

IMPROVEMENTS TO THE RADIANT TIME SERIES
METHOD COOLING LOAD CALCULATION
PROCEDURE

By

BEREKET ASGEDOM NIGUSSE

Bachelor of Science in Chemical Engineering
Addis Ababa University
Addis Ababa, Ethiopia
1989

Master of Engineering Science in Mechanical Engineering
University of New South Wales
Sydney, Australia
1998

Submitted to the Faculty of the
Graduate College of the
Oklahoma State University
in partial fulfillment of
the requirements for
the Degree of
DOCTOR OF PHILOSOPHY
December, 2007

IMPROVEMENTS TO THE RADIANT TIME SERIES
METHOD COOLING LOAD CALCULATION
PROCEDURE

Dissertation Approved:

Dr. Jeffrey D. Spitler

Dissertation Adviser

Dr. Daniel E. Fisher

Dr. Lorenzo Cremaschi

Dr. Alan Noell

Dr. A. Gordon Emslie

Dean of the Graduate College

ACKNOWLEDGEMENTS

First I would like to express my deepest gratitude to my advisor Dr Jeffrey D. Spitler, for his continuous guidance and support over the course of my Ph.D. degree study. I am very grateful for his constructive advice and criticism, without which my success would have been impossible. I would like to this opportunity to thank Dr Daniel Fisher, Dr Alan Noell, and Dr Lorenzo Cramaschi for their time in serving as my advisory committee members.

Next I would like to thank the US State Department for the two-year financial support as Fulbright Scholar. Much of the work was funded by ASHRAE 1326-RP. I am also grateful to ASHRAE for the further financial support provided to me as student Grant-in-Aid.

Finally I would like to express my deepest appreciation for my mother, sisters, brothers, and family members for their encouragement and unconditional love. And my special appreciation goes to my wife Aida Mebrahtu for her support and encouragement.

TABLE OF CONTENTS

Chapter	Page
I. INTRODUCTION	1
1.1 Background	1
1.2 Objectives	13
II. REVIEW OF LITERATURE.....	17
2.1 The Radiant Time Series Method	18
2.1.1 The RTSM Procedure	20
2.1.2 Heat Transfer Phenomena.....	22
2.1.3 RTF Generation	27
2.1.4 Limitations of the Radiant Time Series Method.....	28
2.2 Dynamic Modeling of Thermal Bridges	30
2.2.1 One-Dimensional Conduction Transfer Function.....	32
2.2.2 Steady State Conduction Models.....	36
2.2.3 Multi-dimensional Conduction Dynamic Models	39
III. RTS METHOD IMPROVEMENTS.....	51
3.1 New RTF Calculation Engine	53
3.1.1 The Mathematical Model –Reduced Heat Balance Method	55
3.1.2 Validation of the New RTF Engine	70
3.1.3 1D Finite Volume Method PRF Generation	74
3.1.4 1D RTF Generation in Different Programming Environment.....	76
3.2 Improved Fenestration Model.....	78
3.2.1 Development of Improved Fenestration Model.....	79
3.2.2 Radiative - Convective Split in the RTSM	84
3.2.3 Application of Fenestration Model without Internal Shade.....	98
3.2.4 Application of Fenestration Model with Internal Shade.....	99
3.3 Heat Losses in the RTSM Procedure	100
3.3.1 Derivation of the Mathematical Algorithm.....	101
3.3.2 Dimensionless Loss Conductance.....	115
3.3.3 Performance of Improved RTSM Procedure	118
3.3.4 Heat Losses in the RTSM and TFM Procedures	122
3.3.5 Conclusion and Recommendation	125
3.4 Summary and Conclusions	127

Chapter	Page
IV. PARAMETRIC STUDY OF THE RTSM PROCEDURE.....	131
4.1 Parametric Run Generation.....	132
4.2 Test Zone Parameters.....	134
4.2.1 Zone Geometry and Construction Fabric.....	135
4.2.2 Thermal Mass Types.....	138
4.2.3 Internal Heat Gains and Schedules	139
4.2.4 Glazing Types	140
4.2.5 Interior Shade Model	142
4.2.6 Radiative-Convective Split	143
4.2.7 Solar and Radiant Heat Gain Distribution	144
4.2.8 Design Weather Days	145
4.3 Methodology: HBM and RTSM Implementation.....	147
4.3.1 The HB Method Code.....	148
4.3.2 The RTS Method Code.....	150
4.3.3 The RTSM and HBM Models Comparison.....	151
4.4 Results and Discussion- Original RTSM.....	153
4.4.1 RTSM Peak Design Cooling Load Prediction.....	154
4.4.2 Conclusion and Recommendation	163
4.5 Results and Discussion – Current and Improved RTSM.....	166
V. DYNAMIC MODELING OF THERMAL BRIDGES-METHODOLOGY	175
5.1 Introduction.....	175
5.2 The Equivalent Homogeneous Layer Wall Model	175
5.2.1 Steady State R-value	178
5.2.2 Step-By-Step Procedure.....	178
VI. DYNAMIC MODELING OF THERMAL BRIDGES - VALIDATION	183
6.1 Experimental Validation	184
6.1.1 Guarded Hot Box Dynamic Response Test Facility	184
6.1.2 The Test Procedure and Specimens	186
6.1.3 Experimental Determination of the CTFs.....	190
6.1.4 The Experimental Validation Procedure.....	194
6.1.5 The Equivalent Walls.....	197
6.1.6 Comparison of Conduction Heat Gains	217
6.2 Inter-Model Validation	223
6.2.1 Numerical Validation.....	224
6.2.2 The <i>R</i> -values and the Equivalent Walls	227
6.2.3 Performance of the Equivalent Walls	228

Chapter	Page
6.2.4 Summary and Conclusion	231
6.3 Conclusions and Recommendations	233
6.4 Recommendations for Future Work.....	236
VII. CONCLUSIONS AND RECOMMENDATIONS.....	237
7.1 Conclusions – RTSM Improvements.....	237
7.1.1 Accounting Space Heat Losses.....	238
7.1.2 Improvements to the RTSM Fenestration Model	238
7.1.3 Improvements to the RTF Generation	239
7.1.4 Developments to RTSM Implementation	239
7.1.5 Parametric Study of the Performance of RTSM	240
7.2 Conclusion: Dynamic Modeling of Thermal Bridges.....	243
7.3 Recommendations for Future Work.....	245
REFERENCES	249
APPENDIX.....	259
APPENDIX A: THE NEW RTF ENGINE VALIDATION.....	259
APPENDIX B: 1D FINITE VOLUME METHHOD PRF GENERATION	264
B.1 Derivation of 1D Finite Volume Numerical Model.....	264
B.2 Finite Volume Method PRF Generation Validation	277
APPENDIX C: RTSM IMPLEMENTATION IN OTHER COMPUTING ENVIRONEMNTS	279
APPENDIX D: FENESTRATION MODELS FOR HEAT BALANCE AND RTS METHODS	285

LIST OF TABLES

Table	Page
Table 3.1 Description of zone constructions for RTF generation engine validation.....	70
Table 3.2 RMSE of the RTF of the New RTF Engine.....	71
Table 3.3 Recommended radiative / convective spits for the RTSM procedures	98
Table 4.1 Test Parameter range and levels	134
Table 4.2 Construction Type Materials.....	137
Table 4.3 Thermal Mass Type materials.....	138
Table 4.4 Thermal and Optical Properties of glass window	141
Table 4.5 Optical properties of shade layers.....	143
Table 4.6 Mean Lighting Heat Gain Parameters from ASHRAE 1282-RP.....	144
Table 4.7 Design weather conditions for the fourteen USA locations.....	146
Table 4.8 RTSM and HBM component models	152
Table 4.9 Month of Annual Peak Cooling Load for zones with single pane clear glass.....	159
Table 4.10 RTSM peak cooling load extreme over predictions for glazing without interior shades.....	168
Table 4.11 RTSM peak cooling load extreme over predictions for glazing without interior shades.....	171
Table 6.1 Layer-by-layer descriptions of the ASHRAE RP-515 test walls.....	189

Table	Page
Table 6.2	Surface-to-Surface <i>R</i> -values of ASHRAE RP-515 Test Walls.....204
Table 6.3a	Equivalent walls computed with experimentally determined <i>R</i> - values209
Table 6.3b	Equivalent walls computed with handbook <i>R</i> -values210
Table 6.4a	Air-to-Air CTSF of the test walls generated from experimentally determined conduction transfer functions.....212
Table 6.4b	Air-to-Air CTSF of the EHL walls determined with experimentally determined <i>R</i> -values.....213
Table 6.4c	Air-to-Air CTSF of the EHL walls determined with handbook <i>R</i> - values214
Table 6.5	Results summary of peak heat gains and time shift.....221
Table 6.6	Test walls construction description inter-model validation225
Table 6.7	Surface-to-surface <i>R</i> -value of inter-model validation test walls.....227
Table 6.8	Equivalent walls of inter-model validation test walls.....228
Table 6.9	Peak heat gains and time shift for inter-model validation229

LIST OF FIGURES

Figure		Page
Figure 2.1	Radiant Time Series Method represented as a nodal network. A single wall is shown with the outside surface on the left (Rees at al. 2000)	19
Figure 2.2	The original RTSM cooling load calculation method represented as flow diagram (Rees at al. 2000).....	21
Figure 2.3	Linear-triangular ramp temperature pulse representation.....	41
Figure 3.1	Adiabatic boundary condition for RTF generation: $T_{so}=T_{si}$	58
Figure 3.2	Flow chart of solution scheme I.....	69
Figure 3.3	Solar RTF for lightweight construction zone with no carpet for 50% glazing fraction of the exterior facade.....	72
Figure 3.4	Non-solar RTF for lightweight construction zone with no carpet for 50% glazing fraction of the exterior facade	72
Figure 3.5	Solar RTF for lightweight construction zone with no carpet for 50% glazing fraction of the exterior facade.....	73
Figure 3.6	Non-solar RTF for lightweight construction zone with carpet for 50% glazing fraction of the exterior facade.....	73
Figure 3.7	Peak heat gains calculated using finite volume method versus the State Space method PRFs	76
Figure 3.8	Absorbed component as a fraction of total solar heat gain for different fenestration classes.....	83
Figure 3.9	$TsIn$ and the corresponding MRT of heavyweight construction opaque exterior surfaces and 24°C room air temperature.....	86

Figure	Page
Figure 3.10	<i>TsIn</i> and the corresponding <i>MRT</i> for an opaque surface at peak load for three aspect ratios and 24°C room air temperature87
Figure 3.11	<i>TsIn</i> and the corresponding <i>MRT</i> for single pane clear glass fenestration and 24°C room air temperature.....89
Figure 3.12	<i>TsIn</i> and the corresponding <i>MRT</i> for south facing fenestration at peak load for three aspect ratios and 24°C room air temperature.....90
Figure 3.13	Radiative fractions for fenestration in a heavyweight construction zone and single pane clear glass with 90% glazing fraction.....91
Figure 3.14	Radiative fractions for fenestration in a heavyweight construction zone and single pane clear glass with 50% glazing fraction.....92
Figure 3.15	Radiative Fraction against glazing fraction of exterior facade for heavyweight zone for five glazing types93
Figure 3.16	Radiative fractions against percent glazing of exterior facade for lightweight zone for five different glazing types at peak cooling load condition.....96
Figure 3.17	Radiative fractions against percent glazing of exterior facade for heavyweight zone for five different glazing types at peak cooling load condition.....96
Figure 3.18	RTSM versus the HBM peak cooling loads for single pane clear glass without interior shaded fenestration.....99
Figure 3.19	Current RTSM versus the HBM peak cooling loads for single pane clear glass with interior shaded fenestration100
Figure 3.20	Representation of fenestration inside surface heat balance103
Figure 3.21	The improved RTSM cooling load calculation method represented as flow diagram115
Figure 3.22	Dimensionless loss conductance against glazing fraction for zones with unshaded fenestration117
Figure 3.23	Dimensionless loss conductance against glazing fraction for zone with two exterior facades and interior shaded fenestration117

Figure	Page
Figure 3.24	RTSM peak cooling load vs. HBM for light and heavyweight zone for single pane clear glass without internal shade119
Figure 3.25	Hourly cooling load profile for lightweight zone at 50% glazing fraction for single pane clear glass in Chicago, Illinois.....120
Figure 3.26	Hourly cooling load profile for lightweight zone at 90% glazing fraction for single pane clear glass in Chicago, Illinois.....120
Figure 3.27	RTSM peak cooling load vs. HBM for light and heavyweight zone for single pane clear glass with internal shade121
Figure 4.1	Schematic of Parametric Run Generator.....133
Figure 4.2	Zone orientation and number designations.....136
Figure 4.3	Structure of Heat Balance Method for a Zone149
Figure 4.4	The current RTSM cooling load calculation method represented as flow diagram.....150
Figure 4.5	RTSM annual peak cooling load versus the HBM for the USA weather locations for single pane clear glass160
Figure 4.6	RTSM annual peak cooling load versus the HBM for the USA weather locations for double pane clear glass.....161
Figure 4.7	RTSM annual peak cooling load versus the HBM for the USA weather locations for double pane low-e glass161
Figure 4.8	Maximum RTSM peak cooling load over prediction against glazing fraction for the three glazing types.....162
Figure 4.9	Current RTSM annual peak-cooling load maximum and average over prediction for zone without interior shade.....169
Figure 4.10	Improved RTSM annual peak-cooling load maximum and average over prediction for zone without interior shade169
Figure 4.11	Current and Improved RTSM annual peak-cooling load versus HBM for lightweight zones single pane clear glass without interior shade.....170

Figure	Page
Figure 4.12	Current and Improved RTSM annual peak-cooling load versus HBM for heavyweight zones with single pane clear glass without interior shade.....170
Figure 4.13	Current RTSM annual peak-cooling load maximum and average over prediction for zones with dark roller interior shade.....172
Figure 4.14	Improved RTSM annual peak-cooling load maximum and average over prediction for zones with dark roller interior shade173
Figure 4.15	Current and Improved RTSM annual peak-cooling load versus HBM for lightweight zones with single pane clear glass and dark roller interior shade173
Figure 4.16	Current and Improved RTSM annual peak-cooling load versus HBM for lightweight zones with single pane clear glass and dark roller interior shade174
Figure 6.1	Sectional view of guarded hotbox facility (Brown and Stephenson 1993b)186
Figure 6.2	Flow chart of the experimental validation procedure196
Figure 6.3	Thermal bridge types: (a) sandwiched type; (b) exposed type198
Figure 6.4	ASHRAE RP-515 Test Walls203
Figure 6.5	CTSF plot for the steel stud wall (Wall#1).....215
Figure 6.6	CTSF plot for the steel stud wall (Wall#4).....216
Figure 6.7	CTSF plot for hollow block with insulation and brick exterior finish (wall#5).....216
Figure 6.8	Heat gain for insulated steel stud wall with stucco exterior finish (Wall#1)217
Figure 6.9	Heat gain for pre-cast reinforced concrete slab with steel furring and insulation covered with gypsum board on the exterior (Wall#2)218
Figure 6.10	Heat gain for pre-cast reinforced concrete slab with steel furring and insulation with gypsum board (Wall#3).....218

Figure	Page
Figure 6.11	Heat gain for insulated steel stud wall mounted on reinforced concrete slab (Wall#4)219
Figure 6.12	Heat gain for hollow concrete block with insulation and brick on the exterior and gypsum board (Wall#5)219
Figure 6.13	Heat gain for insulated steel stud wall with brick exterior finish (Wall#6)220
Figure 6.14	Heat gain for solid concrete block wall with insulation and granite veneer exterior finish (Wall#7).....220
Figure 6.15	Summary of peak heat gains for the seven ASHRAE test walls222
Figure 6.16	Handbook R-value errors of the seven ASHRAE test walls.....222
Figure 6.17	Wood and steel stud walls construction details226
Figure 6.18	Heat gain of a wood stud wall for periodic sol-air temperature boundary condition229
Figure 6.19	Heat gain of a warm steel stud wall for steady periodic sol-air temperature boundary condition230
Figure 6.20	Heat gain of a cold steel stud wall for steady periodic sol-air temperature boundary condition230
Figure 6.21	Heat gain of a hybrid steel stud wall for steady periodic sol-air temperature boundary condition231
Figure 6.22	Handbook R-value errors compared to that of the 2D finite volume method.....232
Figure 6.23	Peak cooling load prediction error of the equivalent walls compared to the 2D finite volume method232

CHAPTER I

1 INTRODUCTION

1.1 Background

Design cooling load calculation methods have evolved since their inception during the 1930's. The historical development of cooling load calculation procedures has been strongly influenced by the development and availability of digital computing facilities, and by the desire to provide methods that are of utility to average practicing engineers that can be used with tabulated data (Rees et al. 2000a; Romine 1992).

It is useful to define the terms “heat gains” and “cooling load” and the relationship between them in the context of load calculations. Heat gain is defined as the instantaneous heat flow into a space by conduction, convection and radiation. Cooling load is defined as the amount of heat removed from a space to keep the space air at a fixed desired temperature. Therefore, all heat gains do not necessarily become cooling loads: convective heat gains become cooling load instantaneously, while radiant heat gains are first absorbed by the structure and then released by convection to become a cooling load at a later time. Absorption and re-radiation of radiant heat gains among the surfaces in the zone continues as long as temperature difference exists. Under some circumstances, some of the heat gains may be conducted back out of the space.

The challenge in the early days of the cooling load calculation was primarily to develop procedures to quantify the heat gains. In the 1930s peak-cooling loads were over predicted due to failure to account for thermal mass effects of construction in the load calculation (Houghten et al. 1932; James 1937; Kratz and Konzo 1933). Analytical equations for computing transient conduction heat gains through homogeneous layer constructions exposed to solar radiation were developed. Houghten, et al., (1932) used Fourier analysis and assumed sinusoidally varying outside surface temperatures. Alford, et al., (1939) improved this by assuming sinusoidally varying outdoor air temperature and accounting for solar radiation separately. Despite an effort to develop a rigorous analytical procedure for computing transient heat conduction, there was little success in establishing a general quantitative relation suitable for practicing engineers.

The electric analogy method of predicting heat flow through walls based on the identity of the transient heat flow and flow of electricity can be implemented experimentally and can closely match direct thermal measurements (Paschkis 1942). An electric analog thermal circuit of an embedded tube cooling slab model was developed using electrically equivalent resistance, capacitance, and source terms (Kayan 1950). This allowed determination of the slab surface temperatures, temperature isotherms in the slab and heat transfer rates.

By the mid 1940s, the American Society of Heating and Ventilation Engineers (ASHVE), a predecessor of the American Society of Heating, Refrigeration and Air Conditioning Engineers (ASHRAE), developed a manual method for calculating the heat gain through

various external surfaces with equivalent temperature differentials (ETD) values. The ETD values were often 20 to 40 degrees Fahrenheit above the difference between outside and inside air temperatures (Rees et al. 2000a; Romine 1992). In the ETD method two procedures were involved: the ETD were generated from experimentally measured surface temperatures and conductance (Rees et al. 2000a) for transient conduction heat gain, and the instantaneous solar heat gains through glazing were calculated using heat fluxes and shading coefficients. The ETD method excessively overestimated cooling load due to the assumption that the heat gains instantaneously caused cooling loads on the system. The delays of solar heat gains before becoming cooling load were well understood but simple quantitative relations for these effects were not available until the 1940s and 1950s. Designers made various approximations to compensate for the over prediction of cooling loads (Romine 1992).

Transient conduction heat gain calculation procedures through external surfaces developed using Fourier analysis assumed periodic variation of sol-air temperature as the external driving temperature, constant indoor air temperature, and fixed outside and inside conductance¹ (Mackey and Wright 1944; Mackey and Wright 1946). The sol-air temperature is a concept derived from the equivalent temperature (Billington 1987) used then in UK. It is defined as the temperature that would give the same amount of heat transfer as that of the actual outdoor air temperature and solar radiation incident on the surface. Mackey and Wright (1946) formulated semi-empirical relations to estimate inside surface temperatures for multi-layered walls based on an analytic solution for

¹ A fixed value of combined outside conductance of 4.0 (Btu/hr·ft²·°F) is still commonly used after 60 years.

multi-layered walls. The damping and delay effects of the surface thermal mass on the inside surface temperature were accounted using a decrement factor and time lag. Developing an equation for the inside surface temperatures using the sol-air temperature to account for the incident solar flux provided the first convenient manual procedure for computing instantaneous heat gains. The heat gains were computed from the inside surface temperature and room air temperature, assuming a fixed combined inside conductance.

Later, Stewart (1948) used this procedure to tabulate the ETD for various construction assemblies, surface exterior colors, surface orientations, latitude angles and hours of the day. The tabulated ETD values were adjusted for use with walls and roofs overall heat transfer coefficient, instead of combined inside conductance.

This concept was then adopted by ASHRAE as the total equivalent temperature difference and time averaging (TETD/TA) method in the 1960s. The TETD/TA load calculation method first introduced in the 1967 Handbook of Fundamentals (ASHRAE 1967; Rees et al. 2000a; Romine 1992). The TETD/TA method mainly involves two steps: calculation of heat gains components from all sources and conversion of these heat gains into cooling loads. The TETD replaced the ETD with improved tables and equations for the equivalent temperature differences. Walls and roofs were characterized by two parameters -decrement factor (ratio of peak heat gain to the peak heat gain that would occur with no thermal mass in the wall) and time lag (delay in peak heat gain compared to peak sol-air temperature). The TETD could then be calculated knowing sol-

air temperature, room air temperature, and decrement factors and time lags. Conversion of the instantaneous heat gains into cooling loads using the time averaging technique is a two step procedure: first, split the instantaneous heat gain into convective and radiant components using recommended radiative /convective splits; second, the radiative component of the heat gain is time averaged depending on the thermal mass of the construction to get the cooling loads. For lightweight construction, the hourly radiant cooling load is the radiant component of heat gain time averaged over a 2 to 3 hour period prior to and including the time of maximum load conditions. For heavyweight construction, the hourly radiant cooling load is the radiant component of heat gain time averaged over a 5 to 8 hour period prior to and including the time of maximum load conditions (ASHRAE 1967). The total hourly cooling load is the sum of the convective component and the hourly radiant cooling load.

The work described above did not explicitly consider interactions between heat gain components. The earliest attempt to model zone dynamics involving conduction through the envelope, solar heat gains and the radiant exchange among surfaces and convection between surfaces and room air utilized physical (electric and hydraulic) analogies in the 1940s and 1950s. However, the analogies remained research tools as it was not feasible for practicing engineers to build electric circuits, nor were the insights gained reduced to manual calculation procedures.

Leopold (1948) used a hydraulic analogy to investigate zone dynamics. The model included thermal storage, radiation, convection, and conductions. Thermal capacitance

was represented by vertical tubes in series connection attached to a distribution header connected to a storage tank, and resistances were represented by restricted tube. Radiation absorbed by surfaces was represented by liquid flow from a pump through a calibrated restriction, and temperatures were represented by fluid pressure. The hydraulic model demonstrated dynamics of zones and gave some insights to the limitations the load calculation procedures.

Despite all efforts to improve the accuracy of load calculation procedures, peak cooling load computed using the ASHVE Guide 1952 over predicted by 16 to 32 % compared to values measured in a small single story residential house with large glass exposure due to failure to account for the storage effect (Gilkey et al. 1953). Similarly, a field survey made on single family houses over a wide range of climates and construction fabrics revealed over sizing of cooling equipment capacity due to failure to account for the thermal mass effects of building structures (Willcox et al. 1954).

Dynamic modeling of thermal mass effects of structures and furnishing in a building was attempted using analog computers by solving the electrical equivalent thermal circuit of actual buildings (Willcox et al. 1954). The model used pure resistances to represent doors, windows, blinds and infiltration. Distributed resistances and capacitances were used to represent walls, roofs and partitions. The outdoor and indoor temperatures were represented by potential differences. With this approach, the authors found it difficult to construct a circuit that both had a one-to-one physical correspondence with the building, and which gave a good match to transient thermal measurements. They did find that they

could “tune” a simpler circuit to give the correct dynamic response, but this has limited usefulness for design load calculations. However, they had better success with an analog computer, which utilizes amplifiers and allows better measurement of intermediate values. The analog computer’s calculated response was only 7% higher than the actual thermal measurements.

The work of Brisken and Reque (1956), in developing what they called the ‘Thermal Response Method’, was the first attempt to use digital computers by representing a wall using two-lump (one-resistance and two-capacitance) thermal circuit that was connected to outdoor sol-air temperature and indoor air temperature nodes using outside and inside combined conductance. The two differential equations for the two-lump thermal circuit were solved using the Laplace transform method to determine the room response to a unit square pulse applied at the sol-air temperature while the room air temperature was constant. The method was not adopted in the ASHVE Guide, but the approach later became the basis for development of the conduction transfer function method with a unit triangular pulse adopted by ASHRAE for transient conduction heat gain calculations.

A procedure for computing room response factors using a detailed thermal circuit model involving radiation exchange among inside surfaces and room furnishings, convection between surfaces and room air, and various room heat sources was developed by Mitalas and Stephenson (1967). An effort to provide a more rigorous load calculation procedure led to the development of conduction transfer functions for transient conduction through homogeneous multi-layered constructions (Stephenson and Mitalas 1971). The transfer

function method (TFM) for computing zone thermal response and cooling load was first published in the 1972-Handbooks of Fundamentals (ASHRAE 1972). The method relied on a set of tabulated room transfer function coefficients.

Given the enormous (in the 1970s) computational efforts required by the TFM and the lack of computer resources and skills of practicing engineers there was a need for a method that could be used manually. As a result, a simplified procedure called the Cooling Load Temperature Difference / Cooling Load Factor (CLTD/CLF) method was developed under ASHRAE RP-138 by Rudoy and Duran (1975). The CLTD/CLF method is a single step load calculation procedure. CLTD values were calculated by dividing the cooling load due to a particular wall or roof using the TFM by the U-value of the constructions. Due to its simplicity, the CLTD/CLF method replaced the TETD/TA methods as the ASHRAE-recommended manual load calculation procedure. However, the CLTD/CLF method had limitations due to a lack of tabulated CLTD/CLF design data that matched the wide range of design conditions faced by practitioners. Thus, designers showed continued interest into TETD/TA method due to its flexibility for manual load calculations and adaptations for various building envelope assemblies and design locations (Romine, 1992).

ASHRAE's continued commitment to refine load calculation procedures, to investigate effects of different building design parameters, and to provide accurate design data led to new research directions in the 1980s. ASHRAE-funded research project 472-RP characterized room response based on fourteen building design parameters. Generating,

tabulating, and printing the whole range of the CLTD/CLF data on the basis of the fourteen design parameters became an impractical task (Sowell 1988c). However, ASHRAE maintained the CLTD/CLF method, which later became the Cooling Load Temperature Difference /Solar Cooling Load / Cooling Load Factor (CLTD/SCL/CLF) method, as a manual load calculation procedure by tabulating CLTDs for representative families of walls and roof assemblies and developing a mapping procedure for the actual constructions. Software for generating CLTD and CLF data based on the weighting factors and conduction transfer function coefficients developed in ASHRAE RP-472 was developed as part of ASHRAE RP-626 (Spitler et al. 1993b). Spitler, et al. (1993a) introduced a new factor, the solar cooling load (SCL), for converting solar heat gain into cooling load. Though the TFM required high computational resources, it remained the only computational design cooling load calculation procedure recommended by ASHRAE until the late 1990s.

The Transfer Function Method was not well received (Romine 1992) by practicing engineers for the following reasons:

- Intimidating look of the equations
- Required iterations and convergence may take three to five successive design day calculations
- Computer resources and a lack of computing skills also limited its implementation for load calculations

A simple and yet reasonably accurate load calculation procedure that did not involve iterative processes was highly desired by ASHRAE to replace the manual procedures. An

ASHRAE funded project (RP-875) for continued improvements of load calculation procedures led to the development of the Heat Balance Method (HBM) (Pedersen et al. 1997) and the Radiant Time Series Method (RTSM) (Spitler et al. 1997) for calculating peak cooling loads.

The HBM was first implemented in the 1960s by Kusuda in NBSLD, later by Walton in 1980s in Building Loads Analysis and System Thermodynamics (BLAST) and in Thermal Analysis Research Program (TARP) as cited by Pedersen, et al. (1997). However, a complete description of the procedure for load calculation purposes had not been available. The first complete description of the heat balance method formulation starting from the fundamental principles, and covering implementation and solution techniques as applied for peak cooling load calculation was presented by Pedersen, et al., (1997). Since the heat balance method is based on the fundamental principles of the physics involved, it is commonly used as a reference model for simplified load calculation programs.

The RTSM closely followed the HBM hourly cooling load profile and in most cases slightly overpredicted the peak cooling load; however, the over predicted peak cooling load was significant for zones with large amount of single pane glazing and cool design weather conditions (Rees et al. 1998). The radiant time series method (RTSM) was developed as a spreadsheet method intended to replace the TETD/TA and the CLTD/SCL/CLF methods. It also effectively replaced the TFM. The radiant time series method (RTSM) as a simplified load calculation procedure was adopted as a

nonresidential building load calculation procedure by ASHRAE and published in Pedersen, et al. (1998) and the 2001 *–Handbook of Fundamentals* (ASHRAE 2001). Experimental validation of the heat balance and the radiant time series methods has been done in test cells at Oklahoma State University (Chantrasrisalai et al. 2003; Iu et al. 2003).

ASHRAE research project RP-942 compared the peak cooling load predictions made with the RTSM to those made with the heat balance method (HBM) using a parametric run investigation tool (Rees et al. 1998; Spitler and Rees 1998). Although ASHRAE 942-RP identified building design parameters that lead to over predictions of peak cooling load, the project did not result in design guidance for practicing engineers.

The radiant times series method (RTSM) has effectively replaced the manual load calculation procedures and has attracted interest due to:

- Its amenability to spreadsheet implementations as opposed to the Transfer Function Method, which requires iteration.
- Captures and depicts the physics involved in the Conduction Time Series Factor (CTSF) and Radiant Time Factor (RTF) coefficients, unlike the Transfer Function Method.
- Has essentially the same accuracy as the TFM.

However, the RTSM also has the same approximations as the TFM that, in some cases, lead to over prediction of peak-design cooling load:

- The RTSM replaces the outside heat balance by an exterior boundary condition known as the sol-air temperature, which allows the use of fixed combined conductance of convection and radiation.
- The RTSM computes the radiant heat gain from the interior surfaces as if they all radiate to the room air temperature instead of performing inside surface and room air heat balances. This allows treatment with a linearized radiation coefficient, which is combined with the convection coefficient. This assumption can over predict the instantaneous heat gain, which again contributes to the RTSM peak cooling load overprediction.
- The RTSM uses an adiabatic boundary condition when computing Radiant Time Factors (RTF), causing the RTF to always sum to one. When these RTF are used, this approach conserves the entire solar and internal heat gains during conversion to cooling load, and there is no way that the RTSM can account for any heat gains conducted back out. As a result, the RTSM tends to over predict the peak-cooling load when there is a large amount of single pane glazing or other highly conductive surfaces.

The resulting over predictions was shown in 942-RP to be as high as 37%. It would be very helpful for designers to have guidance as to when the RTSM is likely to give significant overprediction.

1.2 Objectives

The previously published research in the RTSM cooling load calculation procedure has only identified the likely over of peak cooling load and the conditions favorable for over prediction but non them provided a procedure for accounting the heat gain loss and did not provide guidance on the limitation of the RTSM. Therefore, one of the objectives of this thesis is to develop an algorithm that reduces the RTSM peak cooling load likely over prediction significantly and establish the limitations of the RTSM in a form of design guidance. Furthermore, ten years of experience with the RTSM has indicated several improvements that would be helpful for design engineers. These include an improved RTF generation procedure, developing a numerical procedure for periodic response factor generation, updated fenestration modeling and investigated a procedure for treating thermal bridges. These improvements are discussed briefly below.

The RTSM needs radiant time factors (RTF) for the zone to be analyzed. The *ASHRAE Handbook of Fundamentals* (ASHRAE 2001; ASHRAE 2005) has given tabulated RTF for specific cases, but the accuracy resulting from users choosing the “nearest” zones has not been investigated. The original presentation of the procedure utilized a full blown HBM program to generate the RTF. While this approach works, the HBM program has many features and data that are not needed for generating RTF. Therefore, one of the objectives of this thesis is to develop a simplified procedure and implement the algorithm for computing RTF, as described in Section 3.1. Also investigated is a direct method of calculating periodic response factors as an alternative to converting conduction transfer function coefficients back to response factors for use in the RTF generation procedure. A

one-dimensional finite volume numerical fully-implicit formulation for generating periodic response factor will be developed. The finite volume periodic response generator and the simplified RTF generator algorithm will also be implemented in other computing environments. Furthermore, the RTF generation has been investigated with constant radiation coefficient with the intent of reducing the computational time.

The radiant time series method load calculation procedure was developed based on the shading coefficients and optical properties of double-strength glass for computing solar heat gains. Developments in fenestration models and availability of a new set of fenestration data – solar heat gain coefficients - replaced the use of shading coefficients in fenestration modeling. Moreover, the shading coefficient data are no longer available. Therefore, one of the objectives of this thesis is investigation of a new fenestration model using window manufacturer's data and the new set of tabulated glazing and fenestration data available in the ASHRAE's Handbook of Fundamentals as presented in Section 3.2. Improved fenestration model for the RTSM will be investigated and integrated that make use of these new developments. Moreover, a new set of radiative / convective splits for fenestration solar and conduction heat gains will be established.

It has been identified that the likely over prediction of the RTSM procedure is due to failure to account for the space radiant heat gains conducted back to the outside. In this thesis an algorithm for accounting the radiant heat gain loss by conduction will be derived and investigated in Section 3.3.1. The procedure accounts for solar and internal radiant heat gains conducted back out through fenestrations and highly conductive mass

less surfaces. Furthermore, the likely overprediction of peak cooling load by the RTSM will be investigated parametrically over a wider range of building design parameters to characterize its limitations and develop design guidance for practicing engineers. This is covered in Chapter Four.

Another challenge faced by designers is the treatment of thermal bridges in wall and roof constructions. Steady state treatment of thermal bridges is covered in the *ASHRAE Handbook of Fundamentals* (ASHRAE 2005). Dynamic modeling of thermal bridges has been a research interest in building energy and load calculation applications for about two decades. Despite repeated efforts to develop multi-dimensional conduction models capable of dynamic modeling of thermal bridges, these models have never been integrated into design load calculation procedures for several reasons. Therefore, another objective of this thesis is to investigate an approximate one-dimensional dynamic model of thermal bridges that can be directly implemented into design cooling load calculation procedures, and develop design recommendations usable by practicing engineers. This is covered in Chapters Five and Six.

Before addressing these three chapters, the thesis gives an in-depth literature review of the Radiant Time Series Method and the treatment of thermal bridges in Chapter Two. Improvements to the Radiant Time Series Method procedure are discussed in Chapter Three. Parametric investigation of the Radiant Time Series Method to establish the limitations based on adapted fenestration model is covered in Chapter Four. Chapters Five and Six deal with approximate one-dimensional dynamic modeling of thermal

bridges methodology and the validation, respectively. Conclusions and recommendations for future work are given in Chapter Seven.

CHAPTER II

2 REVIEW OF LITERATURE

The literature review covers two separate topics related to building energy analysis and load calculation methods. The first section deals with developments in Radiant Time Series method, and the second section deals with dynamic and steady state modeling of thermal bridges.

The first part of the literature survey (Section 2.1) describes the development of the Radiant Time Series Method (RTSM) as a simplified design cooling load calculation procedure, discusses the key assumptions introduced to derive the RTSM procedure, and explains in detail the limitation of the RTS method in predicting the peak design cooling, and discusses the necessary conditions for the RTSM peak cooling load overprediction. The second part of the literature survey (Section 2.2) deals with dynamic and steady state modeling of thermal bridges in relation to building energy analysis and load calculation program. It discusses the importance of steady state and dynamic modeling of thermal bridges in building energy analysis and load calculation application, reviews previously published dynamic modeling techniques for thermal bridges and explains why these models have not been adopted.

It also presents a brief summary of response factors and conduction transfer functions and the associated one-dimensional conduction modeling procedures. In addition it summarizes recommended approximate procedures for steady state analysis of thermal bridges.

2.1 The Radiant Time Series Method

The Radiant Time Series Method (RTSM) was introduced as a simplified design load calculation procedure (Spitler et al. 1997). The RTSM was intended to replace ASHRAE's simplified load calculation procedures: the cooling load temperature difference/solar cooling load/cooling load factor (CLTD/SCL/CLF) method, the total equivalent temperature difference/time averaging (TETD/TA) method, and the Transfer Function Method (TFM). The radiant time series method can be thought as a two-stage process (Spitler et al. 1997). The first stage of this process is to calculate all the radiant and convective heat gains of the zone. The second stage is the conversion of these gains into contributions to the cooling load on the zone air.

Several key approximations have been employed in simplifying the RTSM in order to avoid the iteration steps in the procedure so as to make the method suitable for spreadsheet implementation. The first simplifying assumption in the radiant time series method is the treatment of exterior and interior convection and radiation coefficients using combined constant conductance. This simplification in effect entails the assumption that surfaces exchange long wavelength radiation with air node. This assumption allows

the replacement of individual surface heat balances and represents each wall by a simplified nodal network as shown in Figure 2.2 (Rees et al. 2000a).

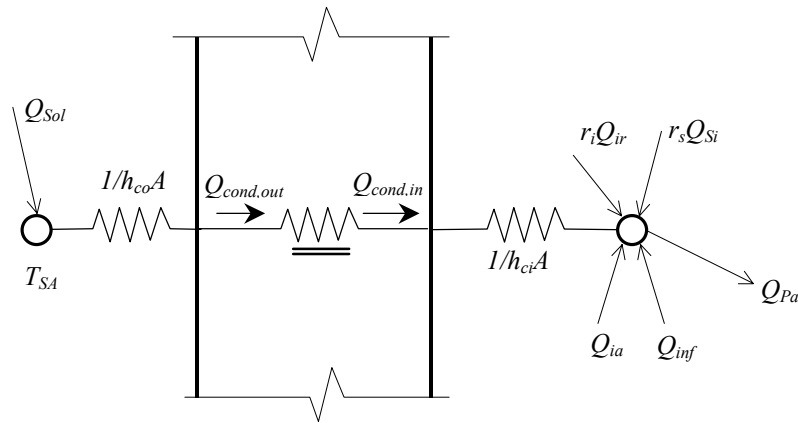


Figure 2.1 Radiant Time Series Method represented as a nodal network. A single wall is shown with the outside surface on the left (Rees et al. 2000a)

The second approximation is periodicity of the design weather conditions. The radiant time series method takes advantage of the periodicity of the design day sol-air temperature and constant room air temperature to develop the periodic response factor. Conduction heat gains are calculated by periodic response factors (PRF) or Conduction Time Series Factors (CTSF) driven by the difference between the design day periodic Sol-air temperature T_{SA} and room air temperature T_a , which is assumed constant. The periodic response factors replace the CTF in the heat balance method and eliminate the iterative conduction heat gain calculation, which is inherent in load calculation methods involving transfer functions. This assumption is key in that it avoids the iteration step and hence makes the RTSM suitable for spreadsheet implementation (Rees et al. 2000a; Spitler et al. 1997). The CTSF are determined from periodic response factors divided by the overall U -value of the construction.

The third simplifying approximation in the RTSM is the conversion of the radiant components of the heat gains into cooling load using the radiant time factors (RTF), which replaces the air heat balance. The radiant gains at each hour are converted by a series of twenty-four room response factors known as the radiant time factors (RTF). The contribution of the internal heat gains Q_{ir} and the transmitted solar heat gains Q_s to the load appear at the room air node as shown in the nodal network diagram (Figure 2.1) but multiplied by the radiant time factors r_i and r_s , respectively. These contributions are summed up to get the total hourly load. Cooling load is defined as the rates at which heat must be removed from the space to maintain a constant room air temperature and is represented as Q_{Pa} in Figure 2.1.

The fourth approximation in the RTSM is that solar and internal heat gains are divided into radiative and convective components using fixed radiative / convective splits (Rees et al. 1998; Spitler et al. 1997).

2.1.1 The RTSM Procedure

The RTSM procedure, in terms of processing the input data and steps to arrive at the 24-hourly cooling loads, is described as follows and the calculation flow diagram is shown in Figure 2.2. The first step of the RTS method is calculation of all internal heat gains. This is done in exactly the same way as for the Heat Balance Method. All gains that are independent of the zone surface temperatures hence can be computed at the beginning of the simulation and stored as hourly values for later use. These include solar gains through

glazing, infiltration (assuming fixed internal air temperature), and internal gains, which are determined from the 24 hours schedule and peak internal heat gain.

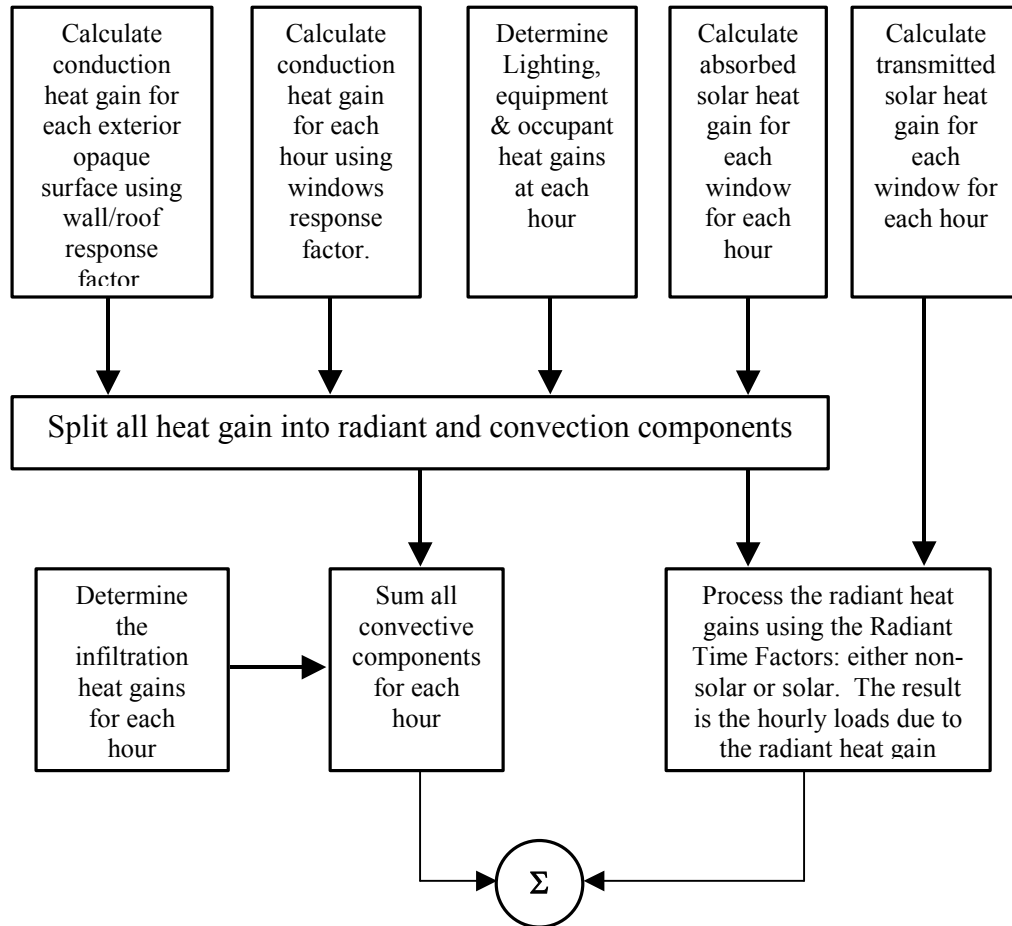


Figure 2.2 The original RTSM cooling load calculation method represented as flow diagram (Rees et al. 2000a)

The periodic response factors operate on the sol-air and internal dry bulb temperatures. The hourly values of the sol-air temperature and the room air temperatures are known at the beginning of the calculation. Once the conduction heat gains through the individual surfaces have been calculated, the next important step is to divide all the gains into

radiant and convective components. This is done using fixed radiative / convective splits for each type of heat gains.

The second stage of the RTS calculation procedure is to convert all the heat gains into contributions to the load at the air node. Convective components of the gains make instantaneous contributions to the cooling load while the radiant components of the heat gains are converted to cooling loads by means of the radiant time factors (RTF). The hourly contributions of the radiant gain to the cooling load are calculated from the 24-hourly radiant gains and the RTF. The radiant time factors are zone dynamic response characteristic, which are dependent on the overall dynamic thermal storage characteristics of the zone and defines how the radiant gain at a given hour is redistributed in time to become contributions to the cooling load at future hours. The contributions of the past and current radiant gains are simply added to the hourly convective gains to give the hourly cooling load.

2.1.2 Heat Transfer Phenomena

This section describes the specific practices and assumptions used by the RTSM to model some of the principal zone heat transfer mechanisms.

Exterior Convection and Radiation

The RTS Method uses a fixed exterior surface conductance combined with a sol-air temperature to model exterior convection and radiation. This is one of the first simplifying assumptions of the radiant time series method.

Transient Conduction Heat Transfer

The RTS Method treats external and internal excitation of conduction heat flow separately. In the RTS procedure, transient conduction heat transfer due to external excitation is modeled using a set of 24 periodic response factors. Given the constant zone air temperature T_a and the current and 23 past values of sol-air temperature $T_{SA\theta}$, the current hour's conduction heat gain per unit surface area is given by:

$$\dot{q}_{cond,i,t}'' = \sum_{j=0}^{23} Y_{Pj} (T_{SA,i,\theta-j\delta} - T_a) \quad (2.1)$$

where,

$\dot{q}_{cond,i,t}''$ = the current hour conduction through the i^{th} surface, Btu/h·ft² (W/m²)

Y_{Pj} = the periodic response factors at j hours from the present, Btu/h(W)

$T_{SA,i,\theta-j\delta}$ = the sol-air temperature of the i^{th} surface j hour from the present, °F(°C)

T_a = the constant room air temperature, °F(°C)

The periodic response factors Y_{Pj} include both the interior and exterior surface conductance. Periodic response factors can be computed from response factors (Spitler et al. 1997), from the generalized form of the CTFs (Spitler and Fisher 1999a), and frequency domain regression method (Chen and Wang 2005). The sol-air and inside temperatures are known at the beginning of the calculation, therefore the heat gains due to conduction can be calculated straightforwardly without the need for any iteration, which makes the RTSM amenable for spreadsheet implementation. These gains subsequently have to be divided into radiant and convective components.

Interior Convection and Radiation

The RTS Method uses fixed combined interior radiation and convection conductances. The convection and radiation coefficients are added (as a resistance) into the wall. This approach, though it simplifies the procedure, has the effect of having the wall radiating to the zone air temperature. In most cases, this causes the RTSM to slightly over-predict the peak cooling load (Rees et al. 2000a).

The RTS Method uses radiant time factors (RTF) to convert and redistribute the radiant part of the conducted gain. Analogous to periodic response factors, radiant time factors are used to convert the cooling load for the current hour based on current and past radiant gains. The radiant time factors are defined such that r_0 represents the portion of the radiant gains convected to the zone air in the current hour. r_1 represents the portion of the previous hour's radiant gains that are convected to the zone air in the current hour, and so on (Spitler and Fisher 1999b). The cooling load due to radiant heat gain is given by:

$$Q_t = \sum_{j=0}^{23} r_j q_{t-j\delta} \quad (2.2)$$

Where

Q_t = the current hour cooling load, Btu/h(W)

$q_{t-j\delta}$ = the radiant gain at j hours ago, Btu/h(W)

r_j = the j^{th} radiant time factor, Btu/h(W)

Transmitted and Absorbed Solar Radiation

Calculation of transmitted and absorbed solar radiation associated with fenestration is a very important part of the design cooling load calculation procedure. The response of the zone is dependent not only on the value of the transmitted and absorbed solar energy but also on its distribution in the zone. Two simple procedures applicable for load calculation purposes have evolved: (1) the use of normal solar heat gain coefficient and transmittance and absorptance correction for angle dependence using a reference standard DSA glass angle correction coefficients (Spitler et al. 1993a), (2) the use of angle dependent beam solar heat gain coefficient and constant diffuse solar heat gain coefficient tabulated values (ASHRAE 2005). The first approach allows separate treatment of transmitted and absorbed solar radiation. Though transmitted and absorbed components are calculated separately, the procedure is based on approximate analysis analogous to the concept of shading coefficient. This was adopted as a standard procedure but with demise of the shading coefficients a new procedure is needed.

The second approach is used in a combined treatment of transmitted and absorbed components. In the second approach the solar heat gain coefficient includes both the transmitted portion of the solar heat gain and the inward flow fraction of the absorbed component. This therefore precludes the separate treatment of the absorbed solar heat gain, which has both radiative and convective components. Likewise, the RTSM uses the solar radiant time factor to convert the beam and diffuse solar heat gains into cooling loads. The diffuse solar gains are treated in a similar way to internal short and long wavelength radiant gains. As noted previously in the discussion on internal convection

and radiation heat transfer, some of the solar radiation that is re-radiated can be conducted to the outside. The RTSM cannot account for this, and so for some zones and design weather condition tends to over-predict the cooling loads.

Internal Heat Gains

In the radiant time series method the hourly schedules and peak gain rate for the three type of internal heat gains (e.g. people, lights, and equipment) are specified by the user along with the respective radiative/convective splits. Though the split between radiative and convection actually depends on the zone airflow rates and surface temperatures, constant values are used even in detailed building energy analysis programs. In the RTSM the radiative component heat gain contribution on the cooling load is estimated with the radiant time factors. The RTSM does not account for the portion of the radiant gain that is conducted to the outside and so for some zone constructions tends to over-predict the cooling loads. The degree of overprediction depends on the zone construction conductance, and design weather conditions. This has been one of the limitations of the RTSM procedure and is discussed in Section 2.1.4.

2.1.3 RTF Generation

Radiant time factors (RTF) are dynamic response characteristics of a zone when a zone is excited by unit heat gain pulse. (Spitler et al. 1997) described two procedures for generating RTF coefficients. The first method uses a load calculation program based on the heat balance method (Pedersen et al. 1997).

The radiant time factors are generated by driving a heat balance model of the zone with a periodic unit pulse of radiant energy under adiabatic wall conditions. The radiant time factors are therefore different for every combination of zone construction and geometry. In principle, they are also different for every chosen distribution of radiant pulse. Thus far two types of distributions have been commonly used for a given zone (Spitler et al. 1997). One is found assuming an equal distribution (by area) of radiant pulse on all zone surfaces and is used for all diffuse radiant gains. A second set is found with the unit pulse of radiant energy added at the floor surface and in some cases to the furniture as well to treat beam solar gains. The conversion of radiant gains by the use of radiant time factors, where there is no requirement for knowledge of past temperatures or cooling loads, again avoids the iteration processes.

The second method demonstrated by (Spitler and Fisher 1999b) is to generate radiant time factors directly from a set of zone weighting factors using the existing ASHRAE database (Sowell 1988a; Sowell 1988b; Sowell 1988c). This approach would use a computer program to map a given zone to the fourteen zone characteristic parameters in the database and transform the weighting factors to radiant time factors using matrix manipulation. However, the custom weighting factors do not represent all possible zone constructions. Use of a weighting factor database requires some approximations to fit the fourteen selection parameters. Therefore, development of an RTF generating tool that fits practical design condition is essential for RTSM implementations.

One important assumption in calculating the radiant time factors is imposing adiabatic boundary condition for all surfaces in the zone. As the consequence of this assumption the radiant pulse used to generate the radiant time factors is then only redistributed in time, otherwise its energy is entirely conserved in the zone. In the RTSM, since no solar and internal radiant heat gains are conducted out of the zone, this often leads to slight over-prediction of the peak-cooling load. However, for zones with large amount single pane glazing, and cooler summer design weather conditions, a significant portion of the radiant heat gains can be conducted out, and those never become part of the cooling load. In these cases a much larger over-prediction relative to the heat balance method is expected (Rees et al. 2000a; Rees et al. 1998; Spitler et al. 1997).

2.1.4 Limitations of the Radiant Time Series Method

Quantitative comparison with the heat balance method shows that the RTSM tends to over predict the peak cooling loads (Rees et al. 1998; Spitler et al. 1997). Parametric investigations conducted for 945 zones cases showed that the peak load is slightly over predicted (Spitler et al. 1997). The heat balance method uses a detailed fundamental and rigorous mathematical model for the outside and inside surface heat balance. For medium and light weight construction, in particular zones with large amount of single pane glazing, the peak loads were over predicted significantly. In another similar study (Rees et al. 1998) made quantitative comparison of 7,000 different combinations of zone type, internal heat gains, and weather day. The result shows that the RTSM cooling load profile closely follows that of the heat balance cooling load; however, it over predicted the peak load for majority of the test cases when a radiative heat gain is large and zones

are made with large amount of single pane glazing. For a heavy weight construction mid-floor, northeast corner zone, with 90% of the exterior wall area consisting of single-pane glass (Rees et al. 1998) the RTSM over predicted the peak-cooling load by 37%. Three main reasons have been pointed out for peak cooling load over prediction: (1) the use of adiabatic boundary condition for the RTF generation, (2) combined treatment and constant assumption of convection and radiation coefficients, which makes the zone internal surfaces to radiate to the room air, and (3) simplification of the sol-air temperature calculations.

Rees et al. (1998) concluded that the RTS method enforces conservation of radiant heat gains by ignoring the heat gain conducted to the outside environment as the principal reason for over prediction of peak cooling load. For internal surfaces with conditioned adjacent zones, the adiabatic boundary condition is a reasonable approximation; however, for external surfaces the adiabatic boundary condition in some cases very conservative approximation. Zones for which the peak design cooling load occurs in winter or zones located at lower design weather temperatures can be shown (with the HBM) to conduct a large amount of heat gains through the exterior surfaces with very low conductance (e.g. single pane glazing windows). On the other hand, the RTSM conserves the entire radiant heat gains and has no procedure to account for the heat gain conducted to the outside. Therefore, the RTSM over predicts the peak design cooling load slightly for hot and warm cooling design weather locations, while it tends to over predicts more and more for cold design weather conditions.

Experimental validation of radiant time series cooling load calculation method revealed that reflection loss of solar heat gain from the zone with high glazing fraction is significant (Iu et al. 2003). Though the re-reflection and direct transmission losses can be computed they require detailed input data of glazing optical properties, zone geometry and orientations. In fact this phenomenon is likely to cause significant loss only in highly glazed buildings.

2.2 Dynamic Modeling of Thermal Bridges

Dynamic modeling of thermal bridges has been an area of interest in building energy analysis and design load calculation programs. Building energy analysis and load calculation programs developed in the USA use one-dimensional conduction transfer functions to predict heat conduction through the building envelope. However, many wall and roof constructions contain composite layers (e.g. steel studs, and batt insulation) that lead to local multidimensional heat conduction. The element with very high thermal conductivity is often referred to as a thermal bridge. Thermal bridges are important for both steady state and dynamic heat conduction.

Several publications (Brown et al. 1998; Carpenter et al. 2003b; Kosny and Christian 1995b; Kosny et al. 1997b; Kosny and Kossecka 2002; Kosny et al. 1997c) indicate that one-dimensional approaches cannot predict heat transmission through building envelopes without errors, especially for walls with thermally massive elements and a high disparity in the thermal conductivity of layer materials. Numerical studies indicate that thermal bridge effects of steel stud walls can reduce the thermal resistance of the clear wall by up

to 50% (Kosny et al. 1997a). Similar studies on metal frame roofs showed that the thermal bridge effect reduces the effective thermal resistance of the clear cavity values by as high as 75% (Kosny et al. 1997c).

However, there is a limitation in the use of one-dimensional response factor or conduction transfer functions methods when it comes to analysis of composite walls such as stud walls. This is a common problem in modeling heat conduction in steel stud walls and the ground where one-dimensional analysis cannot predict the heat conduction without significant error. Multi-dimensional heat conduction effects are either ignored or not accounted properly. The one-dimensional analysis may be valid for homogeneous layer wall; however, at the edges and corners, heat transfer significantly deviates from that of the one-dimensional analysis. In practice, the edge and corner effects are simply ignored. Numerical and experimental investigations showed that ignoring the edge effects could under predict the heat transmission by over 10% (Davies et al. 1995). However, for portions of walls not near the edges, one-dimensional analysis can be a reasonable approximation for lightweight walls without significant thermal conductivity disparity, such as those made from wood studs (Davies et al. 1995). Therefore, the need for multi-dimensional transient heat conduction models in building energy analysis and load calculation programs is crucial for accurate prediction of building energy consumption and peak load estimation; hence, it is also necessary for reliable HVAC equipment sizing and thermal comfort prediction. The following section discusses the one-dimensional dynamic conduction modeling commonly used in load calculation and energy analysis programs in the USA.

2.2.1 One-Dimensional Conduction Transfer Functions

Transient conduction heat transfer through building envelopes can be calculated using lumped parameter methods, numerical methods, frequency response methods and conduction transfer function methods. Conduction transfer functions have been used most commonly in load calculation and building energy analysis programs due to their computational efficiency and accuracy. The response factors are time series solutions of transient heat conduction that relate the current heat flux terms to current and past temperatures. Conduction transfer function coefficients are derived from response factors, which are determined using Laplace transform method (Kusuda 1969; Mitalas 1968; Stephenson and Mitalas 1971), or numerically (Peavy 1978). Conduction transfer function coefficients can be also determined directly using frequency-domain regression (Wang and Chen 2003), stable series expansion based on the Ruth stability theory (Zhang and Ding 2003), and State Space method (Seem 1987; Strand 1995). The next sections presents the use of response factor and transfer function coefficients in one-dimensional conduction.

Heat conduction through building structures is represented by one-dimensional partial differential heat equation and the Fourier's law of heat conduction as follows:

$$\frac{\partial q''(x,t)}{\partial x} = \rho c_p \frac{\partial T(x,t)}{\partial t} \quad (2.3)$$

$$q''(x,t) = -k \frac{\partial T(x,t)}{\partial x} \quad (2.4)$$

Where

- q'' = is the heat flux, (W/m² K)
- T = is the temperature, (°C)
- k = is the thermal conductivity, (W/m K)
- ρ = is the density, (kg/m³)
- c_p = is the specific heat of the solid, (kJ/kg K)

The solution of equations 2.3 and 2.4 can be represented as time series solutions called response factors. The time series solution of the heat conduction equation is determined for a unit triangular ramp excitation of the temperatures on both the internal and external surfaces of a wall. The response factors can be determined using Laplace Transform method (Clarke 2001; Hittle 1992; Kusuda 1969; Stephenson and Mitalas 1971), numerical methods (Peavy 1978), and time domain methods (Davies 1996). The current heat flux at interior surface of the wall $\dot{q}_{i,t}''$ in terms of current and past boundary temperatures as inputs and the response factors is given by:

$$\dot{q}_{i,t}'' = \sum_{n=1}^{\infty} T_{i,t-n+1} Z_n - \sum_{n=1}^{\infty} T_{o,t-n+1} Y_n \quad (2.5)$$

The heat flux at the external surfaces $\dot{q}_{o,t}''$ is given by:

$$\dot{q}_{o,t}'' = \sum_{n=1}^{\infty} T_{i,t-n+1} Y_n - \sum_{n=1}^{\infty} T_{o,t-n+1} X_n \quad (2.6)$$

Where

$\dot{q}_{i,t}''$: heat flux at the interior surfaces at time step t , W/m^2

$\dot{q}_{o,t}''$: heat flux at the external surfaces at time step t , W/m^2

$T_{i,t-n+l}$: interior boundary temperature at time step $t-n+l$, $^{\circ}\text{C}$

$T_{o,t-n+l}$: exterior boundary temperature at time step $t-n+l$, $^{\circ}\text{C}$

X : is the self-coupling response factor; the heat flux at the exterior surface for triangular ramp input of the exterior boundary temperature and zero interior boundary temperature ($\text{W/m}^2 \text{K}$).

Y : is the cross coupling response factor; the heat flux at either surface for triangular ramp input of the boundary temperature at the other surface, ($\text{W/m}^2 \text{K}$).

Z : is self-coupling response factor of the interior surface for triangular ramp input of the boundary temperature at the interior surface and zero exterior boundary temperature, ($\text{W/m}^2 \text{K}$).

The primary advantage of the response factor method is that for a given building structure, assuming constant thermo-physical properties, the response factors need to be determined only once. Numerical methods such as finite difference or finite element methods generally require high computational time; however, they allow variable time step and variable thermo-physical property simulations.

Conduction transfer function methods are further refinements of response factor methods.

The replace many of the higher order terms of the response factors and the past

temperatures with the past heat fluxes; hence, use fewer coefficients (Hittle, 1992) (McQuiston et al. 2005; McQuiston 2000). The heat fluxes at the interior and exterior surfaces of a wall in terms of conduction transfer functions are given by:

$$q_{i,t}'' = \sum_{m=1}^M Z_{k,m} T_{i,t-m+1} - \sum_{m=1}^M Y_{k,m} T_{o,t-m+1} + \sum_{m=1}^M F_m q_{i,t-m} \quad (2.7)$$

$$q_{o,t}'' = \sum_{m=1}^M Y_{k,m} T_{i,t-m+1} - \sum_{m=1}^M X_{k,m} T_{o,t-m+1} + \sum_{m=1}^M F_m q_{o,t-m} \quad (2.8)$$

Where

$X_{k,m}$: the m^{th} conduction transfer coefficient for the exterior self-coupling term of order k, (W/m² K)

$Y_{k,m}$: the m^{th} conduction transfer coefficient for the cross coupling term of order k, (W/m² K)

$Z_{k,m}$: the m^{th} conduction transfer coefficient for the interior self-coupling term of order k, (W/m² K)

F_m : is defined as the flux history term coefficients (-).

2.2.2 Steady State Conduction Models

Multi-dimensional and in particular two-dimensional steady state conduction models have been used to study and investigate the accuracy of the approximate one-dimensional thermal resistance calculation procedures for thermal bridges. Studies made on multi-dimensional steady state heat conduction analysis of composite walls have indicated that the heat fluxes deviate significantly from that of an approximate one-dimensional heat

conduction models that ignore the thermal bridges. This has been demonstrated using numerical and experimental analysis of steady state heat conduction in building wall specimens (Barbour and Goodrow 1995; Brown et al. 1998; Carpenter and Schumacher 2003; Kosny and Christian 1995a; Kosny and Christian 1995c; Kosny et al. 1997a; Kosny et al. 1997b; Thomas and Antar 1998). Compared to dynamic analysis, steady state models for heat transfer of thermal bridges are well developed. The next section briefly discusses ASHRAE's recommended approximate one-dimensional steady heat conduction models.

Approximate Steady State Models

Steady state heat transfer through composite material walls is commonly treated with one-dimensional models that utilize some approximations in representing the thermal resistance of composite walls. ASHRAE recommends the following methods: isothermal plane method, parallel path method, the zone method and modified zone method and insulation/framing adjustment factor method to compute the overall thermal resistance based on qualitative criteria (ASHRAE 2005).

Isothermal Plane Method

This method assumes that for layer materials with high thermal conductivity the temperature at each plane remains isothermal. Composite layers sandwiched in between these two isothermal plane layers are combined using area weighted parallel heat flow path method. Then the overall resistance is determined from layer resistances using a series sum of resistances. This method is recommended for concrete blocks where web

and the core section are combined using area-weighted parallel heat flow path method and then combined in series with the face and air film resistances. For widely distributed metal members with high cross-sectional area constructions such as roof decks the isothermal plane method under-predicts the overall resistance; hence, the zonal method is recommended (ASHRAE 2001).

Parallel Path Method

The parallel heat flow path method assumes no heat flow in the lateral direction; hence, the heat flow path in the construction is principally longitudinal. The resistance is calculated from the area-weighted average of the individual thermal transmittances of the different parallel heat flow paths in the construction. This method predicts the overall-resistance of a construction with reasonable accuracy for wood frame or wood stud walls, where the disparity in thermal conductivity between the wood and the cavity insulation is small. The actual overall thermal resistance lies in between the isothermal plane and the parallel path methods (Barbour and Goodrow 1995; Brown et al. 1998; Gorgolewski 2005; Thomas and Antar 1998). Another method developed as extension of the parallel path method is parallel path correction factor method (ASHRAE 2005). The thermal resistances along the stud and center of wall are area weighted to get the overall average thermal resistance. The parallel path correction factor F_c method is recommended for the metal stud walls.

Modified Zone Method

For building envelopes with widely spaced metal members such as steel stud walls, the actual overall thermal resistance lies in between the isothermal plane and parallel path methods (Barbour and Goodrow 1995; Gorgolewski 2005). The ASHRAE zone method was introduced for calculating overall resistance for such constructions (ASHRAE 2005). The zone method extends the parallel heat flow path method to account the local highly conductive region as a separate path for the heat flow and divides the construction into two zones. The zone method determines the width of zone containing the metal element as function of the distance from the stud face to the surface of the construction. Studies have shown that zone method does not consider the thermal bridge region of influence or the metal zone width dependency on stud spacing, stud depth and sheathing thermal conductivity (Barbour and Goodrow 1995; Kosny and Christian 1995a). The modified zone method was introduced to improve the zone method by including the metal zone area dependency on: ratio of resistivity of cavity insulation to sheathing materials, thickness of sheathing insulation, and stud flange area (Kosny and Christian 1995a).

Insulation / Framing Adjustment Method

Thermal resistance of wall assemblies containing metal framing can be calculated using insulation /framing adjustment factors. Such framing factors are provided by ASHRAE / IESNA standard 90.1-2004 (ASHRAE 2005). The adjustment factor corrects the resistance of the core insulation for the metal frame effect. It is also called correction factor method.

Gorgolewski Method

The Gorgolewski (2007) proposed a semi-empirical correlation for computing the steady state R -value of light frame steel stud walls. This procedure uses weighted average of isothermal plane and parallel path method R -values. The weighting parameter is calculated from semi-empirical correlation that depends on the geometry of the steel frame and the isothermal and parallel path methods R -values and hence is suitable for programming application as it does not involve subjectivity.

The following section discusses development in multidimensional conduction dynamic modeling method and the barriers for their implementation.

2.2.3 Multi-dimensional Conduction Dynamic Models

There have been repeated efforts to develop multidimensional dynamic heat transfer model that produce CTFs in one-dimensional form for energy analysis and load calculation programs. Previously published methods for dynamic modeling of multi-dimensional conduction proposed for use in building energy analysis and load calculation programs include: numerical methods, numerical CTF method, equivalent wall methods and state-space method. The later methods were developed with the intention to use in developing one-dimensional CTF coefficients. However, their adoption has been delayed for several reasons. Nevertheless, there remains a clear need for a simple one-dimensional approximate dynamic model for modeling of construction with thermal bridges. The next section discusses previously published multidimensional conduction dynamic models and their limitations.

Numerical Methods

Numerical models of multi-dimensional conduction heat transfer have been developed, but are still limited to research use (Davies, et al., 1995). Numerical methods include finite difference, finite volume and finite element techniques. The third generation building simulation program, ESP-r, uses the finite control volume energy conservation method (Clarke 2001; Nakhi 1995). ESP-r, a whole building energy simulation program developed at the University of Strathclyde offers multidimensional heat conduction analysis of walls, edges, corners and the ground; however, the multi-dimensional heat conduction model has limitations on the composite layer specification and, at best, is difficult to use. Numerical methods require high computational time since it involves solving the nodal variables at each time step. Therefore, implementation of multi-dimensional heat conduction finite difference or finite element methods for real composite walls requires higher computational time and computer memory. The lack of graphical user interface for automatic building geometry and construction material acquisition has been a hurdle for the development of spatial discretization for use in the multidimensional conduction model.

Burch et al. numerical CTF method

Burch et al. (1992) presented a numerical procedure for calculating CTF coefficients that accounts for thermal bridge effects of metal studs, aluminum frame windows and metal frames on office building envelopes. The method solves the conduction equation numerically using finite difference techniques by applying linearly varying boundary conditions that replicate the triangular ramp temperature boundary conditions as shown in

Figure 2.3. Then the principle of superimposition is used to determine the response factors from the three linear temperature excitations at base time steps of 2δ . The heat flux at a particular surface yields the required response factors. The numerical procedure of determining the response factors for multidimensional conduction models can be summarized as follows (Burch et al. 1992):

- i. Develop the triangular ramp unit excitation (Figure 2.3) representation of the boundary temperature at one of the surfaces of interest while the other face of the surface is kept at zero temperature (Hittle, 1992).
- ii. Determine the numerical solution of the heat flux at the surface interest by summing the individual heat fluxes of the cells or nodes for each excitation. This yields one of the response factors. In a similarly way the other response factors can be determined.
- iii. The CTFs coefficients are determined from the response factors using recursive algorithms (Hittle, 1992).

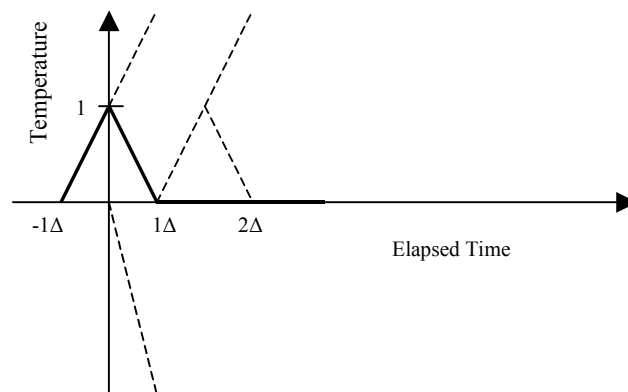


Figure 2.3 Linear-triangular ramp temperature pulse representation

The Burch et al. (1992) finite difference procedure based CTF coefficients determination method requires a separate standalone transient heat conduction analysis program with a spatial discretization scheme. Thus, the Burch et al. method is difficult to be integrate into existing building energy analysis and load calculation programs without significant modifications of their codes (Burch et al. 1992).

Equivalent Wall Method

Kossecka (1998) and Carpenter et al. (2003a) developed the concept of an equivalent wall, which replicates multi-dimensional thermal dynamics of the complex composite wall with a simple homogeneous layer wall. The generated equivalent wall, which has the same dynamic behavior to that of the real composite wall, is represented by one-dimensional response factors or conduction transfer function that can be implemented in the commonly used building energy analysis and load calculation programs (Kosny and Kossecka 2002). Generating equivalent walls requires proper identification of the thermal mass and negligible mass resistance components from the construction layer configuration. The thermal characterization of constructions can be defined by a parameter called thermal structure factor (Kossecka 1998). The concept of thermal structure factor is presented next.

Thermal Structure Factors

Thermal structure factors, which are dimensionless parameters, define the thermal energy storage characteristic of building structures when it goes through two successive steady state ambient temperature transitions (Kossecka 1998; Kossecka and Kosny 2002).

Thermal structure factors of a wall depend on the resistance and thermal capacities of the layers and their sequence of arrangements in the wall. Thermal structure factors (φ) of building structures (Carpenter et al. 2003a; Kossecka 1998; Kossecka and Kosny 2002) are given by:

$$\varphi_{ii} = \frac{1}{C} \int_0^L \rho c_p (1 - \theta)^2 dx \quad (2.9)$$

$$\varphi_{ie} = \frac{1}{C} \int_0^L \rho c_p \theta (1 - \theta) dx \quad (2.10)$$

$$\varphi_{ee} = \frac{1}{C} \int_0^L \rho c_p \theta^2 dx \quad (2.11)$$

Besides, the following identity needs to be met by the thermal structure factors

$$\varphi_{ii} + 2\varphi_{ie} + \varphi_{ee} = 1 \quad (2.12)$$

Where

C Overall thermal capacity of the wall, (J/m² K)

c_p specific heat of a layer in the wall, (J/kg K)

ρ density of a layer in the wall, (kg/m³)

L thickness of the wall, (m)

θ dimensionless temperature, (-)

φ_{ii} Interior structure factor (-)

φ_{ie} core structure factor (-)

φ_{ee} exterior structure factor (-)

A high interior thermal structure factor (φ_{ii}) implies that the higher thermal mass layer is located near the interior surface and most of the resistance is located near the exterior surface of the wall. Vice versa, a high exterior thermal structure factor (φ_{ee}) indicates that the higher thermal mass layer is located near the exterior surface and most of the resistance is located near the interior surface of the wall. And a high core thermal structure factor (φ_{ie}) implies that the higher thermal mass layers are located at the center of the wall and the resistances are placed symmetrically on both sides of the wall. The relationships between response factors and thermal structure factors (Carpenter et al. 2003a; Kossecka 1998; Kossecka and Kosny 2002) are given:

$$\delta \sum_{n=1}^{\infty} n X_n = -C \varphi_{ii} \quad (2.13)$$

$$\delta \sum_{n=1}^{\infty} n Y_n = C \varphi_{ie} \quad (2.14)$$

$$\delta \sum_{n=1}^{\infty} n Z_n = -C \varphi_{ee} \quad (2.15)$$

Where

X_n : the n^{th} term exterior self-coupling response factor, (W/m² K)

Y_n : the n^{th} term cross coupling response factor, (W/m² K)

Z_n : the n^{th} term interior self-coupling response factor, (W/m² K)

C Overall thermal capacity of the wall, (J/m² K)

φ_{ii}	Interior structural factor (-)
φ_{ie}	core structural factor (-)
φ_{ee}	exterior structural factor (-)
δ	time step, (s)

Equivalent wall Generation Procedure

The equivalent wall generation requires five steps (Carpenter et al. 2003a). These steps are summarized as follows:

- (1) Develop a three-dimensional model of the building envelope to exact dimensions using multi-dimensional dimensional heat conduction solver computer programs.
- (2) Generate three-dimensional response factors using numerical methods and use them to determine the three dimensional conduction transfer function;
- (3) Calculate the thermal structure factors of the composite wall using the three dimensional response factors determined in step 2 and the thermal structure factor identity;
- (4) Generate the fictitious equivalent wall. The equivalent wall generation requires selecting random set of resistances for each layers of the wall and calculating the capacitance or randomly specifying the capacitance and calculating the resistances. A three layer fictitious wall is recommended for simplicity (Carpenter et al. 2003a). The material layer configuration, i.e., the relative position of the high thermal mass and the high resistance layers in the fictitious wall layers configuration must resemble that of the actual wall.

- (5) The transfer function coefficients for the three-dimensional numerical model and the equivalent wall model matching is done by trial-and-error until reasonable accuracy is achieved by adjusting the resistance and/or capacitance of the equivalent wall layers. The steady state resistance, thermal response factors and structure factors of the real wall and the fictitious equivalent wall must be the same.

State Space Method

The state space method can be used to determine conduction transfer function coefficients that can represent multidimensional transient heat conduction in walls. The state space method is based on first order differential equation representation of transient heat conduction by spatially discretizing the conduction domain and representing the inputs by continuous, piecewise linear functions (Seem 1987). The advantage of the state space method compared to the Laplace transform method (Hittle, 1992) is that it can be extended to solve multidimensional transient heat conduction problems. The state space method is represented in the form of equations as follows:

$$\left[\frac{dT_i}{dt} \right] = [A][T_i] + [B][T_b] \quad (2.16)$$

$$[q] = [C][T] + [D][T_b] \quad (2.17)$$

Where

T_i vector of n interior node temperatures as state variables, °C (°F)

- A a constant coefficient transition matrix with size of $n \times n$
 t the time, (s)
 B the constant coefficient matrix of input vector of size $(n \times p)$
 T_b vector of p boundary temperatures as inputs, °C(°F)
 q vector of p heat fluxes as outputs, $W/m^2 \cdot K$ ($Btu/h \cdot ft^2 \cdot ^\circ F$)
 C a constant coefficient matrix of the output vectors of size $(m \times n)$
 D constant coefficients matrix of the input vector of size $(m \times p)$

Solution of equations 2.16 and 2.17 for constant elements matrix of A and B in a compact representation is given by:

$$q_t = \sum_{j=0}^{j=n} (S_j T_{t-j\delta}) - \sum_{j=1}^{j=n} F_j q_{t-j\delta} \quad (2.18)$$

Where

- S_j are the conduction transfer function coefficients, $(W/m^2 \cdot K)$
 F_j are the coefficients of the past heat flux history terms, (-)

Two-dimensional state space method

Seem (1987) demonstrated that the state space method can be applied to model multi-dimensional transient heat conduction in building envelopes. In the state space method, the heat conduction domain is discretized in multi-dimensions; hence, the multi-dimensional heat conduction effects in composite walls such as those with steel studs can

be modeled accurately. Therefore, the state space method can model dynamics of walls; however, as the conduction domain becomes complex, the number of nodes required for accurate modeling also increases. Consequently, evaluation of the exponential matrix becomes cumbersome or sometimes almost impossible (Amjad et al. 2003).

Barrier to Use of Dynamic Multi-dimensional Models

Three multidimensional dynamic thermal bridge models, which could be integrated into existing one-dimensional conduction transfer function procedures, have been proposed. The multidimensional dynamic CTF models are: the equivalent wall method, the state space method, and the numerical CTF method. Beyond other reasons, implementation and integration of these models into the existing programs has been delayed due to inherent limitations in the development of the multi-dimensional dynamic procedures, and high computational resource requirement. These barriers to implementation in whole building load calculation / energy simulation programs include:

- The equivalent wall and the Burch et al., numerical CTF models require either separate standalone multidimensional transient heat conduction analysis numerical programs or integration of a significant multi-dimensional conduction subprogram.
- Models with spatial discretization requirements need both an implementation of the discretization procedure and user interface to support this level of details. Given the complexity of providing an interface to specify a whole building, this may be too much of a refinement.

- The equivalent wall method thermo-physical properties determined by trial-and-error could be out of range for typical building materials properties.
- Although the state space method does not require a separate standalone numerical program, a spatial discretization tool is necessary. On the other hand, the state space method can be integrated with existing building energy analysis and load calculation programs most conveniently if an automatic building envelope discretization and/or interactive user interface for material specification and construction model reduction program is made available. However, the multi-dimensional state space method will suffer from a numerical accuracy problem that grows as the number of nodes increases.

CHAPTER III

3. Radiant Time Series Method Improvements

This chapter covers several improvements to the Radiant Time Series Method (RTSM). These improvements include: new algorithm for generating Radiant Time Factors (RTF) and developing a one-dimensional finite volume numerical method periodic response factor generating procedure, adapting an improved fenestration model and establishing radiative / convective splits, developing a procedure for accounting heat losses through fenestration to the outside, and facilitating implementation of the RTSM procedure in different computation environments.

There are several approaches for generating the RTF for a given building zone. Since these procedures have been adopted directly or indirectly from a full-blown heat balance method (HBM) procedure, they tend to have some unnecessary overhead and a simpler method developed specifically for RTF generation is highly desirable. Derivation of the reduced HBM RTF engine is described in Section 3.1. The new radiant time factors (RTF) generating algorithm utilizes periodic response factors (PRF) to model transient conduction as described in Section 3.1.1. Currently available PRF generation procedures convert conduction transfer function coefficients generated using Laplace and State Space method.

This procedure is undesirable for use in VBA and SCILAB type computational environments. Therefore, a one-dimensional finite volume numerical procedure for computing periodic response factors has been implemented and investigated. The finite volume numerical procedure implementation is discussed in Section 3.1.2. Derivation of the algorithm and validations are given in APPENDIX-B.

As part of this research, an improved fenestration model compatible with currently available fenestration data will be adapted to the RTSM. Furthermore, a new set of radiative / convective splits compatible with the improved fenestration model has been established. The improvement in the RTSM fenestration model is described in Section 3.2.

The previously published RTSM cooling load procedure² (Rees et al. 2000a; Spitler et al. 1997) does not account for the solar and internal radiant heat gains conducted back out of the zone. Ignoring these back losses is the principal reason that the RTSM over predicts the peak-cooling load. An approximate algorithm that accounts for zone radiant loss in the RTSM procedure has been derived and is described in Section 3.3.

For all improvements described in this section, results and discussed are provided for each Sections. However, for improvement to the fenestration model and the heat losses accounting procedure, it is highly desirable to demonstrate satisfactory performance over a wider range of cases. Such a study is the subject of Chapter 4.

² Referred to as the “original RTSM procedure” in this thesis.

3.1 New RTF Calculation Engine

The Radiant Time Series Method (RTSM) converts the radiant component of the heat gains into cooling loads using the Radiant Time Factors (RTF), a 24-term series. The 24 hourly radiant time factors describe the dynamic response characteristics of a zone. Two procedures were developed for RTF generation (Spitler et al. 1997). Currently there are five approaches available for generating the radiant time factors: (1) software that comes with the book Cooling and Heating Load Calculation Principles (Pedersen et al. 1998), (2) software that comes with the book by McQuiston et al. (2005), (3) software developed as based on the ASHRAE toolkit (Iu 2001), (4) tabulated RTF values in the ASHRAE Handbook of Fundamentals, and (5) RTF generated from zone heat gain weighting factors. The first four approaches use the full heat balance method as a calculation engine to compute the RTFs. The HBM programs that come with the books by Pedersen et al. and McQuiston et al. are limited to twelve surfaces only for any zone and the RTF generating software developed by Iu is limited to six surfaces. The McQuiston et al. and Pedersen, et al. programs are full load calculation programs that treat the RTF as an auxiliary output. The McQuiston et al. and Iu programs have interfaces that allow users to select material layer thermo-physical properties from a database. The interface used by McQuiston et al. accepts much more information than is actually necessary to generate the RTF. The tabulated values in the Handbook of Fundamentals were generated for limited building design conditions using Pedersen et al. program. But the accuracy of the RTSM peak cooling load resulting from the users choosing the “nearest” zone has not been investigated.

An alternative approach (Spitler and Fisher 1999b) is to generate radiant time factors directly from a set of zone heat gain weighting factors using the existing ASHRAE 472-RP database (Sowell 1988a; Sowell 1988b; Sowell 1988c). These weighting factors were developed for use with the Transfer Function Method (TFM). This approach would use a computer program to map a given zone to the fourteen zone parameters in the database and transform the weighting factors to radiant time factors using matrix manipulation. However, the 472-RP weighting factors do not represent all possible zone designs and construction types. ASHRAE's 472-RP weighting factors were generated for combination of discrete building design parameters; hence, the RTF generated from these weighting factors represent only specific buildings. User judgment is required to match an existing building to one of the combinations of discrete building design parameters.

In conclusion, the existing approaches all suffer from being too cumbersome, requiring too much user judgment, or too limited with regard to the number of zones surfaces. Therefore, development of an RTF coefficient-generating tool that handles a wide range of practical design conditions is desirable. Such a tool should meet the following requirements:

- i. capable of generating RTF for a wide variety of practical building constructions, including a practical number of building surfaces, i.e. more than twelve.
- ii. simple user interface that does not require unnecessary information.
- iii. can be integrated with other applications such as spreadsheets by eliminating unnecessary features and source code. It would be preferable to

minimize the required calculations and eliminate the use of DLLs if possible.

- iv. The methodology should take advantage of the steady periodic nature of the boundary condition. When this is done, the methodology can benefit from matrix algebra easily accessed in modern computing languages and environments such as SCILAB or MATLAB.

The new RTF calculation engine is derived from an inside surface heat balance and room air heat balance for adiabatic zone. The simplified procedure eliminates several steps of the HBM, particularly the exterior surface heat balance and eliminates input data that are not necessary for the RTF generation. The new RTF generating program is first developed as a FORTRAN DLL which may be called from a spreadsheet. Then, it will be implemented in VBA and SCILAB. The following section describes the derivation of the mathematical algorithm for the RTF generation program.

3.1.1 The Mathematical Model -Reduced Heat Balance Method

The formulation of the mathematical model for the radiant time factor generating procedure makes use of the major assumptions used in the Heat Balance Method (HBM) (Pedersen et al. 1997); that surfaces (walls, roofs, windows, etc) can be treated as having uniform surface temperatures, uniform long wave and short wave length radiation; surfaces are gray; one-dimensional conduction is valid and surfaces are exposed to steady periodic boundary conditions. The simplified heat balance procedure for RTF generation uses an inside surface heat balance, steady periodic boundary condition, constant

convection coefficients and constant room air temperature. The simplified HB procedure for RTF generation eliminates the following procedures that are part of the full heat balance method: outside surface heat balance, weather data, solar radiation calculations, shading calculations, infiltration and ventilation. Because this simplified version of the HBM uses a smaller number of heat balance steps, it will be referred to here as the “Reduced Heat Balance Method” (RHBM). In the next section, the RHBM is described step-by-step.

The inside surface heat balance for the i^{th} surface is given by:

$$\dot{q}_{conv,i}'' + \dot{q}_{cond,i}'' + \dot{q}_{rad,i}'' + \dot{q}_{gain,i}'' = 0 \quad (3.1)$$

Where,

$\dot{q}_{conv,i}''$ = convection heat flux from the room air to the i^{th} surface, Btu/h·ft²
(W/m²)

$\dot{q}_{cond,i}''$ = the i^{th} surface conduction heat flux from the outside surface to the inside surface, Btu/h·ft² (W/m²)

$\dot{q}_{rad,i}''$ = radiant heat flux from other internal surfaces to the i^{th} surface, Btu/h·ft²
(W/m²)

$\dot{q}_{gain,i}''$ = radiant heat gain flux of the i^{th} surface from lights, people and equipments, Btu/h·ft² (W/m²)

Conduction Model

The RTSM uses air-to-air periodic response factors to compute conduction heat gain driven by steady periodic exterior sol-air temperature and a constant indoor air temperature. For RTF generation, surface-to-surface periodic response factors are used with steady periodic surface temperatures computed with the reduced heat balance method. The transient conduction heat flux at the inside surface using surface periodic response factors (Spitler et al. 1997) for steady periodic boundary conditions is given by:

$$\dot{q}_{cond,i,t}'' = \sum_{j=0}^{23} Y_{Pj} T_{Out,i,t-j\delta} - \sum_{j=0}^{23} Z_{Pj} T_{In,i,t-j\delta} \quad (3.2)$$

Where,

$T_{In,i,t-j\delta}$ = inside surface temperature j^{th} hours before the current hour, °F (°C)

$T_{Out,i,t-j\delta}$ = outside surface temperature j^{th} hours before the current hour, °F (°C)

Y_{Pj} = surface-to-surface cross periodic response factor, Btu/h·ft²·°F (W/m²·°C)

Z_{Pj} = surface-to-surface inside periodic response factor, Btu/h·ft²·°F (W/m²·°C)

The transient heat conduction equation can be simplified further using the appropriate boundary conditions.

Boundary Conditions

For all surfaces in a zone, the outside surface temperature is assigned the inside surface temperature to maintain the equivalent temperature as the boundary condition. This approach emulates an adiabatic boundary condition by forcing an equal amount of heat flow from the other side of the surface, hence balancing the heat flow into the construction. This condition is represented as follows:

$$\dot{q}_{cond,i,t}'' = \sum_{j=0}^{23} (Y_{Pj} - Z_{Pj}) T_{In,i,t-j\delta} \quad (3.3)$$

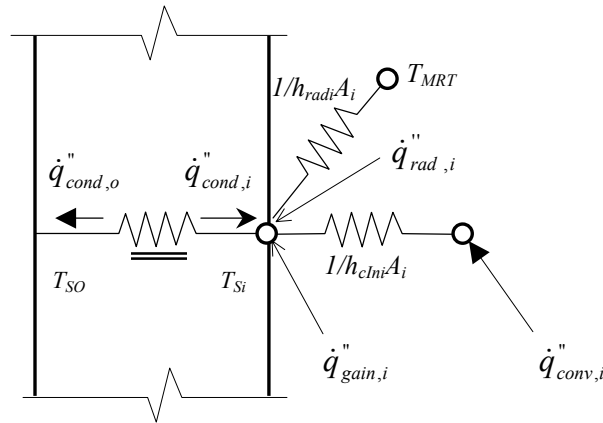


Figure 3.1 Adiabatic boundary condition for RTF generation: $T_{so}=T_{si}$.

Convection Model

The RTSM procedure is formulated to use fixed convection coefficients. This assumption is not required in the Heat Balance Method. Heat transferred from the room air to the zone surfaces by convection using a constant convection coefficient is given by:

$$\dot{q}_{conv,i,t}'' = h_{cIn,i} (T_r - T_{In,i,t}) \quad (3.4)$$

Where,

$T_{In,i,t}$ = inside temperature of the i^{th} surface at time t , °F (°C)

T_r = constant room air temperature, °F (°C)

$h_{cIn,i}$ = convection coefficient of the i^{th} inside surface, Btu/h·ft²·°F (W/m² °C)

$\dot{q}_{conv,i,t}''$ = convection heat flux at the i^{th} surface at time t , Btu/h·ft² (W/m²)

Internal Longwave Radiation Model

The internal long wave radiation model assumes zone air is transparent to long wave radiation and considers the zone surfaces as gray and the long wavelength radiation as diffuse. With these assumptions, long wavelength radiation in building can be modeled using the uniform radiosity method, the total gray exchange factors method (Hottel and Sarofim 1967), the mean radiant temperature and balance (MRT/balance) method (Walton 1980) or the Mean Radiant Temperature Network (MRTNet) method (Carroll 1980).

The uniform radiosity and the total gray exchange factor method require exact view factors. The uniform radiosity method involves solving the radiosity at every time step hence the method is computationally intensive, which makes it unsuitable for building applications. The total gray exchange factor method combines the surface properties and geometries into the gray exchange factors, which can be computed at the beginning of the

simulation and eliminates the simultaneous solution at every time step. However, it requires exact view factors. In real buildings, calculation of exact view factors is computationally intensive and the furnishings and other internal heat sources cannot be easily represented and are mobile during the lifetime of the buildings. Hence, any gains in accuracy facilitated using the exact view factors are unlikely to be realized in practice. Therefore, the extra effort introduced in specifying locations and dimensions of furnishings is unlikely to be rewarded with any tangible benefit.

The advantage of the MRT/ balance and MRTNet methods is that both use approximate view factors based on area and emissivity and allow an approximate representation of furnishings and partitions surfaces. In the MRT/balance method each surface exchanges radiation with a fictitious mean radiant temperature calculated from area-emissivity-surface temperature product weighted of the remaining surfaces viewed by the surface. The radiation flux imbalance resulting from approximate view factors in the MRT/balance method is balanced by redistributing it to the surfaces.

In the MRTNet method each surface exchanges radiation with a single fictitious mean radiant temperature of the zone that is computed from all surfaces. The radiation coefficient linking the each surface is corrected for each surface depending on the surface and MRT temperature of the zone and hence balances the zone radiation exchange. Both MRT methods essentially have the same accuracy (Liesen and Pedersen, 1997). Therefore, due to simplicity, the mean radiant temperature network (MRTNet) method (Carroll 1980) has been selected for use in the RTF generation algorithm. With the

MRTNet method, each surface in the zone is linked to a fictitious single radiant node.

The radiation heat transfer from the fictitious node to the surface is given by:

$$\dot{q}_{rad,i,t} = h_{rad,i,t}(T_{MRT,t} - T_{In,i,t}) \quad (3.5)$$

Where

$T_{MRT,t}$ = mean radiant temperature of the zone at time t , °F (°C)

$h_{rad,i,t}$ = radiation coefficient of the i^{th} surface at time t , Btu/h·ft²·°F (W/m²·°C)

The MRT radiation model (Carroll 1980) requires a two step update of the radiation coefficients for each time step. First, initialize the radiation coefficients for each surface to the reference temperature as follows:

$$h_{rad,ref} = \frac{4\sigma\bar{T}_{ref}^3}{1/F_i + (1 - \varepsilon_i)/\varepsilon_i} \quad (3.6)$$

Where

\bar{T}_{ref} = mean reference temperature in absolute scale, °R (°K)

$h_{rad,ref}$ = radiation coefficient at reference temperature of 300K, Btu/h·ft²·°F
(W/m²·°C)

F_i = the MRTNet view factor for i^{th} surface, (-).

ε_i = the longwave emissivity of i^{th} inside surface, (-).

The MRTNet view factor is an approximate view factor that compensates for the self-weighting in the mean radiant temperature, T_{MRT} , is given by:

$$F_i = 1 / (1 - A_i F_i / \sum_{i=1}^N A_i F_i) \quad (3.7)$$

Where

N = the number of surfaces in the zone

Since the F_i appears on both sides of the equation, iteration is required after setting the initial values of F_i to unity (Carroll 1980). However, the MRT network view factors can be calculated at the beginning of the simulation during the initialization phase.

The hourly radiation coefficient that links each surface to the single fictitious mean radiant temperature in Celsius and Fahrenheit scales, respectively, is updated at each time step as follows:

$$h'_{rad,i,t} = (0.865 + T_{In,i,t} / 200) h_{rad,ref} \quad (3.8a)$$

$$h'_{rad,i,t} = (0.775 + T_{In,i,t} / 360) h_{rad,ref} \quad (3.8b)$$

Then the mean radiant temperature, T_{MRT} , is calculated from weighted average of the product of surface temperatures, surface area and the updated radiation coefficient as follows:

$$T'_{MRT,t} = \frac{\sum_{i=1}^N A_i h_{rad,i,t} T_{In,i,t}}{\sum_{i=1}^N A_i h'_{rad,i,t}} \quad (3.9)$$

Again the radiation coefficients are adjusted using the updated mean radiant temperature in Celsius and Fahrenheit scales, respectively, as follows:

$$h_{rad,i,t} = (0.865 + T'_{MRT,t} / 200) h'_{rad,i,t} \quad (3.10a)$$

$$h_{rad,i,t} = (0.775 + T'_{MRT,t} / 360) h'_{rad,i,t} \quad (3.10b)$$

Then the corrected radiation coefficient of the individual surface is used to compute the room mean radiant temperature ($T_{MRT,t}$) as follows:

$$T_{MRT,t} = \frac{\sum_{i=1}^N A_i h_{rad,i,t} T_{In,i,t}}{\sum_{i=1}^N A_i h_{rad,i,t}} \quad (3.11)$$

So, for each iteration of the heat balance, a fixed two-step iteration to determine the radiation coefficient and the MRT is done as given in Equations 3.7 to 3.11.

Radiant Heat Gain Distribution Model

Computing the precise distribution of long-wave radiation from internal sources requires knowledge of the exact location / position, surface area and temperature of the sources. This approach creates additional complexity to internal radiation exchange models. Therefore, the conventional approach is to distribute the internal radiant heat gains

uniformly to all surfaces in the zone, based on an area weighted or an area-absorptance product weighted distribution model. Similarly, internal short wave radiation heat gain can be reasonably represented by uniform distribution as most of the cases have diffuse sources. For transmitted solar radiation an accurate distribution model could track the sun's position and the resulting sun patch hour-by-hour. However, partial surface irradiation is incompatible with the one-dimensional and uniform surface temperature assumptions used in the conduction and radiation exchange sub-models. Therefore, the most commonly used distribution model is to distribute the transmitted beam solar on the surfaces that are most likely to intercept the solar radiation - the floor and the furnishings. Transmitted diffuse solar heat gain is treated like long wavelength radiant heat gains and distributed uniformly.

The two different distributions are the genesis of the two different RTF series. Long wave length RTF is generated by distributing the heat gain pulse uniformly to all surfaces in the zone. The solar RTF is generated by distributing the heat gain 50% to the floor and 50% to the furniture.

Derivation of the Reduced HBM Algorithm

Substituting the individual heat balance components into the heat balance equation (3.1)

for the i^{th} surface yields:

$$\begin{aligned}
 A_i h_{cIn,i} (T_r - T_{In,i,t}) + A_i \sum_{j=0}^{23} (Y_{Pj} - Z_{Pj}) T_{In,i,t-j\delta} \\
 + A_i h_{rad,i,t} (T_{MRT,t} - T_{In,i,t}) + A_i \dot{q}_{gain,i,t} = 0
 \end{aligned} \tag{3.12}$$

For each surface the heat balance equation 3.12 can be reduced to the form shown below:

$$\begin{aligned}
 A_i(h_{cln,i} + Z_{P0} - Y_{P0} + h_{rad,i,t})T_{ln,i,t} + A_i \sum_{j=1}^{23} (Z_{Pj} - Y_{Pj})T_{ln,i,t-j\delta} \\
 = A_i h_{cln,i} T_r + A_i h_{rad,i,t} T_{MRT,t} + A_i \dot{q}_{gain,i,t}
 \end{aligned}
 \tag{3.13}$$

Solution Schemes

At least two solution schemes for solving Eqn. 3.13 can be developed: *solution scheme I* involves setting up the reduced heat balance equation for all 24 hours for each surface and then marching through each surface until the 24-hourly surface temperatures for all surfaces converge. *Solution scheme II* involves setting up the heat balance equation so as to solve for the inside temperatures of all the surfaces in the zone at every hour, and then march through each hour. These two solution schemes are described in the next two sections.

Solution Scheme I

For a particular surface, the reduced heat balance (equation 3.13) can be written for 24 hours in compact matrix notation:

$$[\Omega][\mathbf{T}_m] = [\Gamma]
 \tag{3.14}$$

The Matrix Ω will have dimensions of 24 by 24 and is given by the following expression:

$$\Omega = \begin{bmatrix} (Z_{f0}-Y_{f0})+h_{rad,i,1}+h_{cIn,i} & (Z_{p23}-Y_{p23}) & (Z_{p22}-Y_{p22}) & \cdots & (Z_{p1}-Y_{p1}) \\ (Z_{p1}-Y_{p1}) & (Z_{f0}-Y_{f0})+h_{rad,i,2}+h_{cIn,i} & (Z_{p23}-Y_{p23}) & \cdots & (Z_{p2}-Y_{p2}) \\ (Z_{p2}-Y_{p2}) & (Z_{p1}-Y_{p1}) & (Z_{f0}-Y_{f0})+h_{rad,i,3}+h_{cIn,i} & \cdots & (Z_{p3}-Y_{p3}) \\ \vdots & \vdots & \vdots & \ddots & \vdots \\ (Z_{p22}-Y_{p22}) & (Z_{p21}-Y_{p21}) & (Z_{p20}-Y_{p20}) & \vdots & (Z_{p23}-Y_{p23}) \\ (Z_{p23}-Y_{p23}) & (Z_{p22}-Y_{p22}) & (Z_{p21}-Y_{p21}) & \cdots & (Z_{f0}-Y_{f0})+h_{rad,i,24}+h_{cIn,i} \end{bmatrix} \quad (3.15)$$

The Matrix Γ is a 24-element column vector and is given by the following expression:

$$\Gamma = \begin{bmatrix} h_{cIn,i}T_r + h_{rad,i,1}T_{MRT,1} + \dot{q}_{gain,i,1}'' \\ h_{cIn,i}T_r + h_{rad,i,2}T_{MRT,2} + \dot{q}_{gain,i,2}'' \\ h_{cIn,i}T_r + h_{rad,i,3}T_{MRT,3} + \dot{q}_{gain,i,3}'' \\ \vdots \\ h_{cIn,i}T_r + h_{rad,i,23}T_{MRT,23} + \dot{q}_{gain,i,23}'' \\ h_{cIn,i}T_r + h_{rad,i,24}T_{MRT,24} + \dot{q}_{gain,i,24}'' \end{bmatrix} \quad (3.16)$$

The inside surface temperatures for a particular surface are determined from Eq. 3.17 as follows:

$$[\mathbf{T}_{in}] = [\Omega]^{-1}[\Gamma] \quad (3.17)$$

In this scheme, the 24 hourly values of surface temperature are solved for each surface sequentially; this is done iteratively until all surface temperatures for all hours are converged.

The radiation coefficients and the Ω matrix elements need to be updated at each iteration step. Thus, the repeated matrix inversion is computationally intensive. Further

simplification of the RTF generation algorithm has been investigated using fixed radiation coefficients. This is presented in Section 3.1.4.

Solution Scheme II

In solution scheme II the surface temperatures are solved for all surfaces at every hour. This solution scheme also can be formulated in matrix notation; however, it is formulated as an iterative procedure. For an hour-by-hour march through all the surfaces at each step, the heat balance equation can be solved iteratively from the following equation:

$$T_{In,i,t} = \frac{h_{cIn,i}T_r + \sum_{j=1}^{23}(Y_{Pj} - Z_{Pj})T_{In,i,t-j\delta} + h_{rad,i,t}T_{MRT,t} + \dot{q}_{gain,i,t}}{(h_{cIn,i} + Z_{P0} - Y_{P0} + h_{rad,i,t})} \quad (3.18)$$

As with solution scheme I the radiation coefficients and the mean radiant temperatures must be updated at each iteration step until the surface temperature converges. The convergence criterion can apply on the surface temperature or the RTFs. The zone radiant time factor is determined from the inside surface temperatures, zone air temperature, convection coefficients and zone surfaces inside areas. The sum of the convection heat transfer from each surface per unit heat gain pulse of the zone is the hourly radiant time factor coefficient and is computed as follows:

$$[r_t] = \frac{1}{\dot{q}_{gain}} [\Delta T_{In}] \cdot [Ah_{cIn}] \quad (3.19)$$

Where

\dot{q}_{gain} = heat gain pulse with which the zone is excited, Btu/hr (W)

$[r_i]$ = a column vector of 24-element radiant time factor coefficients, (-)

$[Ah_{cln}]$ = a row vector of N-elements of the product of inside surface area and convection coefficients, (-)

$[\Delta T_m]$ = a 24 by N matrix of the difference between inside surface temperature and the room air temperature, (K)

The convergence criteria employed is that when the change in the sum of the RTFs changes less than 0.00001 between the successive iteration steps, the solution is considered converged. Solution scheme I is adapted in all subsequent sections and implementations in all other computing environments.

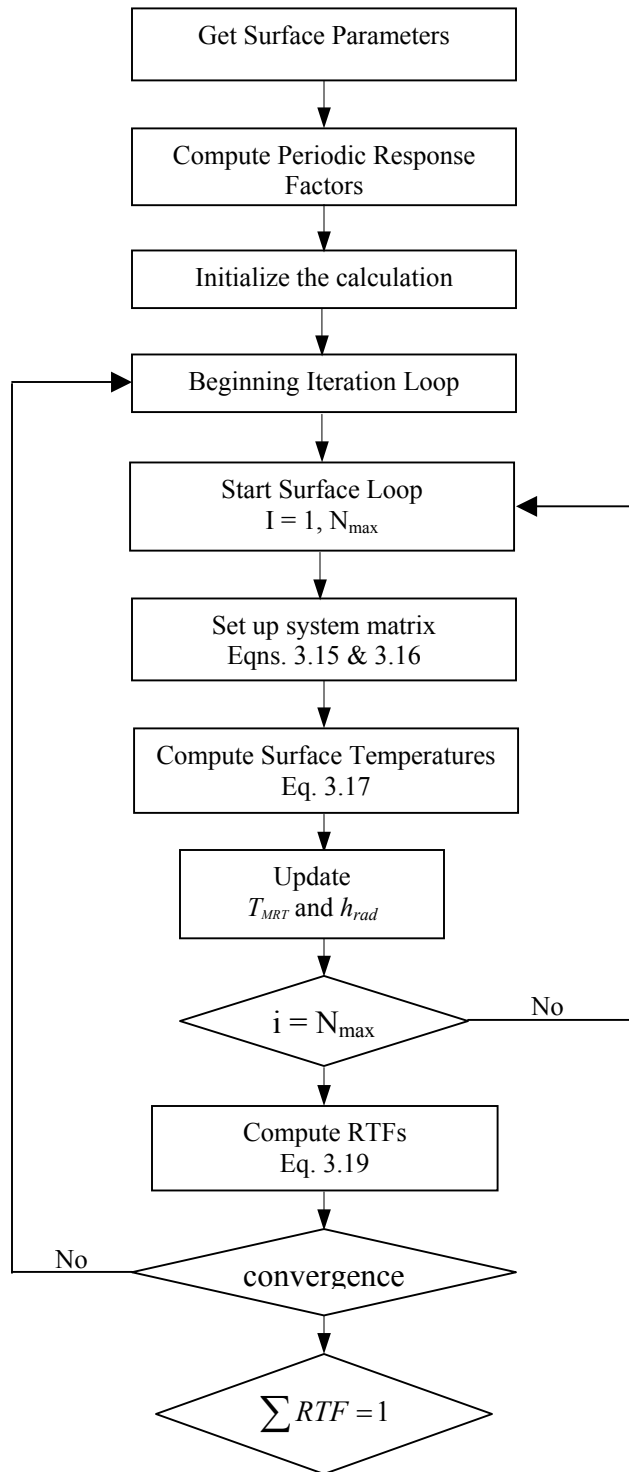


Figure 3.2 Flow chart of solution scheme I

3.1.2 Validation of the New RTF Engine

The new RTF generating engine has been validated against the full-blown heat balance method FORTRAN program originally developed by Pedersen et al. (1997). The test zone geometry and construction fabrics are given in Table 3.1. Three construction types: light, medium and heavy weight constructions were used for the validation. Each zone has a single exterior surface with single pane clear glass and 50% glazing fraction of the exterior facade. Zones were modeled with and without carpeting.

Table 3.1 Description of test zone constructions for RTF generation algorithm validation

Fabric Element	Lightweight	Mediumweight	Heavyweight
External wall	steel siding, 2 in insulation, air space, ¾ in gypsum	4in face brick, 2 in insulation, air space, ¾ in gypsum	4in face brick, air space 2 in. insulation, 8 in HW concrete, ¾ in gypsum
Roof/Ceiling	4 in. LW concrete, ceiling air space, acoustic tile	4 in. HW concrete, ceiling air space, acoustic tile	8 in. HW concrete, ceiling air space, acoustic tile
Partition	¾ in. gyp, air space, ¾.in. gypsum	¾ in. gyp, air space, ¾.in. gypsum	¾ in. gyp, 8 in. HW concrete block, ¾.in. gypsum
Floor	Acoustic tile, ceiling air space, 4 in. LW concrete	Acoustic tile, ceiling air space, 4 in. HW concrete	Acoustic tile, ceiling air space, 8 in. HW concrete
Furnishing	1 in. wood @ 50% of floor area	1 in. wood @ 50% of floor area	1 in. wood @ 50% of floor area
Carpeting	Resistance layer of 2.73 ft ² h °F/Btu	Resistance layer of 2.73 ft ² h °F/Btu	Resistance layer of 2.73 ft ² h °F/Btu

Notes:

1. Surface layers are listed in order from the outside of the room to the inside of the room.
2. The test zone is 15ft x 30ft x 9ft high. The test zone has one exterior wall, 30 ft long.
3. The % glazing is fraction of the exterior facade.
4. Long wavelength absorptance of 0.9 were used for all inside surfaces

The following two heat gain pulse distribution models were used for the RTF generation:

(1) area weighted uniform distribution model for non-solar RTF, and (2) for the solar-RTF generation 50% to the floor and 50% to the thermal mass surfaces. The RTF plots are shown in Figures 3.3 to 3.6. The RTF plots for medium and heavyweight construction zones are shown in Appendix A. Root mean square errors (RMSE) of the

RTF were computed for the 24-hourly values of the New RTF Engine and the HVAC Load Explorer, a full-blown heat balance program, that come with a book by McQuiston et al (2005). The RMSE for three test zone construction types is given in Table 3.2.

Table 3.2 RMSE of the RTF of the New RTF Engine

Zone Construction	Without Carpet		With Carpet	
	Non-solar	Solar	Non-solar	Solar
Heavyweight	0.00013	0.00022	0.00014	0.00027
Mediumweight	0.00008	0.00012	0.00008	0.00015
Lightweight	0.00027	0.00037	0.00007	0.00017

The RMSE is calculated as follows:

$$RMSE = \sqrt{\frac{1}{24} \sum_{j=0}^{23} (RTF_{NewRTF Engine, j} - RTF_{HVAC Load Explorer, j})^2} \quad (3.20)$$

The RMSE of the RTF computed using the New RTF engine are within the convergence limits of the program used to generate the reference RTF. The maximum errors are observed for most of the cases in the first three terms of the RTF as is evident from the plots in Figures 3.3 to 3.6 and Figures 1A to 8A shown in the Appendix A.

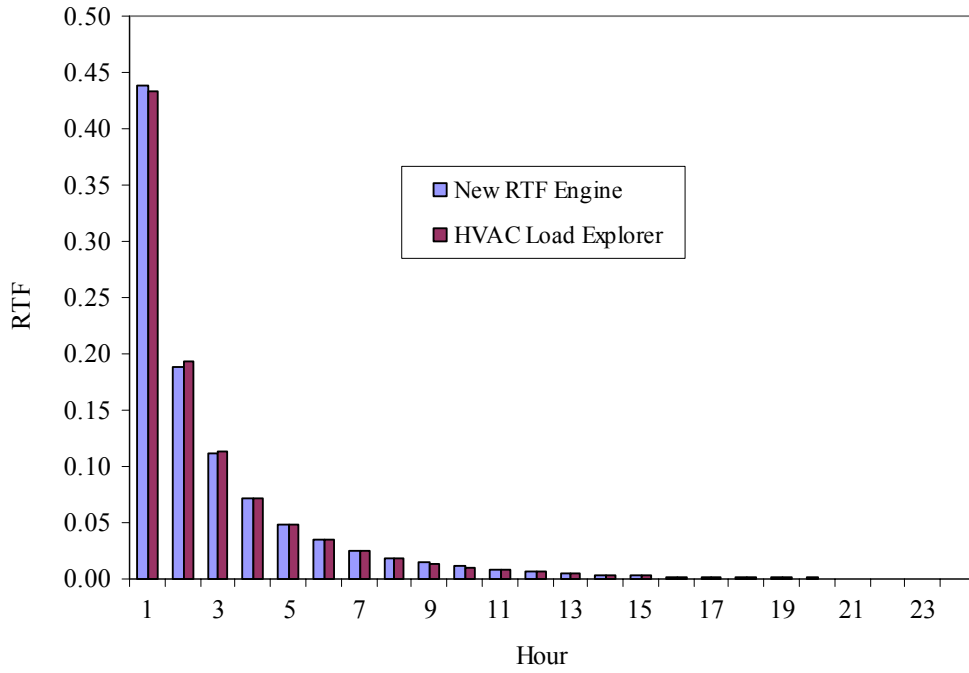


Figure 3.3 Non-solar RTF for lightweight construction zone with no carpet for 50% glazing fraction of the exterior facade

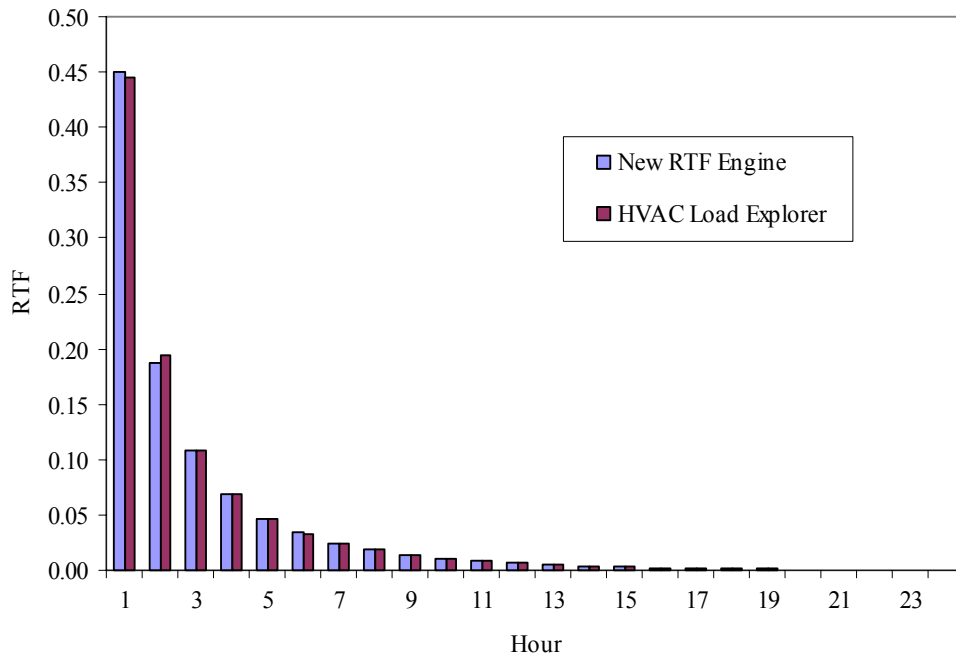


Figure 3.4 Solar RTF for lightweight construction zone with no carpet for 50% glazing fraction of the exterior facade

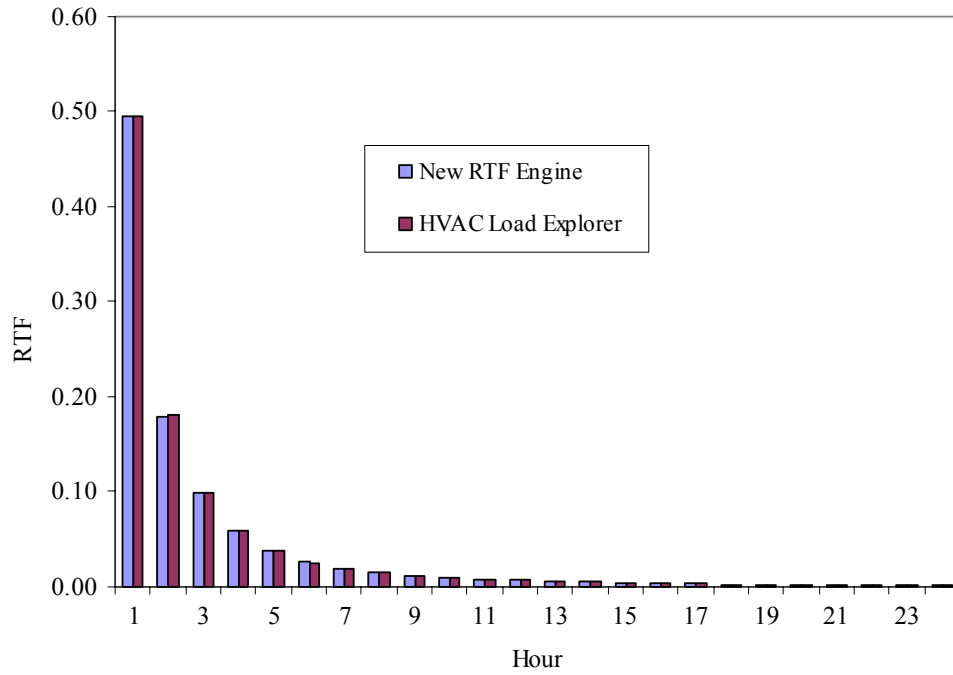


Figure 3.5 Non-solar RTF for lightweight construction zone with carpet for 50% glazing fraction of the exterior facade

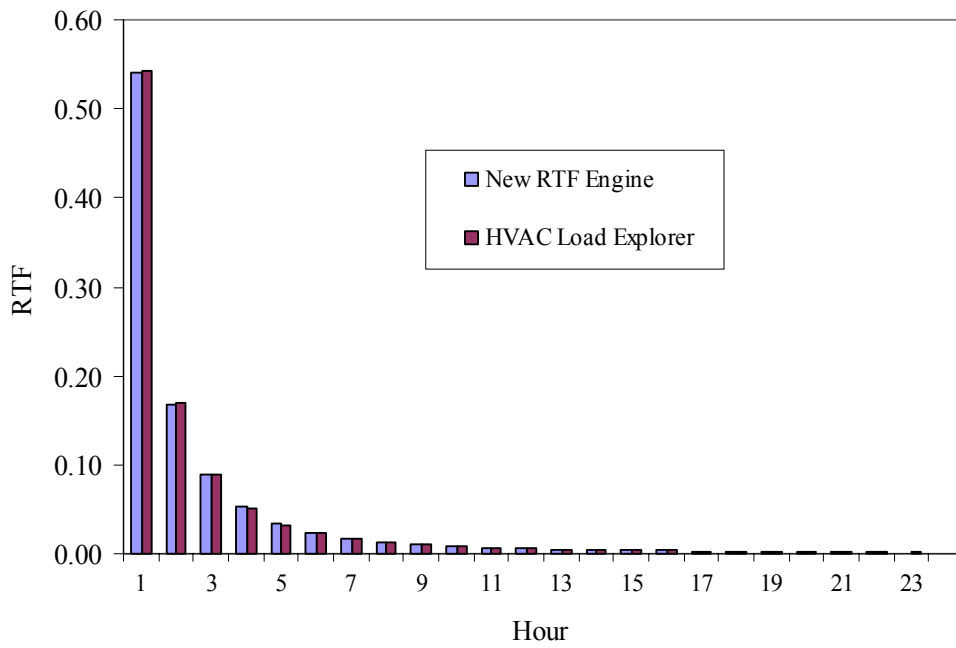


Figure 3.6 Solar RTF for lightweight construction zone with carpet for 50% glazing fraction of the exterior facade

3.1.3 1D Finite Volume Method PRF Generation

Although, Spitler et al. (1997) demonstrated the use of non-periodic response factors to generate PRF, most others implementations have used an existing Laplace or State Space method based CTF generation procedure, then converted the CTF to PRF using the Spitler and Fisher (1999b) procedure. This procedure may be less than ideal for two reasons:

1. Computing CTF then converting to PRF for use in RTSM involves an extra effort.
2. Since the RTSM is intended to be a spreadsheet method, it would be best if the entire procedure could be encapsulated within the spreadsheet. With Microsoft Excel, the VBA programming language allows procedural programming “within” the spreadsheet. Therefore, computation of PRF is possible within the spreadsheet. Laplace and State Space methods for CTF generation might be implemented but significant complexity is a formidable barrier to such an implementation. Consider that the FORTRAN 90 implementations (Iu et al. 2004) of the Laplace and State Space Methods are 1000 and 2000 lines long, respectively.

Therefore, a simpler approach is investigated here, using a 1-D finite volume method fully implicit scheme. For comparison purposes, the implementation investigated here was written in SCILAB and only takes 150 lines. In FORTRAN 90 it takes about 450 lines. A uniform gridding scheme, in each layer, and zero thickness boundary nodes (Patankar 1991) are used, which allows the imposition of realistic boundary conditions.

Moreover, a higher order treatment is used for flux calculation. This method is described fully in Appendix B.

Validation of Periodic Response Factor Generation

The 1D finite volume method (FVM) periodic response factor generation algorithm has been validated against the Spitler and Fisher (1999a) procedure, which is converting CTFs generated using the State Space method. Two types of validations: directly comparing the PRFs generated by these two procedures and by comparing peak heat gains computed for the 82 ASHRAE (ASHRAE, 1997) wall and roof assemblies are done. ASHRAE's Wall10 and Wall37 were used for direct comparison of the PRFs. The 24-hourly PRF terms computed using these two procedures are shown in Figures B.5 and Figure B.6 in the Appendix B. As can be seen, the PRFs are nearly identical. The finite volume procedure produces accurate results; however, it requires smaller time steps compared to the State Space method.

The FVM PRF generation is also validated by computing heat gains for typical design day with sol-air temperature as a boundary condition. ASHRAE's 42 Roofs and 41 Walls (ASHRAE, 1997) are used for the validation. The peak heat gains computed with the FVM periodic response factors were plotted against the peak heat gains computed using the PRF determined by converting the CTFs of the State Space Method. Figure 3.7 compares the results; as expected with nearly identical PRFs, the computed heat gains are also nearly identical. The maximum peak heat gain error is in the range -0.7% to 2.2%

and the average error is -0.03%. The RMSE of the error is 0.02 W/m². As conduction heat gain is typically a small part of the cooling load, this accuracy is sufficient.

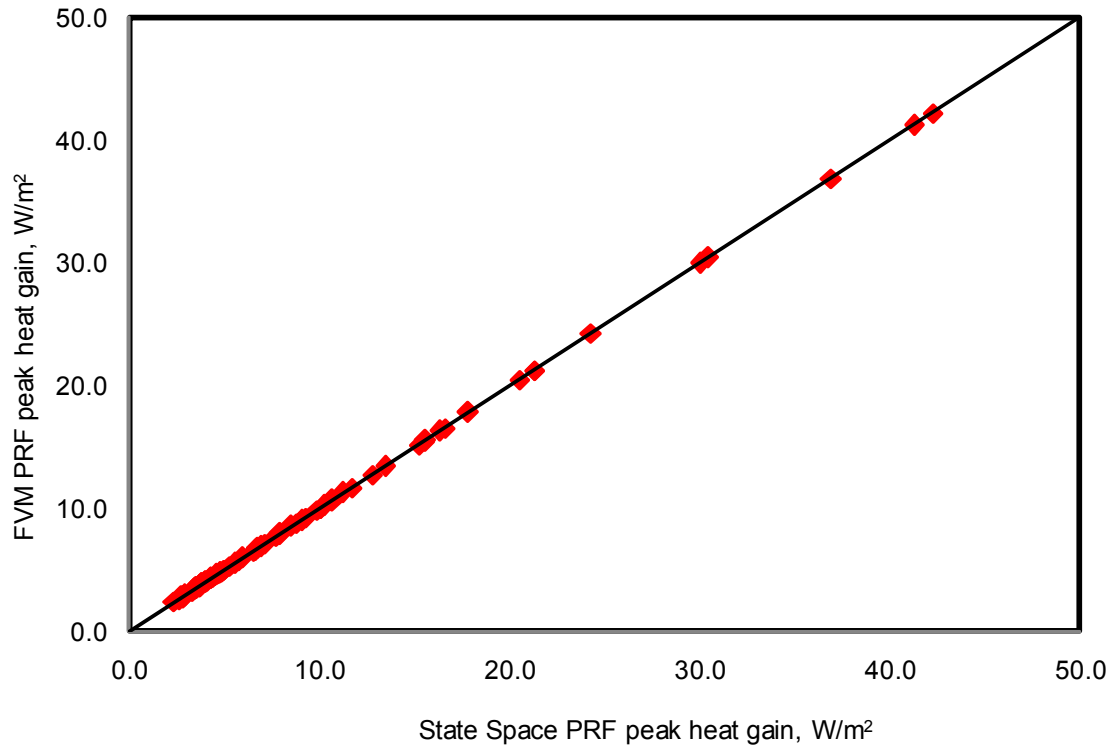


Figure 3.7 Peak heat gains calculated using finite volume method versus the State Space method PRFs

3.1.4 RTF Generation in Spreadsheet or MATLAB Type Environment

With respect to implementation in a spreadsheet environment, the reduced HBM is presented in Section 3.1.1 represents a significant improvement to using the full-blown HBM procedure. To fully facilitate generation of RTF generation in spreadsheet environments and / or MATLAB-like environments, it is advantageous to:

1. Generate surface-to-surface periodic response factors using compact algorithms.
2. Select a solution scheme that makes use of built-in compact matrix formulations.

3. Investigate the use of constant radiation coefficient with the intention of reducing the computational effort.

The RTF generation algorithm has also been implemented in the SCILAB programming environment to take advantage of the built-in compact matrix algebra. The implementation has been demonstrated successfully. The algorithm reads the periodic response factors from a text input file and uses 146 lines of code to generate the RTF. The SCILAB code for the RTF generation is given Appendix B.

The RTF generation implementation in VBA has been validated against a full-blown heat balance method program results using six test zones based on light, medium and heavy construction in Table 3.1 with and without carpets. The RMSE of the RTF generated using the VBA program compared to the full-blown heat balance method program varied in the range from 0.0002 to 0.003. The RTF should sum to one. The RTF generated with the VBA program sum within 0.000001 of one. For the SCILAB case, the RTF sum to within 0.00001 of one. The RMSE of the RTF generated in SCILAB compared to full-blown heat balance method is in the range from 0.0008 to 0.0044. These errors are within the convergence limits of the RTF sum.

The RTF generation algorithm described in Section 3.1.1 requires repeated matrix inversions and/or iterations; hence it is computationally intensive. The RTF generation procedure can be formulated with an approximation using a constant radiation coefficient, calculated with Eq. 3.6 at the reference temperature and never corrected. The

constant radiation coefficient avoids the system matrix update at every iteration and thereby reduces the computational time by about one-half compared to a variable radiation coefficient. Appendix C shows a few cases where this approximation has been compared to more detailed approaches (i.e. with variable radiation coefficient) and it gives nearly identical results. For the three cases, the hourly cooling load error computed in VBA by using constant radiation coefficients was less than $0.02 \text{ Btu/hr}\cdot\text{ft}^2$ or the error was in the range -0.04% to 0.0% of the peak load. Further validation is recommended for this simplification.

3.2 Improved Fenestration Model

The radiant time series method (RTSM) was originally developed for use with shading coefficients and double-strength glass angular properties for computing solar heat gain through fenestration glazing systems. There have been new developments in glazing system data and fenestration models made available since the RTSM was first introduced. Solar heat gain can be computed with solar heat gain coefficients that effectively replace shading coefficients and data published by window manufacturers and ASHRAE are in the form of solar heat gain coefficient (SHGC) rather than shading coefficients. The RTSM cooling load calculation procedure needs to adapt these developments. Therefore, one of the objectives of this thesis is to adapt a fenestration model for the RTSM procedure³ that makes use of the recent developments and new fenestration data.

³ After adapting the fenestration models and the associated radiative/convective splits, the RTSM is referred to as the “current RTSM procedure”.

The improved fenestration model is covered in four sections: development of improved fenestration model, parametric investigation of radiative / convective splits for fenestrations conduction and solar heat gains, application of fenestration model without interior shades, and application of fenestration models with interior shade. Section 3.2.1 deals with development of the improved fenestration models and discusses the challenge of the application of the improved model due to lack of complete window manufacturer's data. Parametric investigation to determine radiative / convective splits for conduction and solar heat gains is discussed in Section 3.2.2. Applications of the improved fenestration model for glazing without and with interior shade are discussed in Sections 3.2.3 and 3.2.4, respectively.

3.2.1 Development of Improved Fenestration Model

The fenestration model used for the RTSM is kept simple as it is intended for a simplified load calculation procedure. The fenestration model proposed for the RTSM uses the solar heat gain coefficient (*SHGC*) and interior attenuation coefficient (*IAC*) (ASHRAE 2001; ASHRAE 2005). The *IAC* accounts for the attenuation of solar heat gain by interior shading device. The *SHGC* is a property of the glazing system that combines the transmittance and the inward flow fraction of the absorbed solar radiation. The RTSM treats the radiant fraction of the absorbed component of solar heat gains using non-solar radiant time factors. The fenestration model requires angle dependent *SHGC*. The *SHGC* combines the transmitted and absorbed components of solar heat gain that needs to be treated separately. Different approaches that require angle dependent *SHGC* and transmittances have been investigated to develop procedures for computing the absorbed

component of solar heat gains. These approaches did not seem to maintain the simplicity required and at the same time required more input data than available. However, window manufacturers usually provide normal solar heat gain coefficient, normal visible transmittance, and U -value of the glazing system. Therefore, a fenestration class procedure that uses normal solar heat gain coefficient and tabulated angular correction method originally developed by Barnaby et al. (2005) has been proposed to overcome the problem of lack of angle dependent SHGC. The fenestration model adopted for the RTSM requires the following input parameters:

1. Normal beam SHGC
2. Diffuse SHGC
3. Angular Correction
4. Interior attenuation coefficient (IAC)
5. Radiative / Convective splits

The radiative / convective split is required to account for the treatment of the absorbed component and its importance is more important for glazing with interior shades as discussed in Section 3.2.2. The solar heat gain through a glazing system without internal shading device (ASHRAE 2005) is given by:

$$\dot{q}_{SHG}'' = E_{ND} \cdot \cos \theta \cdot SHGC(\theta) + (E_d + E_r) \cdot SHGC_d \quad (3.21)$$

where

$$\dot{q}_{SHG}'' = \text{total solar heat gain, Btu/h}\cdot\text{ft}^2 \text{ (W/m}^2\text{)}$$

θ = angle of incidence between the sun's rays and normal to the surface,
radian

E_{ND} = normal direct irradiation, Btu/h·ft² (W/m²)

E_d = diffuse irradiation from the sky, Btu/h·ft² (W/m²)

E_r = diffuse irradiation reflected from the ground or other surfaces, Btu/h·ft²
(W/m²)

$SHGC(\theta)$ = beam solar heat gain coefficient, (-)

$SHGC_d$ = diffuse solar heat gain coefficient, (-)

The solar heat gain for a fenestration system with interior shading devices (ASHRAE 2005) is given by:

$$\dot{q}_{SHG}'' = [E_{DN} \cdot \cos \theta \cdot SHGC(\theta) + (E_d + E_r) \cdot SHGC_d] \cdot IAC \quad (3.22)$$

Where,

IAC = interior attenuation coefficient, (-)

The solar heat gain calculated with Eqns. 3.21 and 3.22 includes transmitted radiation and radiation absorbed by the windows or shades that flows into the space. In the original RTSM cooling load calculation procedure the transmitted components are assumed 100% radiant while the absorbed component is composed of radiative and convective fractions. The original RTSM procedure uses a 63%/37% radiative / convective split for the absorbed component of solar heat gain (Spitler et al. 1997) for fenestration without

interior shades. The challenge for practicing engineers is that window manufacturers usually do not provide all input data required by fenestration models. Determination of radiative / convective splits for conduction and solar heat gains of fenestration is discussed in detail in Section 3.2.2. In the absence of angular dependent SHGC mapping procedures proposed by Barnaby et al. (2005) can be introduced. The proposed mapping procedure is presented next.

Mapping Manufacturer's Windows

Window manufacturers usually provide the solar heat gain coefficients and visible transmittance at normal incident angle and overall U -value of the fenestration system. ASHRAE (2005) provides angle dependent solar heat gain coefficients, transmittance and absorptance of glazing systems but this data set is not linked to specific manufacturer's window. The challenge is how to map between the manufacturer's windows and the tabulated ASHRAE's angle-dependent data.

The proposed mapping procedure is as follows:

- Start with manufacturer's normal solar heat gain coefficient, visible transmittance and U -value.
- Selecting a tabulated set of optical properties of glazing system data for which normal $SHGC$ is nearest to the manufacturer's normal $SHGC$ and visible transmittance based on type of glazing (e.g. clear glass, tinted glass, low-e, reflective coating, number of panes, and thickness of the glass panes).

- Correct the *SHGC* of the tabulated values using the ratio of normal *SHGC* given by the manufacturers to the tabulated normal *SHGC* value. This step provides approximate beam and diffuse *SHGC* for the manufacturer's window.

The mapping procedure can reasonably duplicate the angular dependent solar heat gain coefficient; however, the transmittance and absorptance of a glazing system cannot be mapped explicitly since different combinations of the latter two optical properties can produce the same solar heat gain coefficient. The absorbed component of solar heat gain for several glazing systems has been computed from tabulated optical properties and is shown in Figure 3.8. The absorbed component is a small fraction of the solar heat gain for single and double pane clear glazing systems. But it could be as high as 40% for low-e and coated multiple pane glazing systems. For instance, for the high performance green tinted triple pane glazing system (29c) shown in Figure 3.8, the absorbed fraction is as high as 38% for incident angles up to 40°.

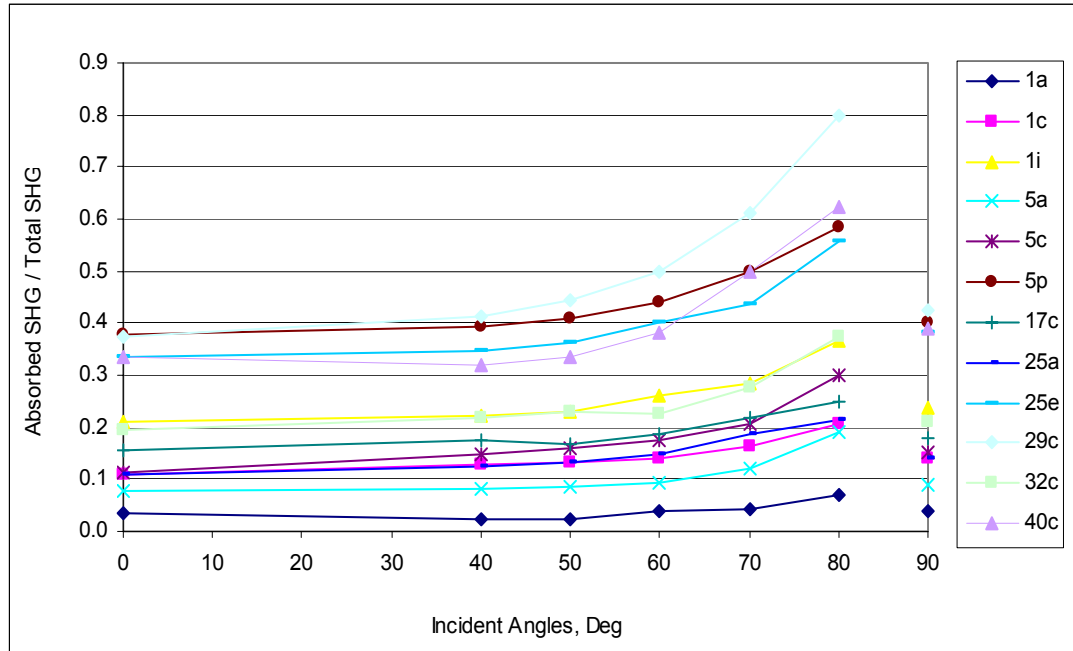


Figure 3.8 Absorbed components as a fraction of total solar heat gain for different fenestration classes

In the presence of interior shades the characteristics of solar heat gain changes both quantitatively and qualitatively. Depending on the transmittance of the interior shades the transmitted fraction can be as low as zero. Therefore, the adapted fenestration model requires a procedure for computing an optimum overall radiative / convective split for different glazing and shade combinations. The next section discusses computation of radiative / convective splits for use in current and improved RTSM cooling load calculation procedure.

3.2.2 Radiative – Convective Splits in RTSM

In the radiant time series method (RTSM) heat gains are first divided into radiative and convective components and the radiant component is converted into cooling load using the 24 term radiant time factors. In the original RTSM, radiative / convective splits of

63%/37% is used for conduction heat gain through fenestrations, walls, floors and absorbed component of fenestration solar heat gain. The introduction of an improved fenestration model that uses Solar Heat Gain Coefficient (*SHGC*) and Interior Attenuation Coefficients (*IAC*) requires a new set of radiative / convective splits. This section discusses the parametric investigation and the rationale in determining the radiative / convective splits for conduction and solar heat gain in the RTSM procedure. This analysis is intended to determine a fixed radiative / convective split for the different heat gains that represent a wide range of practical building design conditions.

Determination of Radiative / Convective Splits

In the RTSM cooling load calculation procedure, as long as the sol-air temperature remains above the room air temperature, the space experiences net heat gain by conduction. This is not necessarily true in real buildings. In the heat balance method, conduction heat gain depends on the inside and outside surface heat balance. The radiative fraction of conduction heat gain that finally appears as radiant heat gain depends on the radiant heat exchange with the other surfaces in the zone. For some surfaces in a zone the radiant flux can be negative when the inside surface temperature (T_{sIn}) is less than the corresponding mean radiant temperature (MRT) seen by the surface. The radiative / convective split determined from the fluxes can only be meaningful in the context of RTSM when the fluxes are positive, i.e. heat gain to the space and computed at peak hour.

In the following section the radiative / convective split first investigated for a few zones computation is discussed in the order to help understand the physics. First, surface temperatures are computed in order to show the direction of radiant and convective heat transfer of conduction heat gain through opaque surfaces, then conduction through fenestrations and, finally, solar heat gain of fenestrations are discussed.

Conduction Heat Gains – Internal Surface Temperatures

The relationship between opaque constructions inside surface temperatures (T_{sIn}), the mean radiant temperatures (MRT) and room air temperature were investigated using a heavyweight top floor corner zone with exterior facades on the east and south faces. The exterior facades have 90% glazing fraction single pane glass. Three aspect ratios of 0.5, 1.0 and 2.0 on the north-south axis were used. The 24 hourly values of the inside surface temperatures of south and east facing exterior facades remain below the corresponding MRT, and the room air temperature as shown in Figure 3.9. Figure 3.10 shows T_{sIn} and MRT for a range of glazing fraction and three aspect ratios for a 24°C room air temperature.

In general, for zones with large amount of glazing the exterior opaque constructions' the T_{sIn} are lower than the MRT and above the room air temperature (TR). Therefore, these surfaces experience net radiant flux into the construction and convective flux out of the construction.

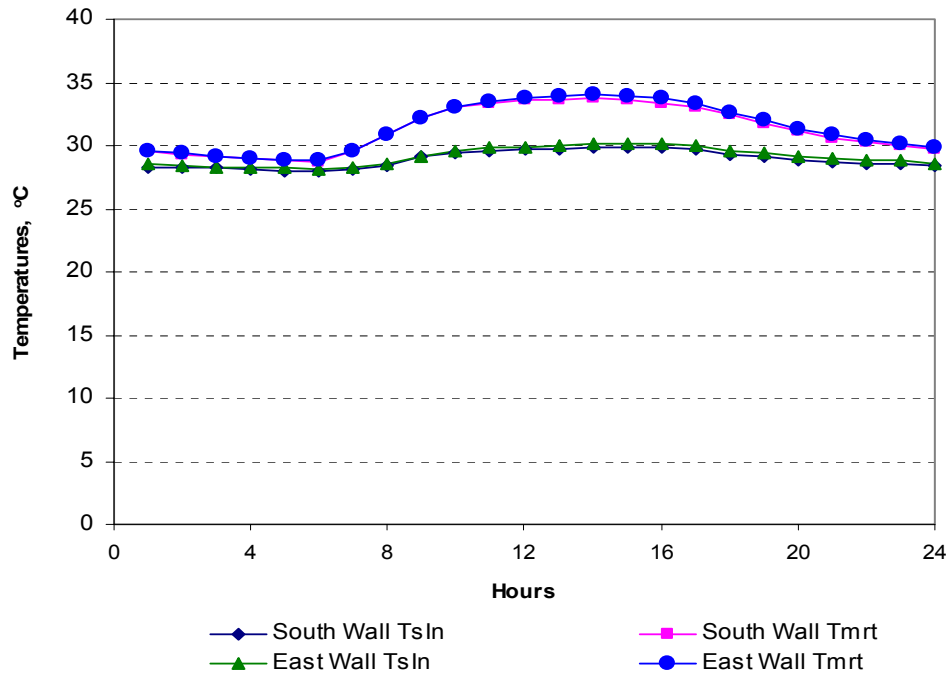


Figure 3.9 $TsIn$ and MRT of heavyweight construction opaque exterior surfaces and 24°C room air temperature

The above analysis would suggest that the radiative fraction should be zero or even negative for cases with high solar or internal heat gains. However, there are cases without high solar or internal heat gains, e.g. warehouses, for which the radiation fraction should have a positive value.

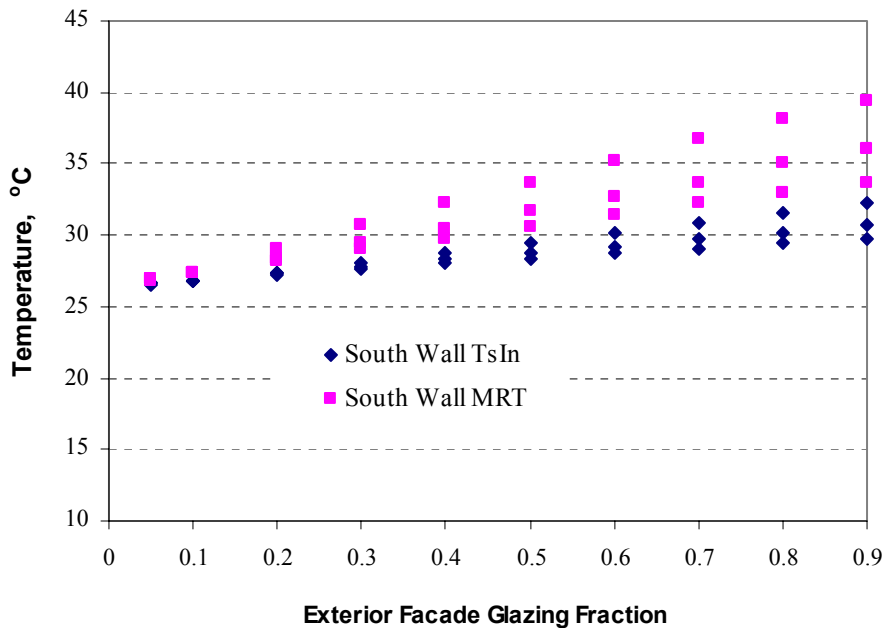


Figure 3.10 T_{sIn} and the corresponding MRT for opaque surface at peak load for three aspect ratios and 24°C room air temperature

Zones with high solar heat gains (zones with large single and double pane clear glass or high solar heat gain coefficient) result in closely similar inside surface temperatures that reduce the net radiant heat exchange with fenestration. Hence the radiant fraction for conduction heat gains in a zone with a large amount of solar and internal radiant heat gains tends to be lower.

This quandary can be resolved by understanding that, for zones with high solar and internal heat gains, the contributions of exterior opaque construction conduction heat gains to the peak cooling load is small. Hence the peak cooling load is not sensitive to radiative / convective splits of conduction heat gains through walls and roofs for these zones, as a small fraction of the total cooling load. Then the question becomes what value of radiative / convective split gives an accurate cooling load over a wide range of

zone types? This question will be addressed using a large set parametric study. The approach taken below is to determine radiative / convective splits for conduction heat gains through opaque surfaces and fenestration based on a parametric study, adjusting the radiative / convective splits to give a good overall match to the HBM. It will be preferable, if possible, to use the same radiative / convective splits for both opaque and transparent surfaces. The following section discusses the interior surface temperature of fenestrations.

Fenestrations Conduction Heat Gain – Internal surface Temperature

As for conduction heat gain, interior surface temperatures are important in determining direction of radiation and convective heat transfer and magnitude of radiative / convective splits. Like the last section, conduction heat gains were investigated for a top floor corner zone with two exterior facades facing south and east direction for July design weather condition of Phoenix, Arizona has been selected for this investigation. The 24 hourly temperatures profile are shown in Figures 3.11 for 90% glazed cases. For this particular zone the fenestration inside surface temperatures remain above the MRT and the room air temperature over the entire day and in particular at the peak cooling load hour. It is evident from these temperature profiles that conduction heat gain through fenestration comprises positive radiative and convective components.

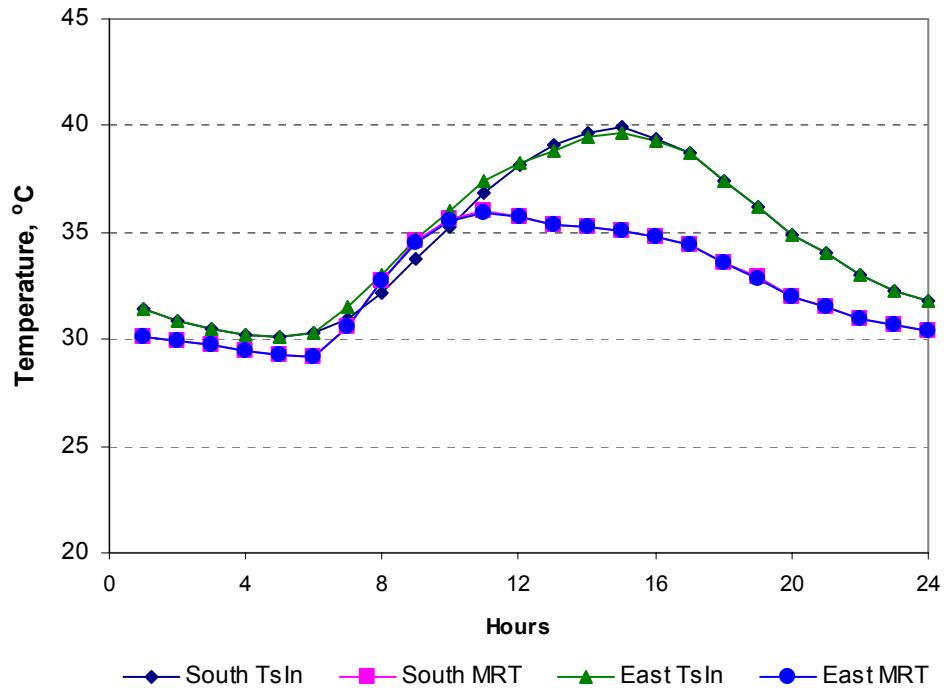


Figure 3.11 $TsIn$ and the corresponding MRT for single pane clear glass fenestration and 24°C room air temperature

The peak hour's temperatures for the three aspect ratios are plotted against glazing fraction in Figure 3.12. For all cases the inside surface temperature ($TsIn$) remain above the corresponding MRT up to 70% glazing fraction. A reverse trend is observed when the glazing fraction exceeds 70% at high aspect ratio. A wider scattering of the mean radiant temperature for higher glazing fraction and aspect ratios is also due to increased solar heat gain and a decrease in thermal mass of the zone.

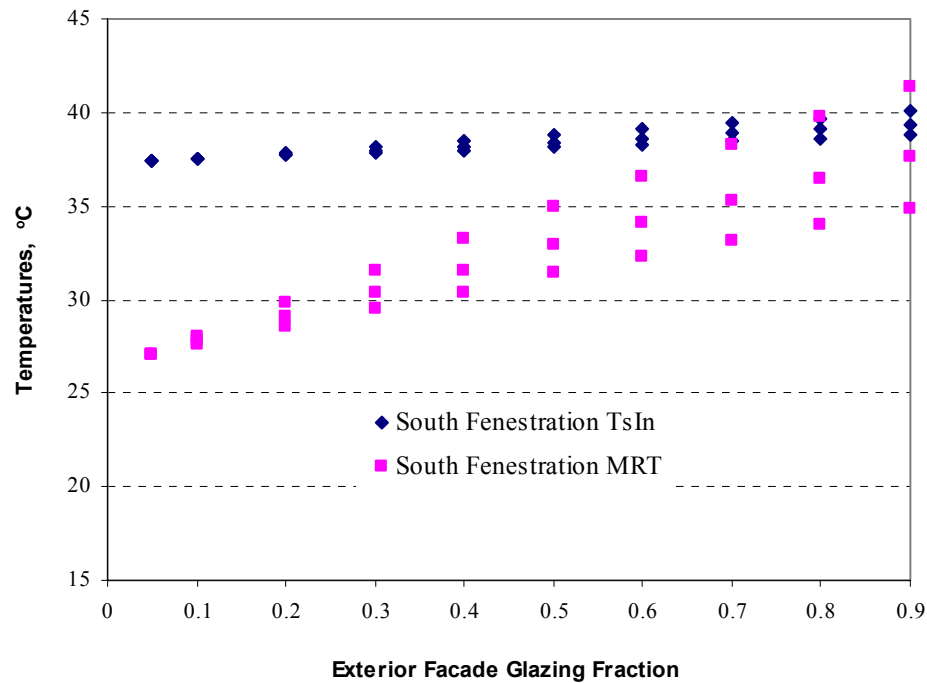


Figure 3.12 $TsIn$ and the corresponding MRT for south facing fenestration at peak load for three aspect ratios and 24°C room air temperature

What is obvious from this plot is that with increasing glazing fraction the difference between the fenestration inside surface and the corresponding MRT it sees is decreasing implying that the net radiative flux decreases while the convective flux increases. This indicates that the radiative fraction decreases when the glazing fraction increases. It is also interesting to observe how the radiative fractions change throughout the day. The hourly radiative fractions of conduction heat gain for a fenestration in a corner zone with south and east facing exterior facades in two different orientations are shown in Figure 3.12. For this zone the peak cooling load occurs at 11AM and the radiative fraction range at the peak hour is 0.08 – 0.11.

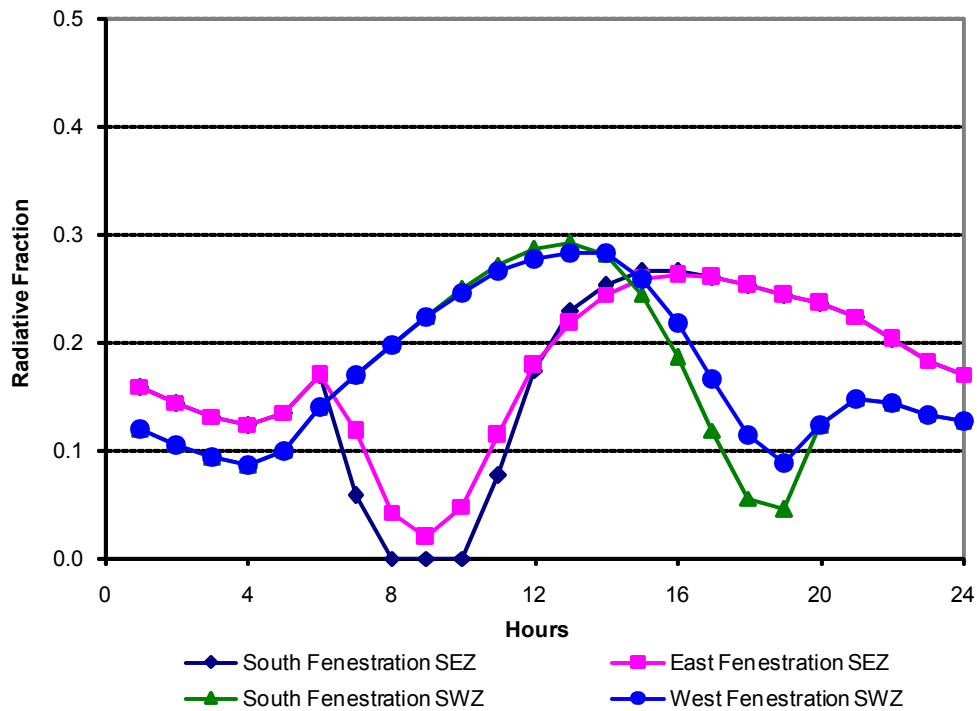


Figure 3.13 Radiative fractions for fenestration in a heavyweight construction zone with two exterior facades single pane clear glass with 90% glazing fraction

For the same building design, a zone with exterior surfaces on the south and west facades with the peak cooling load occurring in the afternoon at 5PM, the radiative fraction lies between 0.12 – 0.17. The radiative fraction varies hourly and is smaller when the temperature differences between the inside surface temperature and its mean radiant temperature is smaller. A similar hourly plot of the radiative fraction for 50% glazing fraction of the exterior facade is shown in Figure 3.14. The radiative fraction for south-east and south-west facing zones were found out to be in the range from 0.33 to 0.34 and from 0.31 to 0.34, respectively. The increase in the radiant fraction with decrease in glazing fraction is directly related to amount of solar heat gain and zone construction fabric.

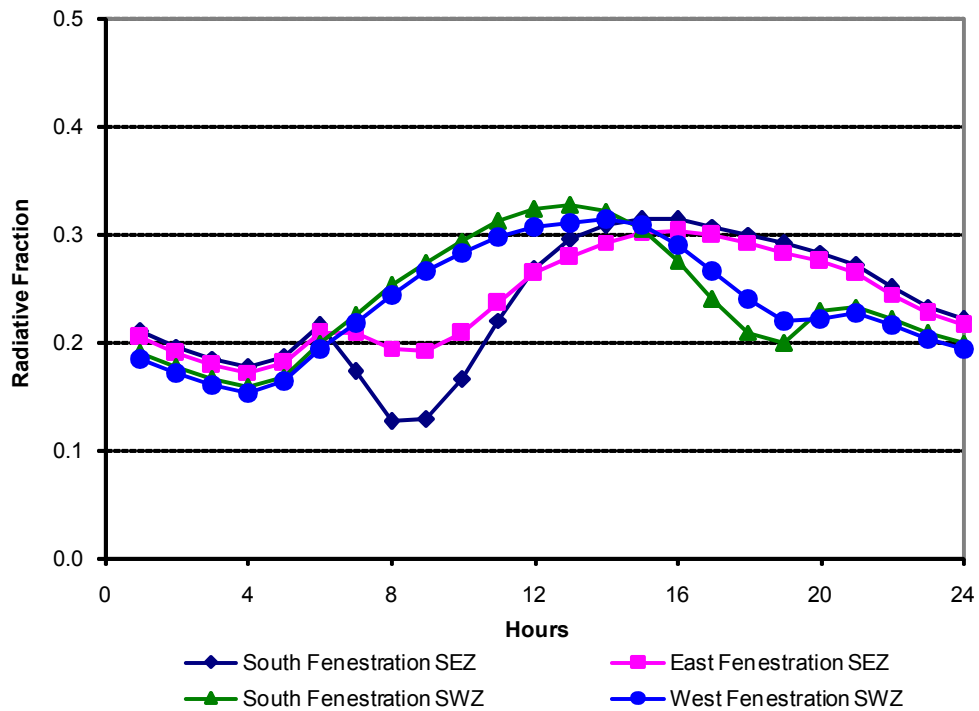


Figure 3.14 Radiative fractions for fenestration in a heavyweight construction zone with two exterior facades single pane clear glass with 50% glazing fraction

The radiative fractions vary very little with change in zone orientation. Glazing fractions change the thermal mass of the zone and hence its dynamic response characteristic. It is possible to deduce from the Figures 3.13 and 3.14 that the higher the glazing fraction the lower the radiative fraction. The radiative fractions determined for a heavyweight construction zone with two exterior facades, five different glazing types, three aspect ratios and ten glazing fractions for July design weather conditions of Phoenix, Arizona are shown in Figure 3.15.

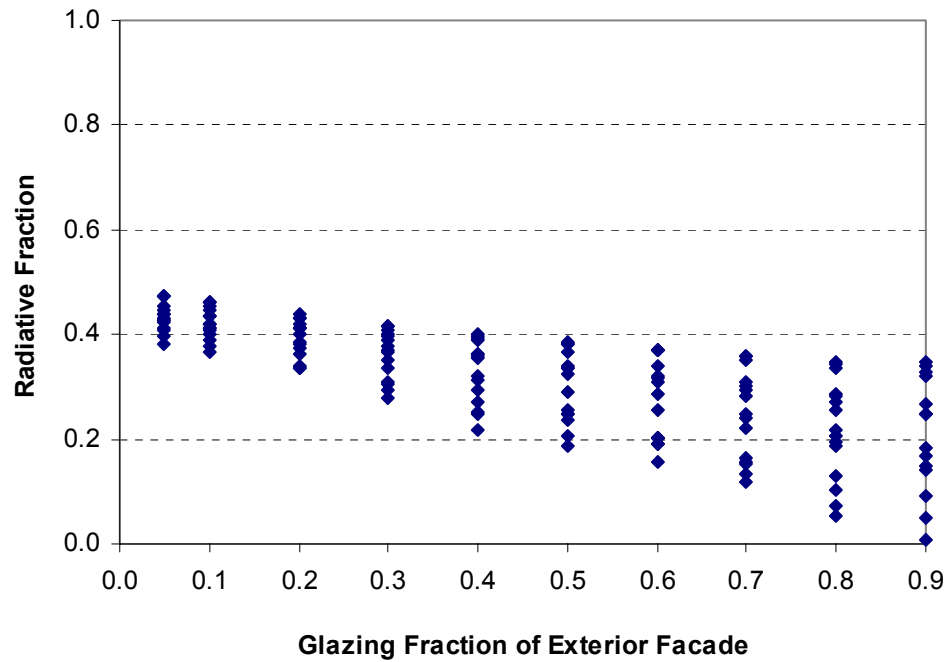


Figure 3.15 Radiative Fraction against glazing fraction of exterior facade for heavyweight zone for five different glazing types at peak cooling load condition

It is evident from this plot that the radiative fraction becomes sensitive to aspect ratio, glazing type and glazing fraction. These three parameters directly or indirectly affect the amount of solar heat gain.

Given that radiative fractions vary between 0.0 and 0.46 for just the above combinations of aspect ratio, glazing type and glazing fraction, it would be difficult or impossible to recommend a single value based on this analysis. Rather, large-scale parametric studies will be used to test possible values.

Solar heat gains Radiative Convective Split

The use of solar heat gain coefficients (SHGC) and interior attenuation coefficients (IAC) to compute fenestration solar heat gain for the RTSM requires introduction of radiant fraction to estimate the convective and radiant components. The introduction of radiant fraction is important to model fenestration with interior shades since the attenuation coefficient accounts only for the reduction of solar heat gain but does not quantify the change in radiative / convective split. Though the solar heat gain radiative / convective split depend on different building design parameters, two types of preliminary investigations were conducted - one for fenestration without interior shade and another for fenestration with shade.

Fenestration without Internal Shade

For most glazing types the transmitted component, which is 100% radiant, is the largest fraction of solar heat gain. The absorbed solar heat gain comprises radiant and convective components. Taken together, the radiant fraction is the larger portion for almost all unshaded glazing types. Since the original and current RTSM cooling load calculation procedures do not account for the radiant heat loss by conduction, the treatment of solar heat gain as 100% radiant doesn't lead to under prediction of the peak cooling load. The effect of this assumption has been investigated parametrically. This assumption is not realistic for fenestration system with internal shades since a substantial portion of solar heat gains can be convective. Detailed radiative / convective split analysis over a wide range of building design conditions were conducted to determine the optimum radiative fraction range and is presented in the following section.

Fenestration with Internal Shade

The fenestration model adopted for the RTSM uses the interior attenuation coefficients (*IAC*) to account for the reduction of solar heat gain by interior shading devices. ASHRAE provides tabulated *IAC* for different combination of glazing system and interior shading devices (ASHRAE 2001; ASHRAE 2005). Interior shading devices have two effects: first, reduction of solar heat gain, which is taken care by using the interior attenuation coefficient; second, increase in the relative proportion of the absorbed component. Therefore, the use of *IAC* accounts for the attenuation effect but not to changes in the relative proportions of transmitted and absorbed components. The absorbed solar heat gain change from short wave to long wave and the long wave radiation exchange with the other surface in zone depends on the inside surface temperatures, long wavelength emissivities and zone geometry.

In this investigation five different glass types were investigated: single pane clear glass, double pane clear glass, two double pane low-e glasses, and double pane reflective coated glass. The investigation included typical internal heat gains and the following building design parameters: glazing types, glazing fractions, interior shades, construction fabrics (light and heavyweight), furnishings thermal mass, aspect ratio, number of external facades and zone orientations were varied. The radiative fractions representing a wide range of building design conditions are shown in Figures 3.16 and 3.17.

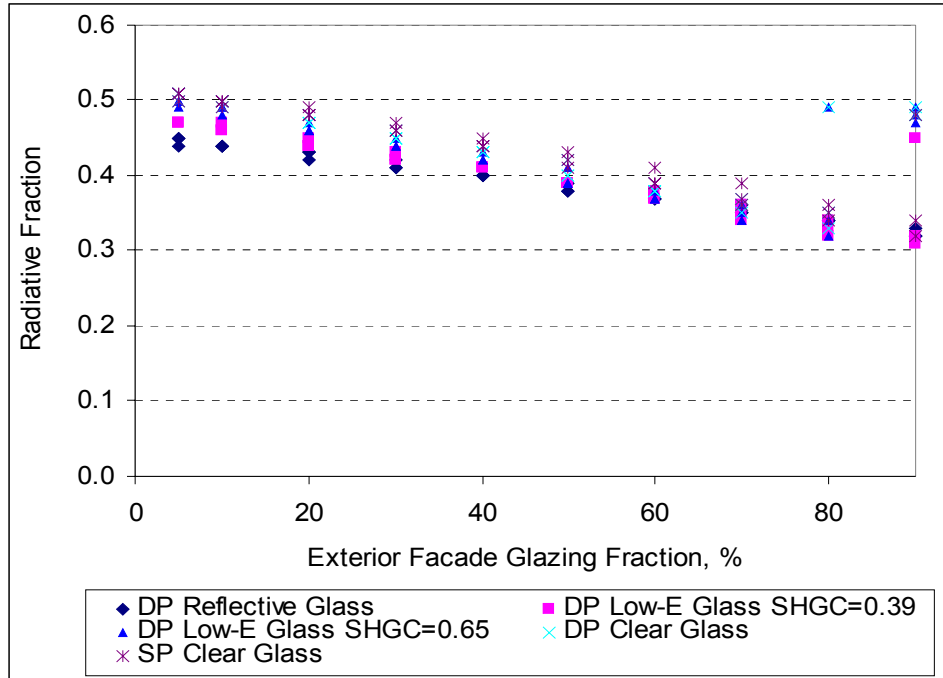


Figure 3.16 Radiative fractions against percent glazing of exterior facade for lightweight zone for five different glazing types at peak cooling load condition

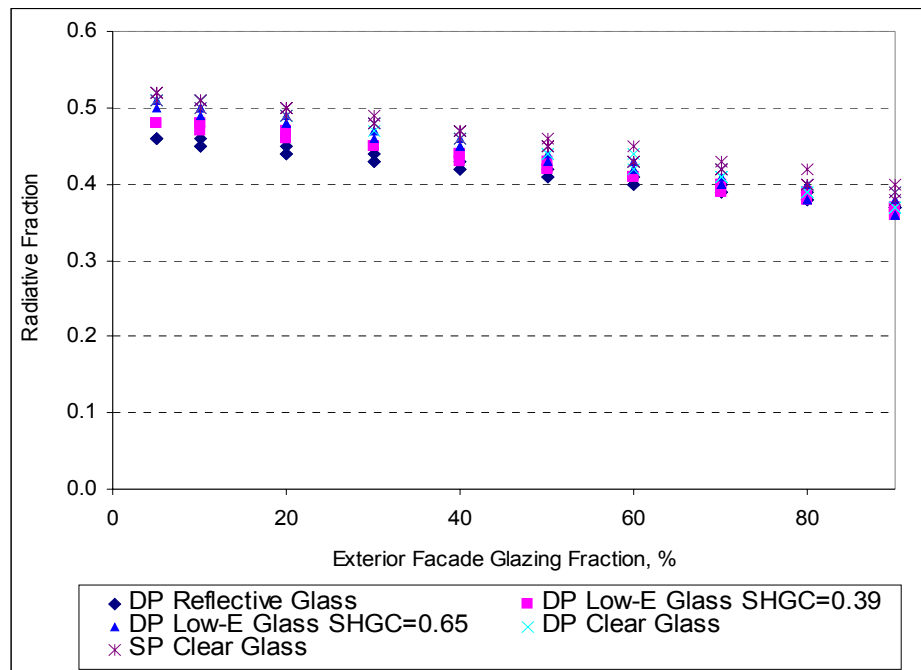


Figure 3.17 Radiative fractions against percent glazing of exterior facade for heavyweight zone for five different glazing types at peak cooling load condition

The radiative fractions at peak cooling load conditions primarily depend on the construction fabric thermal mass, glazing fraction, and shade type and are in the range from 0.30 to 0.53.

Recommended Radiative / Convective Splits for the RTSM

As shown in the above sections, radiative fractions for each heat gain vary widely at peak cooling load condition. They vary even more widely at off-peak conditions. This suggests the insights gained from this study can be used to help guide an iterative approach of choosing candidate values, then testing these values against a wide range of test zones. This testing was done with the parametric analysis tool described in Chapter four.

Using the parametric run tool, candidate radiative / convective splits were tested against the HBM for approximately a half million cases. Recommended radiative / convective splits were chosen in order to give minimal over prediction while avoiding all but the most minor under predictions. In order to meet this objective, two values of the radiative / convective split were utilized for window conduction heat gain and solar heat gain for shaded glazing, depending on SHGC. Furthermore, the radiative / convective splits for “Improved RTSM”, to be introduced in Section 3.3 below, were investigated.

The resulting recommendations for both methods (and those given for the original RTSM) are summarized in Table 3.3.

Table 3.3 Recommended radiative / convective splits for the RTSM procedures

Descriptions	Radiative Fraction Original RTSM	Radiative Fraction Current RTSM	Radiative Fraction Improved RTSM
Conduction			
Walls	0.63	0.46	0.46
Window	0.63	0.33 SHGC > 0.50	0.33 SHGC > 0.50
		0.46 SHGC < 0.50	0.46 SHGC < 0.50
Floor	0.63	0.46	0.46
Roof	0.84	0.60	0.60
Solar heat gain, un shaded glazing			
Transmitted	1.00	1.00	0.90
Absorbed	0.63		
Solar heat gain, shaded glazing			
Transmitted		0.33 SHGC > 0.50	0.33 SHGC > 0.50
Absorbed		0.46 SHGC < 0.50	0.46 SHGC < 0.50

The performance of the RTSM with these recommended radiative / convective splits is fully investigated in Chapter Four. However, the performance of the method is briefly summarized here.

3.2.3 Application of Fenestration Model without Internal Shade

537,600 test zones are created by varying: glazing fraction, glazing type (five glazing types), light and heavyweight construction (exterior Wall, Partition, Roof, and Floor), four top floor corner zones, three aspect ratios (0.5, 1., and 2.), two levels of internal schedules, two levels of thermal mass, and fourteen July 21 design day US weather locations. For cases with single pane glazing the performance of the original and current RTSM in the matching the HBM predicted peak-cooling loads is shown in Figure 3.18. As can be seen, the current RTSM performs about as well or slightly better than the original RTSM. (Here, “performance” is judged against the criterion that the simplified procedure should be minimally over predicts while avoiding under prediction).

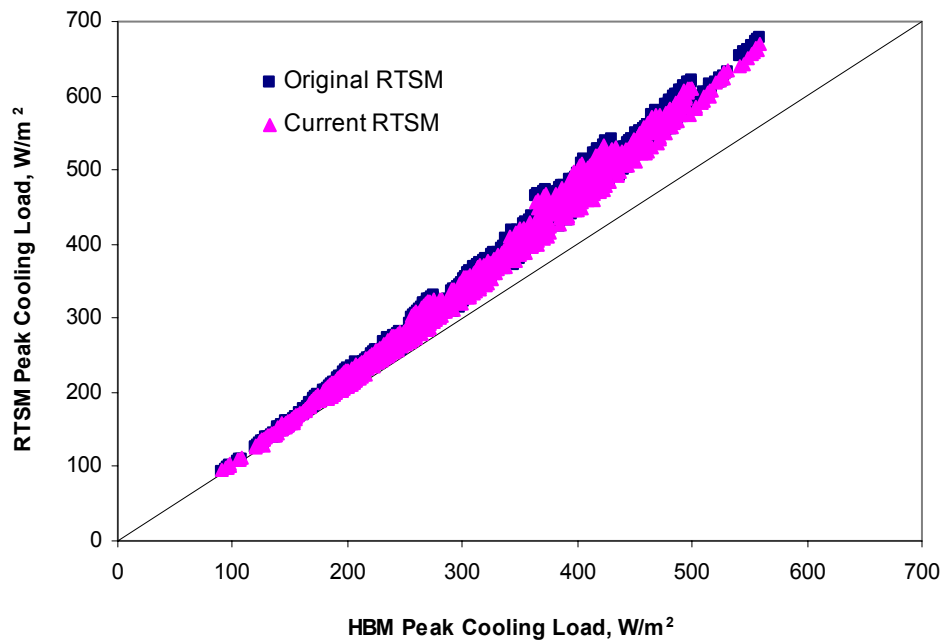


Figure 3.18 RTSM versus the HBM peak cooling loads for single pane clear glass without interior shaded fenestration

3.2.4 Application of Fenestration Model with Internal Shade

A similar analysis, for 403,200 test cases was done by varying: glazing fraction, glazing type (five glazing types), light and heavyweight construction (exterior Wall, Partition, Roof, and Floor), a top floor south west corner zone, three aspect ratios (0.5, 1., and 2.), two levels of internal schedules, two levels of thermal mass, fourteen July 21 design day US weather locations and the three interior shade types. Since the original RTSM did not explicitly address shaded glazing, only results for the current RTSM are shown in Figure 3.19. Performance is even better than that for unshaded glazing. This is due to the reduced solar heat gains making a smaller contribution to the peak cooling load.

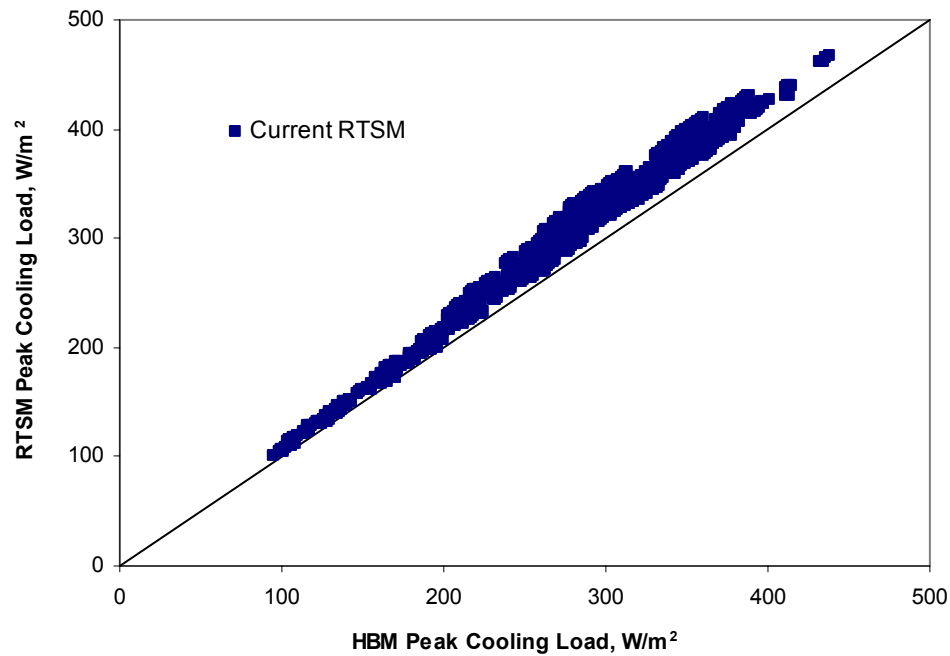


Figure 3.19 Current RTSM versus the HBM peak cooling loads for single pane clear glass with interior shaded fenestration

3.3 Heat Losses in the RTSM Procedure

The failure of the RTSM procedure to account for radiant heat gains conducted back out has been identified (Rees et al. 1998; Rees et al. 2000b); however, the challenge has been to come up with an appropriate physical/conceptual and mathematical model that can account for the loss and be incorporated into the RTSM without unduly complicating the procedure. The conceptual model and the approximations introduced in deriving the mathematical model can be summarized as follows:

- The total solar and radiant heat gains are distributed to the zone inside surfaces including furnishings based on: long wave length radiant and short wave length solar heat gains are assumed to be distributed using area-absorptance product of the inside surface of the space.

- The procedure assumes the fenestration inside surfaces radiate to the room air. This assumption decouples the long wavelength radiation exchange among the surfaces in the zone and allows each surface to be treated separately.
- Uses a fixed combined inside surface conductance. This assumption along with previous approximations allows introducing the concept of inside sol-air temperature concept.
- The surface heat balance ignores the thermal mass of the fenestration; hence, steady state analysis is valid.
- Short-wave retransmission losses are ignored both in the HBM and RTSM. The window is assumed opaque to long wavelength radiation.

These assumptions and approximations along with the conceptual model leads to the formulation of an algorithm that accounts for radiant heat gain instantaneously conducted through fenestrations using a dimensionless loss conductance.

3.3.1 Derivation of the Mathematical Algorithm

The procedure assumes steady state conditions, considering the thermal mass of the fenestration to be negligible, and estimates how much of the radiant (solar and internal heat gains) are conducted back out of the windows. Fenestration conduction heat gain calculations in the original RTSM consider only the effects of the outdoor and indoor air temperatures:

$$\dot{q}_{cond}'' = U(T_o - T_a) \quad (3.23)$$

Solar heat gain coefficients are mainly intended for rating of the fenestration and do not take into account the fenestration interaction with the space heat gains and other inside surfaces. In reality, the fenestration interaction with the space heat gain may lead to net conduction heat gain into the space or conduction back out depending on the amount of space heat gain, outdoor air temperature and fenestration conductance.

What is missing in the original RTSM procedure is a procedure that integrates the effect of space solar and radiant internal heat gains and the outdoor air temperature into the fenestration conduction analysis. Derivation of the adapted fenestration conduction equation that combines these effects along with the assumptions introduced is described next. The following assumptions were introduced to formulate the heat conduction equation that account for the space heat gain loss:

- The total solar and internal radiant heat gains are distributed to the zone inside surfaces including furnishings based on: long wavelength radiant and short wavelength solar heat gains are assumed to be distributed using area-absorptance product of the inside surface of the space.
- Uses combined inside surface conductance.
- The surface heat balance ignores the thermal mass of the fenestration; hence, steady state analysis is valid.
- Short wave retransmission losses are ignored both in the HBM and RTSM. The window is assumed opaque to long wavelength radiation.

The derivation of the radiant heat gain back loss equations is developed based on area-absorptance product radiant heat gains distribution model as a generalized expression. For this approach, long and short wavelength radiant heat gains and inside surface absorptivities would have to be tracked separately. But the expression can be reduced further to much simpler form with area-weighted distribution model. The parametric run results presented in Section 3.3.3 are based on area-weighted distribution models.

Fenestration inside Surface Heat Balance

The thermal network representation of a fenestration with solar and internal heat gain flux absorbed on the inside surface is shown in Figure 3.20.

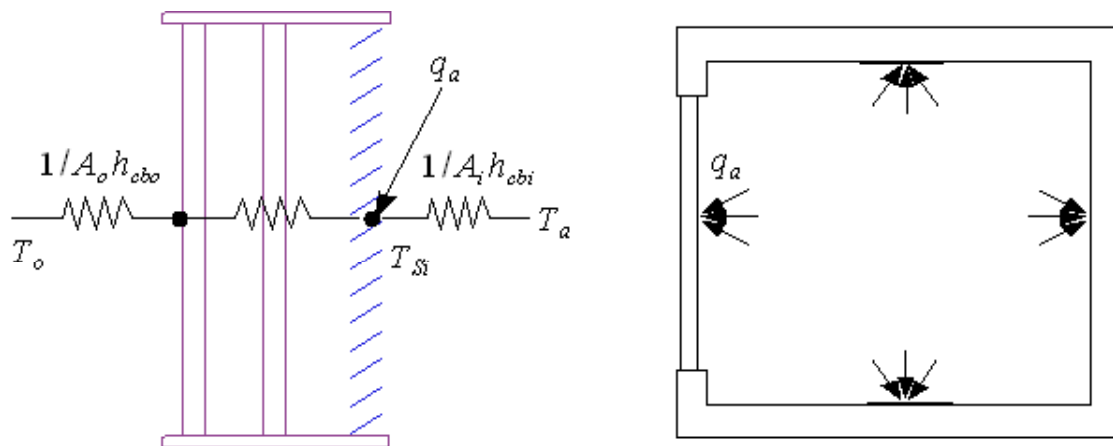


Figure 3.20 Representation of fenestration inside surface heat balance

Using combined inside conductance and a prescribed the space radiant heat gain distribution model, the instantaneous fenestration inside surface heat balance assuming a steady state condition by ignoring the thermal mass is given by:

$$U_{si}(T_o - T_{si}) + h_{cb,i}(T_a - T_{si}) + \dot{q}_a'' = 0 \quad (3.24)$$

Where,

U_{si} = the U value from outdoor air to the inside surface, W/m²·K

T_o = outdoor air temperature, °C

T_a = indoor air temperature, °C

$h_{cb,i}$ = inside surface combined conductance, W/m²·K

T_{si} = the inside surface temperature, °C

\dot{q}_a'' = the space radiant heat gains distributed to the inside surface of the fenestration, W/m²

Solving Eq. 3.24 for the inside surface temperature yields:

$$T_{si} = \frac{U_{si}}{U_{si} + h_{cb,i}} T_o + \frac{h_{cb,i}}{U_{si} + h_{cb,i}} T_a + \frac{\dot{q}_a''}{U_{si} + h_{cb,i}} \quad (3.25)$$

The U_{si} is related to the air-to-air U -value and the inside combined conductance by:

$$\frac{1}{U} = \frac{1}{h_{cb,i}} + \frac{1}{U_{si}} \quad (3.26)$$

Starting from Eqn (3.26), the following simplifications can be derived for the coefficients in Eqn 3.25.

$$\frac{U_{si}}{U_{si} + h_{cb,i}} = \frac{U}{h_{cb,i}} \quad (3.27)$$

$$\frac{h_{cb,i}}{U_{si} + h_{cb,i}} = \frac{U}{U_{si}} \quad (3.28)$$

$$\frac{1}{U_{si} + h_{cb,i}} = \frac{U}{U_{si}h_{cb,i}} \quad (3.29)$$

Substituting Eqs. 3.27, 3.28, and 3.29 into Eq. 3.25 and simplifying yields:

$$T_{si} = \frac{U}{h_{cb,i}}T_o + \frac{U}{U_{si}}T_a + \frac{U}{U_{si}h_{cb,i}}\dot{q}_a'' \quad (3.30)$$

An inside sol-air temperature may be defined as an artificial air temperature that gives the same heat gain/loss as the combined radiation and convection:

$$U(T_o - T_{SAi}) = h_{cb,i}(T_{Si} - T_a) \quad (3.31)$$

Or

$$T_{SAi} = T_o - \frac{h_{cb,i}}{U}(T_{si} - T_a) \quad (3.32)$$

Substituting for the inside surface temperature (Eq. 3.30) into Eq. 3.32 yields:

$$T_{SAi} = T_o - \frac{h_{cb,i}}{U} \left(\frac{U}{h_{cb,i}} T_o + \frac{U}{U_{si}} T_a + \frac{U}{U_{si} h_{cb,i}} \dot{q}_a'' - T_a \right) \quad (3.33)$$

Simplifying yields:

$$T_{SAi} = T_o - T_o - \frac{h_{cb,i}}{U_{si}} T_a - \frac{1}{U_{si}} \dot{q}_a'' + \frac{h_{cb,i}}{U} T_a \quad (3.34)$$

$$T_{SAi} = h_{cb,i} \left(\frac{1}{U} - \frac{1}{U_{si}} \right) T_a - \frac{1}{U_{si}} \dot{q}_a'' \quad (3.35)$$

$$T_{SAi} = h_{cb,i} \left(\frac{1}{h_{cb,i}} \right) T_a - \frac{1}{U_{si}} \dot{q}_a'' \quad (3.36)$$

$$T_{SAi} = T_a - \frac{1}{U_{si}} \dot{q}_a'' \quad (3.37)$$

The conduction heat gain through the i^{th} window (fenestration) that includes the effects of radiant heat gains absorbed on the inside surface is then given by:

$$\dot{q}_{cond}'' = U(T_o - T_{SAi}) \quad (3.38)$$

Substituting for the inside sol-air temperature T_{SAi} and rearranging yields:

$$\dot{q}_{cond}'' = U(T_o - T_a) + \left(\frac{U}{U_{si}} \dot{q}_a'' \right) \quad (3.39)$$

And, rearranging Eqns. 3.26 gives:

$$\frac{U}{U_{si}} = 1 - \frac{U}{h_{cb,i}} \quad (3.40)$$

Substituting Eq. 3.40 into Eq 3.39 allows the elimination of U_{si} .

$$\dot{q}_{cond}'' = U(T_o - T_a) + \left(1 - \frac{U}{h_{cb,i}} \right) \dot{q}_a'' \quad (3.41)$$

$$\dot{q}_{cond}'' = U(T_o - T_a) + \dot{q}_a'' - \frac{U}{h_{cb,i}} \dot{q}_a'' \quad (3.42)$$

The first two terms in Eq. 3.44 represent the conduction heat gain and the radiant heat gain flux absorbed by the inside fenestration surface, respectively. The last term is the amount of space radiant heat gain conducted back out through the fenestration. The amount of space heat gain absorbed by the fenestration depends on the heat gain distribution and surface properties. To simplify the procedure, the heat gain absorbed by the fenestration inside surface needs to be expressed in terms of the space heat gain and prescribed distribution function. Area-absorptance product weighted distribution can be used to approximate the heat absorbed by surfaces. Using this distribution model the space radiant heat gain absorbed by a surface is given by:

$$\dot{q}_a'' = \left(\frac{A_j \alpha_j}{\sum_{j=1}^N A_j \alpha_j} \right) \frac{\dot{q}_{HG}}{A_j} \quad (3.43)$$

Where,

\dot{q}_{HG} = the space solar and internal radiant heat gains, W

N = the number of surfaces of the zone

α_j = the absorptance of the j^{th} surface appropriate to short and long wavelength heat gain type, (-)

Eq. 3.43 may reduce to simple area-fraction provided the inside absorptance of the surfaces in the zone are the same. For a first order approximation of the space radiant heat gain loss the area fraction should be sufficient. Substituting Eq. (3.43) into Eq. (3.42) the expression for conduction heat gain/loss flux that combines the effect of the space radiant heat gain is given by:

$$\dot{q}_{cond,j}'' = U(T_o - T_a) + \left(\frac{A_j \alpha_j}{\sum_{j=1}^N A_j \alpha_j} \right) \frac{\dot{q}_{HG}}{A_j} - \frac{U}{h_{cb,i}} \left(\frac{A_j \alpha_j}{\sum_{j=1}^N A_j \alpha_j} \right) \frac{\dot{q}_{HG}}{A_j} \quad (3.44)$$

$$\dot{q}_{cond,j} = UA_j(T_o - T_a) + \left(\frac{A_j \alpha_j}{\sum_{j=1}^N A_j \alpha_j} \right) \dot{q}_{HG} - \frac{U}{h_{cb,i}} \left(\frac{A_j \alpha_j}{\sum_{j=1}^N A_j \alpha_j} \right) \dot{q}_{HG} \quad (3.45)$$

Further simplification of the overall heat conduction equation that takes into account the space radiant heat gain may lead to four different approaches for implementing in the RTSM cooling load calculation procedure:

- An improved heat conduction equation which would replace the existing equations for fenestration heat gain due to temperature difference between the inside and outside can be developed. Instead of using the inside air temperature, an expression for inside sol-air temperature can be developed and utilized. Although this follows the physics in a way analogous to the exterior sol-air temperature, it seems likely to be confusing to users of the method. (Approach I)
- A dimensionless loss coefficient, u^* , can be developed and applied to all of the radiant heat gains. (Approach II)
- A correction to the first term of the radiant time factor series can be made. (Approach III)
- A modified heat conduction equation that accounts for the heat gain loss can be formulated. (Approach IV).

The derivation for all four approaches utilizes an interior sol-air temperature as described below. However, for the II, III and IV approach, interior sol-air temperature is eliminated.

Approach I

The first approach would be to use the concept of equivalent indoor “sol-air temperature” for window conduction heat gain calculations that includes the space radiant heat gain. The instantaneous conduction heat gain through a fenestration surface can be written as a function of the outside air temperature and the equivalent indoor sol-air temperature as follows:

$$\dot{q}_{cond} = UA(T_o - T_{SAi}) \quad (3.46)$$

$$T_{SAi} = \left(T_a + \frac{1}{h_{cb,i}} \left(\frac{A_j \alpha_j}{\sum_{j=1}^N A_j \alpha_j} \right) \frac{\dot{q}_{HG}}{A_j} \right) \quad (3.47)$$

Where,

$h_{cb,i}$ = fenestration inside surface combined conductance, (W/K·m²)

T_a = room air temperature, (°C)

$T_{SA,i}$ = inside sol-air temperature of the fenestration surface, (°C)

U = the air to air heat transfer coefficient of the fenestration based on combined inside and outside conductance, (W/m²·K)

Alternatively, for the case where all internal absorptivities are approximately equal, the sol-air temperature equation can be collapsed to:

$$T_{SAi} = T_a + \frac{\dot{q}_{HG}}{h_{cb,i} A_{room}} \quad (3.48)$$

Where,

$$A_{room} = \text{the interior surface area of the room, m}^2$$

In other words, the inside sol-air temperature is simply the indoor air temperature plus the sum of all radiant heat gains divided by the product of the inside surface conductance and the room inside surface area. This procedure requires calculating the equivalent “sol-air temperature” for each window surface in the zone.

Approach II

The second approach basically keeps the window conduction heat gain calculation procedure the same as the standard RTSM procedure but corrects the space heat gain.

The corrected space heat gain is given by:

$$\dot{q}_{net\ gain} = \dot{q}_{HG} - u^* \cdot \dot{q}_{HG} \quad (3.49)$$

$$u^* = \left(\sum_{j=1}^M \frac{U}{h_{cb,i}} \left(\frac{A_j \alpha_j}{\sum_{j=1}^N A_j \alpha_j} \right) \right) \quad (3.50)$$

Where,

$$u^* = \text{dimensionless loss conductance of the space, (-)}$$

Alternatively, for the case where all internal absorptivities are approximately equal, Eq.

3.51 can be collapsed to:

$$u^* = \left(\frac{1}{A_{room} h_{cb,i}} \sum_{j=1}^M U_j A_j \right) \quad (3.51)$$

Where,

$\dot{q}_{net,gain}$ = net space radiant heat gain corrected for heat gain conducted back out, W

\dot{q}_{HG} = sum of all radiant heat gain of the space shortwave and long wavelength, W

M = number of windows in the zone

The dimensionless heat loss conductance of the zone applies to the current hour radiant heat gains from all sources. The second term in Eq. 3.49, which is absent in the original RTSM procedure, represents part of the space heat gain instantaneously conducted back out through the j^{th} fenestration surface. u^* is positive, hence the negative sign indicates that the solar heat gain after repeated reflection and absorption is partly conducted back out depending on the fenestration conductance. The total space heat gain conducted back out through fenestration is determined by adding the individual fenestration surfaces contributions as shown in Eq. 3.52.

$$\dot{q}_{Loss} = \left[\sum_{j=1}^M \left(\frac{U}{h_{cb,i}} \right) \left(\frac{A_j \alpha_j}{\sum_{j=1}^N A_j \alpha_j} \right) \right] \cdot \dot{q}_{HG} \quad (3.52)$$

Where,

M = the number of fenestrations in the zone, (-)

The assumptions introduced to derive Eq. 3.51 are in many ways similar to the simplification used in the derivation of the RTSM. It is evident from Eq. 3.51 that the space heat gain that could be conducted back out depends on the amount of solar heat gain into the space, the dimensionless conductance of the space, and the space heat gain distribution. In reality solar and internal radiant heat gain could be conducted back out through opaque exterior constructions; however, the amount is smaller compared to that of the fenestrations; hence, can be ignored.

Approach III

Examining the form of the correction factor in Eq. 3.45 shows that it operates on the current hour of the solar and internal radiant heat gains, as does the first term of the radiant time factor series. The correction factor can be readily integrated to the radiant time factors and the original RTSM calculation procedure is retained. Therefore, approach III can be introduced as a correction to the first term of RTF. The beauty of the third approach is that it can be implemented simply by subtracting the dimensionless heat loss conductance from the first term of the radiant time factors without any change to the

original RTSM procedure. The corrected radiant time factors, solar and non-solar, are given by:

$$\bar{r}_{s,0} = (r_{s,0} - u^*) \quad (3.53)$$

$$\bar{r}_{ns,0} = (r_{ns,0} - u^*) \quad (3.54)$$

Therefore, approach III simply reduces to correcting the instantaneous term (the first term) of the radiant time factors. u^* is a positive dimensionless conductance determined from construction fabrics, area and absorptance of the surfaces. The effect of this approach is then it will correct all radiant heat gains that are operated by radiant time factors. Therefore, approach III automatically accounts for the conduction loss from the radiant fraction of conduction heat gains through the fenestrations, which cannot be done without extra effort in approaches II and I.

Approach IV

The conduction heat gain through fenestrations that accounts for the effect of the space radiant heat gain can be formulated using the Eq 3.48 for sol-air temperature and Eq. 3.46 and is given by:

$$\dot{q}_{cond} = UA \left(T_o - T_a - \frac{\dot{q}_{HG}}{h_{cb,i} A_{room}} \right) \quad (3.55)$$

Implementation Procedure

Implementation of the improved RTSM procedure is shown in a form of flow chart in Figure 3.21.

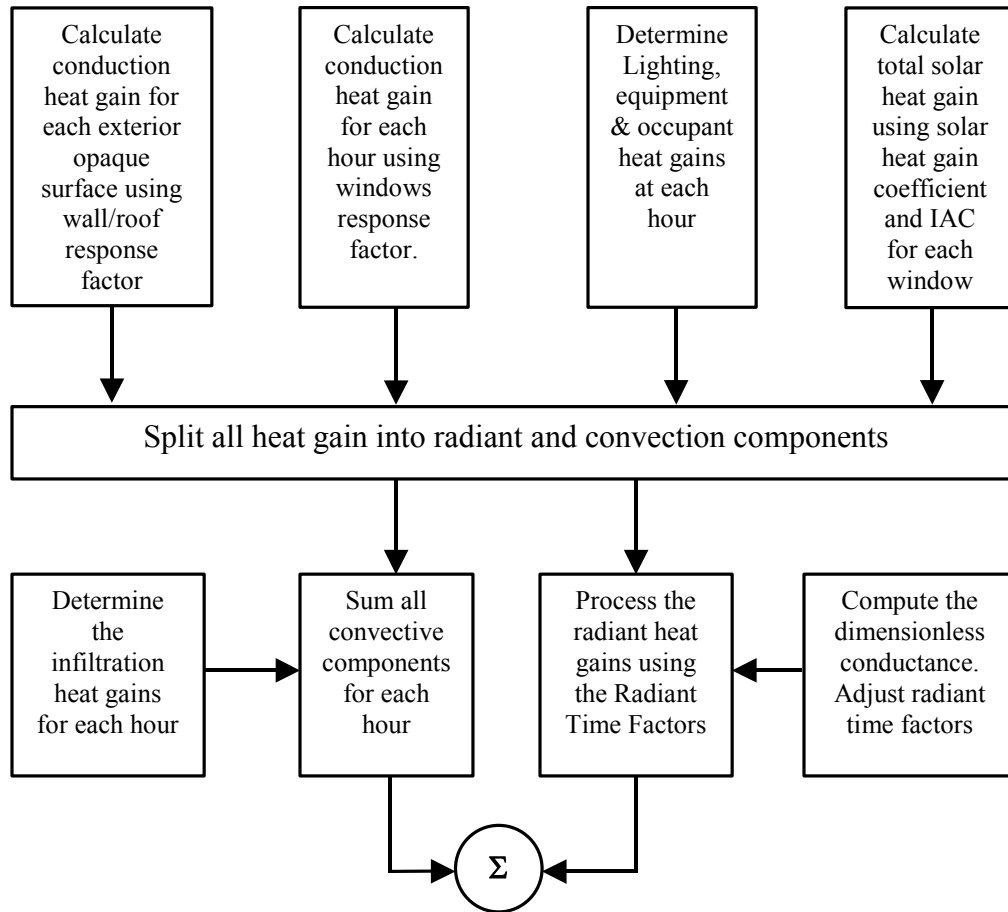


Figure 3.21 Improved Radiant Time Series cooling load calculation method represented as flow diagram

3.3.2 Dimensionless Loss Conductance

The modified conduction heat gains Eqs 3.45 for j^{th} fenestration surface that accounts for the effects of the space solar and internal radiant heat gains using a uniform area-weighted distribution model is given by:

$$\dot{q}_{cond,j} = UA_j(T_o - T_a) + \left(\frac{A_j}{A_{room}}\right)\dot{q}_{HG} - \frac{U}{h_{cb,i}}\left(\frac{A_j}{A_{room}}\right)\dot{q}_{HG} \quad (3.56)$$

Or

$$\dot{q}_{cond,j} = UA_j(T_o - T_a) + \frac{A_j}{A_{room}}\left(1 - \frac{U}{h_{cb,i}}\right)\dot{q}_{HG} \quad (3.57)$$

The first term in Eq. 3.57 is the conduction heat gain for steady state conduction as is commonly implemented in the original RTSM. The second term is the fraction the space solar and radiant heat gain absorbed based on distribution model assigned to the j^{th} fenestration surface. If summed over surfaces in the zone is equal to the space radiant heat gain. The last term is the fraction that conducted back out. The difference between the last two terms is the net radiant heat gain of the space. The modified conduction equation can also be formulated using superposition principle. Dimensionless loss conductance computed for a corner zone with two exterior facade surfaces are shown in Figures 3.22 and 3.23. Five different glazing types with different U -values with and without interior shades are shown. A constant combined conductance of 3.56 ($W/m^2 \cdot K$) was used for the air gap between the glazing and the interior shade. The dimensionless loss conductance is directly proportional to the U -value of the fenestration system, the inside combined conductance and glazing fraction of the exterior facade as it is also evident from Eq 3.51. The maximum value for a zone with two exterior facades at 90% glazing fraction and single pane clear glass is about 0.17 for aspect ratio of 0.5. It is also evident from these plots the radiant heat gain loss are not significant when the glazing U -value are small like low-e insulating glasses and in particular when it involves interior shades. The dimensionless conductance increases for decreasing aspect ratio.

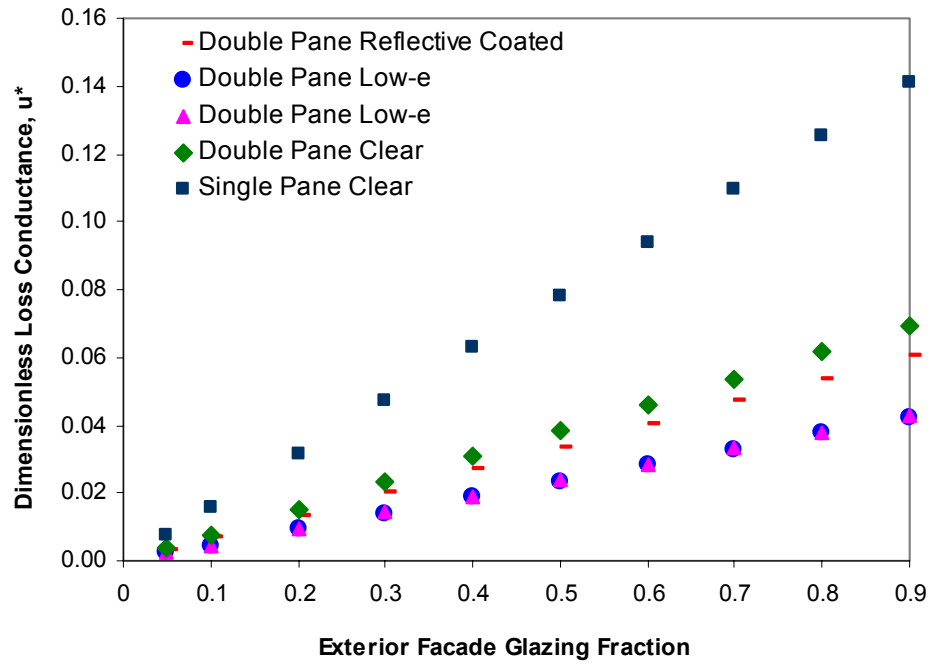


Figure 3.22 Dimensionless loss conductance for zone with two exterior facades and unshaded glazing

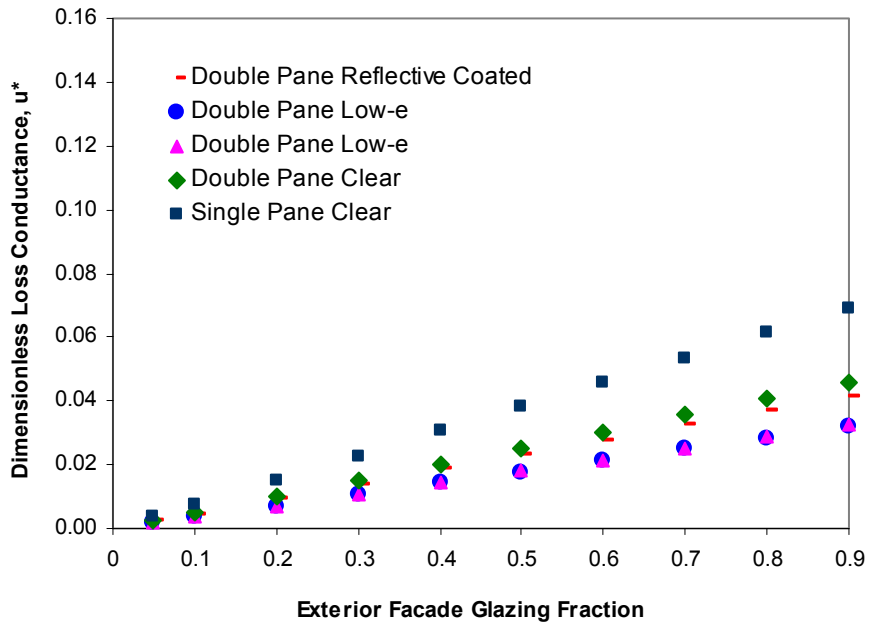


Figure 3.23 Dimensionless loss conductance for zone with two exterior facades for shaded glazing types

3.3.3 Performance of the Improved RTSM Procedure

The improved RTSM cooling load calculation procedure performance has been tested over a wider range of building design parameters combination for a zone with two exterior facades facing south and west with different glazing types and shades for fourteen USA design day weather and locations for the month of July. Building design parameters range and levels given in Table 4.1 were used. The performance of current and improved RTSM procedures was determined using the parametric run tool and the recommended radiative / convective splits given in Table 3.3. The results are presented for fenestration without and with interior shades as follows.

Fenestration without Interior shades

A total of 537600 test zones were investigated by varying: glazing fraction, glazing type (five glazing types), light and heavyweight construction (exterior Wall, Partition, Roof, and Floor), four top floor corner zones, three aspect ratios (0.5, 1., and 2.), two levels of internal schedules, two levels of thermal mass, and 14 July 21 design day US weather locations. The RTSM peak cooling load plot against that of the HBM is shown for single pane clear glass in Figure 3.24. The improved RTSM peak cooling load over prediction for zones with large amount of single pane clear glazing has been improved dramatically from as high as 26.8% to 8.8% at 90% glazing fraction of the exterior facades.

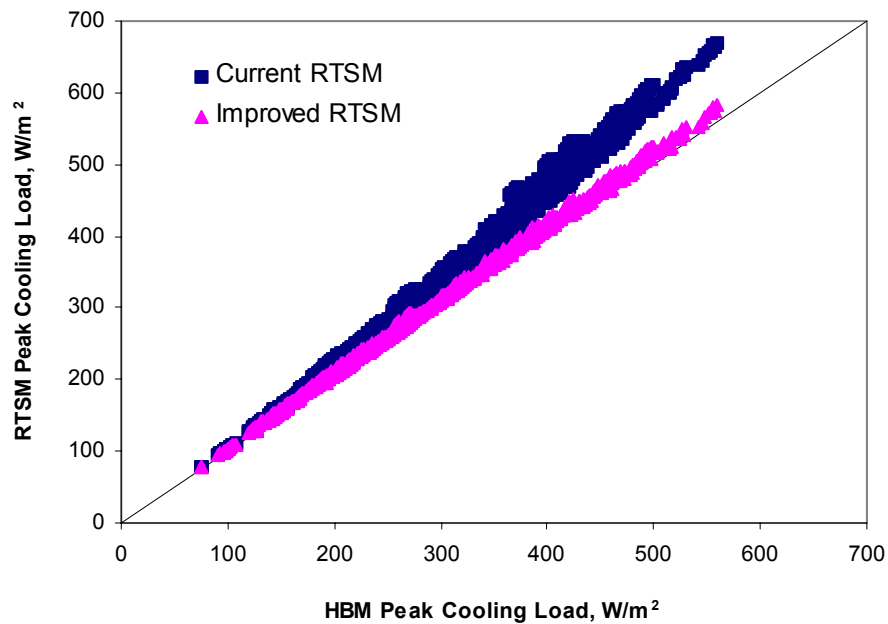


Figure 3.24 RTSM peak cooling load vs. HBM for light and heavyweight zone for single pane clear glass without internal shade

The hourly cooling load profile of the RTSM procedures were compared with the reference model, the heat balance method, for July design day weather in Chicago, Illinois (peak design temperature of 34.6°C). A top floor corner zone with single pane clear glass both on the south and west exterior facades was used. The improved RTSM cooling load profile behaved well and closely follows that of the HBM compared to the current RTSM as shown in Figure 3.25 and 3.26. The peak-cooling load maximum over prediction for the current and improved RTSM at 50% glazing fraction of the exterior facade is 12.6% and 5.8%, respectively. The peak cooling load over prediction of the current RTSM increases proportionally with the glazing fraction and it is 22.2% at 90% glazing fraction whereas the improved RTSM over prediction is 9.3% only.

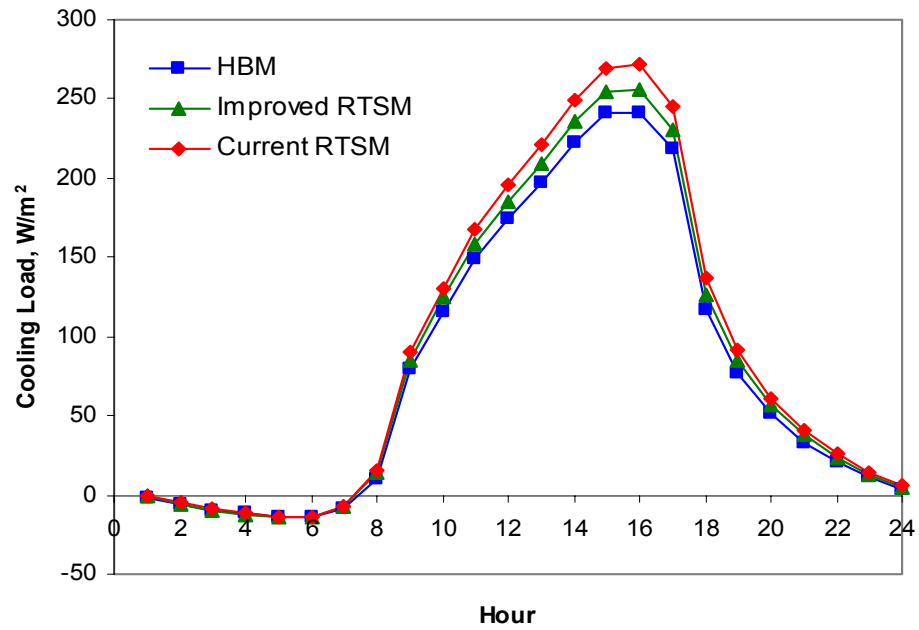


Figure 3.25 Hourly cooling load profile for lightweight zone at 50% glazing fraction for single pane clear glass in Chicago, Illinois

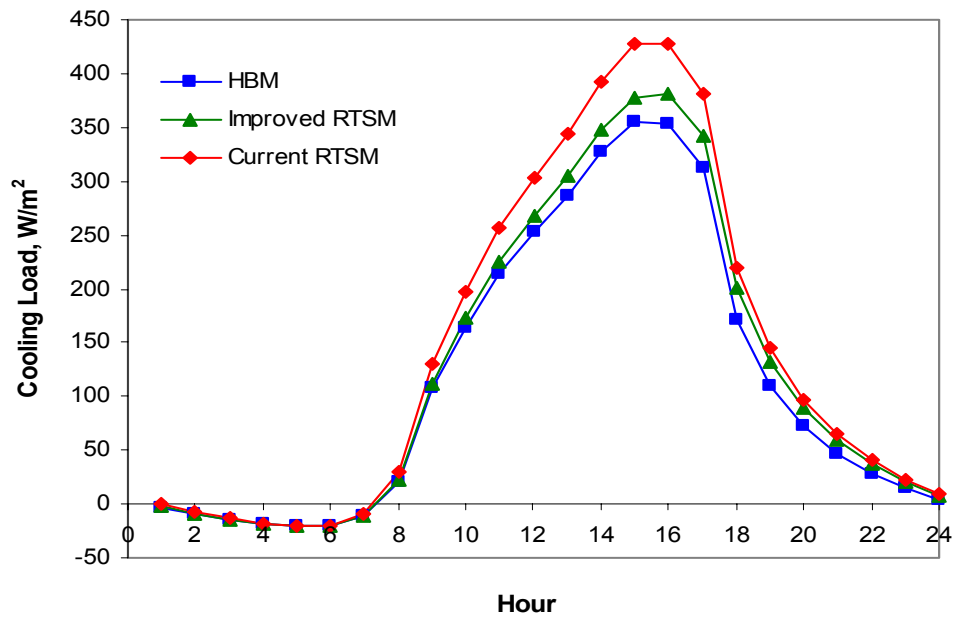


Figure 3.26 Hourly cooling load profile for lightweight zone at 90% glazing fraction for single pane clear glass in Chicago, Illinois

Fenestration with Interior shades

A total of 403,200 test zones were investigated by varying: glazing fraction, glazing type (five glazing types), light and heavyweight construction (exterior Wall, Partition, Roof, and Floor), a top floor south west corner zone, three aspect ratios (0.5, 1., and 2.), two levels of internal schedules, two levels of thermal mass, fourteen July 21 design day US weather locations and the three interior shade types. The RTSM peak cooling loads versus that of the HBM are shown in Figure 3.27.

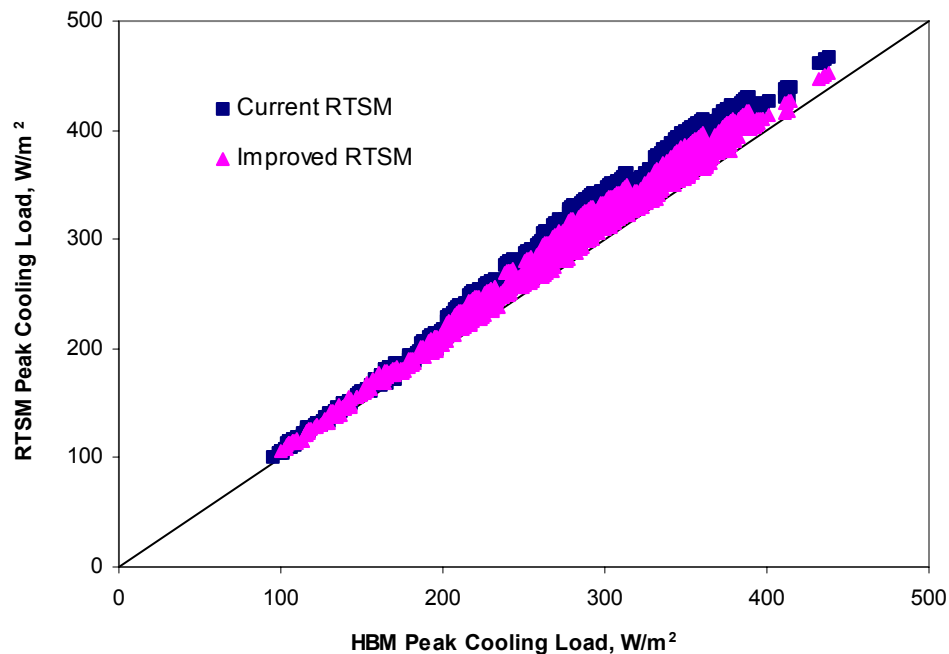


Figure 3.27 RTSM peak cooling load vs. HBM for light and heavyweight zone for single pane clear glass with internal shade

The improvement in the peak cooling prediction of the improved RTSM procedure is not significant mainly due to: (1) a reduction in the amount of solar heat gain due to shade, and (2) reduction in the dimensionless loss conductance for shaded fenestration due to air gap resistance as shown in Figure 3.23.

The RTSM peak cooling load over predictions in design weather location of Atlanta, Georgia for lightweight construction zone with dark roller interior shaded and single pane clear glass is well below 6% for current procedure and well below 3% for the improved procedures. However, the peak cooling load over prediction is relatively higher for heavyweight construction zones and can be as high as 12% and 9% for current and improved RTSM, respectively. The main reason for marked difference in performance of the RTSM for light and heavy weight construction zones is the use of fixed radiative fraction for all construction types.

Heavyweight construction zone with interior shaded fenestration surfaces require higher radiative fractions due to the lower mean radiant temperatures they see compared to lightweight construction zones. Based on higher radiative fractions for heavyweight construction zones the RTSM peak cooling load predictions would have been less. The higher sensitivities of the RTSM performance to construction fabrics for fenestration with shades is that most of the solar heat gains is transmitted into the space via radiation exchange after being absorbed by the shade. Moreover, the radiant fraction is dependent on the mean radiant temperatures of surfaces viewed by the fenestration, which also depends on the zone construction fabrics. As the results the radiative fraction of solar and conduction heat gains of fenestrations with interior shades shows more sensitivity compared to fenestration without interior shade, for which the solar heat gain is mainly transmitted component.

The RTSM peak cooling over prediction shows good match with the HBM for larger aspect ratios. The higher over prediction at lower aspect ratio in particular to heavyweight construction zones is due to large amount of solar heat gain per unit floor area and the sensitivity of the radiative / convective split to construction fabrics. However, the improved RTSM procedure peak cooling load shows less sensitivity to aspect ratio compared to the current RTSM procedure.

3.3.4 Heat Losses in the TFM Procedure

Spitler and Fisher (1999) introduced a relationship between the RTSM radiant time factors and the weighting factors of the TFM using the steady periodic nature of the design day cooling load calculation. On this basis, it seems likely that a similar heat losses correction could be derived for the TFM. Indeed, this is the case. The derivation is given in this section.

The current hour cooling loads are related to the hourly present and past heat gains using the heat gain weighting factor transfer function method formulation described by Kerrisk (1981) and is given by:

$$Q_{\theta} = \sum_{j=0}^2 v_j q_{\theta-j\delta} - \sum_{k=1}^2 w_k Q_{\theta-k\delta} \quad (3.58)$$

Calculation of steady periodic radiant time series coefficient matrix is defined in terms of the zone weighting factors coefficient matrices and is given by:

$$\mathbf{R} = \mathbf{W}^{-1}\mathbf{V} \quad (3.59)$$

Where \mathbf{W} is the cooling load weighting factor coefficient matrix, \mathbf{V} is the heat gain weighting factor coefficients matrix, and \mathbf{R} is the radiant time factors coefficient matrix. The dimensionless loss conductance is introduced to account for the space radiant heat gain conducted back out and acts on the current hour of the radiant time factors. For a steady periodic design day load calculation the corrected radiant time factors coefficient matrix is given by:

$$\bar{\mathbf{R}} = \mathbf{R} - u^* \mathbf{I} \quad (3.60)$$

Where $\bar{\mathbf{R}}$ is the corrected radiant time factor coefficients matrix and \mathbf{I} is the identity matrix. Taking the steady periodic nature of the design day load calculation the improved RTSM procedure that accounts for the radiant heat back loss can be related to the transfer function weighting factors using the relationship described by Spitler and Fisher (1999) and it is given by:

$$[\bar{\mathbf{R}} + u^* \mathbf{I}]\mathbf{q} = \mathbf{W}^{-1}\mathbf{V}\mathbf{q} \quad (3.61)$$

Where \mathbf{q} is a column vector contains the 24 hourly values of the radiant heat gains. Dropping the heat gains vectors form both sides of the equation and multiplying both sides of the equation by \mathbf{W} and simplifying yields:

$$[\mathbf{WR} + \mathbf{W}u^*\mathbf{I}] = \mathbf{V} \quad (3.62)$$

$$\bar{\mathbf{V}} = \mathbf{WR} \quad (3.63)$$

Where $\bar{\mathbf{V}}$ is the corrected the heat gain weighting factors coefficient matrix.

Substituting Eq. 3.63 into Eq. 3.62 and rearing yields:

$$\mathbf{V} = \bar{\mathbf{V}} + u^*\mathbf{W} \quad (3.64)$$

$$\bar{\mathbf{V}} = \mathbf{V} - u^*\mathbf{W} \quad (3.65)$$

Eq. 3.65 relates the corrected heat gain weighting factor coefficient matrix to the adiabatic (normalized) heat gain TFM weighting factors and cooling load TFM weighting factors coefficient matrix using the dimensionless loss conductance.

3.3.5 Conclusion and Recommendations

It has been a problem to formulate a procedure that accounts for the radiant heat gain loss yet maintains the simplicity of the RTSM procedure. A methodology or an algorithm that accounts for radiant heat gain back loss and mitigates the RTSM peak-cooling load over predictions has been developed. This algorithm introduces a dimensionless loss conductance of a zone that depends on the fenestration U -value, inside combined conductance, fenestration area and the inside surface areas. This algorithm has been tested over wide range building design parameters combination forming 403,200 test cases for shaded fenestration and 537,600 test cases for unshaded one. The modification and implementation of the algorithm maintains the simplicity of the original RTSM

procedure and can be adopted by simply correcting the first terms of the adiabatic radiant time factors. The following conclusions can be drawn from the finding of the parametric run investigation of the RTSM procedure:

- The dimensionless loss conductance that accounts for heat loss of a space has been introduced and can be computed readily from building design parameters – the fenestration U -value and area, inside combined conductance and zone inside surface area. The heat losses are not significant when the glazing U -value is small like in insulating glasses and in particular when it involves interior shades.
- In general the improved RTSM reduces the peak-cooling load over prediction trend of the RTSM procedure dramatically. The peak cooling load over prediction can be reduced fewer than 10% for zones with single pane clear glasses and having two exterior facades for most design weather conditions. The over prediction of peak cooling load is much lower in the glazing fraction is less than 70%. In general peak cooling load over predictions of the RTSM procedure for light weight construction zones is much lower than heavyweight construction zones without interior shaded fenestrations. The improved RTSM peak cooling load over prediction for lightweight construction zones with unshaded fenestration is less 6%.
- Two range solar heat gain radiative / convective splits were recommended that depends on the glazing type for fenestration with interior shades. The improved RTSM procedure works better if several ranges of radiative / convective splits that depend on glazing type for zones without interior shaded fenestration. The radiative / convective split used for solar heat gain in the RTSM procedure

showed strong sensitivity to zone construction fabric for fenestration system with interior shades. Though a fixed value use of radiative fraction for all construction fabrics showed conservative estimate of the RTSM peak cooling load, the over prediction trend can further be reduced by using radiative fraction dependent on the zone construction fabrics as well. With recommended radiative / convective split given in Table 3.3 the maximum over prediction of the improved RTSM may reach as high as 11% for heavyweight construction zones. The over prediction of the RTSM can be further reduced for fenestration system without shades by using a radiative / convective split dependent on the glazing type and construction fabrics.

- Further investigation is required to determine the radiative / convective splits dependency on other types of interior shades like drapery fabrics with wide characteristics of optical properties.

3.4 Summary and Conclusions

The series of improvements to the Radiant Time Series Method investigated developed in this chapter are comprised of improvements of the method, its sub-models, or supporting data, or ease of implementation in various computing environments. These improvements are summarized as follows:

- A one-dimensional finite volume procedure with fully implicit solution scheme has been developed for PRF generation. The PRFs are generated by exciting multi-layered wall with unit height triangular base temperature pulse. The procedure uses uniform gridding for each layer with zero thickness boundary nodes for effective boundary condition imposition. Moreover, higher order expression is used for

response flux calculation. The algorithm has been implemented in FORTRAN 90, VBA and SCILAB. The implementations in these programming platforms required 500, 450 and 150 lines of code, respectively, compared to 2000 lines of FORTRAN 90 for computation of CTF with the State Space method and conversion to PRF. The finite volume procedure has been validated against PRF determined by converting CTF generated using the State Space Method as discussed in Section 3.1.3. The validation was done comparing the peak heat gains computed using these two PRF for typical design day sol-air temperatures and 82 ASHRAE walls and roofs (ASHRAE, 1997). The difference between the peak heat gains is in the range -0.7% to 2.2% and average error is -0.03%. The RMSE of the peak heat gain is 0.02 W/m^2 . This is sufficient accuracy for cooling load calculation, as conduction heat gain is small fraction of cooling loads.

- The RTF generation procedure, which was originally developed using a full-blown heat balance procedure, has been reformulated in a compact form is the “reduced heat balance method” by eliminating unneeded features of the HBM. Due to the compact nature of the algorithm it can take advantage of computing environments with built-in libraries of matrix algebra. This algorithm has been successfully implemented in VBA and SCILAB using 450 and 150 lines of codes, respectively. The procedure has been validated against a full-blown heat balance procedure in Section 3.1.1. For six test zones, the RMSE of the reduced heat balance procedure RTF compared to the full heat balance method was within 0.00007 to 0.00037. This error margin is within the convergence limits of the full-blown heat balance procedure. The reduced heat balance procedure has been further simplified to use constant radiation coefficients

and this results in reducing the computation time by half compared to the variable radiation coefficient implementation. With these simplifications the hourly cooling load errors in a spreadsheet RTSM implementation for three test zones is within 0.02 Btu/hr·ft². The hourly cooling load plots for constant and variable radiation coefficient are shown in Appendix C.

- An improved fenestration model, compatible with recent developments in fenestration data, has been adapted to the RTSM procedure. A new set of radiative / convective splits for fenestration conduction and solar heat gains have been established and are given in Table 3.3. The RTSM fenestration model and the radiative / convective splits fenestration model facilitates the use of manufactures' data and avoids the need for splitting solar heat gain into transmitted and absorbed components.
- An algorithm for accounting heat losses by conduction through highly conductive mass less surfaces such as fenestration has been developed. The algorithm uses a dimensionless loss conductance that can be calculated from zone surface geometry, fenestration U-value and combined inside surface conductance. The dimensionless loss conductance operates on the first term of the radiant time factors and hence maintains the simplicity of the RTSM procedure desired. The approximate correction introduced reduced peak cooling load over predictions of the RTSM procedure significantly for all problem zones. For a parametric study of 403,200 zones with unshaded fenestration the maximum RTSM peak cooling load overprediction is reduced from 26.8% to 8.8%.

CHAPTER IV

4. Parametric Study of the RTSM Procedure

This chapter deals with a parametric investigation conducted to develop quantitative design guidance on the performance of the Radiant Time Series Method (RTSM). First, the range of parameters investigated are described; second, the methodology employed in the parametric investigation is explained and load calculation programs / software utilized for the investigation are discussed; and, third the results and recommendations are given.

Although the RTSM has been adopted by ASHRAE as published cooling load calculation design procedure there is no information available regarding the likely overprediction of the peak-cooling load by the RTSM procedure in the form of design guidance for practicing engineers. It is difficult or impossible for a designer to judge the likely overprediction of the RTSM in the absence of such quantitative design guidance. This parametric study is intended to quantitatively investigate the effect of design parameters that influence the maximum overprediction error of the RTSM and lead to quantitative design guidance. This work will make use of extended version of the parametric run generation tool used in ASHRAE RP-942 but originally developed by Strand as cited by Spitler and Rees (1998).

However, this work has a different goal - providing quantitative design guidance. In addition, improvements to the fenestration model have been incorporated in both HBM and RTSM procedures. The fenestration model is capable of modeling interior shades. The HBM fenestration model uses Klems (2002) algorithm given in appendix-A. The RTSM fenestration model uses solar heat gain coefficient (SHGC), interior attenuation coefficient (IAC) and radiative / convective split as described in Section 5.2. Compared to the previous study (Rees et al. 1998; Spitler and Rees 1998) a much larger number of parametric values and zones have been utilized.

4.1 Parametric Run Generation

This work utilized a revised version of the parametric run generation tool originally developed by Strand as cited by Spitler and Rees (1998). The parametric run generator as shown in Figure 4.1 reads in the input values for each parametric and levels and creates input file each case. Three different “types” of parametric studies can be performed: a “fully populated set”, a “sparsely populated set” and “min-max set” (Spitler and Rees 1998). The parametric run generator then creates a complete set of files for the specified combinations of design parameters and the batch file required for running those combinations. The individual zone input data is created by combining small text files and, where necessary, computing dimensions and writing them into an input file. Previously, the parametric run generator was limited to ten design days. It has been updated to use up to 100 design different design days representing different locations and months. This was needed to allow comparison for a range of months, as many zones do not peak in summer. In this investigation, fourteen USA locations, each with seven

months of design day data, making a total of 98 design weather are utilized. The parametric run generation tool was modified to support a new fenestration model, a range of window glazing types and a range of interior shades.

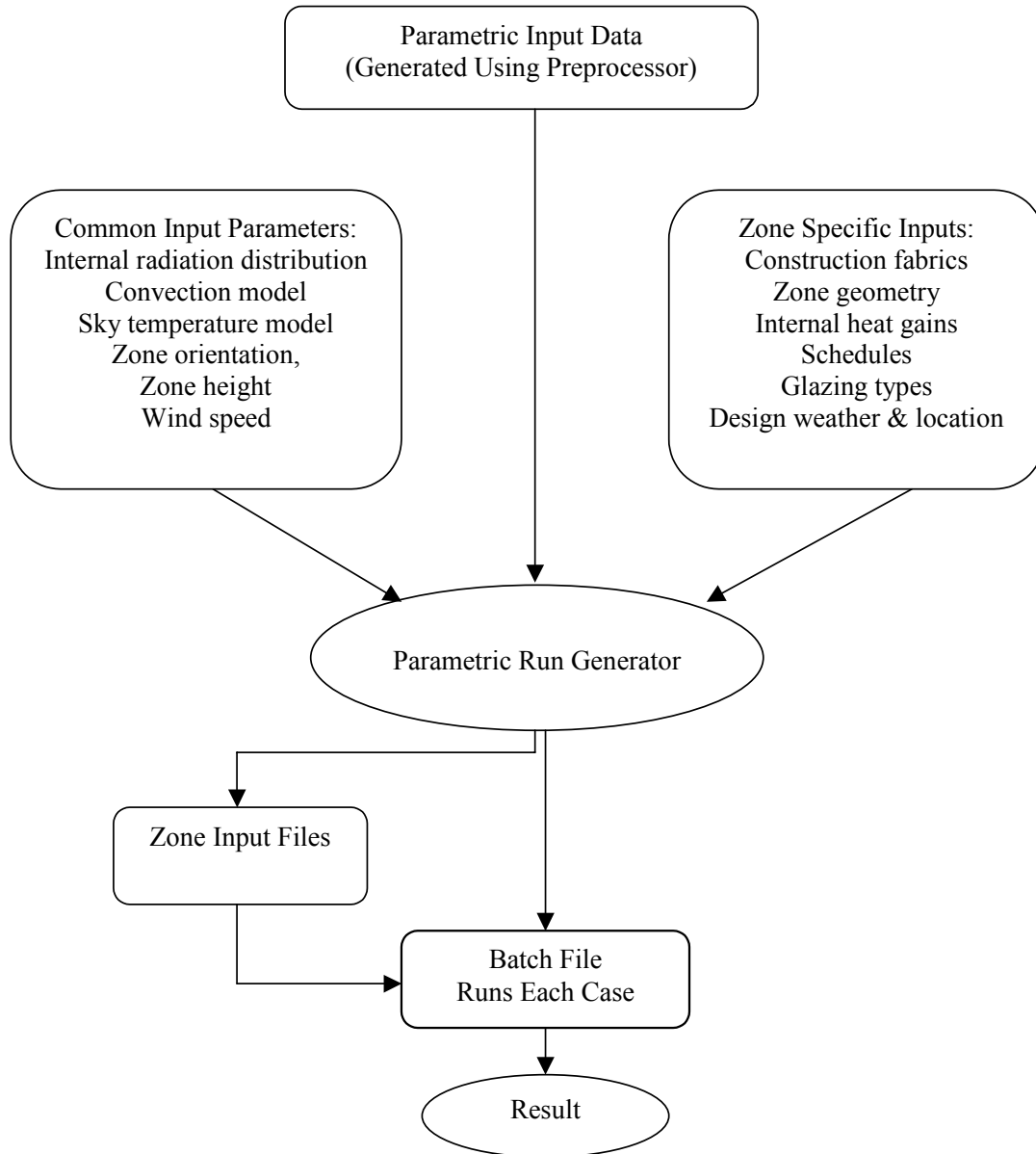


Figure 4.1 Schematic of Parametric Run Generator

4.2 Test Zone Parameters

This section discusses the range of zone parameters investigated in the parametric study. The levels of the nineteen parameters summarized in Table 4.1 control the zone construction, geometry, internal heat gains, and weather conditions. The levels reflect typical values expected in practice. The numbering scheme has been adapted from Spitler and Rees (1998), but not all of their levels are used. For example exterior wall have levels, 1 and 6, levels 2-5 from Spitler and Rees (1998) are not used. Further discussion of the changes in the parameter levels is given in the following sections.

Table 4.1 Test Parameter range and levels

No	Parameter	No. of Levels	Parameter Levels
1	Room size	1	A: (6m east-west axis dimension)
2	Room level	2	m, t (middle & top floor zone)
3	Zone Number ¹	9	1 – 9 (all zone orientations)
4	% Glazing ²	10	5%, 10%, 20%, 30%, ..., 90%
5	People	3	5, 10 and 30 W per 100m ² (5, 10 and 30 per 1076 ft ²)
6	Lighting	3	10, 20, and 30 W/m ² (3.17, 6.34 and 9.51 Btu/h ft ²)
7	Equipment	1	30 W/m ² (9.51 Btu/h ft ²)
8	Infiltration	1	0.5 Air change per hour (ACH)
9	Exterior Wall ³	2	Type 1: light 32.0 kJ/m ² ·K (1.6 Btu/ft ² °F) Type 2: light 137.1 kJ/m ² ·K (6.7 Btu/ft ² °F) Type 3: light 316.6 kJ/m ² ·K (15.5 Btu/ft ² °F) Type 4: light 362.7 kJ/m ² ·K (17.7 Btu/ft ² °F) Type 5: light 520.7 kJ/m ² ·K (25.5 Btu/ft ² °F) Type 6: heavy 550.9 kJ/m ² ·K (26.9 Btu/ft ² °F)
10	Partition	2	Type 1: light 24.9 kJ/m ² ·K (1.2 Btu/ft ² °F) Type 2: heavy 208.9 kJ/m ² ·K (10.2 Btu/ft ² °F)
11	Roof	2	Type 1: light 34.4 kJ/m ² ·K (1.7 Btu/ft ² °F) Type 2: heavy 350.2 kJ/m ² ·K (17.1 Btu/ft ² °F)
12	Floor	2	Type 1: light 78.0 kJ/m ² ·K (3.8 Btu/ft ² °F) Type 4: heavy 540.7 kJ/m ² ·K (26.5 Btu/ft ² °F)
13	Ceiling	2	Type 1: light 78.0 kJ/m ² ·K (3.8 Btu/ft ² °F) Type 4: heavy 540.7 kJ/m ² ·K (26.5 Btu/ft ² °F)

Table 4.1 Test Parameter range and levels (continued)

No	Parameter	No. of Levels	Parameter Levels
14	Window Type ⁴	3	Type 1: single pane clear glass Type 2: double pane clear glass Type 3: double pane low-e glass (SHGC=0.65) Type 4: double pane low-e glass (SHGC=0.39) Type 5: double pane reflective coated glass
15	Thermal mass ⁵	2	Type 1: light 45.6 kJ/m ² ·K (2.2 Btu/ft ² °F) Type 2: light 78.2 kJ/m ² ·K (3.8 Btu/ft ² °F)
16	Aspect Ratio ⁶	3	0.5, 1.0, and 2.0
17	Load Schedule	2	1, and 6 (on all day, stepped schedule)
18	Weather Day ⁷	98	Fourteen weather locations; Each with seven months design weather data.
19	Interior shades ⁸	4	Type 1: no shade Type 2: medium color Venetian blind Type 3: dark roller shade Type 4: close weave dark color Drapery fabrics

1. See Figure 4.2
2. Percent of exterior facade area, computed based on internal dimensions
3. For each of the wall, partition, floor/ceiling, and roof constructions, the thermal capacitance of the construction is specified in parentheses. Layer-by-layer descriptions are given in Table 4.2.
4. Detailed windows descriptions are given in Table 4.4
5. Ratio of north-south dimension to east-west dimension
6. See Section 4.2.3
7. See Section 4.2.8
8. See Section 4.2.5

4.2.1 Zone Geometry and Construction Fabric

The zone floor geometry is determined from two parameters: the east-west axis and aspect ratio. Though the parametric run generation tool allows specifying ten different east-west axis dimensions a fixed value of 6m (19.68ft) has been selected throughout this investigation. The other dimension of the floor is determined by multiplying the east-west dimension by the aspect ratio. It is possible to define arbitrary aspect ratios in the range 0.1 to 9.9; three aspect ratios: 0.5, 1.0, and 2.0 have been considered in this parametric investigation. The purpose of the parametric investigation is to determine the limiting case over prediction of the RTSM; therefore, design parameters were limited to typical design conditions. The specific wall, floor, partition, and ceiling constructions of the zone

are determined by a combination of two parameters: room level and zone number. The zone level (mid floor or top floor) controls the ceiling construction whether it is “roof” or “floor/ceiling”. The zone number determines the location of the zone in a given floor, as shown in Figure 4.2. Accordingly, numbers 1, 3, 5, and 7 have two external walls, and two partition walls. Zone numbers 2, 4, 6, and 8 have one external wall and three partition walls. The external surfaces always have windows as a sub-surface and the window area is defined as a fraction of the base surface area. Ten glazing fractions between 5% and 90% are used for this parametric study.

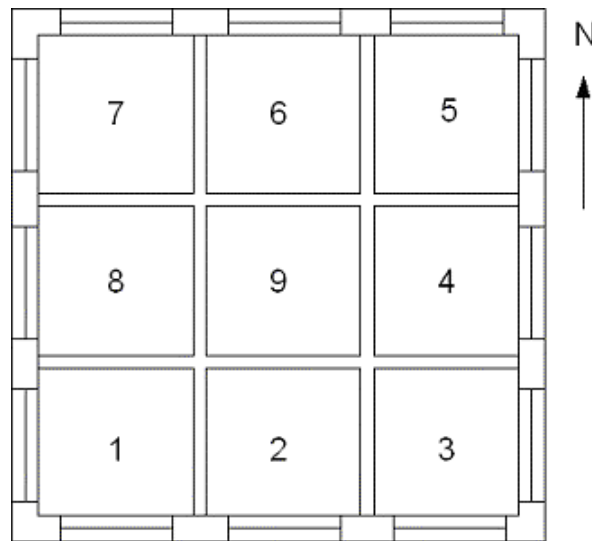


Figure 4.2 Zone orientation and number designations

The areas of all constructions are set with the above parameters. The actual construction for each construction type is then set with the parameters: external wall, partitions, floor/ceiling and roof. The parametric run investigated light and heavy weight constructions taken from previous study (Spitler and Rees 1998) represent typical commonly used construction and their thermal properties are shown in Table 6.2.

Table 4.2 Construction Type Materials (Rees et al. 1998)

Layer Material	Thickness mm (in.)	ρ kg/m ³ (lb/ft ³)	C_p kJ/kg·K (Btu/lb·°F)	k W/m·K (Btu/h·ft·°F)
Exterior Wall Type 2: Brick and Stud Inner Leaf (Wilkins 1996)				
Facing Brick	92(0.625)	1600(50)	0.79(0.39)	0.84(0.49)
Air gap	48(.875)	1.2(0.075)	1.005(0.24)	*
Gypsum sheathing	16(0.625)	800(34)	1.09(0.26)	0.16(0.07)
Insulation (R-19)	150(6.0)	32(2)	0.71(0.17)	0.04(0.02)
Gypsum wall board	16(0.625)	800(50)	1.09(0.26)	0.16(0.09)
Exterior Wall Type 6: Heavyweight Blockwork and Cavity Insulation (Arup R&D)				
Facing brick	100(4)	1600(100)	0.79(0.19)	0.84(0.49)
Air gap	100(4)	1.2(0.075)	1.005(0.24)	*
Insulation	50(2)	32(2)	0.71(0.17)	0.04(0.02)
Solid concrete block	215(8.5)	2100(131)	0.92(0.22)	1.63(0.94)
Plaster	13(0.5)	720(45)	0.84(0.20)	0.16(0.09)
Partition Wall Type 1: Stud Wall Internal Partition				
Gypsum wall board	13(0.5)	800(50)	1.09(0.26)	0.16(0.09)
Insulation	100(4)	32(2)	0.71(0.17)	0.04(0.02)
Gypsum wall board	13(0.5)	800(50)	1.09(0.26)	0.16(0.09)
Partition Wall Type 2: Blockwork Internal Partition				
Plaster	13(0.5)	720(45)	0.84(0.20)	0.16(0.09)
Concrete block	100(4)	2100(131)	0.92(0.22)	1.63(0.94)
Plaster	13(0.5)	720(45)	0.84(0.20)	0.16(0.09)
Floor/Ceiling Type 1: Wood Floor with Gypsum Board Ceiling				
Gypsum wall board	13(0.5)	800(50)	1.09(0.26)	0.16(0.09)
Air gap	190.5(7.5)	1.2(0.075)	1.005(0.24)	*
Pine	200(0.79)	640(40)	1.63(0.39)	0.15(0.09)
Floor/Ceiling Type 4: In-Situ Concrete Slab, Suspended Ceiling, Tile Finish Floor				
Ceiling Tile	10(0.4)	370(23)	0.59(0.14)	0.06(0.04)
Ceiling air space	1000(39)	1.2(0.075)	1.005(0.24)	*
Cast concrete	200(8)	2300(144)	0.9(0.22)	1.73(1)
Screed	70(2.75)	1920(120)	0.88(0.21)	1.4(0.81)
Vinyl tiles	5(0.2)	800(50)	1.26(0.30)	0.6(0.35)
Roof Type 1: Steel Decking Insulated (Wilkins 1996)				
Membrane	10(0.4)	1121(70)	1.67(0.40)	0.19(0.11)
Insulation	150(6)	32(2)	1.21(0.29)	0.04(0.02)
Steel pan	2(0.08)	7689(481)	0.42(0.10)	45(26)
Ceiling air space	1000(39)	1.2(0.075)	1.005(0.24)	*
Ceiling tile	10(0.4)	370(23)	0.59(0.14)	0.06(0.04)
Roof Type 2: Concrete Slab Insulated				
Stone Chippings	13(0.5)	881(55)	1.67(0.40)	1.436(0.83)
Felt and membrane	10(0.4)	1121(70)	1.67(0.40)	0.19(0.11)
Insulation	50(2)	40(2.5)	0.92(0.22)	0.025(0.01)
Cast concrete	150(6)	2300(144)	0.9(0.22)	1.73(1.0)

* all air gap have been give a constant resistance of 0.18 m²·K/W (1 hr·ft²·°F/Btu)

4.2.2 Thermal Mass Types

The RP-942 parametric run data generator tool used a single parameter that specified the type of thermal mass: lightweight (pine) and heavy weight (brick) thermal mass and the ratio of the thermal mass surface area to the floor area (0, 25%, 50%, 100%, 200% and 400%) (Spitler and Rees 1998). The thermal mass of a building may change a lot during the lifetime of a building and will differ from zone to zone in the same building. Thermal mass intercepts the solar and internal radiant gains and releases it at a later time. Thermal mass releases the energy faster or slower depending on the thermal mass of the rest of the building structure; hence, it has a direct effect on the peak cooling load. The large amount of thermal mass is not suitable for establishing the RTSM peak cooling load over prediction limit. Two extreme thermal mass types have been utilized but in terms of surface area an average value is more representative. In this parametric investigation lightweight and heavyweight thermal mass construction based on 50% of the floor surface area were used. The thermal capacitances of the two thermal masses are 45.6 KJ/m² K (2.2 Btu/ft²·°F) and 78.2 KJ/m² K (3.8 Btu/ft²·°F).

Table 4.3 Thermal Mass Type materials (Rees et al. 1998)

Layer Material	Thickness mm (in.)	ρ kg/m ³ (lb/ft ³)	C_p KJ/kg·K (Btu/lb·°F)	k W/m·K (Btu/h·ft·°F)
Thermal Mass Type 2: 25 mm (1in.) Pine				
Pine	25(1)	640(40)	2.803(0.67)	0.15(0.09)
Thermal Mass Type 7: 50 mm (2in.) Brick				
Brick	50(2)	1700(106)	0.92(0.22)	0.55(0.32)

4.2.3 Internal Heat Gains and Schedules

People, lighting and equipment loads were included in the parametric investigation by defining the zone peak heat gain loading. Then the hourly heat gain rates are determined by multiplying the peak heat gain and the 24-hourly heat gain schedules. The parametric run generation tool has six schedule types but only two have been used in this investigation. For the base case analysis the following internal heat gain values were used: 10 people per 100m² for people, 20 W/m² (6.34 Btu/h·ft²) for lighting and 30 W/m² (9.51 Btu/h·ft²) for equipment. Investigation attempted to quantitatively analyze internal heat gain loading impact on the RTS method likely peak cooling load overprediction. It is common practice to use constant radiative / convective split of internal heat gains in RTSM. ASHRAE 942-RP parametric runs generator uses a fixed radiative / convective split for all parametric runs: 70/30 for people, 30/70 for equipment and 67/33 for lighting heat gains. However, for quantitative characterization of the maximum RTSM peak cooling load over prediction there is a need to consider wide range of radiative / convective splits, which also depends on Luminaire type, the space air flow rate and lighting input intensity.

ASHRAE's RP-1282 provided lighting heat gain fractions based on experimental studies on twelve luminaires types (Fisher and Chantrasrisalai, 2006). The RP-1282 recommended five luminaire categories for purposes of setting the radiative / convective split. The recommended ranges were based on studies made on lighting heat input rates in the range 0.9 W/ft² (9.69 W/m²) to 2.6 W/ft² (27.99 W/m²). A typical peak lighting heat gain rate of 1.86 W/ft² (20.0 W/m²) was used in this parametric investigation.

The equipment peak heat gain loading expected in commercial buildings ranges widely and depends on the building usage. An electronic equipment heat gain load study made on office buildings has shown that the actual load factor ranges between 0.32 W/ft² (3.44 W/m²) to 1.33 W/ft² (14.32 W/m²) and if the usage diversity is ignored the maximum loading may reach 1.75 W/ft² (18.8 W/m²) (Wilkins 1998). Average equipment heat gain loading for medical center hospital laboratory spaces can be 6.71 W/ft² (72.2 W/m²) and it could be as high as 10.65 W/ft² (114.6 W/m²) (Wilkins and Cook 1999). The equipment load density is wide range depending on the building usage and industry category; hence, 2.79 W/ft² (30.0 W/m²) has been utilized as a representative typical value over the entire range.

4.2.4 Glazing Types

In general the original RTSM tends to over predict the peak cooling load when the zone has large amount of single pane glazing and exposed to lower outside design air temperature. However, the RTSM peak cooling load overprediction decreases substantially for double pane fenestration systems due to a decrease in conductance and solar heat gain. Therefore, here it is intended to provide design guidance for four categories of fenestration types: single pane clear window, double pane clear windows, double pane low-emissivity glass windows and double pane reflective coated glass windows shown in Table 6.4. The individual glass layer properties were taken from LBNL Optics5 optical glazing database that closely duplicate the system properties given in ASHRAE Handbook of Fundamental (ASHRAE 2005).

Table 4.4 Single Pane Clear Glass Window

Glazing Type 1: Single Pane Clear Glass, Aluminum Frame (1b)		
Layer Material	Thickness	Coating
Clear Glass	0.24 in (6mm)	None
U-factor		6.10 W/m ² ·°C 1.07 Btu/(h·ft ² ·°F)
Shading Coefficient		0.93
Normal SHGC		0.81
Normal Solar absorptance		0.16
Normal Solar Transmittance		0.76
Inside emissivity		0.84
Outside emissivity		0.84
Surface-to-surface thermal conductance		151.7 W/m ² ·°C 26.70 Btu/(h·ft ² ·°F)
Glazing Type 2: Double glazing, Aluminum Frame with thermal break (5a)		
Layer Material	Thickness	Coating
Clear Glass	0.24 in (3 mm)	None
Air gap	½ in (12.7mm)	
Clear glass	0.24 in (3 mm)	None
U-factor		2.86 W/m ² ·°C 0.50 Btu/(h·ft ² ·°F)
Shading Coefficient		0.88
Normal SHGC		0.76
Normal Solar absorptance		0.17
Normal Solar Transmittance		0.70
Inside emissivity		0.84
Outside emissivity		0.84
Surface-to-surface thermal conductance		5.41 W/m ² ·°C 0.95 Btu/(h·ft ² ·°F)
Glazing Type 3: Double glazing, Tinted Low-E Coating, Aluminum Frame with thermal break (21f)		
Layer Material	Thickness	Coating
Bronze	0.24 in (3mm)	None
Air gap	½ in (12.7mm)	
Clear glass	0.24 in (3mm)	Low-E
U-factor		1.76 W/m ² ·°C 0.31 Btu/(h·ft ² ·°F)
Shading Coefficient		0.75
Normal SHGC		0.65
Normal Solar absorptance		0.27
Normal Solar Transmittance		0.59
Inside emissivity		0.84
Outside emissivity		0.84
Surface-to-surface thermal conductance		2.48 W/m ² ·°C 0.44 Btu/(h·ft ² ·°F)

Table 4.4 Thermal and Optical Properties of glass window (Continued)

Glazing Type 4: Double glazing, Tinted Low-E Coating, Aluminum Frame with thermal break (21f)		
Layer Material	Thickness	Coating
Bronze	0.24 in (6mm)	None
Air gap	½ in (12.7mm)	
Clear glass	0.24 in (6mm)	Low-E
U-factor		2.45 W/m ² ·°C 0.43 Btu/(h·ft ² ·°F)
Shading Coefficient		0.45
Normal SHGC		0.39
Normal Solar absorptance		0.61
Normal Solar Transmittance		0.27
Inside emissivity		0.84
Outside emissivity		0.84
Surface-to-surface thermal conductance		1.74 W/m ² ·°C 0.31 Btu/(h·ft ² ·°F)
Glazing Type 5: Double glazing, reflective coated glass, Aluminum Frame with thermal break (5o)		
Layer Material	Thickness	Coating
Bronze	0.24 in (6mm)	None
Air gap	½ in (12.7mm)	
Clear glass	0.24 in (6mm)	Low-E
U-factor		2.50 W/m ² ·°C 0.44 Btu/(h·ft ² ·°F)
Shading Coefficient		0.24
Normal SHGC		0.21
Normal Solar absorptance		0.67
Normal Solar Transmittance		0.11
Inside emissivity		0.84
Outside emissivity		0.84
Surface-to-surface thermal conductance		4.26 W/m ² ·°C 0.75 Btu/(h·ft ² ·°F)

4.2.5 Interior Shade Model

Increasing the solar heat gain augments the RTS method peak-cooling load over prediction. Therefore, here it is intended to investigate interior shading effect on the radiant time series peak cooling load overprediction error. The interior-shading algorithm was implemented based on the approximate shade model developed by Klems (2002). The following assumptions: the glazing is completely shaded, planar, the shade layer is assumed ideally diffuse were used to develop the model. The optical properties

for the three shade types: medium colored Venetian blinds, dark roller shades, and close weave dark color drapery fabric shades were taken from ASHRAE Handbook of Fundamentals (ASHRAE 2005) and are given in Table 4.5.

Table 4.5 Optical properties of shade layers (2005 Handbook of Fundamentals)

Shade element	Optical properties at normal incidence		
	Transmittance	Reflectance	Absorptance
Medium color Venetian blind	0.05	0.35	0.60
Dark Roller shades	0.0	0.20	0.80
Close weave dark color Drapery Fabrics	0.09	0.135	0.775

4.2.6 Radiative / Convective Split

In the past RTSM peak cooling overprediction parametric investigation were conducted with constant radiative / convective splits (Rees et al. 1998; Spitler et al. 1997). Constant 70/30 radiative / convective split for people heat gain is reasonable assumption for the point of view of peak cooling load overprediction. Similarly 30/70 split for office equipment heat gains is conservative estimate. However, for lighting heat gain the radiative / convective split is dependent on the Luminaire type as well (Chantrasrisalai and Fisher 2007a; Chantrasrisalai and Fisher 2007b; Fisher and Chantrasrisalai 2006). Therefore it is of interest to have insight to sensitivity of RTSM peak cooling load overprediction error to radiative / convective splits of lighting heat gain. The parametric investigation has attempted to identify the relative importance of the radiative / convective split on the RTS peak cooling load over prediction for lighting heat gain.

Radiative / convective split recommended for lighting heat gain based on ASHRAE RP-1282 are given in Table 4.6.

Table 4.6 Mean Lighting Heat Gain Parameters from ASHRAE 1282-RP

Luminaires Category	Space Fraction	Radiative Fraction	Convective Fraction
Recessed Fluorescent Luminaires without Lens	0.69	0.58	0.42
Recessed Fluorescent Luminaires with Lens	0.45	0.67	0.33
Downlight Compact Fluorescent Luminaires	0.18	1.00	0.00
Downlight Incandescent Luminaires	0.75	1.00	0.00
Non-In-Ceiling Fluorescent Luminaires	1.00	0.54	0.46

Radiative / convective split of lighting heat gain on the peak cooling load has been investigated. Though, it is important on the peak cooling load prediction, it has little impact on the peak cooling load over prediction error

4.2.7 Solar and Radiant Heat Gain Distributions

In the RTSM and HBM solar and internal radiant heat gains need to be distributed to the surfaces in a zone. The RTSM uses the distribution model for generating the radiant time factors (RTF). The same distribution must be used by the RTSM and HBM to make realistic comparison of peak design cooling loads of these two procedures. In this parametric investigation the transmitted beam solar heat gains is distributed to the floor and internal thermal mass surfaces, 50% each. For transmitted solar diffuse heat gain, short wavelength and long wavelength internal radiant gains area-absorptance product weighted distribution are used.

4.2.8 Design Weather Days

In the RTSM the RTF are generated assuming adiabatic zone. The adiabatic boundary condition is one of the inherent limiting assumptions of the RTSM. On the other hand, the HBM models the building envelope interaction realistically by solving the inside and outside surfaces heat balance equations along with zone air heat balance equations simultaneously using the actual weather data as boundary conditions. Therefore, the RTSM peak-cooling load over prediction shows sensitivities to the peak design outdoor air temperature. Higher design weather temperature (relative to the room design temperature) tends to offset parts of effects of the adiabatic boundary condition assumption; hence, results in smaller RTS peak cooling load over prediction. On the other hand, colder design weather tends to yield higher RTSM peak cooling load over prediction. The RTSM peak cooling load overprediction error also varies across the year primarily due to variation of the peak design temperature and intensity of solar incident. The time of occurrence of annual peak design cooling load depends on many design parameters primarily on: window glazing fraction, fenestration type, construction type, zone orientation, site location, design weather conditions, internal heat gain loadings and infiltration. Mostly for variety of design weather and zone locations the annual peak design cooling load occurs from June to September, but for south facing zones with large amount of glazing for lower end of the latitude angles of the USA locations such as: Atlanta, and Miami with warm winter weather the annual peak design cooling load may occur in November and December due to low solar elevation angles. Fourteen USA representative climate regions were selected for this investigation. Each location uses the

1% ASHRAE design day weather data for seven monthly design weather days from June to December. The fourteen US weather site locations are given in Table 4.7

Table 4.7 Design weather conditions for the fourteen USA locations

Location	Latitude Angle (degree)	Longitude (degree)	Time Zone (hours)
Albuquerque, New Mexico	25.03	106.62	7
Baltimore, Maryland	39.17	76.67	5
Boise, Idaho	43.57	116.22	7
Burlington, Vermont	44.47	73.15	5
Chicago, Illinois	42.00	87.77	6
Duluth, Minnesota	46.82	92.17	6
El Paso, Texas	31.78	106.40	7
Fairbanks, Alaska	64.82	147.87	9
Houston, Texas	29.97	95.37	6
Memphis, Tennessee	35.03	89.97	6
Miami, Florida	25.70	80.27	5
Phoenix, Arizona	33.42	112.02	7
Atlanta, Georgia	39.77	104.87	7
Denver, Colorado	33.65	84.42	5

4.3 Methodology: HBM and RTSM Implementation

The purpose of this parametric investigation is to come up with quantitative characterization of the original RTSM peak cooling load likely overprediction trend compared to the HBM, which uses the most rigorous and fundamental mathematic algorithms. It is not straightforward task to generalize the RTSM peak-cooling load over prediction error when it depends on several building design parameters. Therefore it of interest to define the RTSM peak design cooling loads over prediction error. Here it is defined as the deviation of the RTSM annual peak design-cooling load from that of the HBM. The annual peak design-cooling load is taken as the maximum of the peak-cooling load computed for the hot months of the year from June to December. In the RTSM as a load calculation procedure we are interested on the annual peak design cooling loads. Thus, to encompass possible design conditions the annual peak design cooling loads of the RTSM and HBM were computed for a wide range and different combination of nineteen building design parameters.

The RTSM annual peak design cooling load overprediction error were determined using fully populated parametric run to establish the general overprediction trend for a range of building design parameter such as: glazing type, glazing fraction, design weather, zone location, construction fabric, internal heat gains, schedules, infiltration rates, furniture thermal mass and aspect ratio and interior shades. Furthermore, sensitivity of the maximum error of the RTS annual peak design-cooling load was investigated for other design parameters: internal heat gain rates, radiative / convective split, carpeting and interior shade effects. The following section describes the basic features and component models of the HBM and RTSM utilized in the parametric run tool.

4.3.1 The HB Method Code

For the heat balance method the standalone Fortran program HVAC load explorer engine, which was originally developed by (Pedersen 1997) for ASHRAE RP-875 was used. For the HBM detailed fenestration model developed by Klems (2002) were used. This fenestration model computes the optical properties of the glazing system from the individual layer optical properties. Klems's fenestration model allows incorporating the internal shading as an additional glazing layer with some simplifying approximations. The detailed fenestration model implemented in the parametric investigation tool improves the accuracy of the analysis and allows modeling various glazing types more accurately. Moreover, the RTSM peak cooling load over prediction errors are primarily related to solar heat gain treatment; hence, the accuracy of the fenestration model is essential. The structure of the HBM program is given in Figure 4.3. The HBM sub-models used in the parametric investigations are given Table 4.8.

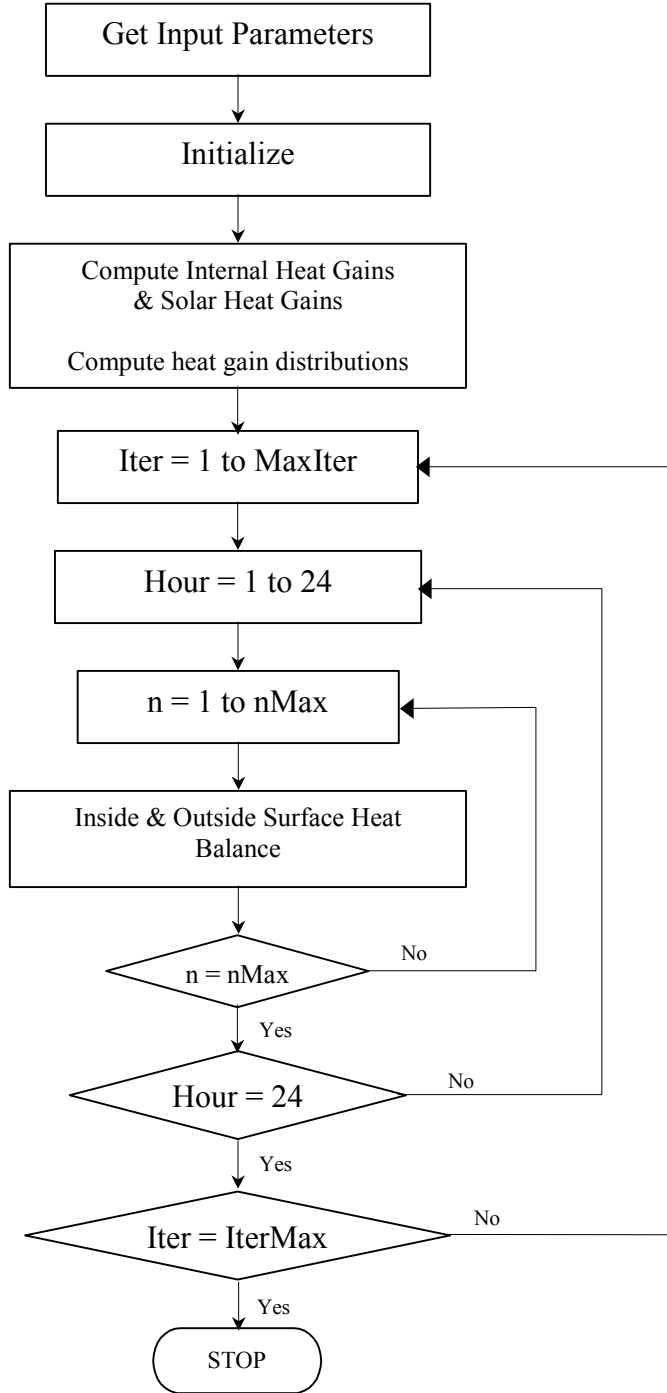


Figure 4.3 Structure of Heat Balance Method for a Zone

4.3.2 The RTS Method Code

The Radiant time series method (RTSM) load calculation procedure, which is regarded as a two-step process, is depicted in Figure 6.4 showing the different components of the heat gain and the sequence of the procedure. In the parametric run the RTSM and the HBM use the same input file generated using by the parametric run generator. The radiant time series method uses the radiant time factors computed using the New RTF Engine described in Section 3.1.

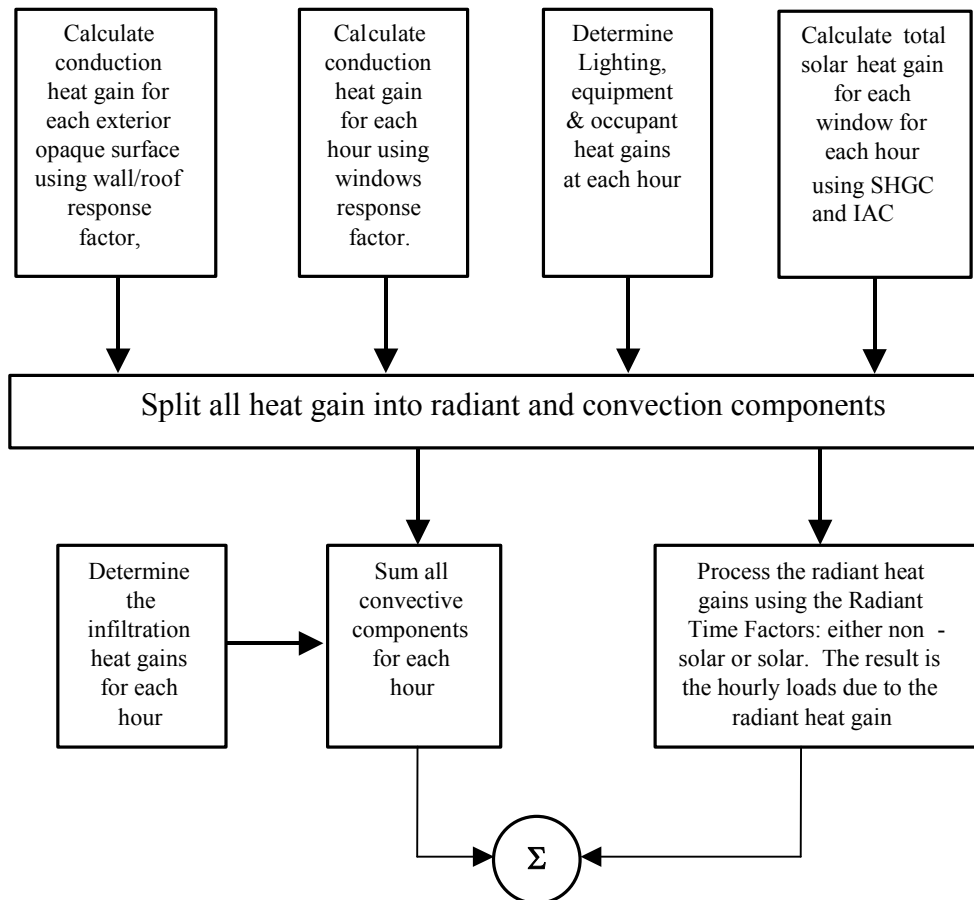


Figure 4.4 The current RTSM cooling load calculation procedure represented as flow diagram

4.3.3 The RTSM and HBM Models Comparison

The heat balance and radiant time series methods use component model to represents the different physical processes in the zone models. The major component models for the HBM and RTSM are described in Table 4.8.

Table 4.8 RTSM and HBM component models

Models	HBM	RTF Generation	RTSM
Solar Irradiance	ASHRAE clear sky model	-	ASHRAE clear sky model
Internal Solar Distribution	Beam Solar: 50% to the floor and 50% to the furniture. Diffuse Solar: area-absorptance product weighted.	Beam Solar: 50% to the floor and 50% to the furniture.	Solar-RTF
Internal Radiant Gain Distribution	Short and Longwave radiation: area-absorptance product weighted.	area-absorptance product weighted.	Non-solar RTF
Outside Boundary condition:	Outside air temperature. The ground surface assigned the outdoor air temperature. Blast sky temperature model.	-	Sol-air temperature
Inside Convection Coefficients	Fixed coefficients: Walls: ▪ $h_c = 4.68$ (W/m ² K) Floor: ▪ $h_c = 4.37$ (W/m ² K) Ceiling: ▪ $h_c = 1.25$ (W/m ² K)	Fixed coefficients: Walls: ▪ $h_c = 4.68$ (W/m ² K) Floor: ▪ $h_c = 4.37$ (W/m ² K) Ceiling: ▪ $h_c = 1.25$ (W/m ² K)	Combined conductance $h_{combined} = 8.3$ (W/m ² K)
Outside Convection Coefficients	$h_c = 17.03$ (W/m ² K)	-	$h_{combined} = 22.03$ (W/m ² K)
Inside Longwave Radiation Model	MRT / Balance (Walton, 1980)	MRTNet (Carroll, 1980)	Surfaces radiating to room air
Fenestration Model	Detailed Model (Klems, 2002)	-	Solar Heat Gain Coefficient
Interior Shade Model	Detailed Model (Klems, 2002)	-	Interior Attenuation Coefficients

4.4 Results and Discussion – Original RTSM

The objective of this chapter is to examine the RTSM annual peak design cooling load prediction performance relative to the HBM using parametric run tool over wide range and combinations of nineteen different building design parameters shown in Table 6.1. The parametric values and level were selected based on typical design values for internal heat gains, schedules, aspect ratio and glazing types, light and heavyweight for construction fabrics, and exterior facade glazing fractions. Furthermore, detailed parametric investigation of the effect of internal heat gain rates and radiative / convective splits for lighting heat gains was conducted.

The RTSM annual peak design cooling load error was established based 376,320 cases of parametric runs for each of the glazing types investigated. Seven months of design day weather were used for each of the fourteen USA weather locations. The RTSM annual peak design cooling load over prediction trend was investigated for typical internal heat gain values (10 people per 100m² occupancy level, 20 W/m² light heat gain intensity and 30 W/m² equipment heat gain loading) and fixed radiative / convective splits. The original RTSM annual peak design cooling load error shows strong correlation to building design parameters that lead to higher solar heat gain such as: glazing fraction of exterior facade, glazing type, number of exterior facades, peak design temperatures, and zone locations. The over prediction trend is also affected by the outdoor air design temperature. Colder design weather increases the over prediction, and hotter design weather tends to decrease the over prediction trend.

The annual peak design-cooling load for the most of the USA occurs in the months from July to September. Though, some weather locations and zones with large glazing facing south may peak in the months from October to December.

4.4.1 RTSM Peak Design Cooling Load Prediction

The RTSM annual peak cooling load over-prediction trend has been investigated, the primary building design parameters contributing to the over prediction has been examined, and the maximum annual peak design cooling load over prediction error of the RTSM for the USA locations has been established.

The analysis presented here demonstrates the sensitivity of the RTSM annual peak design-cooling load over prediction to the different building design parameters. Also explains the relative importance of the design parameters to the RTSM peak-cooling load over prediction. Then establishes the RTSM annual peak-cooling loads maximum over predictions. The effects of building design parameters that have primary effect on the RTSM peak cooling load over prediction: glazing fraction of exterior facade, glazing type, number of exterior facades, peak design temperature, zone location, and construction fabrics, are presented next.

RTSM over Prediction Sensitivity Analysis

The RTSM peak cooling load over prediction sensitivity to different building design parameters has been investigated to establish extreme over prediction limits. The sensitivity analysis helps to establish the relative importance of the building design

parameters on the RTSM over prediction. It has been established that RTSM cooling load over prediction primarily depends on the treatment of solar and internal heat gains. In the following analysis the relative contributions of the different building design parameters to the peak cooling load over prediction error is presented.

Glazing Type

The effect of glazing type on the RTSM over prediction of peak cooling load is demonstrated for a lightweight construction zone with exterior surface in north and east facade for a building located in Atlanta, Georgia. The peak-cooling load over prediction error differences between the glazing types progressively increases with glazing fraction. The over prediction difference between single and double pane clear glasses for 90% glazing fraction can be as much as 13.2%. Based on annual peak design cooling load for Atlanta, Georgia, the extreme peak cooling over prediction for zones with two exterior facades for single pane clear glazing is under 29% at 90% glazing fraction. The higher peak cooling load over prediction error of the RTSM for single pane clear glazing is due to large amount of solar heat gain and conservation of the entire heat gain. However, the HBM may allow part of the radiant heat gain to be conducted back out depending on glazing conductance and temperature difference between outside and inside air temperature. Similar trend is observed for other locations as well but the extent of over prediction depends on the outdoor air temperature for the same building design parameters.

Number of Exterior Facades

The RTSM peak cooling load over prediction error has been examined using lightweight construction zone with single exterior facade for single pane clear glass for two extreme weather locations: Phoenix, Arizona, and Fairbanks, Alaska. The RTSM peak-cooling load over prediction shows dependency on the zone exterior facade orientation for zones with single exterior facade. In general zones facing east and west directions have higher peak cooling load over prediction error compared to south and north facing zones due to large amount of solar heat gains. Depending on the facing direction of the exterior facade the RTSM peak cooling over prediction error may vary between 6 to 12% for zones with single exterior surface at 90% glazing fraction for single pane clear glass. The peak cooling load over prediction for locations with warm design weather condition like Phoenix, Arizona is less by as much as 5% compared to colder design weather location like Fairbanks, Alaska for zones with east and west exterior facades. In the case of zones with south facing exterior facades the over prediction is strongly dependent on the latitude angle as well. Phoenix, which has warm design weather the RTSM over prediction, is less from that of Fairbanks by 2% only. In Fairbanks, Alaska, south facing zones have their peak-cooling load in July. The north facing zones generally has the least peak-cooling load over prediction error compared to any other orientations for zones with single exterior facade.

Peak Design Temperature and Latitude

The RTSM peak-cooling load over prediction also depends on the peak design temperature. The RTSM peak-cooling load depends on the difference between the

outdoor air and indoor air temperatures. In general lower peak design temperatures have higher peak cooling load over prediction error. For zones with two exterior facades the effect of peak design temperature may bring as much as 6% difference on the peak cooling load over prediction between the warmest and coldest summer cooling design weather conditions for the USA for 90% exterior facade glazing fraction. The latitude affects the amount of solar heat gain and hence the RTSM peak cooling loads over prediction error but has secondary effect for zones with two exterior facades. Zones with two adjacent exterior facades the RTSM annual peak design cooling loads over prediction primarily depends on peak design temperature. Peak cooling load over predictions are almost the same for locations with similar design weather conditions but the amount of peak cooling could be different. For instance for a north east zone in Chicago and Atlanta with peak design temperatures of 35.8°C and 34.8°C for the month of July, respectively, their RTSM annual peak cooling load over prediction error closely match at all glazing fractions though there is significant latitude difference.

Construction Fabrics

The RTSM peak-cooling load over prediction has been investigated for lightweight and heavyweight construction zones with single pane clear glazing. On average for the original RTSM peak-cooling load lightweight construction zones over predicted by as much as 3% to 4% higher than that of the heavyweight lightweight construction zones.

The sensitivity analysis has shown that the RTSM annual design peak cooling load over prediction error primarily depends on: glazing fraction, glazing type, zone orientation, number of exterior surfaces, peak design temperature, and construction fabric. The former four building design parameters control the amount of solar heat gain. A secondary effect dependency was also observed on internal heat gain schedule and furnishing thermal mass.

The RTSM peak-cooling load for a given zone and weather location depends on the month at which the load is calculated. The RTSM as peak load calculation procedure is intended for sizing equipments and hence our primary interest should be the annual peak-cooling load. In order to establish the maximum RTSM over prediction limit, the error analysis should be based on the annual peak-cooling load. Therefore, the annual RTSM peak cooling load needs to be determined for the fourteen USA weather locations. The following section defines the basis for the annual peak cooling load calculation for the different weather locations and typical design condition.

RTSM Annual Peak Design Cooling Load

The RTSM annual peak cooling load error sets the maximum design cooling load error expected for a given design weather at annual peak design cooling load computed over a range of combination of several building design parameters such as: zone location, internal heat gain loadings, construction fabrics, fenestration type, glazing fractions of exterior facade, infiltrations, schedules and aspect ratio. The annual peak design-cooling load does not necessarily occur on the warmest month of the year. The combined effect

of peak design temperature, exterior faced orientation and latitude of the location determines the peak cooling load and the time of occurrence. In particular for zones with south facing exterior facade and for lower end latitude (e.g. Atlanta, Georgia, and Phoenix, Arizona) that have warm winter design temperatures the peak cooling load may occur in October and November. Table 4.9 shows the annual peak cooling load occurrence months for zones with different orientation and number of exterior facades. Some zones have multiple peak months depending on the glazing fractions.

Table 4.9 Month of Annual Peak Cooling Load for zones with single pane clear glass

Site Location	Annual Peak Cooling Load Months			
	South East	South West	North East	North West
Zone with two adjacent exterior facade				
Phoenix	7,8,9	7,8,9	7	6,7
Chicago	7,9	7,8	7	7
Atlanta	7,8,9	7,8,9	7	7
Fairbanks	7	7	6	6
Zone with single exterior facade				
Phoenix	9,10	7	6	7
Chicago	8,9,10	7	7	7
Atlanta	8,9,10,11	7	7	7
Fairbanks	7,8	6	6	6

In this investigation, the RTSM peak-cooling load errors were calculated based on annual peak design cooling load for the fourteen USA locations. The original RTSM annual peak-cooling load has been analyzed based on the combinations of the nineteen building design parameters making a total of 376,320 cases parametric run for each glazing type. The annual peak cooling load from the above data set is only fourteen locations, eight zones and ten glazing fraction (making a total of $14 \times 8 \times 10 = 1120$ cases). The parametric run required is 1120 cases only but we cannot determine the annual peak cooling load

month without running the 98 design weather days and other ranges of building design parameters. The annual peak design-cooling loads plot selected from the entire data set for single pane clear glass is shown in Figure 4.5.

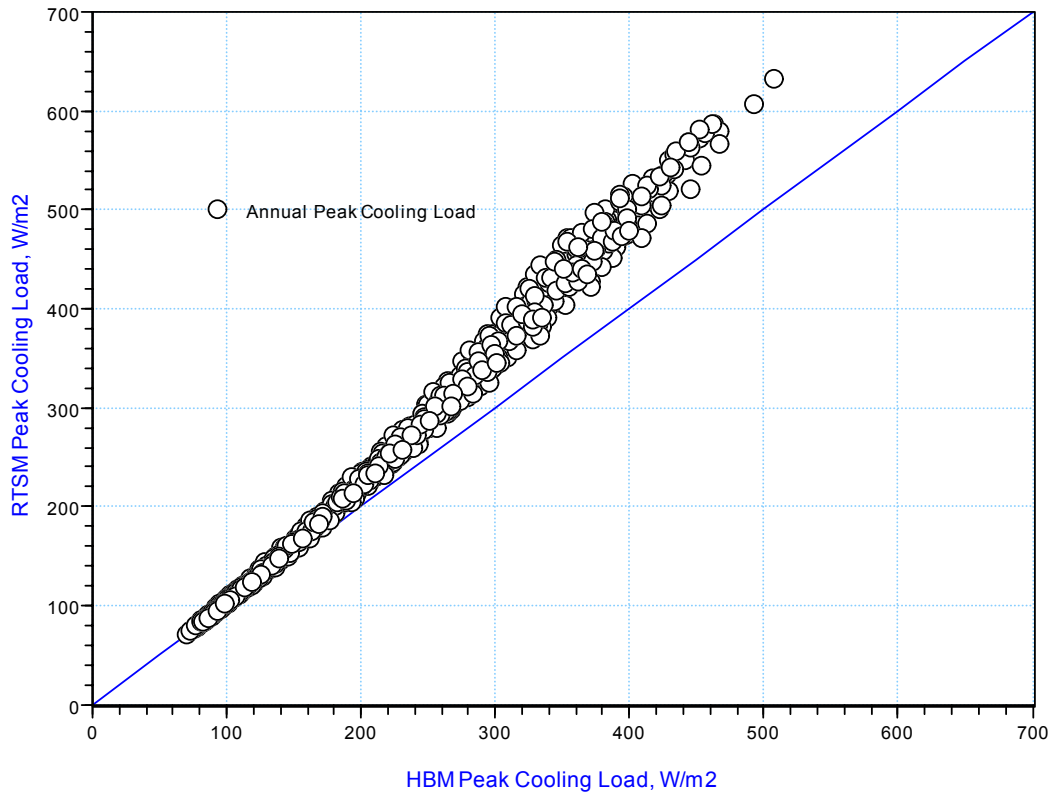


Figure 4.5 RTSM annual peak cooling load versus the HBM for the USA weather locations for single pane clear glass

A similar peak cooling loads plot is shown for double pane clear glass and low-e glass in Figures 4.6 and 4.7, respectively. Based on annual peak cooling load analysis the RTSM extreme over prediction error is fewer than 16% and 12% for double pane clear glass and low-e glass, respectively.

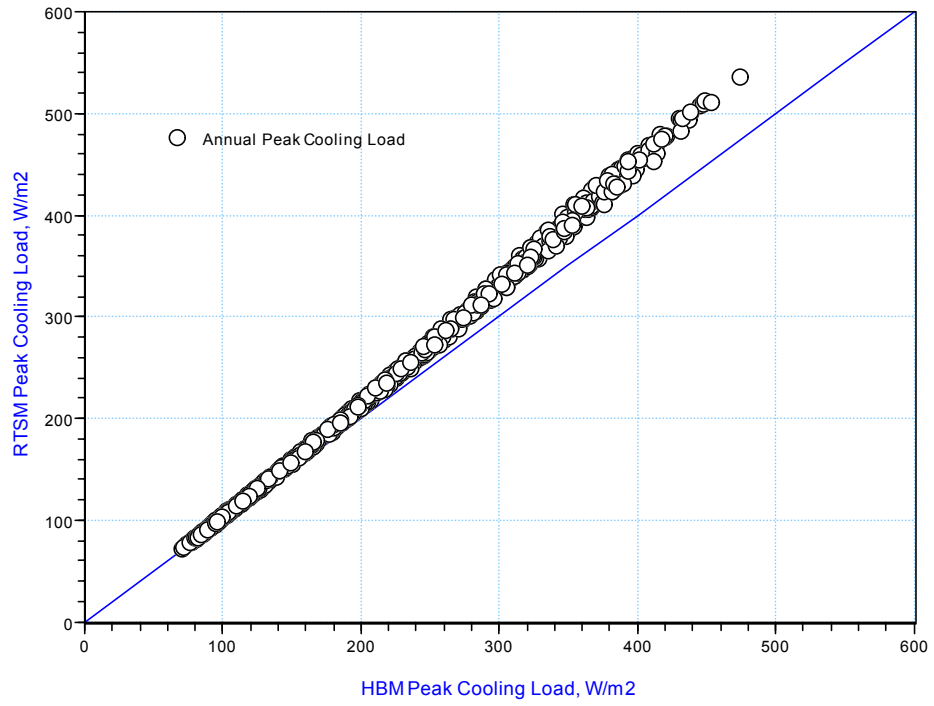


Figure 4.6 RTSM annual peak cooling load versus the HBM for the USA weather locations for double pane clear glass

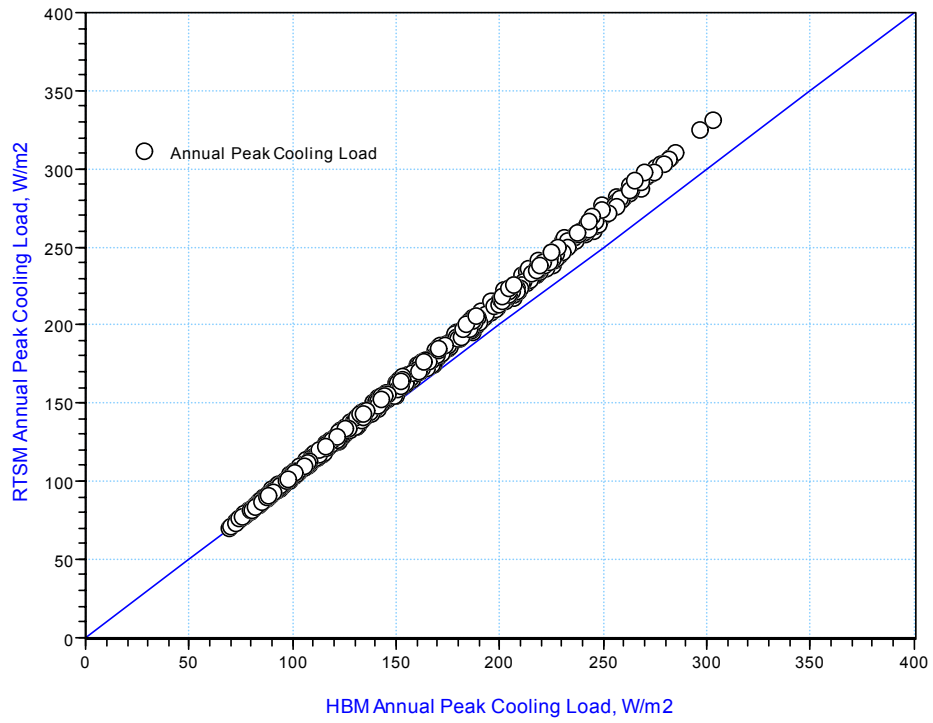


Figure 4.7 RTSM annual peak cooling load versus the HBM for the USA weather locations for double pane low-e glass

The maximum RTSM over prediction errors were determined from the annual peak cooling loads of the fourteen USA weather locations for each glazing type. The maximum RTSM peak cooling load over prediction errors plot against glazing fraction for the three glazing types investigated are shown in Figure 4.8. The extreme RTSM annual peak load over prediction error for zone with two exterior facade and 90% glazing fraction was found out to be 33.5%. The RTSM as design cooling load calculation procedure should be applied carefully for zones with single pane glazing system. If the acceptable over prediction limit were to be set 10% the RTSM can only be used for zones with maximum glazing fraction of 18% for zones with two exterior facades.

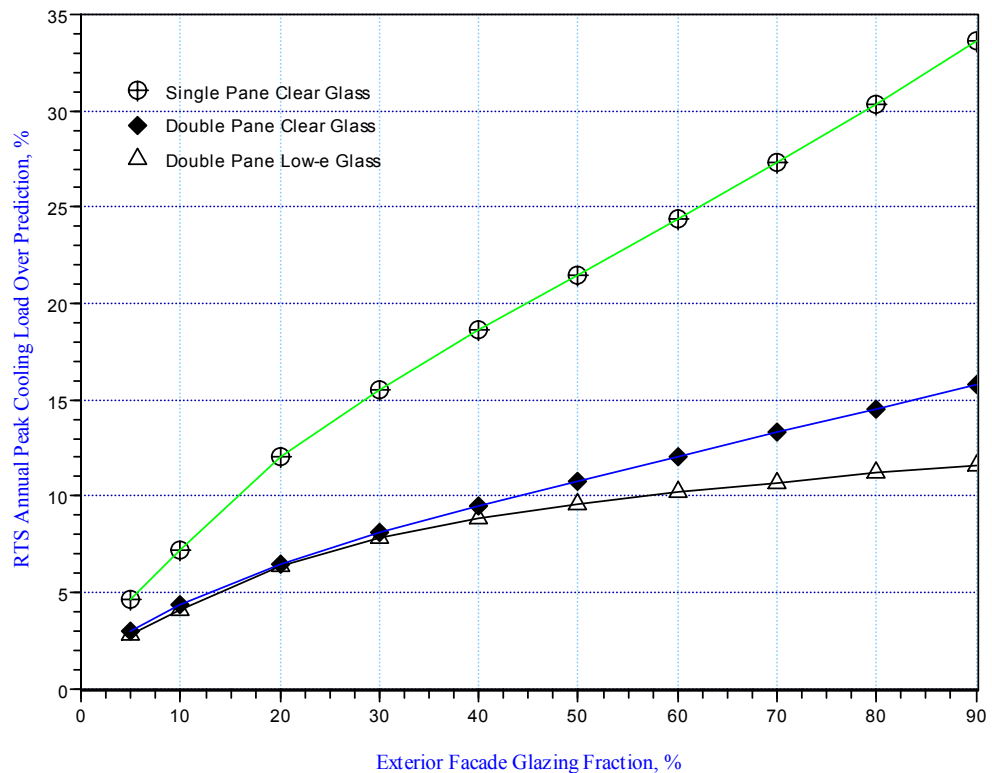


Figure 4.8 Extreme RTSM peak cooling load over prediction against glazing fraction for the three glazing types

In general the RTSM predicts the annual peak-cooling load accurately for zones with double pane-glazed windows compared to single pane. The maximum RTSM annual peak-cooling load over prediction is well below 16% for all glazing fractions. For zones with single exterior facades facing any direction the RTSM maximum over prediction is much below 10% for glazing fraction up to 90%. For zones with two exterior facades and double pane windows the RTSM predicts the annual peak cooling load within 10% of the heat balance method provided the glazing fraction is kept fewer than 45%.

The RTSM as a peak design cooling load calculation procedure performs reasonably for double pane low-e fenestration systems for all grazing fraction levels up to 90% with maximum over prediction limit of 12.0%. The maximum annual peak-cooling load over prediction limit of the RTSM procedure can be kept under 10% provided the glazing fraction is fewer than 60%.

4.4.2 Conclusions and Recommendations

The original RTSM annual peak design cooling load maximum over prediction trend has been established using parametric investigation for three fenestration types and range of building design parameters using fourteen USA weather locations. This investigation was intended to determine limitations of the RTSM and develop design guidance for practicing engineers. 376,320 building zone parametric runs were conducted for each glazing type to determine the maximum RTSM annual peak-cooling load over prediction errors. The following conclusion can be drawn based on the parametric investigation conducted here:

- For the USA weather condition the maximum RTSM annual peak design cooling load over prediction for zones having two adjacent exterior facades with 90% glazing fraction single pane clear glass windows can be as much as 33.5%. This corresponds to weather condition of the month of July in Fairbanks, Alaska. All other locations, which have warmer design weather conditions over predict less.
- For zones with single exterior facade either in the East or West facing direction the maximum over prediction can only be as high as 26.0% for single pane clear glass with 90% glazing. The maximum over prediction for zones with single exterior facade viewing south or north and 90% glazing fraction can be as much as 16.5% and 8.6%, respectively. Zones with single exterior facade facing south can predict the annual design cooling load within 10% of the heat balance method provided the single pane window glazing fraction is kept fewer than 75%. Zones with east or west facing exterior facades for single pane glass windows the RTSM can predict the annual peak design cooling load within 10% of the heat balance method provided the glazing fraction is less than 35%. Similarly for zones with two exterior facades the glazing fraction should be kept under 28%.
- In general the RTSM performs well for double pane clear glass fenestration systems. The RTS method over prediction of annual peak design cooling load is below 12% for one and two exterior facades and glazing fraction levels up to 90%. For zones with two adjacent exterior facades and double pane clear glass the RTSM can predict the annual peak design cooling within 11% of the heat balance method if the glazing fraction is kept less than 50%. Zones with single exterior facade viewing east or west the RTS method can predict the annual peak

cooling load within 9% of the heat balance method for glazing fractions up to 50%. Similarly zones with south or north facing exterior facades maximum over prediction of annual peak cooling load by the RTS method is under 5% for all glazing fraction levels up to 90%.

- The RTSM over predicts the annual peak design cooling loads fewer than 11% for zones with double pane low-e glazing up to 90% glazing fractions. The RTS method maximum over prediction of the annual peak cooling load can be kept under 10% for two exterior facade zones provided the glazing fraction is limited to 55%. Zones with single exterior facade in the south and north facing direction the RTS method predicts the annual peak cooling load by as much as 8.2% and 3.1%, respectively, for 90% glazing fractions.
- The RTSM annual peak-cooling load over prediction correction factor has been introduced. The correlation coefficients vary depending on number of exterior facade and zone locations. The correction predicts the annual peak-cooling load with $\pm 6\%$ of the heat balance method for single pane clear glass fenestration system for two exterior facade zones.
- Radiative / convective split of lighting heat gain on the peak cooling load has been investigated. Though, it is important on the peak cooling load prediction, it has little impact on the peak cooling load over prediction error.

4.5 Results and Discussion – Current and Improved RTSM

The performance of the current and improved RTSM procedures in predicting the peak cooling loads has been established using wide range parametric runs and the recommended radiative / convective splits given in Table 3.5. The maximum and average peak cooling load over predictions for both current and improved RTSM procedures has been established for use as a design guidance. The parametric investigation has been run using the parameters range and levels given in Table 4.1. Four sets of parametric runs were conducted – two for current RTSM and two for improved RTSM. The two parametric runs for each procedure represent fenestration with and without interior shades. The number of parametric runs for each test was limited to 716,800 zones to optimize the computational resource requirements. The nineteen parameters combination for fenestration without interior shade include: four top floor corner zones, two levels of construction fabrics one for lightweight and another for heavyweight for each of surface constructions exterior (type 1 and type 6), partition (type 1 and type 2), roofs (type 1 and type 2) and floor surfaces (type 1 and type 4), five glazing types, ten glazing fractions (5%, 10%, 20%, 30%, ..., 90%), three aspect ratios (0.5, 1.0 and 2.0), two levels of thermal mass (type 2 and type 7), two types of load schedules (type 1 and type 6), and eight representative US weather locations (Burlington, Chicago, Duluth, Fairbanks, Denver, Miami, Phoenix and Atlanta) with seven months of design day data from June to December for each location making 56 design days weather. The remaining parameters were: typical internal (people, lighting and equipment) heat gain levels, typical infiltration rate of 0.5 ACH, and east-west axis size of 6m was used. For the fenestration with interior shade a dark roller shade, which has zero transmittance,

was used. The dark roller shade was selected because it showed the highest tendency for over prediction compared to the other two interior shades given in Table 4.4. A total of 2,867,200 test case parametric runs were conducted. Two sets of annual peak cooling load were extracted for each of the four test cases – one for lightweight and another for heavyweight. Each set has four zones, ten glazing fraction and eight locations making a total of 320 annual peak cooling loads. The maximum over prediction for each glazing type, construction type, glazing fraction and zone location / orientation were selected for each of the four test cases to establish the maximum annual peak cooling load prediction performance of the RTSM procedures. The next section presents the results for fenestration without interior shades and then followed by fenestration with shades.

Application without Interior Shades

The RTSM peak cooling loads maximum and average over predictions for current and improved procedures for zones without interior shaded fenestration have been established are shown in Figures 4.9 and 4.10. For 716,800 zones without interior shaded fenestration, the current RTSM procedure peak cooling over predictions can be as high as 30.5% while it is reduced to 10.5% for improved RTSM procedure. These occur for zones with two exterior facades and with single pane clear glass at 90% glazing fraction. The maximum and average over predictions were estimated from 71,680 zones for each of the ten glazing fractions. The maximum over predictions for improved RTSM was 11.7%. This occurred for zones with two exterior façade surfaces, double pane reflected coated glazing at 90% glazing fraction. Summary of the maximum over predictions for the five glazing types without interior shades are given in Table 4.10.

Table 4.10 RTSM peak cooling load extreme over prediction for glazing without shade

Glazing Types	Current RTSM Extreme Over Prediction, %		Improved RTSM Extreme Over Prediction, %	
	Lightweight Construction	Heavyweight Construction	Lightweight Construction	Heavyweight Construction
Single Pane Clear Glass (SHGC =0.80)	30.4	28.2	10.5	8.3
Double Pane Clear Glass (SHGC =0.76)	14.0	13.1	5.9	6.9
Double Pane Low-e Glass (SHGC =0.65)	8.5	7.8	4.1	5.8
Double Pane Low-e Glass (SHGC =0.39)	10.4	7.9	6.0	5.7
Double Pane Reflective Coated Glass (SHGC =0.21)	18.5	14.5	11.7	9.0

The peak cooling load over prediction levels for the current and improved RTSM do not show distinct range for light and heavy weight construction zones for glazing without interior shades. One reason is for this that the solar transmission into the space does not depend or has little dependence on the inside surface temperatures. Hence the extent of over prediction is similar for all construction types; however, it depends on the glazing type. The dependency of the over prediction on the glazing type partly comes from the amount of absorbed fraction in the total solar heat gain. The RTSM peak cooling load versus the HBM peak cooling loads shown in Figures 4.11 and 4.12 have similar trend for all construction fabric. It is evident from this that the radiant fraction for solar heat gains should be only function of glazing type for fenestration without interior shade.

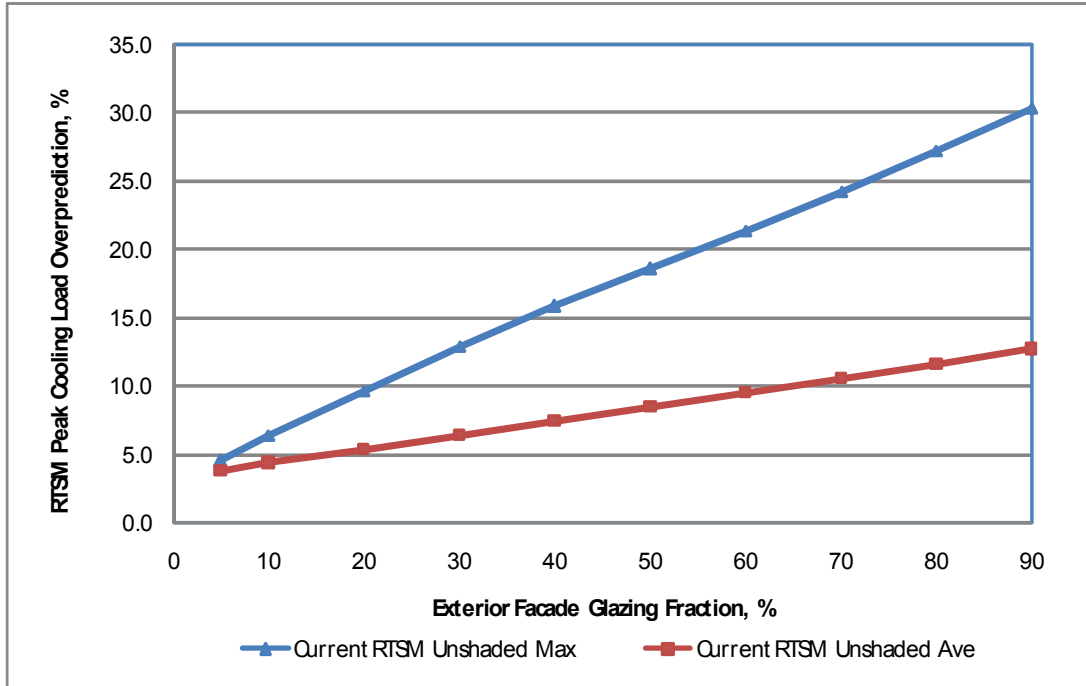


Figure 4.9 Current RTSM annual peak-cooling load maximum and average over prediction for zones without interior shade fenestration

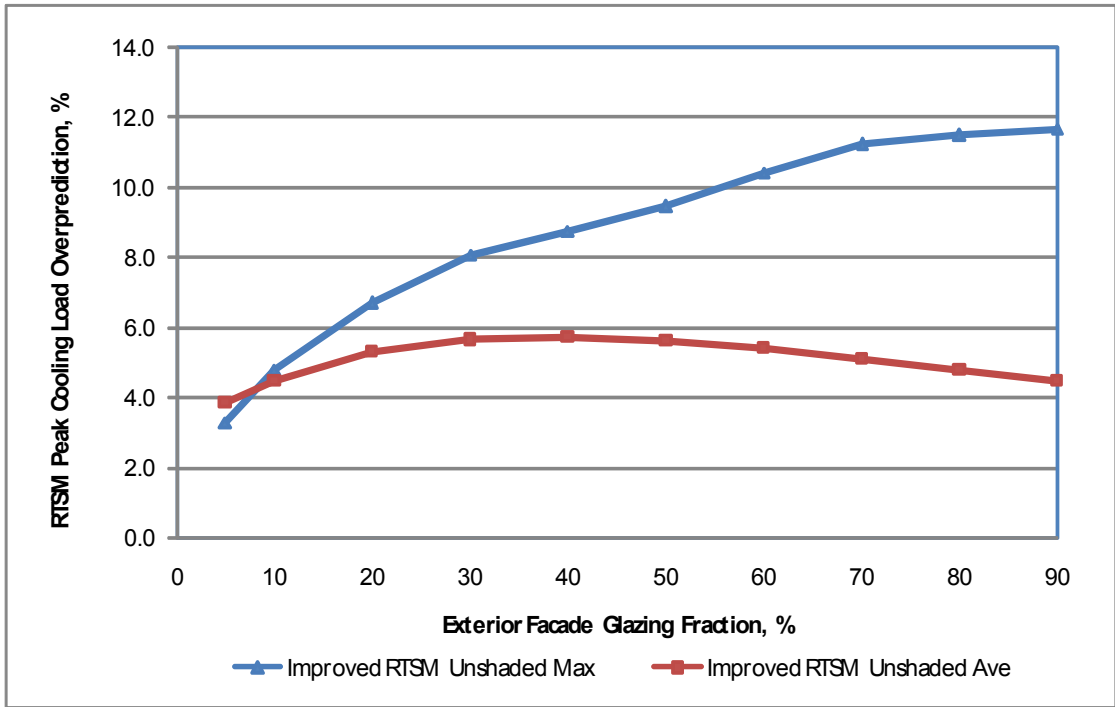


Figure 4.10 Improved RTSM annual peak-cooling load maximum and average over prediction for zones without interior shade fenestration

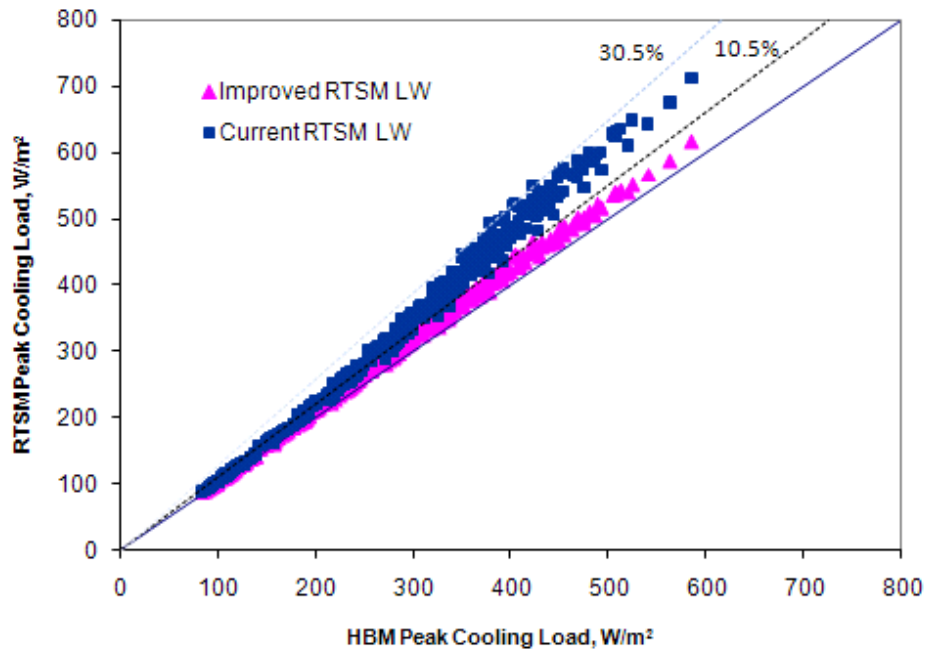


Figure 4.11 Current and Improved RTSM annual peak-cooling load versus HBM for lightweight zones with single pane clear glass without interior shade

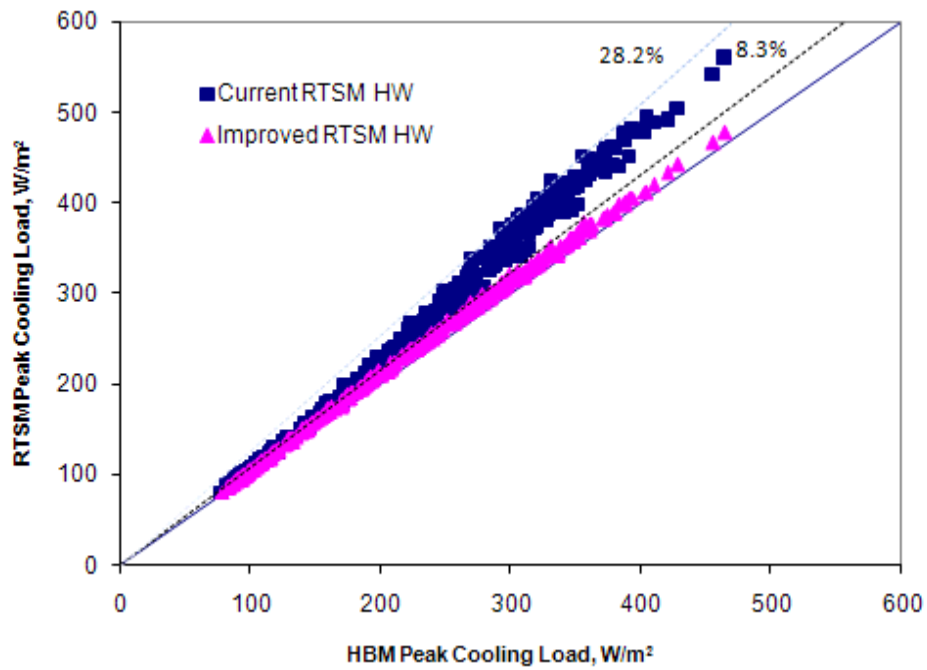


Figure 4.12 Current and Improved RTSM annual peak-cooling load versus HBM for heavyweight zones with single pane clear glass without interior shade

Application with Interior Shades

The maximum peak cooling load over predictions for current and improved RTSM procedures for zones with interior shaded fenestration are shown in Figures 4.13 and 4.14. Summary of the maximum over prediction for different glazing types are shown in Table 4.11. The heavyweight construction zones peak cooling load over prediction is two to three times the value for lightweight zones with single pane and double pane clear glass. Similar trend is observed for glazing types with SHGC less than 0.5 but the difference between the light and heavy weight zone peak cooling loads over predictions are moderate. The RTSM versus HBM peak cooling loads plot shown in Figures 4.15 and 4.16 indicate that the peak cooling load over prediction depends on zone construction fabrics. The sensitivity of the RTSM over prediction to construction type is primarily due to the use of a fixed radiative fraction for all zone construction types. The over predictions for zones with interior shaded fenestration tend to be higher for heavyweight zones than lightweight by 2% - 12% depending on the glazing type.

Table 4.11 RTSM peak cooling load maximum overpredictions for glazing with interior shade

Glazing Types	Current RTSM Extreme Over Prediction, %		Improved RTSM Extreme Over Prediction, %	
	Lightweight Construction	Heavyweight Construction	Lightweight Construction	Heavyweight Construction
Single Pane Clear Glass (SHGC =0.80)	6.4	17.2	3.0	13.2
Double Pane Clear Glass (SHGC =0.76)	7.1	19.9	4.8	17.1
Double Pane Low-e Glass (SHGC =0.65)	7.3	19.6	5.7	17.7
Double Pane Low-e Glass (SHGC =0.39)	8.2	14.2	6.1	11.7
Double Pane Reflective Coated Glass (SHGC =0.21)	11.4	14.2	8.6	11.1

The RTSM peak cooling load overprediction sensitivity decreases for low SHGC glazing types. In general the RTSM peak cooling loads over prediction is smaller when the fenestration has interior shades due to reduction in the amount of solar heat gain. The maximum over predictions of the current and improved RTSM procedures for 716,800 zones with interior shade fenestration are 19.9% and 17.7%, respectively. For current RTSM procedure the maximum over predictions occur at 90% glazing fraction of the exterior facade surfaces. The average overprediction of the current RTSM procedure for zones with interior shade fenestration based on 71,680 zones at 50% and 71,680 zones at 90% glazing fractions are 10.3% and 12.8%, respectively. The improved RTSM procedure reduces the average over predictions of peak cooling load for these 71,680 zones to 8.6% and 9.8%, respectively.

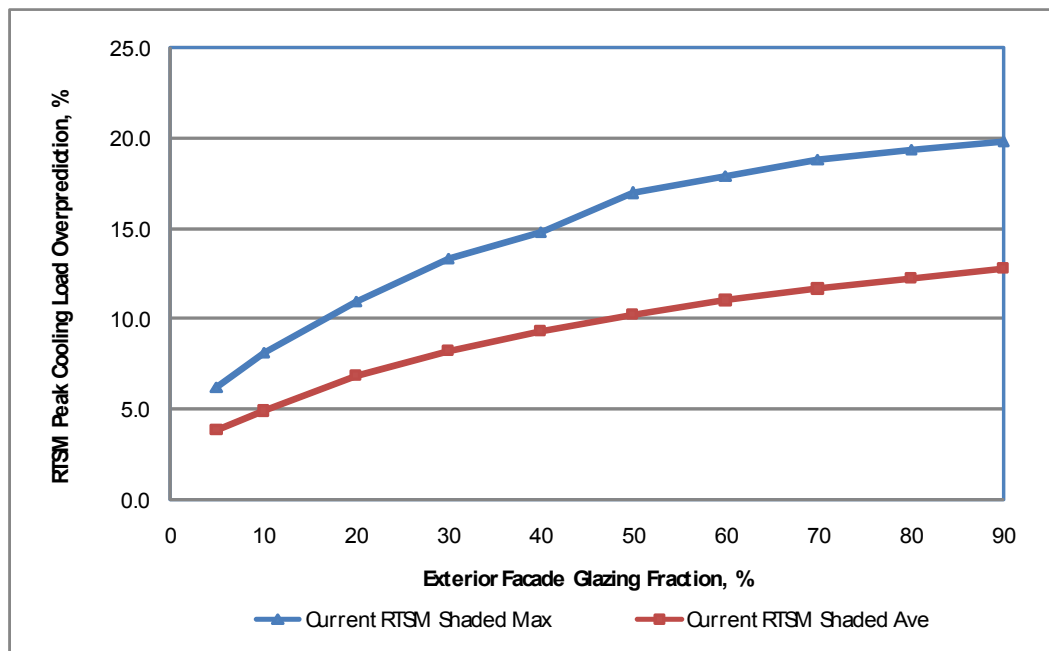


Figure 4.13 Current RTSM annual peak-cooling load maximum and average over prediction for zones with interior shaded fenestration

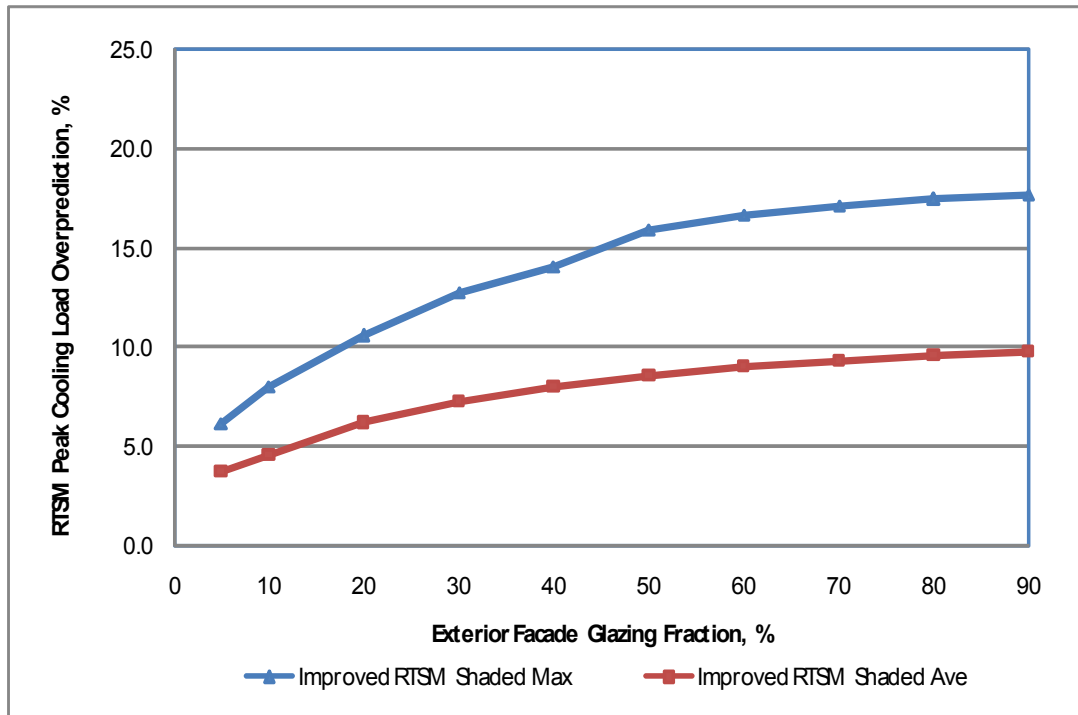


Figure 4.14 Improved RTSM annual peak-cooling load maximum and average over prediction for zones with interior shaded fenestration

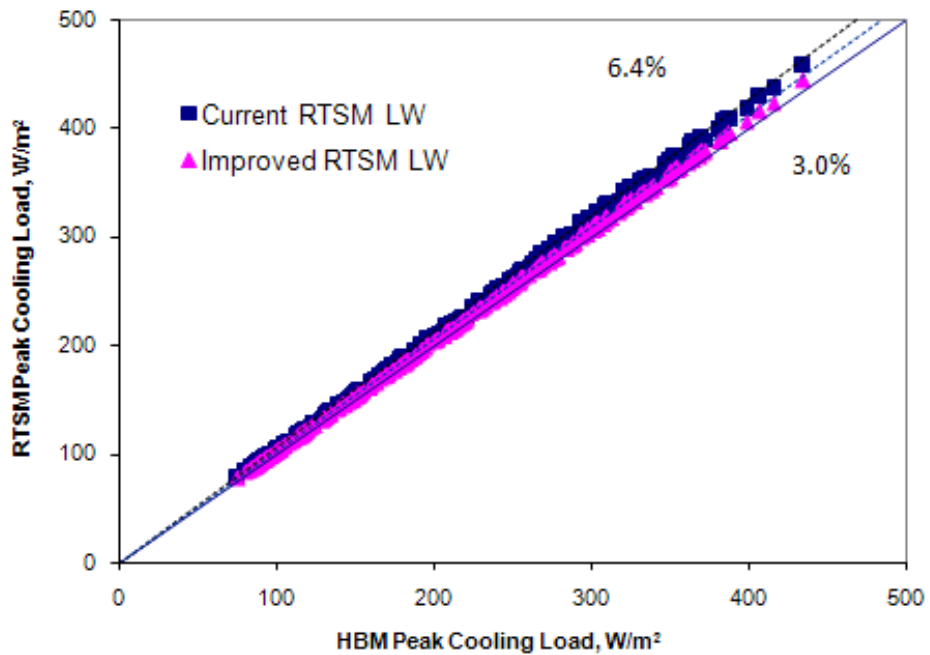


Figure 4.15 Current and Improved RTSM annual peak-cooling load versus HBM for lightweight zones with single pane clear glass and dark roller interior shade

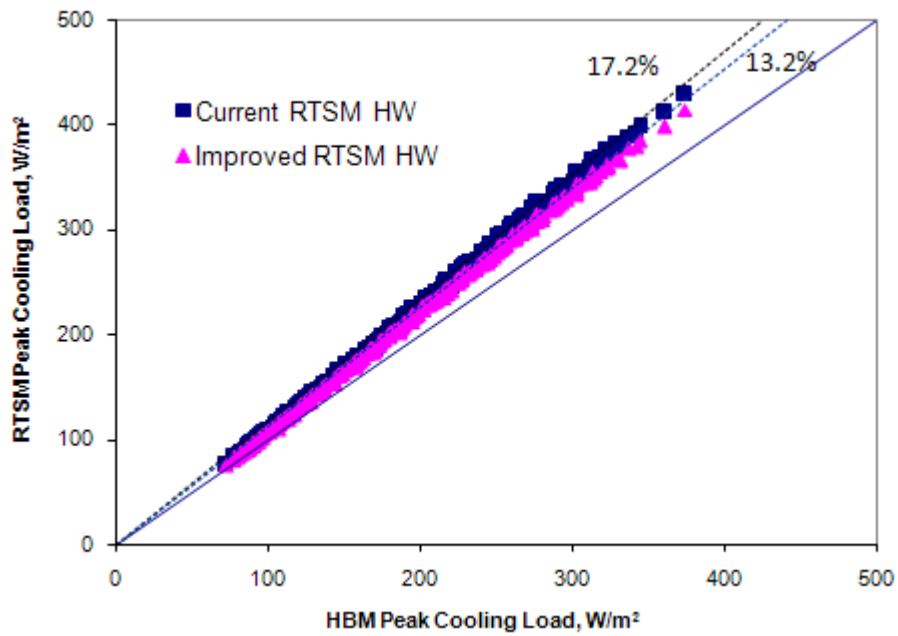


Figure 4.16 Current and Improved RTSM annual peak-cooling load versus HBM for heavyweight zones with single pane clear glass and dark roller interior shade

CHAPTER V

5. Dynamic Modeling of Thermal Bridges – Methodology

5.1 Introduction

Thermal bridges change the internal surface temperatures and the heat flow characteristics of the building envelope. Thermal bridge effects are caused by: large differences in thermal conductivity of the elements of a construction (eg. steel stud walls), and differences between internal and external areas of construction at corners and edges of constructions. The most common thermal bridges are the two-dimensional or “linear” thermal bridges, which occur in composite material constructions with large thermal conductivity disparity, and at the junctions of two or more building envelopes. The consequences of thermal bridges are higher heating and cooling load, which results in needing larger air conditioning equipment, risk of condensation and mould growth resulting from low-surface temperature on the inside surface of the thermal bridge, and thermal discomfort. As a result, the need for dynamic modeling of thermal bridges has been of high interest recently. Building energy analysis and load calculation programs developed in the USA use one-dimensional conduction transfer functions to predict heat conduction through the building envelopes.

In order to properly analyze thermal bridge effect, some form of multi-dimensional transient heat conduction model is needed. There have been repeated efforts to develop multidimensional dynamic heat conduction models that produce CTFs in one-dimensional form for energy analysis and load calculation programs commonly used in USA. However, their implementation has been delayed for several reasons. A multidimensional finite volume numerical method has been also implemented in ESP-r (Nakhi, 1995), which is a whole building energy and environmental simulation program, but this feature is not usable. Therefore, there is an urgent need for simple one-dimensional approximate dynamic modeling procedure for constructions with thermal bridge.

Karambakkam, et al. (2005) proposed a simple one-dimensional approximate procedure for dynamic modeling of thermal bridges. Preliminary numerical validation results suggest that this approximate method gives good results from a few cases investigated. The equivalent homogeneous layer wall model as proposed applies to thermal bridges with a single composite layer. The procedure does not provide guidance when the thermal bridge involves multiple composite layers, in particular when two composite layers are separated by homogeneous layer(s). Furthermore, it does not provide guidance when to use air-to-air or surface-to-surface *R*-value. It also does not provide guidance when a thermal bridge element extends to the surface. This approximate one-dimensional dynamic model will be investigated experimentally and numerically, and limitations of this approximate model will be established.

5.2 Equivalent Homogeneous Layer Model

The equivalent homogeneous layer (EHL) model (Karambakkam, et al., 2005) is an approximate one-dimensional dynamic model based on conservation of the thermal resistance and thermal mass of the actual construction. In this model, an equivalent homogeneous layer(s) replaces the composite material layer(s). The homogeneous layer resistance is computed such that the actual overall resistance is conserved. The overall resistance of the actual construction must first be determined using the best method available. The density and thermal capacity of the equivalent homogeneous layer is determined based on conservation of thermal mass of the actual construction. The equivalent homogeneous layer has the following properties:

- Thickness -same as the thickness of composite layer
- Conductivity is determined from the required resistance of the equivalent homogeneous layer and the thickness of the composite layer
- Density is the volume weighted average of the densities of the composite layer materials.
- Specific heat is determined from a mass weighted average of the specific heats of the composite layer materials.

The accuracy of the EHL model in duplicating the actual construction depends on the accuracy of the steady state thermal resistance or R -value. The equivalent homogeneous layer produces very good match provided there is accurate knowledge of the overall thermal resistance or U -value of the actual construction. The following section discusses ASHRAE's recommended overall thermal resistance, R -value calculation procedures.

5.2.1 Steady State R -Value

Steady state thermal resistances calculation procedures recommended by ASHRAE are described in Section 2.2.2. Though there are three procedures for overall resistance calculation recommended by ASHRAE, still there exists some subjective judgment to be made in selecting the best method for a particular construction type. ASHRAE's recommended R -value / U -value calculation procedure are approximations which sometimes can have significant errors. Therefore, it is worth mentioning that the best R -value / U -value calculation procedure in accuracy poses limitation on the equivalent homogeneous layers. However, if accuracy is desired accurate multidimensional numerical procedures such as finite volume or finite element method can be used to determine the R -value.

The equivalent homogeneous layer model is believed to give good approximation when a composite layer or layers of a construction are fully sandwiched between homogeneous layers. The equivalent homogeneous layer wall model has limitations when the highly conductive element fully penetrates the outermost layers. The following section the procedure for computing the equivalent homogeneous layer model is described.

5.2.2 Step By Step Procedure

The equivalent homogeneous layer model (Karambakkam, et al., 2005) relies on accurate knowledge of the air-to-air or surface-to-surface R -value and the geometry of the actual construction. The step-by-step procedure for calculating the equivalent homogeneous layer model wall for cases with single composite layer is described as follows:

- 1) Determine the handbook⁴ overall resistance of the actual construction based on ASHRAE's recommended methods. The handbook steady-state overall resistance may be determined using the three recommended practices: parallel heat flow path method, isothermal plane method, and the modified zone method (ASHRAE 2005).
- 2) Compute the effective equivalent resistance of the homogenous layer based on the actual overall resistance determined in step (1). The equivalent homogeneous layer resistance is the difference between the actual thermal resistance and the sum of the homogeneous layers resistances in the actual construction and is given by:

$$R_{Hom} = R_T - \sum_{i=1}^N R_{Sl,i} \quad (5.1)$$

where

R_T = the steady state overall thermal resistance of the construction,
(h·ft²·°F/Btu)

R_{Sl} = the thermal resistance of the i^{th} single homogeneous layer in the
construction, (h·ft²·°F/Btu)

R_{Hom} = the thermal resistance of the equivalent homogeneous layer, (h·ft²·°F/Btu)

N = the number of single homogeneous layers in actual construction, (-)

Sl = stands for single homogeneous layer in the actual construction, (-)

⁴ The steady state R -value determined using the procedures recommended in the ASHRAE 2005 *Handbook of Fundamentals* as described in Section 2.2.2.

- 3) Thermal conductivity of the equivalent homogenous layer is obtained by dividing the thickness of the equivalent homogeneous layer with resistance of the equivalent homogeneous layer. The thickness of the equivalent homogeneous layer is equal to the thickness of the composite layer.

$$X_{Hom} = X_{Tot} - \sum_{i=1}^N X_{Sl,i} \quad (5.2)$$

$$k_{Hom} = \frac{X_{Hom}}{R_{Hom}} \quad (5.3)$$

Where

X_{Tot} = the overall thickness of the actual construction, (in)

X_{Hom} = the thickness of the equivalent homogeneous layer, (in)

$X_{Sl,i}$ = the thickness of the i^{th} single homogeneous layer in the construction, (in)

k_{Hom} = the thermal conductivity of the equivalent homogeneous layer,
(h·ft²·°F/Btu-in)

- 4) Density of the equivalent homogeneous layer is determined from densities of the components of the composite layers and the corresponding volume fractions. The product sum of the volume fraction and densities of the components in the composite layer yields the equivalent homogenous layer density and is given by:

$$\rho_{Hom} = \sum_{i=1}^M y_i \rho_i \quad (5.4)$$

where

y_i = the volume fraction of i^{th} component in the composite layer(s), (-)

ρ_i = the density of the i^{th} component in the composite layer(s), (lb_m/ft^3)

ρ_{Hom} = the density of the equivalent homogeneous layer, (lb_m/ft^3)

The constituents' volume fraction in the composite layer is determined from the geometry of the composite layer.

- 5) The specific heat of the homogeneous layer is determined from the product sum of the specific heat, densities and volume fractions of the constituents of the composite layers.

$$C_{P, Hom} = \sum_{i=1}^M y_i \rho_i C_{pi} / \rho_{Hom} \quad (5.5)$$

where

C_{Pi} = specific heat of the i^{th} component in the composite layer(s), ($\text{Btu}/\text{lb}_m \cdot ^\circ\text{F}$)

$C_{P, Hom}$ = specific heat of the equivalent homogeneous layer, ($\text{Btu}/\text{lb}_m \cdot ^\circ\text{F}$)

Once the thickness and thermo-physical properties of the equivalent homogeneous layer have been determined, the equivalent homogeneous layers model wall can be input and analyzed as if were made up of homogeneous layers.

The equivalent homogeneous layer wall model described by Karambakkam et al. (2005) applies to thermal bridges with a single composite layer. It does not provide guidance when the thermal bridge involves multiple composite layers, in particular when two composite layers are separated by homogeneous layer(s). It does not provide guidance whether to use air-to-air or surface-to-surface R -value. It also does not provide guidance when a thermal bridge element extends to the surface. These practical challenges will be addressed in Chapter Six and guidance will be developed. Moreover, the equivalent homogeneous layer model will be validated experimentally, and numerically over a wider range of construction types.

6. Dynamic Modeling of Thermal Bridges – Validation

An approximate one-dimensional homogeneous layer procedure has been proposed for dynamic modeling of thermal bridges in Chapter 3. The model has been tested numerically using a few test samples. Preliminary results (Karambakkam et al. 2005) suggest that the model is promising based on the few limited test cases analyzed. However, the procedure needs to be tested against a wider range of thermal bridge test samples to establish its accuracy and limitations. This chapter is dedicated to experimental and numerical validation of the approximate homogeneous layer one-dimensional thermal bridge model. The experimental validation of the procedure will be done utilizing the work of ASHRAE 515-RP (Brown and Stephenson 1993a; Brown and Stephenson 1993b).

The experimental test data available is limited to seven walls. Therefore, a numerical experiment that covers a wide range of thermal bridges and boundary conditions is also proposed. The numerical experiment uses a 2D finite volume method as a reference model.

The following sections describe the experimental validations already done and are followed by a discussion of the proposed work for the numerical validation. Moreover, the equivalent homogeneous layer will be extended for use with multiple composite layers, application and design guidance procedures will be provided for use with real world thermal bridge types. Besides, guidance will be provided when to use the air-to-air and the surface to-surface R -value.

6.1 Experimental Validation

Experimental validation of the simplified equivalent homogeneous layer (EHL) model is carried out based on the ASHRAE 515-RP seven experimental test of walls Brown and Stephenson (1993a; 1993b). The tests were conducted in a dynamic test facility built by Brown and Stephenson (1993b). The test facility was based on ASTM standard C-236-89, which applies only to a steady state conditions. The above authors extended the methodology to make dynamic tests. The experimental validation describes the test facility and test procedure, the validation and discusses the results.

6.1.1 Guarded Hot Box Dynamic Response Test Facility

The guarded hotbox dynamic response test facility is based on the standard guarded hotbox steady state test setup with additional control features that dynamically update the boundary conditions set points Brown and Stephenson (1993b). The experimental set-up of the guarded hotbox dynamic test facility may be summarized as follows:

- Thermally insulated room chamber with a controlled calorimeter. The calorimeter has a test temperature range $16^{\circ}\text{C} - 26^{\circ}\text{C}$ and a test area of 2440mm by 2440mm for full-scale wall specimen test.
- The calorimeter has equally spaced built-in thermocouples measuring the surface temperatures on both sides of the calorimeter. This allows the measurement of average temperature of both surfaces of the calorimeter. The set point temperatures of the calorimeter surfaces are controlled remotely.
- The specimen surface, which faces the calorimeter, is shielded from direct radiation coming from the calorimeter by a baffle. The baffle is placed between the calorimeter and the specimen. The baffle has enough spacing for circulation of the heated air in the space between the calorimeter and the specimen.
- The calorimeter air heater is placed in between the calorimeter and the baffle. The calorimeter air temperature is sensed and controlled using an analog millivolt controller.
- The well-insulated cold chamber minimizes the interaction of the cold side of the specimen with the surroundings and maintains the cold chamber temperature in the range 0°C to -40°C . Circulating heated air controls the cold chamber temperature. A pre-cooler maintains the circulating air temperatures below the set point.
- The set point temperatures in the calorimeter, room chamber and cold chamber are controlled using a computerized data acquisition system and a remote controller. For the dynamic tests the set point temperature in the calorimeter is updated at the required time interval and the controller regulates the new set point

every time the set point is updated. The set point temperature of the air in the calorimeter can be programmed to the required boundary conditions: constant, ramp and sinusoidal waveforms excitation. The remote computer also records the required temperatures at each time step.

6.1.2 The Test Procedure and Specimens

Using the above test facility, Brown and Stephenson (1993a; 1993b) experimentally determined dynamic response of seven full-scale wall specimens. The test facility described above uses a remote computer that controls the set points for temperature or heat inputs for the steady state and dynamic tests. The steady state test was used to determine the thermal resistance and size the heater power input for three selected exterior air temperatures.

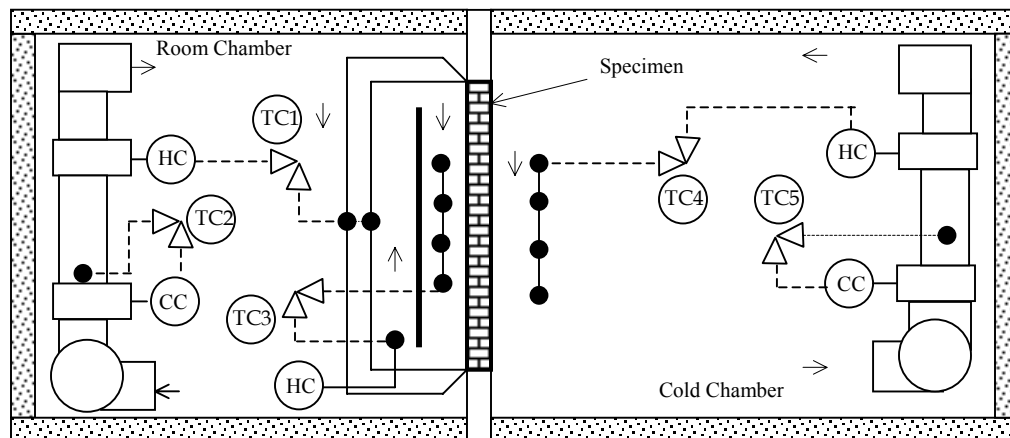


Figure 6.1 Sectional view of guarded hotbox facility (Brown and Stephenson 1993b)

Legend

HC	Heating Coil (Electric Heater)
CC	Cooling Coil (Chilled water coiling coil)
TC1	Metering Box differential temperature cooler
TC2	Room air pre-Cooler controller
TC3	Metering box air temperature controller
TC4	Cold Chamber air temperature controller
TC5	Cold Chamber air pre-cooler controller

The mean interior air temperature was fixed at 21°C [70°F] for all the tests. Thermal resistances of the wall specimens were measured at three different mean exterior air temperatures: -35°C [-31°F], -20°C [-4°F] and -5°C [23°F]. The thermal resistances measured for each specimen at these three temperatures were used to establish the temperature dependent relationship for the thermal resistance.

The dynamic responses of the wall specimens were determined with sinusoidally varying exterior air temperature at a mean value of -20°C [-4°F] and amplitude of 15K [27°F] at a period of 24, 12, and 6 hours. For heavy specimens, walls# 2, 3, 4, 5, and 7, a 48 period was also applied. The calorimeter heat input was fixed at a value determined by steady state heat transfer rate across the specimen at mean exterior temperature of -20°C [-4°F]. The sinusoidally varying exterior air temperature set point is updated every minute and the controller of the cold chamber matches the air temperature to the new set point.

Another set of dynamic response of the wall specimens was measured for sinusoidal varying calorimeter heat input with amplitude of 60W at periods of 24, 12, and 6 hours. For heavy specimens, walls# 2, 3, 4, 5, and 7, a 48 period was also applied. The cold chamber (exterior air temperature) -35°C [-31°F] fixed air temperature was used. For this case, the mean calorimeter heater set point was determined from the steady state heat transfer rate across the specimen measured at a fixed exterior air temperature of -35°C [-31°F]. The full-scale test specimens are described in Table 6.1.

Table 6.1 Layer-by-layer descriptions of the ASHRAE RP-515 test walls

Wall #	Layer-by-layer description		Remark
1	1	Outside film resistance, 0.19 hr·ft ² °F/Btu (0.033 m ² ·K/W)	The composite layer is the layer containing the glass fiber and the steel stud sandwiched between homogeneous layer gypsum boards.
	2	1 in (25mm) Stucco on wire mesh (3 coats)	
	3	0.5 in (12mm) Exterior Gypsum sheathing	
	4	3.5 in (89mm) Glass Fiber Insulation Layer with punched steel studs 16ga, 16 in (406mm) on centers	
	5	0.5 in (12mm) Interior Gypsum board	
	6	Inside film coefficient, 0.44 hr·ft ² °F/Btu (0.078 m ² ·K/W)	
2	1	Outside film resistance, 0.29 hr·ft ² °F/Btu (0.051 m ² ·K/W)	Steel furring 24 in (610mm) on center is placed in the insulation board layer
	2	8 in (200mm) Pre-cast reinforced concrete (#5 re-in bar)	
	3	1 in (25mm) Styrofoam Insulation board	
	4	5/8 in (16mm) Interior Gypsum board	
	5	Inside film coefficient, 0.44 hr·ft ² °F/Btu (0.078 m ² ·K/W)	
3	1	Outside film resistance, 0.24 hr·ft ² °F/Btu (0.043 m ² ·K/W)	Steel furring 24 in (610mm) on center is placed in the insulation board layer
	2	5/8 in (16mm) Interior Gypsum board	
	3	1 in (25mm) Styrofoam Insulation board	
	4	8 in (200mm) Pre-cast reinforced concrete (#5 re-in bar)	
	5	Inside film coefficient, 0.44 hr·ft ² °F/Btu (0.078 m ² ·K/W)	
4	1	Outside film resistance, 0.31 hr·ft ² °F/Btu (0.054 m ² ·K/W)	The composite layer is made from the steel stud and glass fiber and is sandwiched between concrete and gypsum board.
	2	4 in (200mm) Pre-cast reinforced concrete (#5 re-in bar)	
	3	3.5 in (89mm) Fiber Glass Insulation Layer with punched steel studs 20ga, 16 in (406mm) on centers	
	4	5/8 in (16mm) Interior Gypsum board	
	5	Inside film coefficient, 0.45 hr·ft ² °F/Btu (0.079 m ² ·K/W)	
5	1	Outside film resistance, 0.31 hr·ft ² °F/Btu (0.055 m ² ·K/W)	The hollow block layer the voids filled with cement mortar is the composite layer.
	2	2.25 x 3.5 x 7.5 in (57 x 89 x 190 mm) Burned clay brick	
	3	2 in (50 mm) Styrofoam insulation board	
	4	6 x 7.5 x 15.25 (140 x 190 x 390 mm) Hollow Concrete blocks	
	5	0.887 in (22 mm) Air space with steel furring 26 ga.	
	6	5/8 in (16mm) Interior Gypsum board	
	7	Inside film coefficient, 0.44 hr·ft ² °F/Btu (0.078 m ² ·K/W)	
6	1	Outside film resistance, 0.29 hr·ft ² °F/Btu (0.051 m ² ·K/W)	The composite layer is the layer containing the glass fiber insulation and the steel stud. The brick tie effect is ignored.
	2	2.25 x 3.5 x 7.5 in (57 x 89 x 190 mm) Burned clay brick with brick tie	
	3	1 in (25 mm) Air space	
	4	0.5 in (12mm) Exterior Gypsum board	
	5	3.5 in (89mm) Fiber Glass Insulation Layer with punched steel studs 20ga, 16 in (406mm) on centers	
	6	5/8 in (16mm) Interior Gypsum board	
	7	Inside film coefficient, 0.44 hr·ft ² °F/Btu (0.078 m ² ·K/W)	
7	1	Outside film resistance, 0.24 hr·ft ² °F/Btu (0.043 m ² ·K/W)	There are three composite layers place adjacent to each other. The layers include: angle iron, two layers of insulation and air gap.
	2	6 x 7.5 x 15.25 in (140 x 190 x 390 mm) Solid Concrete Block	
	3	3 in (76 mm) Styrofoam Insulation Board	
	4	1 in (25 mm) Styrofoam Insulation Board	
	5	1.8 in (46 mm) Air space	
	6	1.06 in (27mm) Granite Veneer	
	7	Inside film coefficient, 0.45 hr·ft ² °F/Btu (0.079 m ² ·K/W)	
8	1	Outside film resistance, 0.31 hr·ft ² °F/Btu (0.055 m ² ·K/W)	
	2	Homogeneous layer pre cast concrete slab	
	3	Inside film coefficient, 0.44 hr·ft ² °F/Btu (0.078 m ² ·K/W)	

6.1.3 Experimental Determination of the CTF

The conduction transfer functions for the test specimens were determined from measured heat fluxes and/or power inputs, measured temperatures and temperature excitations, measured U -values and test apparatus calibrations. The z -transfer function coefficients are determined from the measured responses and U -values using mathematical manipulations. The following section describes the fundamentals of conduction transfer functions, describes the procedures for determining the responses, and then describes the step-by-step procedure for computing the z -transfer coefficients from the measured responses.

The Laplace transform form of the overall transmission matrix of a multi-layered wall that relates the transform of the interior temperature T_i , exterior temperature T_e , the inside surface heat flux q_i , and the exterior surface heat flux q_e and is given by Carslaw and Jaeger (1959):

$$\begin{bmatrix} T_i \\ q_i \end{bmatrix} = \begin{bmatrix} A & B \\ C & D \end{bmatrix} \cdot \begin{bmatrix} T_e \\ q_e \end{bmatrix} \quad (6.1)$$

The transmission matrix elements A , B , C and D are functions of the thermal properties and dimensions of the individual wall layers and the surface heat transfer coefficients. The matrix element C can be eliminated using the identity $AD-BC = 1$ and the equation 4.1 can be written as follows:

$$\begin{bmatrix} q_i \\ q_e \end{bmatrix} = \begin{bmatrix} D/B & -1/B \\ 1/B & -A/B \end{bmatrix} \begin{bmatrix} T_i \\ T_e \end{bmatrix} \quad (6.2)$$

Where,

D/B = represents response of the internal surface due to variation of the interior environment temperature.

$1/B$ = represents response of the internal surface due to variation of the exterior environment temperature.

A/B = represents response of the external surface due to variation of the exterior environment temperature.

The z-transfer functions are commonly used in building load and energy calculations programs. The following steps describe the procedure to compute the z-transfer function coefficients from the finite number of measured heat fluxes and temperatures. The z-transfer function coefficients are commonly used for calculating responses of walls and are given by:

$$Z\{q_i\} = \frac{D(z)}{B(z)} \cdot Z\{T_i\} - \frac{1}{B(z)} \cdot Z\{T_e\} \quad (6.3)$$

In time-domain form Eq. (4.3) is given by:

$$q_{i,t} = U \cdot \sum_{n=0}^{N_c} (c_n \cdot T_{i,t-n\delta}) - U \cdot \sum_{n=0}^{N_b} (b_n \cdot T_{e,t-n\delta}) - \sum_{n=1}^{N_d} (d_n \cdot q_{i,t-n\delta}) \quad (6.4)$$

where,

U = is the air-to-air heat transfer coefficient, $W/(m^2 \cdot K)$

c = are the inside z-transfer function coefficients, $W/(m^2 \cdot K)$

b = are the cross z-transfer function coefficients, $W/(m^2 \cdot K)$

d = are heat flux history terms coefficients, (-)

Determination of Wall Response

The cross and inside self-response and time constants of the test walls specimens were determined as follows (Brown and Stephenson 1993a; 1993b):

1. The values of “D/B”, the inside self-response, were determined from measured heat flux through the room side (interior) of the specimen in response to an excitation on the room side of the specimen, and from the test apparatus dynamic calibration.
2. The values of “1/B”, the cross response, were determined from measured heat flux through the room side (interior) of the specimen in response to an excitation on the outside of the specimen, and from the test apparatus calibration.
3. A finite number of time constants were determined from the experimental results that best match the response calculated with Eq. 6.5 to the measured value of 1/B using a minimization technique at discrete periods.

$$\frac{1}{B} = \frac{U}{\prod_{n=1}^{\infty} (1 + \tau_n s)} \quad (6.5)$$

Determination of z-transfer Coefficients

The values of d_n coefficients are determined from the poles of the 1/B by matching the denominators of Eq. 6.6 and Eq. 6.5. The number of significant d_n coefficients determined by this procedure is dependent on the magnitude of time constants determined in step 3 above.

$$\frac{1}{B\{z\}} = U \cdot \frac{\sum_{n=0}^{N_b} b_n \cdot z^{-n}}{\sum_{n=0}^{N_d} d_n \cdot z^{-n}} \quad (6.6)$$

The b_n and c_n z-transfer function coefficients of the specimens can be determined by matching the calculated response to the measured response using various mathematic steps. The values of b_n coefficients were determined through the following two mathematical steps:

1. response factors are determined for unit triangular ramp at 1 hour interval using the measured 1/B terms;
2. Then the b_n coefficients were determined by matching response factors generated in step 1 to Eq. 6.6.

The values of “ c_n ” are determined by fitting Eq. 6.7 to the frequency response measured at two periods, typically 24 h and 6h.

$$\frac{D\{z\}}{B\{z\}} = U \cdot \frac{\sum_{n=0}^{N_c} c_n \cdot z^{-n}}{\sum_{n=0}^{N_d} d_n \cdot z^{-n}} \quad (6.7)$$

The test results include the overall and surface-to-surface resistances, the air-to-air z-transfer functions, and amplitude and phase shift at different periods.

6.1.4 The Experimental Validation Procedure

The equivalent homogeneous layer wall model experimental validation process involves comparison of the Conduction Time Series Factors (CTSF) coefficients, peak heat gain, and the peak heat gain timing. For the experimental results, CTSF coefficients are generated from the CTF coefficients computed by Brown and Stephenson (1993a; 1993b), using the procedure described by Spitler and Fisher (1999a). Using the experimentally determined surface-to-surface R -value and the construction description provided by Brown and Stephenson (1993a), the equivalent homogeneous layer model is used to create an equivalent one-dimensional wall description and Seem’s (1987) procedure is used to determine CTF coefficients. From these CTFs, the Spitler and Fisher (1999a) procedure is used to determine CTSF. The two sets of CTSF may be compared directly.

Applications of the two sets of CTSF for a typical design day (Atlanta, Georgia 1% design day weather condition for the month of July with peak dry bulb temperature of 35.7°C and daily range of 10.5K) allows comparison of the hourly heat flux and the peak heat gain timing that reflect the practical accuracy of the equivalent homogeneous layer model for design load calculations. The flow chart of the validation procedure is shown in Figure 6.2. However, practicing engineers do not have measured *R*-values and must rely on one of the methods described in Section 2.2.2. Therefore, the layer-by-layer properties of the equivalent walls generated using the measured and handbook *R*-values are also compared in Table 6.3a and Table 6.3b. In the following sections the equivalent wall generation, the comparison of heat gains, discussions and recommendations are presented successively.

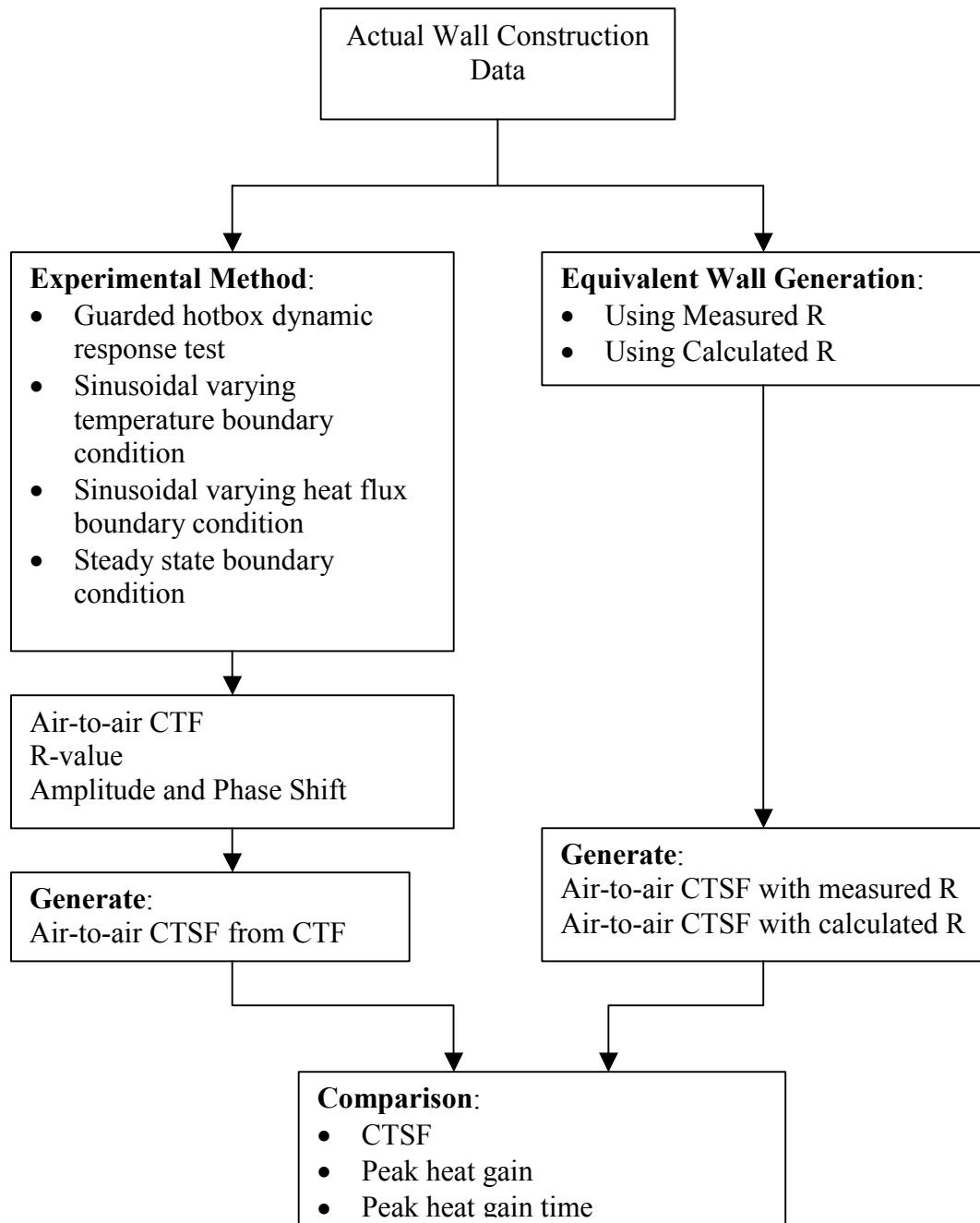


Figure 6.2 Flow chart of the experimental validation procedure

6.1.5 The Equivalent Walls

The equivalent wall model is based on conservation of the construction R -value and thermal mass. It also depends on maintaining the layers' order from the actual construction. Therefore, the equivalent wall generation requires an accurate R -value, detailed geometry and material properties of the actual construction.

The first step in the equivalent wall generation procedure is estimation of steady state R -value. In practice the R -values of a construction with non-homogeneous layers needs to be determined using one of the available procedures described Section 2.2.3.

In this validation, the equivalent walls were generated with measured and handbook R -values. The validation procedure gives insight into how the performance of the proposed approximate one-dimensional dynamic model depends on the accuracy of the R -value. Therefore, determination of handbook R -value of the seven test walls and the approximations and/or assumption introduced is described next.

Implementation of the equivalent wall procedure requires some subjective judgments to be made depending on the composite layer(s) configurations. The type of linear thermal bridges included in this work can be classified depending on the composite layers configurations as follows:

- i. Sandwiched composite layer(s)
- ii. Exposed composite layer

The thermal bridges analyzed here are the linear type with equal inside and outside surface areas. (They are not associated with corners).

Sandwich Composite Layers

Constructions with sandwich type composite layers are common in building wall and roof constructions. The construction may contain one or more composite layer(s) located in adjacent each other or separated by homogeneous layer(s). This type of thermal bridges will have at least three layers – two homogeneous layers and one composite layer. They can be easily replicated easily using the equivalent homogeneous layer wall model. A typical sandwich type thermal bridge is found in a steel stud walls with siding on exterior side and dry wall on the interior side as shown in Figure 6.3(a).

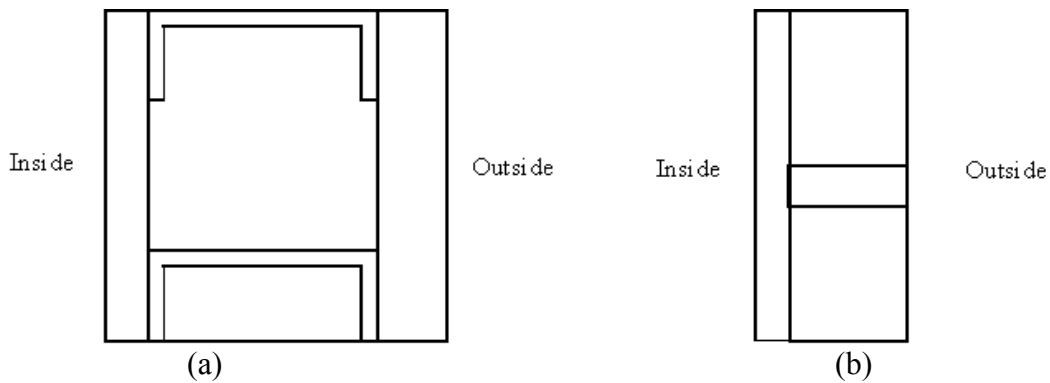


Figure 6.3 Thermal bridge types: (a) sandwiched type; (b) exposed type

Exposed Composite Layer

Thermal bridges involving composite layer(s) exposed to either exterior or interior environments are not common in building constructions. This type of thermal bridge cannot be easily replicated by the equivalent homogeneous layer wall model procedure

given in Section 5.2. In this situation the equivalent homogeneous layer wall model procedure needs to be extended to be applicable to exposed type thermal bridges. A procedure is proposed for this type of thermal bridges in Section 6.1.8.

The Equivalent Walls and Computation of R-value

There are two-types of R -values that can be calculated for a given wall – the air-to-air and surface-to-surface. In general, the choice of R -value depends on the thermal bridge type. The steady state R -value calculation procedures (isothermal plane, parallel path, F_c correction method and zone method) all reflect the steady state temperature distribution pattern in the actual constructions. If isothermal plane method or the parallel path correction method is used for R -value calculations both the air-to-air and the surface-to-surface R -values must give identical equivalent wall layers. However, for R -value calculated using either parallel path or zone method, the air-to-air and the surface-to-surface R -values may give different equivalent wall layers depending on the thermal bridge element configuration in the actual wall. If the thermal bridge element is exposed type or the thermal bridge influence is so strong that significant surface temperature variation exists on either surface, then the air-to-air R -value should be used for the equivalent wall generation. The use of either air-to-air or surface-to-surface R -values for equivalent wall generation depends on the procedure used to determine the overall R -value or U -values. However, the following recommendation can be made:

- For R -values determined using either isothermal plane or the parallel path correction method the use of either R -value gives the same equivalent homogeneous layer.

- For R -values determined using the parallel path or zone methods the properties of the EHL wall vary slightly depending on whether the basis is air-to-air or surface-to-surface R -values. If the parallel path extends to air-to-air node in the R -value calculation then the air-to-air R -value should be used in the equivalent layer determination. If the parallel path method combines the facing layers in series with composite layer then the use of either air-to-air or surface-to-surface R -values gives the same equivalent layer.

For sandwiched type thermal bridges surface to surface R -value are generally sufficient for the equivalent wall generation. For exposed type thermal bridges the air-to-air R -value may be more representative due to possible surface temperature differences. In the later case the equivalent homogeneous layer wall model must be generated using the air-to-air R -value. Therefore, the inside and outside film resistances will be removed from the equivalent wall layers for use in the heat balance method. For use in the RTSM the inside and outside combined conductance are added to the surface-to-surface R -value.

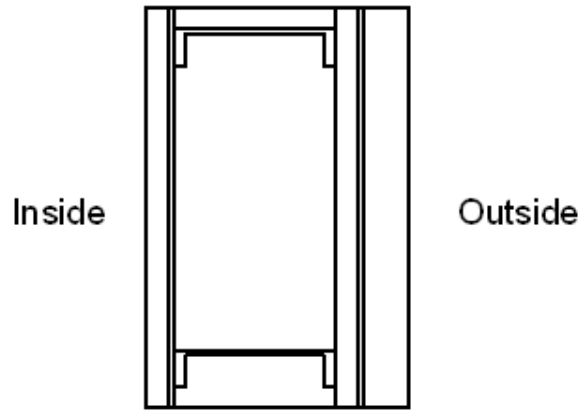
The experimental validation of the EHL wall model was conducted using measured and calculated surface-to-surface R -values. The measured and calculated R -values along with the calculation method are given in Table 6.2. Then the R -values were also computed using the using the isothermal plane, parallel path, F_c correction factor and zone methods. It is advisable to verify whether the modified zone method R -values lie between the isothermal plane and parallel path methods in particular when the zone factor value is

outside the range for which the method is recommended. The section views of the seven test walls are shown in Figure 6.4.

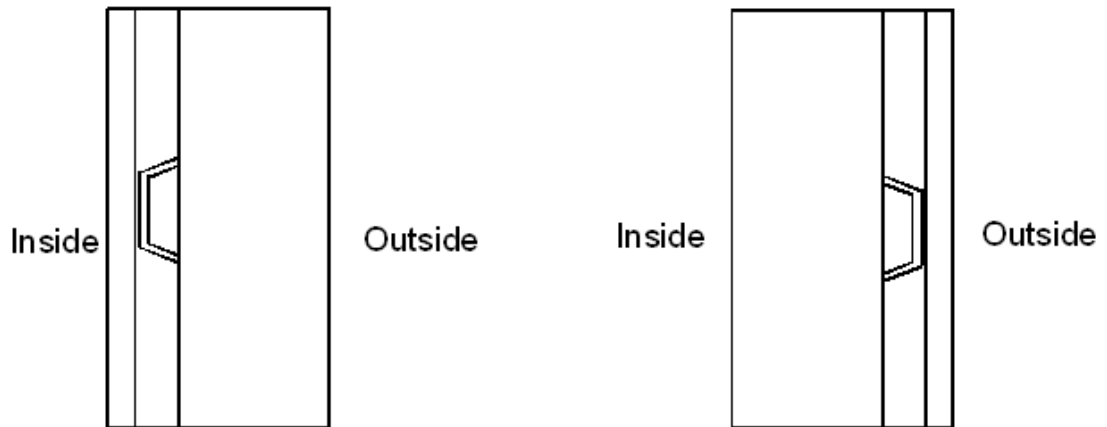
The equivalent homogeneous layers are generated using the procedure described in Chapter 5. The following section discusses the assumptions made and approximations introduced to generate the equivalent homogeneous layer for each of the seven ASHRAE test walls.

The following general principles for when to ignore distributed elements of a composite construction have been followed:

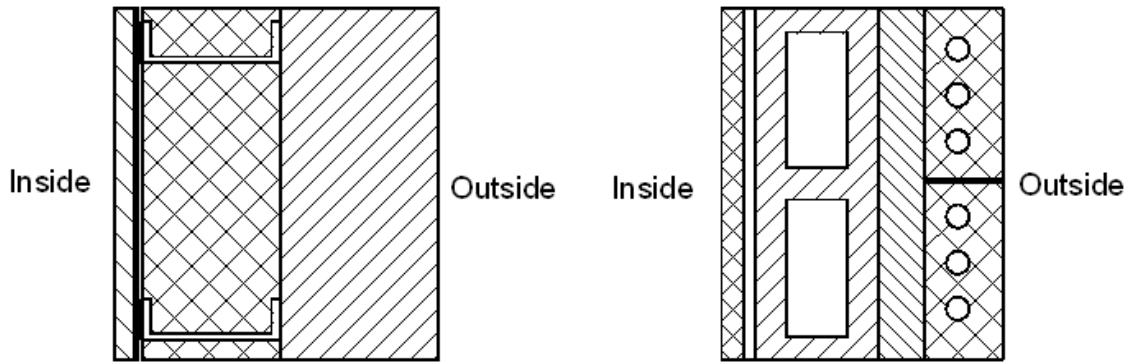
- Small elements of negligible conductance such as brick ties are neglected
- Element aligned parallel to the wall surface, like rebar, for which the thermal mass is important but the increased conductance in the transverse direction of the wall is negligible are neglected for resistance calculation; however, they are included in the layer thermal mass.



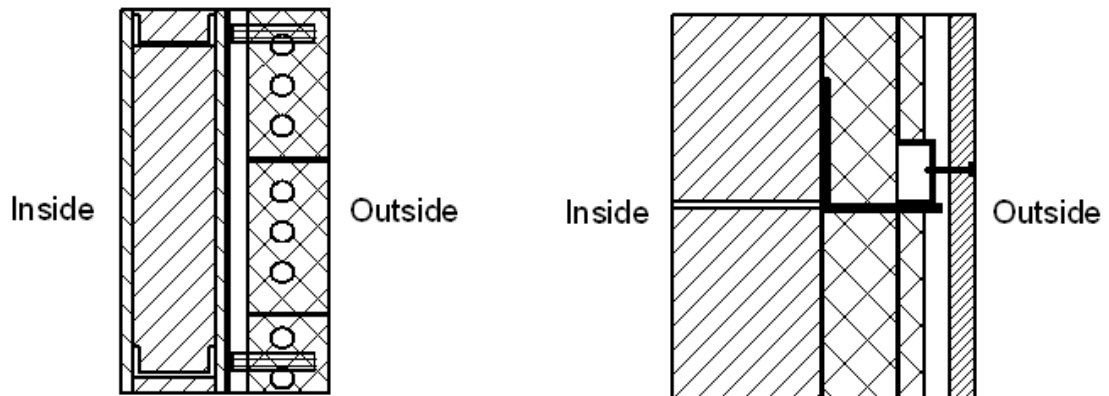
(a) Test Wall#1 steel stud with stucco exterior finish



(b) Test Wall#2: pre-cast concrete with metal furring and insulation; (c) Test Wall#3: pre-cast concrete with metal furring and insulation



(d) Test Wall#4: Insulated steel stud mounted on pre-cast concrete; (e) Test Wall#5: Hollow Block with insulation and brick exterior finish



(f) Test Wall#6: Insulated steel stud wall with brick finish; (g) Test Wall#7: Solid Concrete block with insulation and granite finish

Figure 6.4 ASHRAE RP-515 Test Walls

Table 6.2 Surface-to-Surface R -values of ASHRAE RP-515 Test Walls

Wall #	Measured R -Value ($\text{m}^2 \cdot \text{K}/\text{W}$)	Calculated R -Value ($\text{m}^2 \cdot \text{K}/\text{W}$)	Calculation Method
1	1.17	1.27	F_c Correction Method $F_c = 0.48$
2	0.86	0.88	Zone Method
3	0.83	0.88	Zone Method
4	1.33	1.18	F_c Correction Method $F_c = 0.48$
5	2.14	2.30	Isothermal Plane
6	1.64	1.52	F_c Correction Method $F_c = 0.48$
7	1.66	1.56	Zone Method

Steel stud wall with stucco exterior finish (Wall#1)

The steady state resistance of steel stud walls can be determined using the F_c correction method. The surface-to-surface R -value of the wall based on the parallel path correction factor $F_c = 0.48$ was estimated to be $1.27 \text{ (m}^2 \cdot \text{K}/\text{W)}$. The calculated R -value is higher by 8.6% than the measured value. The steel stud wall has three homogeneous layers and one composite layer as summarized in Table 6.3. The equivalent homogeneous layer wall can be generated using the three homogeneous layers and one equivalent homogeneous layer representing the composite layer. This wall may be considered as “sandwich” type thermal bridge construction.

Pre-cast concrete with metal furring insulation (Wall#2 and Wall#3)

The surface-to-surface R -value can be estimated using the zone method from the three layers by ignoring the reinforcement bar in the concrete. The reinforcement bar does not

act as thermal bridge element since it is parallel to the inside and outside surface areas and hence has negligible effect on the thermal resistance. The R -value determined using the zone method is given in Table 6.3. Test specimen wall#3 is the same construction but the layers are in reverse order. Therefore both walls should have the same steady state thermal resistance or R -value. However, the slight difference in experimental measurement due to instrumentation error or change in the property of the test specimen may cause difference in the R -values.

These wall constructions each have two homogeneous layers and one composite layer. The composite layer is made from Styrofoam insulation board and steel furring. An equivalent homogeneous layer that replaces the composite layer was determined. The metal reinforcement bars (rebar) in the concrete slabs are accounted for in thermal mass calculations. This wall may be considered as “sandwich” type thermal bridge construction.

Insulated steel stud mounted on pre-cast concrete (Wall#4)

The surface-to-surface R -value of the insulation is determined using the insulation/framing adjustment factor in ASHRAE/IESNA *Standard* 90.1-2004, in Table A9.2B $F_c=0.48$. The handbook R -value ($1.18 \text{ m}^2\cdot\text{K}/\text{W}$) is lower than the measured value ($1.33 \text{ m}^2\cdot\text{K}/\text{W}$) by 11.3% as shown in Table 6.2. Ignoring the metal reinforcement bars in the concrete slab, the insulated steel stud wall can be considered a “sandwich” type thermal bridge construction. The glass fiber and the steel stud constitute a composite

layer hence can be replaced by an equivalent homogeneous layer. The equivalent wall consists of three homogeneous layers as summarized in Table 6.3.

Hollow Block with insulation and brick exterior finish (Wall#5)

The surface-to-surface R -value was determined by applying the isothermal plane method for the hollow block layer. The estimated R -value ($2.30 \text{ m}^2\cdot\text{K}/\text{W}$) is lower than the measured R -value ($2.14 \text{ m}^2\cdot\text{K}/\text{W}$) by 7.5%. All layers except the hollow block section may be considered as homogeneous layers. The hollow block voids are filled with cement mortar and hence are considered as composite layers. Thus, an equivalent homogeneous layer was generated for the hollow block section of the wall. The brick's thermal mass was corrected for the voids. All in all the equivalent homogeneous layers wall contain five homogeneous layers as summarized in Table 6.3. The voids in the brick are a small fraction of the heat flow path area and the thermal conductivity of the brick material is significantly higher than the void conductance. Therefore, ignoring the void resistance has little effect on the overall thermal resistance of the construction.

Insulated steel stud wall with brick finish (Wall#6)

The surface-to-surface R -value was estimated with F_c correction method. The estimated R -value ($1.52 \text{ m}^2\cdot\text{K}/\text{W}$) is lower than the measured R -value ($1.64 \text{ m}^2\cdot\text{K}/\text{W}$) by 7.3%. The brick ties were ignored in steady state thermal resistance calculations. The steel stud wall with air space and brick veneer finish can be considered to have only one composite layer section if the brick ties are ignored. This wall is a sandwich type thermal bridge. The equivalent homogeneous layer for the composite can be determined using the procedure

described in Chapter 5 and the resulting equivalent wall has five homogeneous layers as shown in Table 6.3.

Solid Concrete block with insulation and granite finish (Wall#7)

This wall consists of a homogeneous layer solid concrete block to which an angle iron is mounted with bolted connection to support insulation layers. The angle iron extends through the insulation layers and supports the Veri-trust channel. The wall has an air gap and a granite veneer exterior finish. The granite veneer is secured by galvanized steel butterfly clip that extends through the air gap and screwed to the Veri-trust channel as shown in Figure 6.4g. The insulation and the angle iron form composite layer, the air gap and Veri-trust channel for the second composite layer and the granite veneer and the butterfly clip can be considered as the third composite layer. The solid concrete block could also be considered as the fourth composite layer due to the anchoring bolt.

The surface-to-surface R -value was estimated using the zone method for the composite layer containing the insulation and angle iron. The width of the thermal bridge metal section is assumed to be half of that of the angle iron width. The Veri-trust channel was ignored, as it is aligned perpendicular to the main heat flow path. The butterfly clip has been also ignored due to small heat flow paths area compared to total surface area. The estimated R -value ($1.77 \text{ m}^2\cdot\text{K}/\text{W}$) is higher than the measured R -value ($1.69 \text{ m}^2\cdot\text{K}/\text{W}$) by 4.7%.

All the composite layers are adjacent to each other. The composite layers containing the two insulation layers and the air gap can be lumped together to form an equivalent homogeneous layer. Therefore, the equivalent homogeneous layer wall will be formed from the solid concrete block, the equivalent homogeneous layer and the granite veneer. The effect of the Veri-trust channel on the thermal mass is included. For the seven walls, the various ASHRAE methods for predicting steady-state resistances predict the R -values within $\pm 11.3\%$. In general, the equivalent homogeneous layer model may be expected to be no more accurate than the estimate of steady state resistance. The experimental validation results given in Section 6.1.4 reflect the importance of the R -value on the accuracy of the proposed model.

The R -value calculation methods and approximations introduced in the equivalent wall generation for the test walls have been previously discussed. The layer-by-layer description of the equivalent walls determined using the measured and handbook R -values are given in Table 6.3a and Table 6.3b, respectively. The difference between the two equivalent walls generated using the measured and handbook R -values is the composite layer (equivalent homogeneous layer) thermal resistance; otherwise the number of layers, layers order, and thermal mass of the construction are the same. The following sections discuss the effects of R -values have on the equivalent wall CTSFs.

Table 6.3a Equivalent walls computed with experimentally determined *R*-values

Wall No.	Layers Description	Thickness (mm)	Conductivity (W/m·K)	Density (Kg/m ³)	Specific Heat (kJ/kg·K)	Resistance (m ² ·K /W)
1	Outside Air Film					0.043
	Stucco wire mesh	25	0.720	1856.0	0.840	0.035
	Ext. gypsum sheathing	12	0.162	800.0	1.090	0.074
	Equivalent Layer	89	0.085	14.5	4.250	1.043
	Int. gypsum sheathing	12	0.162	800.0	1.090	0.074
	Inside Air film					0.079
2	Outside Air Film					0.051
	Concrete slab	200	1.728	2451.8	0.869	0.116
	Equivalent Layer	25	0.040	38.6	1.036	0.624
	Interior Gypsum board	16	0.160	800.0	1.090	0.100
	Inside Air film					0.078
3	Outside Air Film					0.051
	Ext. Gypsum board	16	0.16	800.00	1.09	0.100
	Equivalent Layer	25	0.04	36.15	1.07	0.640
	Concrete slab	200	1.73	2663.55	0.83	0.120
	Inside Air film					0.078
4	Outside Air Film					0.043
	Reinforced Concrete slab	102	1.728	2240.0	0.920	0.059
	Equivalent Layer	89	0.070	46.8	0.565	1.272
	Interior Gypsum board	16	0.160	800.0	1.090	0.100
	Inside Air film					0.079
5	Outside Air Film					0.055
	Burned Clay Brick	89	0.780	1920.0	0.790	0.114
	RSI Insulation	50	0.029	28.8	1.220	1.724
	Equivalent Layer	140	3.353	1323.7	0.834	0.042
	Air Gap	22				0.160
	Interior Gypsum board	16	0.160	800.0	1.090	0.100
	Inside Air film					0.078
6	Outside Air Film					0.051
	Burned Clay Brick	89	0.78	1918.33	0.79	0.110
	Air Gap					0.210
	Interior Gypsum board	12	0.16	800.00	1.09	0.080
	Equivalent Layer	89	0.08	46.85	0.56	1.140
	Interior Gypsum board	16	0.16	800.00	1.09	0.100
	Inside Air film					0.078
7	Outside Air Film					0.043
	Solid Concrete Masonry	140	1.728	2100.0	0.920	0.081
	Equivalent Layer	148	0.093	217.3	0.564	1.599
	Granite Finish	27	2.600	2600.0	0.880	0.010
	Inside Air film					0.079

Table 6.3b Equivalent walls computed with handbook *R*-values

Wall No.	Layers Description	Thickness (mm)	Conductivity (W/m-K)	Density (Kg/m ³)	Specific Heat (kJ/kg-K)	Resistance (m ² -K /W)
1	Outside Air Film					0.043
	Stucco wire mesh	25	0.720	1856.0	0.840	0.035
	Ext. gypsum sheathing	12	0.162	800.0	1.090	0.074
	Equivalent Layer	89	0.090	14.5	4.250	0.987
	Int. gypsum sheathing	12	0.162	800.0	1.090	0.074
	Inside Air film					0.079
2	Outside Air Film					0.051
	Concrete Slab	200	1.728	2451.8	0.869	0.116
	New Equivalent Layer	25	0.038	38.6	1.036	0.666
	Interior Gypsum board	16	0.160	800.0	1.090	0.100
	Inside Air film					0.078
3	Outside Air Film					0.051
	Gypsum board (Interior)	16	1.728	2240.0	0.920	0.100
	Equivalent Layer	25	0.038	38.6	1.036	0.666
	Concrete slab	200	1.728	2240.0	0.920	0.116
	Inside Air film					0.078
4	Outside Air Film					0.043
	Reinforced Concrete slab	102	1.728	2240.0	0.920	0.059
	Equivalent Layer	89	0.088	46.9	0.565	1.016
	Interior Gypsum board	16	0.160	800.0	1.090	0.100
	Inside Air film					0.079
5	Outside Air Film					0.055
	Burned Clay Brick	89	0.780	1920.0	0.790	0.114
	RSI Insulation	50	0.029	28.8	1.220	1.724
	Equivalent Layer	140	0.693	1323.7	0.834	0.202
	Air Gap	22				0.160
	Interior Gypsum board	16	0.160	800.0	1.090	0.100
	Inside Air film					0.078
6	Outside Air Film					0.051
	Burned Clay Brick	89	0.780	1919.3	0.790	0.114
	Air Gap	0	0.000	0.0	0.000	0.210
	Interior Gypsum board	12	0.160	800.0	1.090	0.075
	Equivalent Layer	89	0.088	46.9	0.565	1.017
	Interior Gypsum board	16	0.160	800.0	1.090	0.100
	Inside Air film					0.078
7	Outside Air Film					0.043
	Solid Concrete Masonry	140	1.728	2100.0	0.920	0.080
	Equivalent Layer	148	0.088	217.3	0.564	1.680
	Granite	27	2.600	2600.0	0.880	0.010
	Inside Air film					0.079

Comparison of the Conduction Time Series (CTSF)

The Conduction Time Series factors (CTSF) were computed three different ways:

- Using the conduction transfer functions computed by Brown and Stephenson (1993a; 1993b), the CTSF were computed using the procedure given by Spitler and Fisher (1999a). These values are given in Table 6.4a.
- Using the conduction transfer functions computed by the state space method from the equivalent wall generated using the measured *R*-value, the CTSF were computed using the procedure given by Spitler and Fisher (1999a). These values are given in Table 6.4b.
- Using the conduction transfer functions computed by the state space method from the equivalent wall generated using the handbook *R*-value, the CTSF were computed using the procedure given by Spitler and Fisher (1999a). These values are given in Table 6.4c.

Table 6.4a Air-to-Air CTSF of the test walls generated from experimentally determined conduction transfer functions

CTS#	ASHRAE 515-RP Test Walls#						
	1	2	3	4	5	6	7
0	0.103200	0.011537	0.015849	0.018255	0.024967	0.005248	0.008559
1	0.457622	0.036539	0.033612	0.137050	0.026803	0.077499	0.019711
2	0.273223	0.078689	0.061717	0.173911	0.033232	0.169579	0.052201
3	0.104275	0.093715	0.075496	0.143111	0.040494	0.174652	0.081376
4	0.038769	0.090233	0.077523	0.112984	0.046567	0.141962	0.093821
5	0.014401	0.082053	0.074315	0.089003	0.050934	0.108306	0.093424
6	0.005349	0.073670	0.069315	0.070106	0.053662	0.081426	0.086705
7	0.001987	0.065980	0.063949	0.055221	0.055006	0.061029	0.077844
8	0.000738	0.059067	0.058742	0.043496	0.055254	0.045714	0.068837
9	0.000274	0.052874	0.053866	0.034261	0.054666	0.034238	0.060465
10	0.000102	0.047330	0.049362	0.026986	0.053462	0.025642	0.052959
11	0.000038	0.042367	0.045222	0.021257	0.051816	0.019204	0.046329
12	0.000014	0.037924	0.041424	0.016743	0.049869	0.014383	0.040509
13	0.000005	0.033948	0.037944	0.013188	0.047726	0.010772	0.035413
14	0.000002	0.030388	0.034756	0.010388	0.045470	0.008067	0.030956
15	0.000001	0.027201	0.031836	0.008183	0.043163	0.006042	0.027058
16	0.000000	0.024349	0.029161	0.006445	0.040852	0.004525	0.023652
17	0.000000	0.021796	0.026710	0.005077	0.038570	0.003389	0.020673
18	0.000000	0.019510	0.024466	0.003999	0.036343	0.002538	0.018070
19	0.000000	0.017464	0.022410	0.003150	0.034187	0.001901	0.015795
20	0.000000	0.015633	0.020527	0.002481	0.032115	0.001424	0.013806
21	0.000000	0.013994	0.018802	0.001954	0.030134	0.001066	0.012068
22	0.000000	0.012526	0.017222	0.001539	0.028248	0.000798	0.010548
23	0.000000	0.011213	0.015775	0.001212	0.026459	0.000598	0.009220

Table 6.4b Air-to-Air CTSF of the EHL walls determined with experimentally determined *R*-values

CTSF	ASHRAE 515-RP Test Walls#						
	1	2	3	4	5	6	7
0	0.079140	0.011980	0.015578	0.007118	0.022151	0.001579	0.008830
1	0.497214	0.021668	0.022806	0.099980	0.020809	0.045743	0.012537
2	0.304794	0.055322	0.049974	0.172089	0.023713	0.144186	0.039737
3	0.088837	0.079857	0.070516	0.153820	0.033122	0.172429	0.074886
4	0.022609	0.085918	0.076497	0.122886	0.043857	0.150046	0.092626
5	0.005588	0.082847	0.075072	0.096636	0.052220	0.118337	0.094408
6	0.001372	0.076647	0.070853	0.075835	0.057520	0.090511	0.088360
7	0.000336	0.069767	0.065806	0.059496	0.060185	0.068570	0.079683
8	0.000082	0.063091	0.060706	0.046675	0.060850	0.051794	0.070721
9	0.000020	0.056902	0.055837	0.036617	0.060089	0.039086	0.062347
10	0.000005	0.051263	0.051294	0.028726	0.058351	0.029488	0.054811
11	0.000001	0.046163	0.047095	0.022536	0.055976	0.022244	0.048131
12	0.000000	0.041562	0.043229	0.017680	0.053212	0.016780	0.042245
13	0.000000	0.037417	0.039676	0.013870	0.050237	0.012658	0.037071
14	0.000000	0.033685	0.036414	0.010881	0.047179	0.009548	0.032529
15	0.000000	0.030324	0.033419	0.008536	0.044125	0.007203	0.028542
16	0.000000	0.027298	0.030671	0.006697	0.041138	0.005433	0.025044
17	0.000000	0.024575	0.028148	0.005254	0.038256	0.004098	0.021974
18	0.000000	0.022123	0.025833	0.004122	0.035505	0.003092	0.019280
19	0.000000	0.019915	0.023708	0.003233	0.032900	0.002332	0.016917
20	0.000000	0.017928	0.021758	0.002537	0.030447	0.001759	0.014843
21	0.000000	0.016139	0.019968	0.001990	0.028149	0.001327	0.013024
22	0.000000	0.014529	0.018325	0.001561	0.026004	0.001001	0.011427
23	0.000000	0.013079	0.016818	0.001225	0.024006	0.000755	0.010027

Table 6.4c Air-to-Air CTSF of the EHL walls determined with handbook *R*-values

CTSF	ASHRAE 515-RP Test Walls#						
	1	2	3	4	5	6	7
0	0.078143	0.012495	0.015831	0.007980	0.025924	0.001651	0.009357
1	0.495753	0.021360	0.023853	0.105520	0.024560	0.047902	0.011401
2	0.306182	0.053569	0.051130	0.174424	0.026216	0.147321	0.032663
3	0.089580	0.077946	0.070585	0.153712	0.033204	0.173662	0.065803
4	0.022845	0.084442	0.075953	0.122183	0.041764	0.149960	0.086741
5	0.005655	0.081815	0.074371	0.095788	0.048682	0.117728	0.092324
6	0.001390	0.075974	0.070185	0.074965	0.053240	0.089749	0.088787
7	0.000341	0.069381	0.065236	0.058656	0.055719	0.067803	0.081378
8	0.000084	0.062935	0.060246	0.045894	0.056597	0.051080	0.072916
9	0.000021	0.056932	0.055483	0.035909	0.056313	0.038449	0.064645
10	0.000005	0.051443	0.051035	0.028096	0.055212	0.028934	0.057031
11	0.000001	0.046462	0.046918	0.021983	0.053559	0.021771	0.050200
12	0.000000	0.041955	0.043124	0.017200	0.051545	0.016382	0.044141
13	0.000000	0.037883	0.039633	0.013458	0.049312	0.012326	0.038796
14	0.000000	0.034205	0.036422	0.010530	0.046963	0.009275	0.034090
15	0.000000	0.030883	0.033472	0.008239	0.044571	0.006978	0.029952
16	0.000000	0.027884	0.030759	0.006446	0.042187	0.005251	0.026315
17	0.000000	0.025176	0.028267	0.005044	0.039847	0.003951	0.023120
18	0.000000	0.022731	0.025977	0.003946	0.037576	0.002973	0.020312
19	0.000000	0.020524	0.023872	0.003088	0.035389	0.002237	0.017845
20	0.000000	0.018530	0.021937	0.002416	0.033295	0.001683	0.015678
21	0.000000	0.016731	0.020160	0.001890	0.031301	0.001266	0.013774
22	0.000000	0.015106	0.018526	0.001479	0.029408	0.000953	0.012101
23	0.000000	0.013639	0.017025	0.001157	0.027616	0.000717	0.010631

The CTSF of three test walls – Wall#1, Wall#4 and Wall#5 were selected for demonstration of the performance of the equivalent wall model. The CTSF plots of the three test walls are shown in Figures 6.5, 6.6 and 6.7. The two equivalent walls of each test wall have the same thermal mass for each layer and the same thermal resistance for all layers but the equivalent layer.

In general, all the three sets of CTS match reasonably well. Interestingly, there does not appear to be a one-to-one correspondence between the error in the *R*-value and the error

in the CTSF. Figure 4.6 represents a case with fairly high error in the handbook R-value (-11.3%) yet the CTSF are very similar. Figure 4.7 represents a case with lower error in the R-value (7.0%) but a noticeably larger deviation in the calculate CTSF. It can be concluded from this observation that EHL wall model accuracy depends not only on the magnitude of the thermal resistance but also may depend on the location of the equivalent homogeneous layer in the construction.

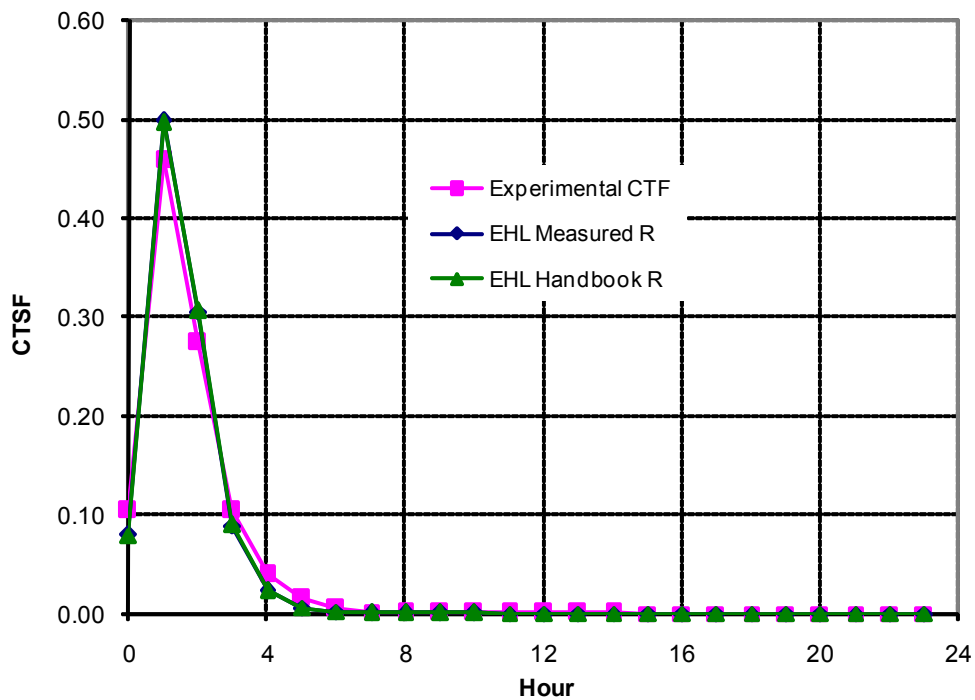


Figure 6.5 CTSF plot for the steel stud wall (Wall#1)

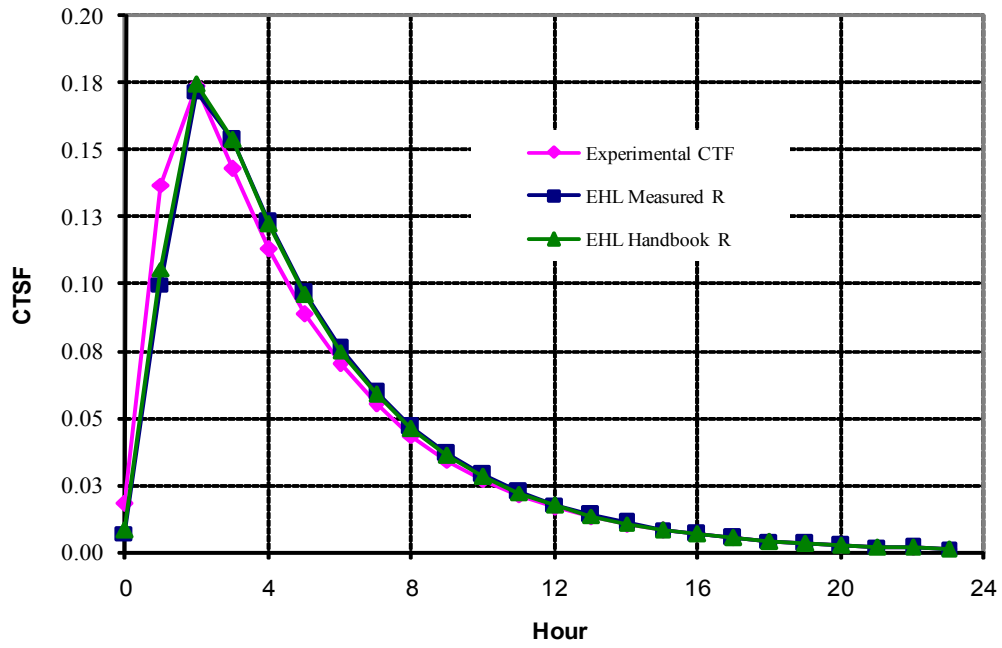


Figure 6.6 CTSF plot for the steel stud wall (Wall#4)

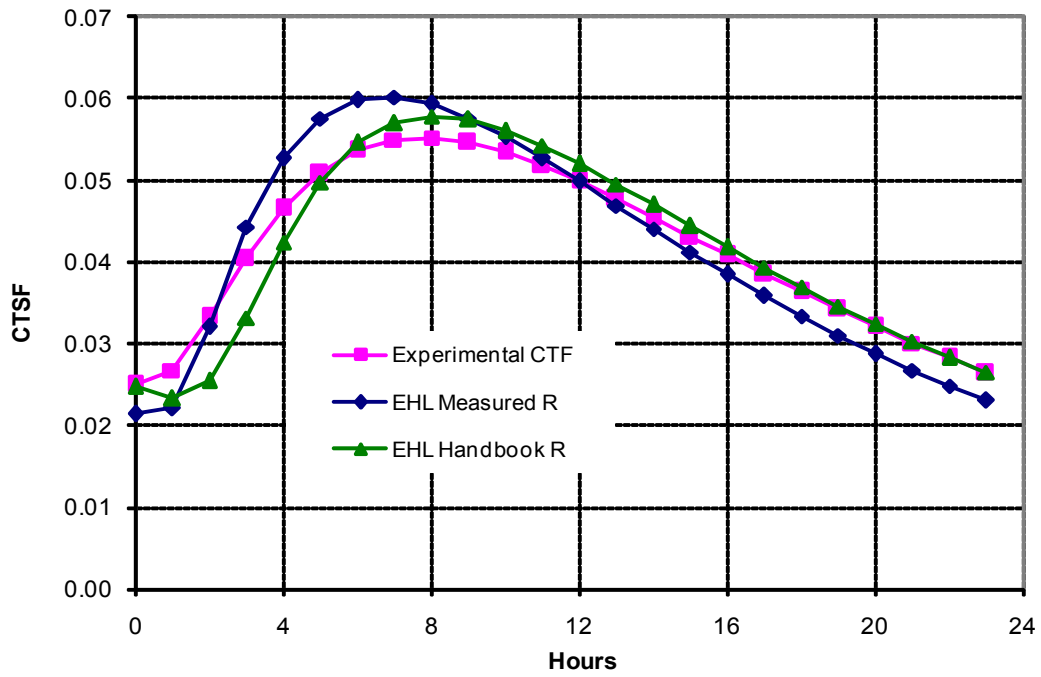


Figure 6.7 CTSF plot for hollow block with insulation and brick exterior finish (wall#5)

6.1.6 Comparison of Conduction Heat gains

The equivalent wall model validation was conducted by computing the conduction heat gains using – the CTSF generated from experimentally determined CTFs, CTSF of the equivalent wall generated using the measured R -value, and the CTSF of the equivalent walls generated using handbook R -value. The heat gains were calculated for Atlanta, Georgia the 1% design day weather condition for the month of July. The hourly heat gain plots for the seven test walls are shown in Figures 6.10 to 6.16.

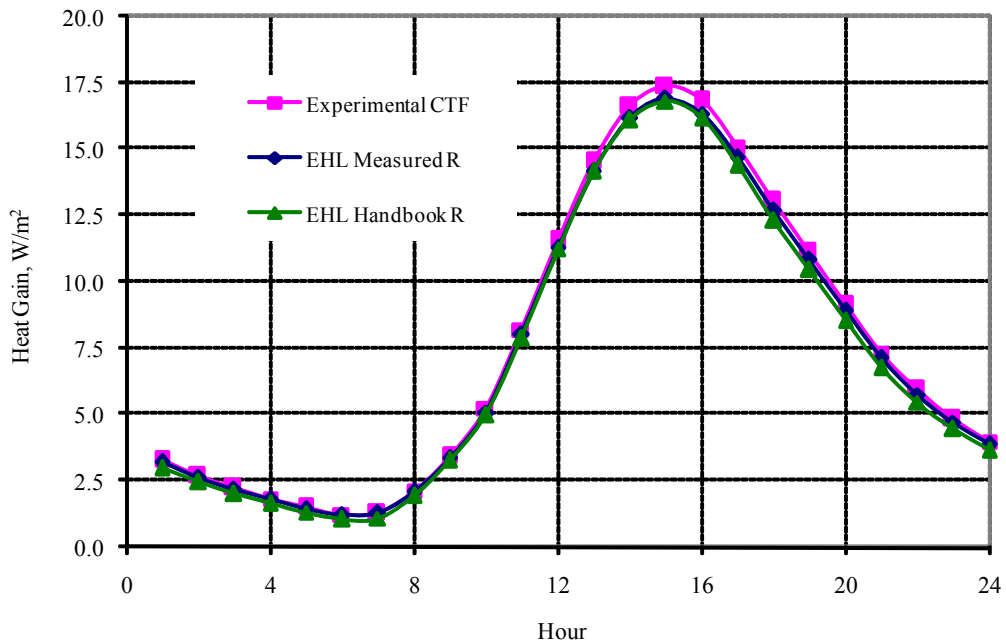


Figure 6.8 Heat gain for insulated steel stud wall with stucco exterior finish (Wall#1)

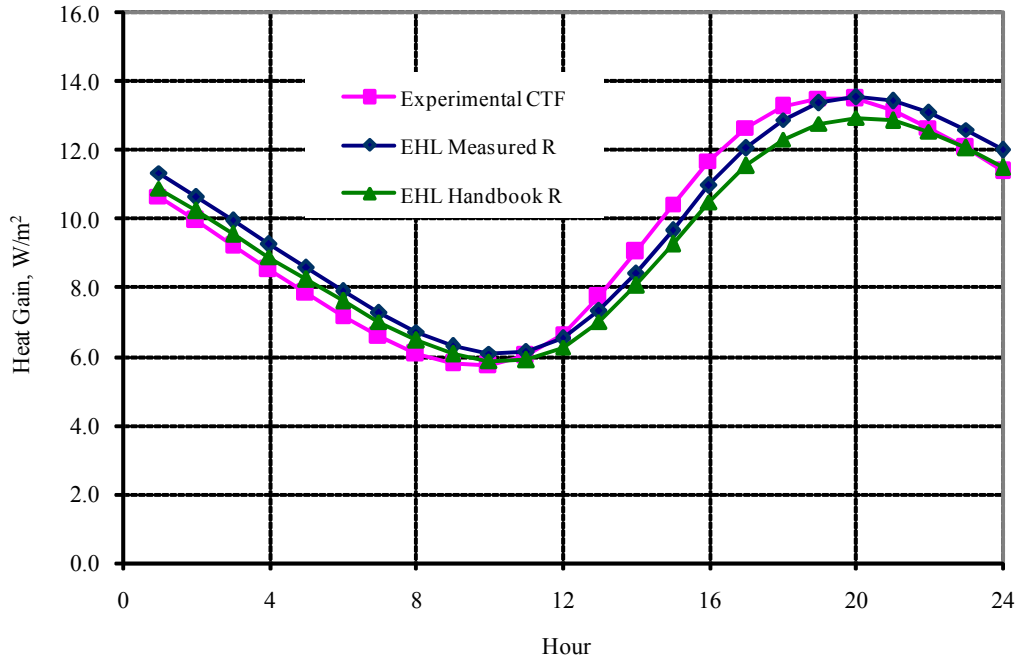


Figure 6.9 Heat gain for pre-cast reinforced concrete slab with steel furring and insulation covered with gypsum board (Wall#2)

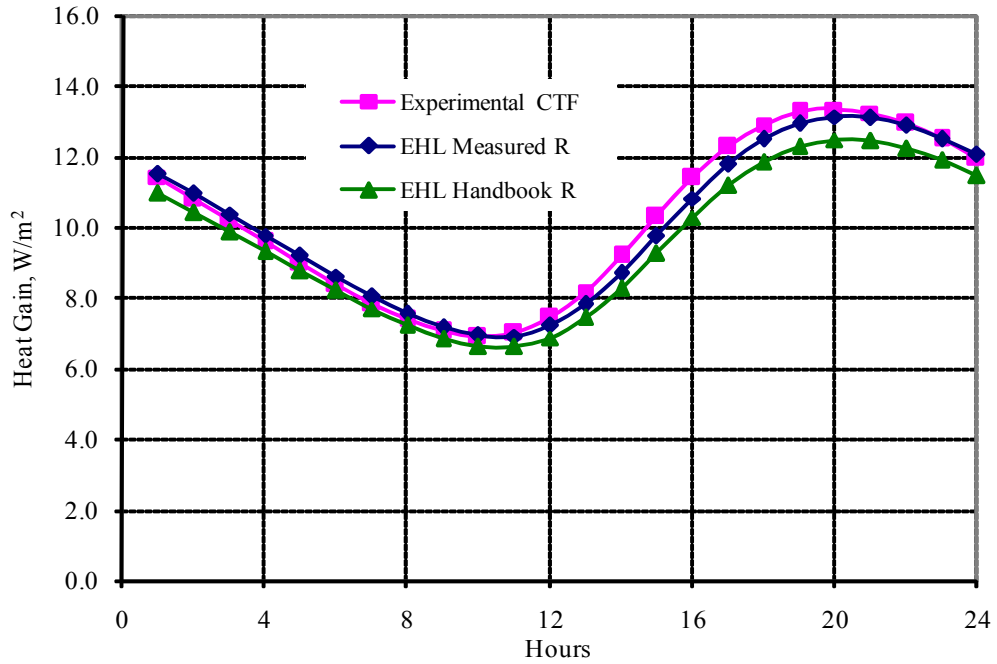


Figure 6.10 Heat gain for pre-cast reinforced concrete slab with steel furring and insulation covered with gypsum board (Wall#3)

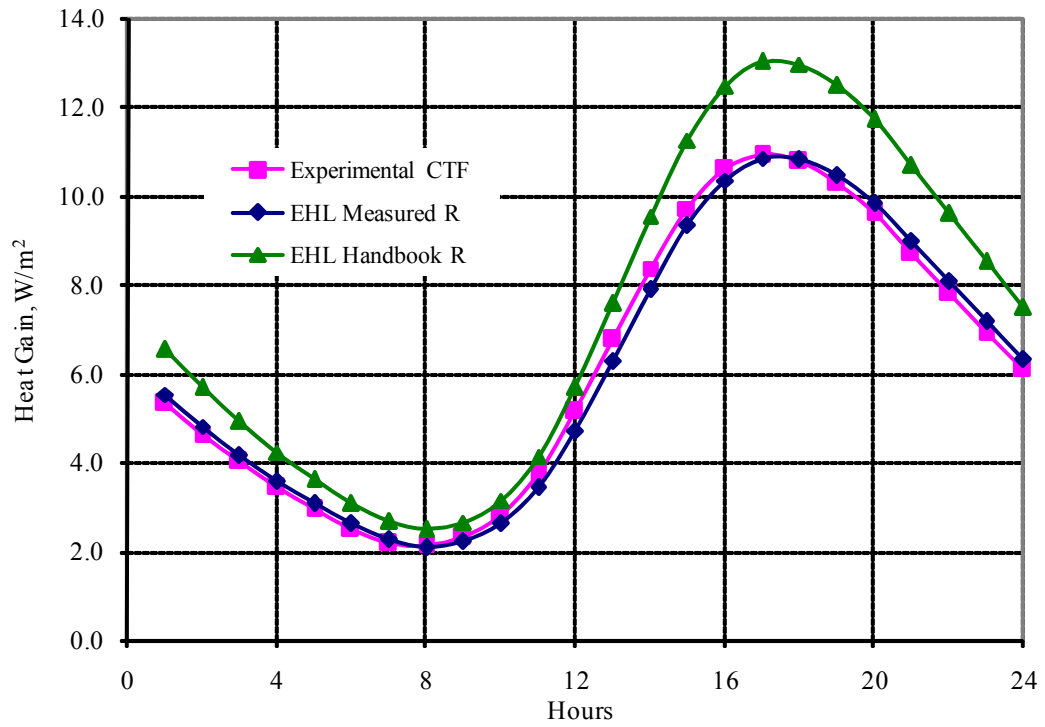


Figure 6.11 Heat gain for insulated steel stud wall mounted on reinforced concrete slab (Wall#4)

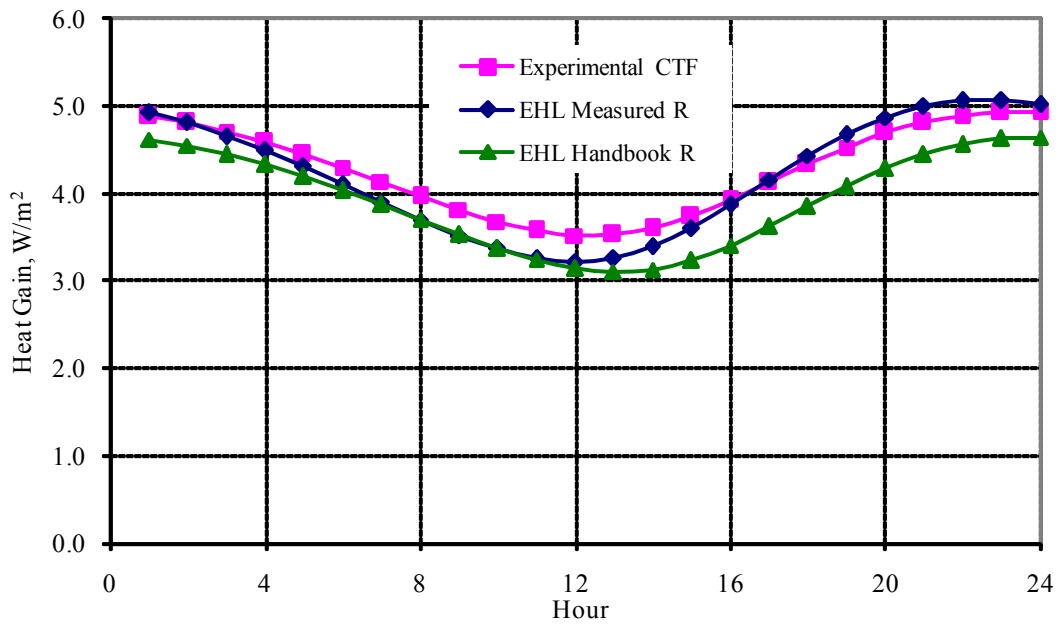


Figure 6.12 Heat gain for hollow concrete block with insulation and brick on the exterior and gypsum board on the interior (Wall#5)

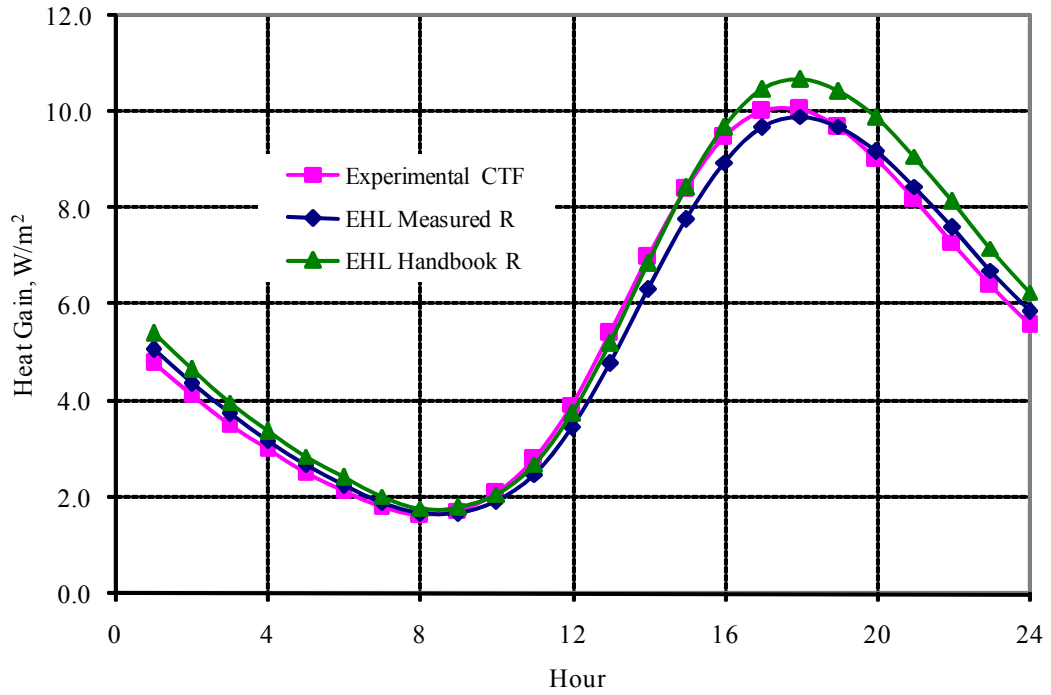


Figure 6.13 Heat gain for insulated steel stud wall with brick exterior finish (Wall#6)

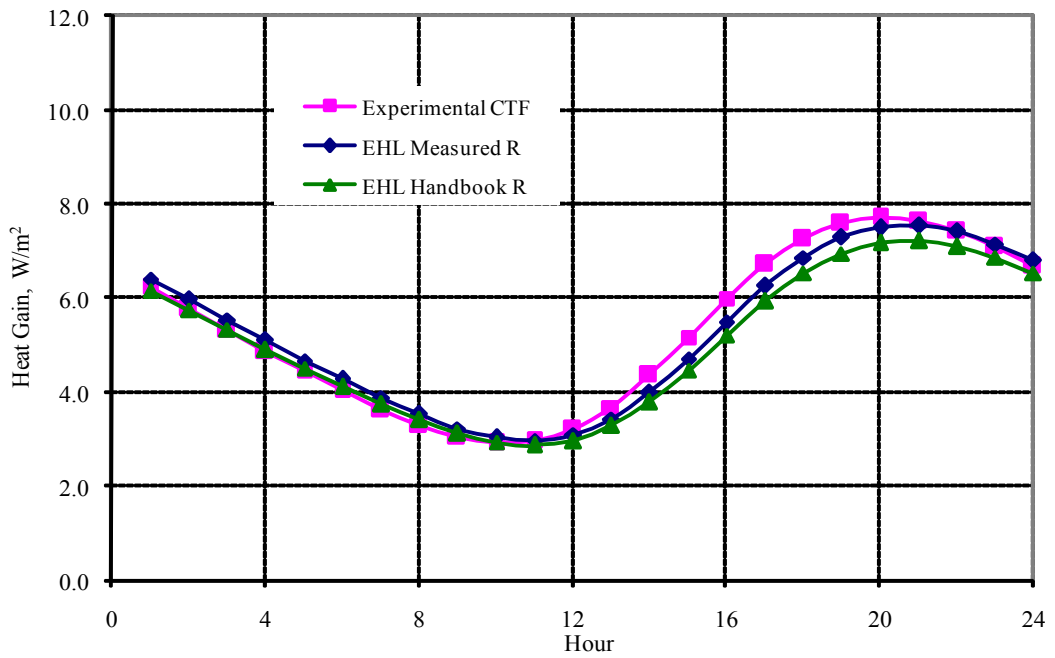


Figure 6.14 Heat gain for solid concrete block wall with insulation and granite veneer exterior finish (Wall#7)

For each of the three approaches, the resulting peak heat gains of the equivalent wall generated using the measured and handbook values matched well with those computed using the experimentally determined CTFs as shown in Table 6.5.

Table 6.5 Results summary of peak heat gains and time shift

Wall #	Peak Heat Gain, W/m ²			Peak Heat Gain Hour, hours		
	Experimental CTF	EHL With Exp. R	EHL With Est. R	Experimental CTF	EHL With Exp. R	EHL With Est. R
1	16.9	17.0	16.8	15	15	15
2	13.5	13.5	13.0	19	20	20
3	13.4	13.1	12.5	20	20	20
4	10.9	10.8	13.0	17	17	17
5	4.9	5.1	4.6	23	23	24
6	10.1	9.9	10.7	18	18	18
7	7.7	7.6	7.2	20	21	21

The peak heat gain error calculated for the two equivalent walls generated using the measured and handbook R-values are summarized and given in Figure 6.15. The peak heat gain of the equivalent wall model calculated using the measured R-values agreed within $\pm 2.6\%$ of the experimental results. For comparison purposes, Figure 6.16 shows errors in the handbook R-values for each wall.

Also reasonably good heat gain match were found between the equivalent walls generated using the handbook R-value and experimentally determined CTFs. However, deviations were observed where the handbook R-value showed large differences from that of the experimental values.

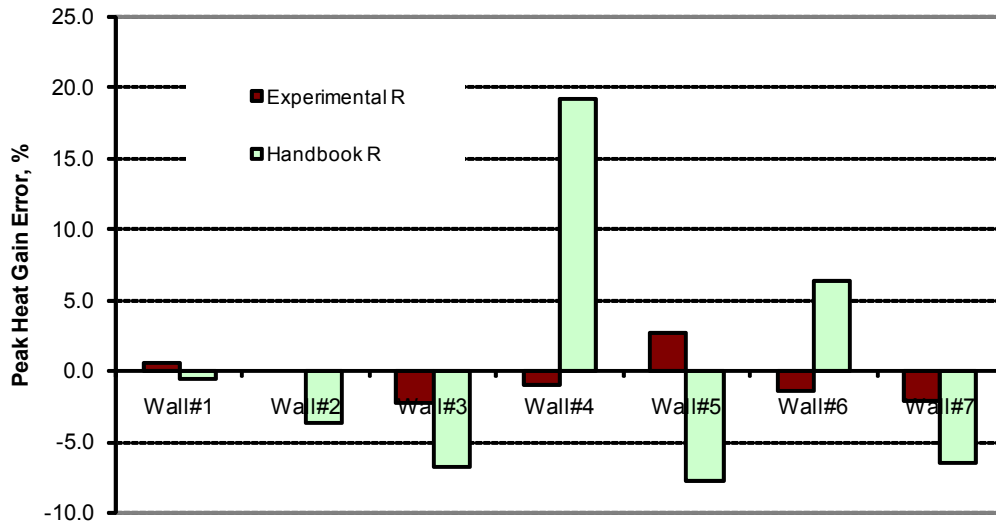


Figure 6.15 Summary of peak heat gains for the seven ASHRAE test walls

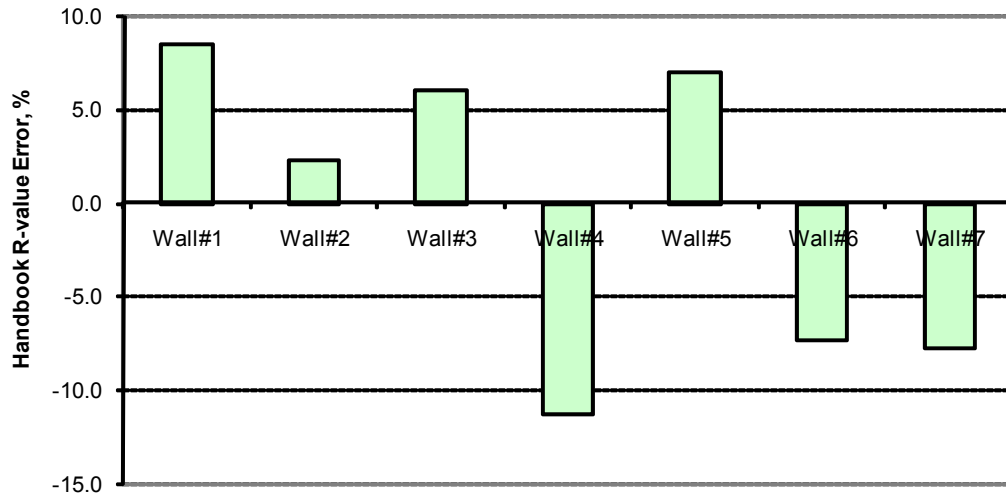


Figure 6.16 Handbook *R*-value errors compared to experimental values the seven ASHRAE test walls

For the equivalent wall determined using the handbook *R*-value agreed within $\pm 8\%$ of the experimental results for all test walls except for the insulated steel stud wall with reinforced concrete slab siding (test wall#4). It is evident from the *R*-values given in

Table 6.2 that the higher the peak heat gain deviation for this wall is due to large difference between measured and the handbook R -values. The higher error of the handbook R -value for wall#4 is may be explained by failure of the F_c correction method for steel stud walls with thick reinforced concrete siding.

The peak heat gain timing of the equivalent walls matched well with timing computed with experimentally measured CTFs as shown in Table 6.5. The wall#2, wall#5 and wall#7 show one hour shift in the peak heat gain occurrence. The reinforced concrete slab walls with insulated steel furring siding (test wall#2 and wall#3) have identical layers. However, the measured R -values reported are slightly different presumably attributed to experimental errors.

6.2 Inter-model Validation

The experimental validation is based on a limited number of thermal bridge wall specimen tests. Moreover, the ASHRAE 515-RP experimental results provide air-to-air conduction transfer coefficients, which limit the experimental validation to convective type boundary conditions only. Therefore, it is desirable to augment the experimental validation of the equivalent homogeneous layer model with additional wall types and boundary conditions. Since developing a new experimental facility is beyond the scope of this project, a numerical inter-model validation using a wide range of test specimens and boundary conditions is necessary.

The numerical validation is intended to augment the experimental validation and demonstrate the suitability of implementation of the equivalent homogeneous layer wall model in the one-dimensional energy analysis and load calculation programs. A two-dimensional finite volume numerical method is used as a reference model for the inter model validation. The validation has been done based on three generic steel stud constructions identified by Gorgolewski (2007) and a wood stud wall. All the test specimens in the numerical validation are sandwich type linear thermal bridges. The description of the test walls is given next.

6.2.1 Numerical Validation Test Walls

Gorgolewski (2007) came up with three generic type steel stud walls commonly used in building walls and roofs construction. These generic constructions were used as representative test specimens for the numerical validation. For completeness wood stud wall test specimen has been included. These test specimens are described next and their construction layers thermo-physical properties are given in Table 6.6 and their section views are shown in Figure 6.17.

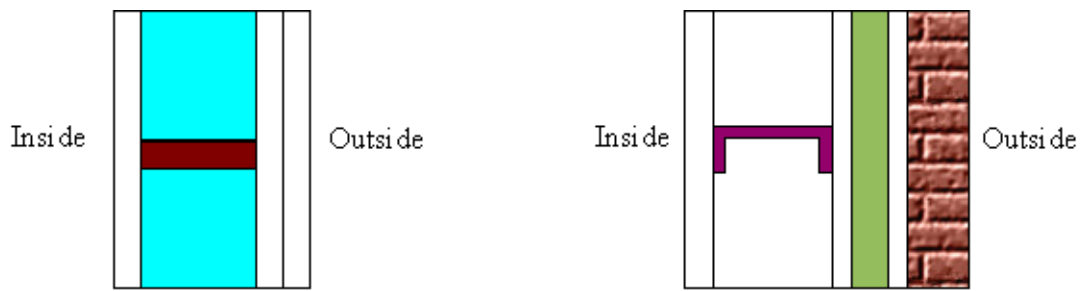
Wood Stud Wall: the wood stud consists of wood siding on the exterior, after that plywood, then a composite layer with fiberglass insulation and wood stud wall in parallel and Gypsum interior finish. The stud has 88.9 mm depth and 38.1 mm width. The stud center-to-center spacing is 406.4 mm. The actual wood stud wall layer is given in Table 6.6.

Table 6.6 Test walls layers description for inter-model validation

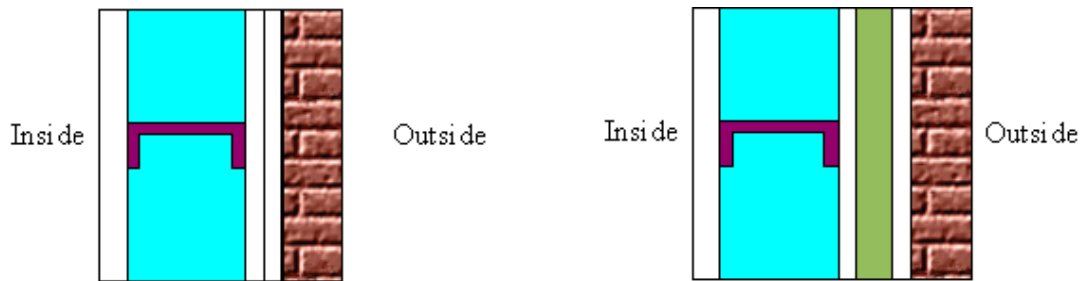
Layers	Thickness (mm)	Conductivity (W/m·K)	Density (Kg/m ³)	Specific Heat (kJ/kg·K)	Resistance (m ² ·K /W)
Actual wall layers – wood stud wall					
Wood Siding	12.7	0.072	544.0	1.255	0.176
Plywood	12.7	0.115	544.0	1.213	0.110
Wood Stud	88.9	0.114	576.0	1.632	
Fiber Glass Insulation	88.9	0.046	84.8	0.962	
Gypsum	12.7	0.160	800.0	1.088	0.079
Actual wall layers – cold light steel stud wall					
Brick	102	0.720	1920.0	0.790	0.142
Clear Air Cavity	50	0.250	1.2	1.007	0.200
Plywood	20	0.115	544.0	1.213	0.174
Steel Stud	100	45.3	7600.0	0.500	
Fiber Glass Insulation	100	0.029	14.5	0.710	
Plaster Board	15	0.100	800.0	1.090	0.150
Actual wall layers – warm light steel stud wall					
Brick	102	0.720	1920.0	0.790	0.142
Clear Air Cavity	50	0.250	1.2	1.007	0.200
Rigid Insulation	50	0.046	84.8	0.962	1.087
Plywood	20	0.115	544.0	1.213	0.174
Steel Stud	100	45.3	7600.0	0.500	
Air Gap	100	0.560	1.2	1.007	
Plaster Board	15	0.100	800.0	1.090	0.150
Equivalent homogeneous layer wall – hybrid light steel stud wall					
Brick	102	0.720	1920.0	0.790	0.142
Clear Air Cavity	50	0.250	1.2	1.007	0.200
Rigid Insulation	50	0.046	84.8	0.962	1.087
Plywood	20	0.115	544.0	1.213	0.174
Steel Stud	100	45.3	7600.0	0.500	
Fiber Glass Insulation	100	0.029	14.5	0.710	
Plaster Board	15	0.100	800.0	1.090	0.150

Warm Frame Steel Stud Wall: the warm steel frame wall construction has no insulation in between the steel studs and the insulation layer is on the exterior side. This type of construction maintains the steel frame temperature close to the indoor air temperature and is common for domestic design in the UK. The steel stud has 100 mm depth, 38.1 mm width, 1.5 mm thickness and 609.6 mm center-to-center spacing. The layer-by-layer description of the cold steel stud wall is given in Table 6.6.

Cold Frame Steel Stud Wall: the cold steel frame wall construction has insulation in between the steel studs only and there is no insulation layer on the exterior side. This type of construction has high degree of thermal bridge effects. The steel stud has 100 mm depth, 38.1 mm width, 1.5 mm thickness and 609.6 mm center-to-center spacing. The layer-by-layer description of the cold steel stud wall layers is given in Table 6.6.



(a) Wood stud wall; (b) warm frame steel stud wall



(c) Cold frame steel stud wall; (d) hybrid frame steel stud wall

Figure 6.17 Wood and steel stud walls construction for numerical validation

Hybrid Frame Steel Stud Wall: the hybrid steel frame wall construction has insulation on the exterior side and in between the steel stud layer. This is the most common type construction used for domestic walls and roofs application (Gorgolewski 2007). The steel stud has 100 mm depth, 38.1 mm width, 1.5 mm thickness and 609.6 mm center-to-center spacing. The layer-by-layer description of the hybrid steel stud layer is given in Table 6.6.

6.2.2 The R-values and The Equivalent Walls

The handbook surface-to-surface R -values of the wood stud and the steel stud walls were calculated using the parallel path method and the F_c correction method, respectively, as recommended by ASHRAE (2005). The R -values calculated using the 2D finite volume numerical program, and ASHRAE's recommended procedures are given in Table 6.7. The equivalent wall generated of the four test walls are given in Table 6.8.

Table 6.7 Surface-to-surface R -values of the inter-model validation test walls ($\text{m}^2 \cdot \text{K}/\text{W}$)

Test Walls	2D Finite Volume Method	Handbook	Handbook Method
Wood stud wall	2.10	2.09	Parallel Path
Warm steel stud wall	1.95	1.91	$F_c (=0.90)$
Cold steel stud wall	2.69	2.39	$F_c (=0.55)$
Hybrid steel stud wall	3.92	3.59	$F_c (=0.55)$

Table 6.8 Equivalent walls for inter-model validation test walls

Layers	Thickness (mm)	Conductivity (W/m·K)	Density (Kg/m ³)	Specific Heat (kJ/kg·K)	Resistance (m ² ·K /W)
Equivalent homogeneous layer wall – wood stud wall					
Wood Siding	12.7	0.072	544.0	1.255	0.176
Plywood	12.7	0.115	544.0	1.213	0.110
Equivalent layer	88.9	0.052	130.9	1.239	1.725
Gypsum	12.7	0.160	800.0	1.088	0.079
Equivalent homogeneous layer wall – warm light steel stud wall					
Brick	102	0.720	1920.0	0.790	0.142
Clear Air Cavity	50	0.250	1.2	1.007	0.200
Rigid Insulation	50	0.046	84.8	0.962	1.087
Plywood	20	0.115	544.0	1.213	0.174
Equivalent Layer	100	0.050	47.4	0.564	2.013
Plaster Board	15	0.100	800.0	1.090	0.150
Equivalent homogeneous layer wall – cold light steel stud wall					
Brick	102	0.720	1920.0	0.790	0.142
Clear Air Cavity	50	0.250	1.2	1.007	0.200
Plywood	20	0.115	544.0	1.213	0.174
Equivalent Layer	100	0.053	47.4	0.564	1.897
Plaster Board	15	0.100	800.0	1.090	0.150
Equivalent homogeneous layer wall – hybrid light steel stud wall					
Brick	102	0.720	1920.0	0.790	0.142
Clear Air Cavity	50	0.250	1.2	1.007	0.200
Rigid Insulation	50	0.046	84.8	0.962	1.087
Plywood	20	0.115	544.0	1.213	0.174
Equivalent Layer	100	0.050	47.4	0.564	2.013
Plaster Board	15	0.100	800.0	1.090	0.150

6.2.3 Performance of the Equivalent Walls

The steady periodic heat gains for the four test walls were determined using sol-air temperature as boundary condition of ASHRAE’s 1% design day weather data of Atlanta, Georgia. The hourly heat gains of the equivalent walls generated for *R*-values computed using 2D finite volume numerical method and the handbook procedures and then compared to that of a 2D transient finite volume numerical program. For the equivalent walls the hourly heat gains were computed using conduction time series factors (CTSF)

generated using the Spitler and Fisher (1999a) procedure. The hourly heat gain plots are shown in Figures 6.19 to 6.22. Summary of the peak heat gains is shown in Table 6.9.

Table 6.9 Results summary of peak heat gains and time shift

Wall #	Peak Heat Gain, W/m ²			Time Shift in hours	
	2D Finite Volume Program	EHL 2D Finite Volume R	EHL Best Est. R	EHL 2D Finite Volume R	EHL Best Est. R
1	9.2	9.50	9.50	-1	-1
2	7.99	7.73	7.91	0	0
3	5.66	5.79	6.08	0	0
4	3.47	3.50	3.86	0	0

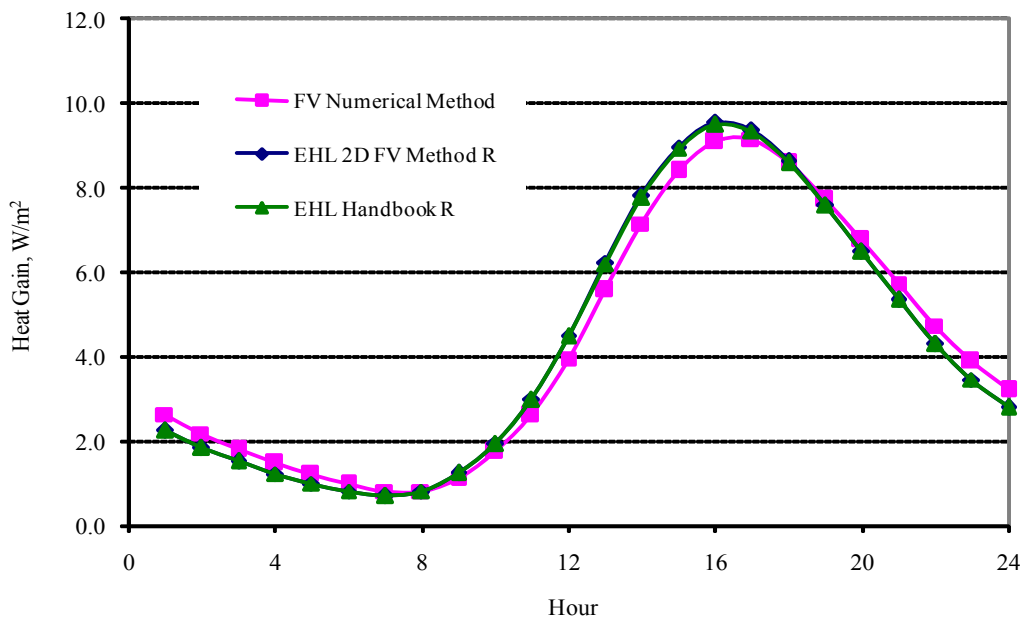


Figure 6.18 Heat gain at the inside surface of a wood stud wall for periodic sol-air temperature boundary condition

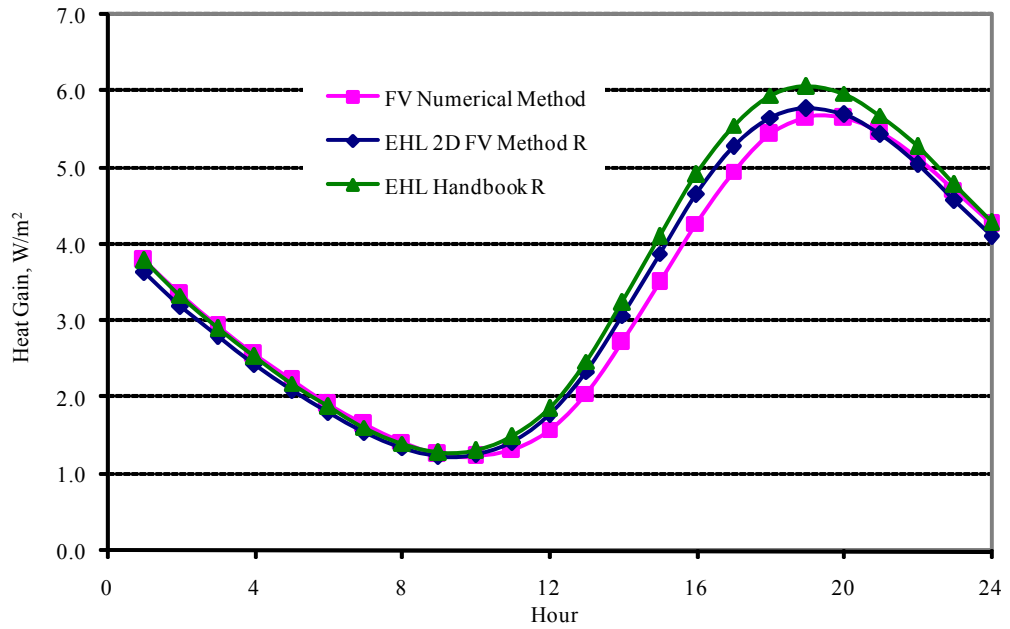


Figure 6.19 Heat gain of a cold steel stud wall for steady periodic sol-air temperature boundary condition

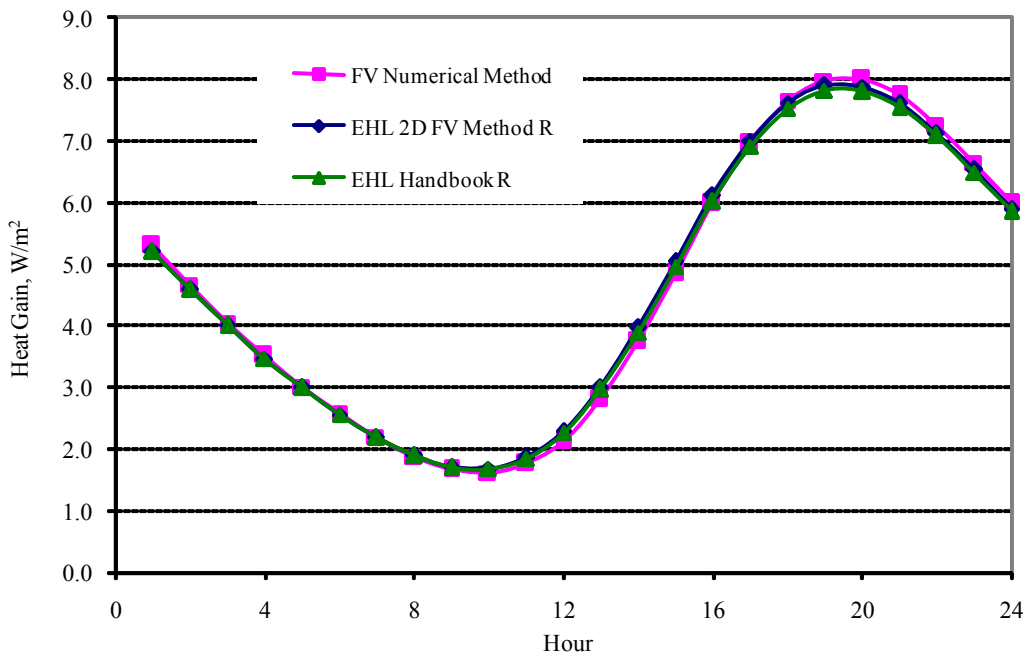


Figure 6.20 Heat gain of a warm steel stud wall for steady periodic sol-air temperature boundary condition

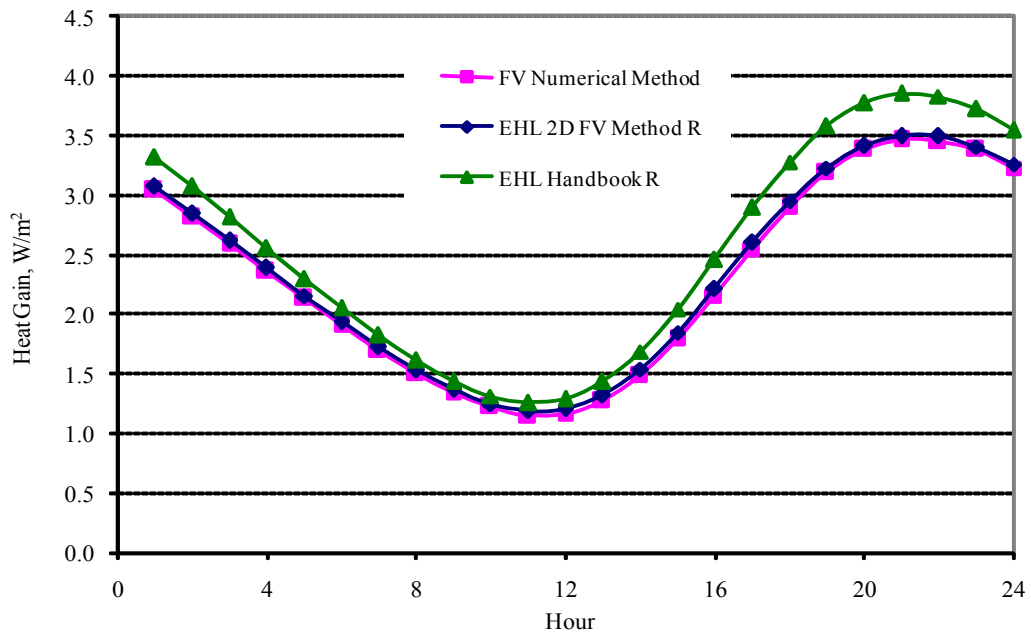


Figure 6.21 Heat gain of a hybrid steel stud wall for steady periodic sol-air temperature boundary condition

6.2.4 Summary and Conclusion

The numerical validation has also confirmed that the approximate one-dimensional equivalent homogeneous layers wall model can predict the peak heat gain very well but the performance is as good as the accuracy of the steady state R -value. The peak heat gain error for the equivalent wall of the cold frame light steel stud wall, which has the handbook R -value error of 11.3%, was only 7.3% as shown in Figure 6.22 and 6.23. Similarly the peak heat gain error of the equivalent wall of warm frame light steel stud wall, which has the handbook R -value error of 8.3%, is 11.1%. This clearly indicates that the peak heat gain errors depends not only the magnitude of the R -value error but also on the order of the layers and the magnitude of the thermal bridge composite layer resistance relative to the other layers in the construction.

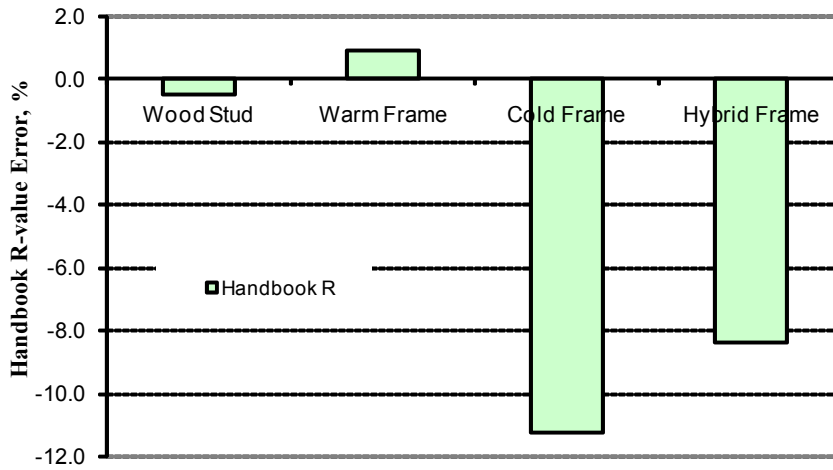


Figure 6.22 Handbook *R*-value errors compared to that of the 2D finite volume method

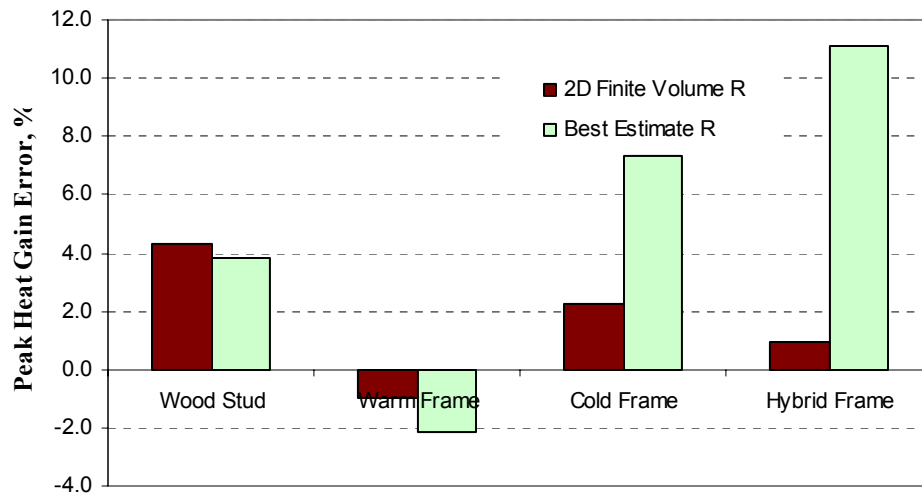


Figure 6.23 Peak cooling load prediction error of the equivalent walls compared to the 2D finite volume method

The cold and hybrid frame steel stud test walls, which have higher handbook *R*-value error, the layer orders has been reversed from the outside to inside to investigate how the relative position of the composite or thermal bridge layer change affects the peak heat

gain prediction of the equivalent wall. The reversed layers order equivalent walls are identical since the steady state R -values are the same. For the reversed layers order the cold and hybrid steel stud equivalent walls peak heat gains reduced to 5.0% and 10.2% from 7.3% and 11.1%, respectively. This change in the peak heat gain error shows how the relative position of the thermal bridge composite layer may affect the peak heat gain prediction performance of the equivalent wall. It can be inferred from these that it is essential to maintain the number of layers and the layers order as in the actual construction whenever possible.

The equivalent wall model predicts the peak cooling load within $\pm 2.5\%$ of a 2D finite numerical program provided the steady state R -values are determined using two-dimensional numerical programs. In fact this suggests that a numerical program that can generate equivalent walls can be developed and readily integrated into existing one-dimensional energy analysis and load calculation programs. However, this requires a standalone 2D user interface for construction geometry and material layer specification to compute accurate steady state R -value and then generate the equivalent wall.

6.3 Conclusion and Recommendations

The experimental and the inter-model validations have confirmed that the equivalent homogeneous layer wall model can replicate the peak heat gains of walls with thermal bridges with the accuracy primarily limited by the estimate of the R -values. This has been demonstrated using the seven ASHRAE RP-515 test walls and a wood stud wall, and three generic type steel frame walls identified by Gorgolewski (2007).

When measured R -values are used, the EHL model agreed within $\pm 2.6\%$ of the experimental results. When standard methods recommended by ASHRAE for estimating the R -values were used, the peak heat gains for six of walls were predicted within $\pm 7.7\%$ of the peak heat gain determined using the measured CTFs. For the seventh wall, an insulated steel stud wall mounted on reinforced concrete slab, a peak heat gain error of 19.3% was observed. This is primarily due to an 11.3% deviation of the handbook R -value from the measured R -value.

The inter-model validation also confirmed that the equivalent wall for light steel stud walls predicts the peak heat gain within $\pm 2.5\%$ of that of the actual wall provided that the R -values were determined using the 2D numerical model. The errors in the R -values for the numerical test walls computed with standard method were in the range 0.5% to 11.3%. For the cold frame steel stud test wall with the R -value error of 11.3%, the peak heat gain error was 7.3%.

It can be concluded from experimental and numerical validation that the EHL walls duplicate the dynamics of walls with thermal bridges provided the thermal resistances of the actual construction and the thermal mass of the composite layer are predicted accurately and the layers order are maintained as in the actual wall. It can be said that the equivalent homogeneous layer dynamic model is as good as the accuracy of the R -value estimate.

The EHL wall model accuracy dependency on the layers order has been investigated by reversing layers order for cold and hybrid steel stud test walls. The reversed layer and the actual walls have the same R -values. Interestingly, reversing layers order brought 31.5%, and 8.1%, respectively, reduction in the peak heat gain prediction error. This clearly indicates that the EHL wall model performance also slightly depends on the location of the thermal bridge layer relative to highly resistive and massive layers in the construction.

General Recommendation

The following guidelines are additional recommendation that help to improve implementation of the equivalent homogeneous layer wall model to thermal bridges:

- i. Maintain the number of layers and the layer order in the actual wall construction as much as possible. Otherwise, it is recommended to keep at least three homogeneous layers in the equivalent wall whenever possible.
- ii. The overall thickness of the equivalent wall must be the same as that of the actual wall and the thermal mass and the sequence must correspond to each layer in the actual construction.
- iii. Air gaps adjacent to composite layers should remain as a separate layer unless elements of the composite layers such as tie-rods, screws or bolts protrude into the air gap layer. In the later case combine the air gap with composite layer. Then the thickness of the equivalent homogeneous layer is the sum of the composite layers and that of the air gap thickness. The thermal mass of the equivalent layer must then include that of the air gap as well.

- iv. If the composite layer has significant thermal mass difference along the principal heat flow direction then divide the composite layer into two homogeneous layers reflecting the realistic thermal mass distributions.
- v. If there are two composite layers separated by homogeneous layers, then there must be two equal homogeneous layers one for each. Then, the equivalent layers will be apportioned based on the thermal resistance ratio of the dominant elements in the two composite layers. But the equivalent layers thermal masses should be based on the actual constructions in each composite layer.
- vi. The reinforcement metal bars in the concrete slab can be ignored in the thermal resistance calculation. Treat the concrete slab as if it is homogeneous layer but correct the thermal mass for the effect of the reinforcement bar.

6.4 Recommendation for Future Work

The equivalent homogeneous layer wall model is suited only for sandwich type thermal bridge constructions. Two limitations of the equivalent homogeneous layer wall model that has been identified: when thermal bridge element is exposed to interior or exterior environments, and when multiple composite layers are separated by homogeneous layer in sandwich type thermal bridges. The multi-composite layers can be lumped together. But this needs to be validated either experimentally or numerically. Therefore, these two limiting cases of the equivalent homogeneous layer wall model require further investigation hence are recommended as a future work.

7 Conclusions and Recommendations

In this thesis a series of investigations of the Radiant Time Series Method (RTSM) have been conducted, in some cases leading to improvements to the method, its sub-models, supporting data, or facilitation of implementation in a wide range of computing environments. These developments include:

1. The improved RTSM procedure, which accounts for transmission of radiant heat gains back to the outside by conduction through fenestration or other high conductance surfaces.
2. Modification of fenestration model: adapted the RTSM to use recent developments in fenestration models and data. A new set of radiative / convective splits have been established.
3. Development of the reduced heat balance method for RTF generation.
4. Development of simplifications to facilitate implementation of the RTSM in a range of computing environments.
5. Parametric investigation to establish the limitations of the RTSM and provide design guidance.

Furthermore, an approximate one-dimensional dynamic model for thermal bridges has been investigated and design guidance for practicing engineers has been established. The dynamic model of thermal bridges can be used with other energy analysis and load calculation procedures as well in the following sections, conclusions based on the findings are summarized and recommended future works are presented.

7.1 Improvement to the Radiant Time Series Method

The improvements of the RTSM procedure correspond to the first four developments listed above. The findings are summarized in the following sections:

7.1.1 Accounting for Heat Losses in RTSM

An algorithm for correcting the space radiant heat gains to account for radiant loss by conduction has been derived as discussed in Section 3.3.1. The procedure accounts for solar and internal radiant heat gains conducted back out through fenestrations. The algorithm is formulated using a dimensionless loss conductance that can easily be computed from the fenestration U -value, inside combined conductance and total area of the zone surfaces including furnishings. The procedure has been implemented by correcting the first term of the radiant time factors and hence maintains the simplicity desired in the RTSM procedure. The peak cooling load over prediction trend of the RTSM procedure has been improved dramatically, as discussed below in section 7.1.5. With this addition, the current RTSM procedure is referred to as the improved RTSM procedure.

7.1.2 Improvements to the RTSM Fenestration Model

The RTSM fenestration models have been adapted to the use of solar heat gain coefficients (SHGC) currently available from window manufacturers and interior attenuation coefficients (IAC) as appear in the current (2005) ASHRAE Handbook of Fundamentals. Since SHGC do not give information about the split between transmitted and absorbed components, as was available with previous models which used shading coefficients, new radiative / convective splits were needed. These were determined with a parametric study described in Section 3.2 and are summarized in Table 3.5. The performance of the new set of radiative / convective splits has been characterized with parametric investigation summarized in Section 7.1.5.

7.1.3 Improvements to the RTF generation

An algorithm for generating Radiant Time Factors (RTF) based on the reduced heat balance procedure has been derived, as discussed in Section 3.1, and validated against a full-blown heat balance program. The new RTF engine uses periodic response factors, which are generated from conduction transfer functions (CTFs) computed using the state space method. The reduced heat balance method eliminates the unneeded features in the HBM, such as the outside heat balance and treatment of solar radiation, and it uses compact matrix notation. Hence implementation of the method can take advantage of programming environments with built-in matrix algebra or matrix algebra libraries. Furthermore, a constant radiation use in the system matrix has been investigated, which may reduce the RTF generation time by one-half without loss of accuracy. This is desirable for implementation in VBA.

7.1.4 Developments in RTSM Implementations

Implementation of the RTSM in different computing environments has been hindered by computational efforts required to generate the periodic response factors (PRF) and the radiant time factors (RTF). Specifically, the RTSM was intended for use as a spreadsheet method, yet it originally required a full-blown HBM program to generate the PRF and RTF. The developments to facilitate implementations of the RTSM in other computing environments are summarized as follows:

- An alternative procedure for generating periodic response factors (PRF) that uses a one-dimensional finite volume numerical method has been developed and successfully implemented in VBA and FORTRAN 90. This algorithm has some advantages over the Laplace and State Space methods in that it's based on fundamental concepts understandable by senior level undergraduate students and is suitable for implementation in any computational platform. In particular its suitability for use with VBA is convenient for implementation of the RTSM in spreadsheets.
- The reduced HBM RTF generation algorithm has also been implemented in VBA and SCILAB. Its implementation in VBA makes the RTSM entirely a “spreadsheet procedure” – thus no external DLL or other computer programs are needed.

7.1.5 Parametric Study of the Performance of RTSM

Performance of the current and improved RTSM procedures has been investigated using a total of 2,867,200 zones representing a wide range of building constructions, zone geometries, fenestrations with and without interior shading, and design weather and

locations. In the discussion below, the term “current RTSM” refers to the original RTSM (Spitler et al. 1997) procedure with the new fenestration model. The term “Improved RTSM” procedure refers to the current RTSM with heat loss correction applied. This investigation was intended to establish the limitations of the RTSM peak cooling prediction quantitatively as design guidance for practicing engineers. The following conclusions can be deduced from the parametric investigations conducted:

- The extreme peak cooling over prediction trend of the RTSM procedure showed strong dependency on:
 - ♦ glazing fraction – over prediction increases with glazing fraction
 - ♦ glazing types – high SHGC increases the amount of solar heat gain for unshaded fenestration and hence increases the over prediction
 - ♦ peak design temperature – lower peak design temperatures tend to increase the peak cooling over prediction
 - ♦ zone orientation – zones in the east and north-east zones tend to peak in the morning, hence tending to increase the over prediction
 - ♦ number of exterior facade surfaces – increasing the exterior facades increases in the over predictions
 - ♦ interior shades – reduce the amount of solar heat gain and hence reduce the peak cooling load over prediction
 - ♦ construction fabric – without interior shaded fenestration, light and heavyweight construction tend to have the same over predictions. However, for zones with interior shaded fenestration, heavyweight construction zones tend to result in higher overpredict than lightweight

zone construction. This not endemic to the method but is an effect of the single radiative fraction for all SHGC applied to all zones.

- The improved RTSM procedure reduced the over prediction of peak cooling load significantly, in particular for fenestrations without interior shades. For 716,800 zones without interior shading, the current RTSM over predictions are as high as 30.5% while it is reduced to 10.5% for the improved RTSM procedure. The maximum over prediction occurs for zones with single pane clear glass on two exterior facade surfaces. The over prediction for other glazing types and zone constructions are summarized in Table 4.10.
- The average over prediction of peak cooling load of the current RTSM for 71,680 zones at 50% and 71,680 zones at 90% exterior facade glazing fraction for fenestration without interior shades are 8.4% and 12.7%, respectively. Overall the improved RTSM gives substantially lower over predictions for the entire range of problem zones. The average over predictions for the same 71,680 zones reduced to 5.6% and 4.5%, respectively.
- The over prediction is smaller when the fenestration has interior shades due to reduction in the amount of solar heat gain. The maximum over predictions of the current and improved RTSM procedures for 716,800 zones with interior shade fenestration are 19.9% and 17.7%, respectively. For the current RTSM procedure this occurs at 90% glazing fraction of the exterior facade. The average overpredictions of the current RTSM procedure for zones with interior shaded fenestration at 50% (71,680 zones) and 90% (71,680 zones) glazing fractions are

10.3% and 12.8%, respectively. The improved RTSM procedure only reduces the average over predictions of peak cooling load for these zones to 8.6% and 9.8%, respectively.

- As the result of the use of a fixed radiative fraction for all construction fabrics, the RTSM peak cooling load over prediction is different with light and heavyweight constructions. Peak cooling load over predictions for zones with shaded windows tend to be higher for heavyweight zones than lightweight zones by 2% - 12% depending on the glazing type. The over prediction trends for different glazing types are summarized in Table 4.11.

7.2 Conclusions: Dynamic Modeling of Thermal Bridges

The approximate one-dimensional procedure, the equivalent homogeneous layer (EHL) wall model, proposed by Karambakkam et al. (2005) has been validated against experimental results published by Brown and Stephenson (1993a; 1993b). As the experimental validation test specimens were limited to seven test walls, a wood stud wall and three generic steel stud walls identified by Gorgolewski (2007) have been validated against a 2D finite volume program. Brown and Stephenson derived conduction transfer functions (CTFs) for each wall. These CTFs and the conduction time series factors (CTSFs) developed with the equivalent homogeneous layer (EHL) wall model were used to compare peak heat gains for a typical sol-air temperature profile. For inter-model validation using 2D finite volume program, peak heat gains computed with EHL-model derived CTFs were compared to peak heat gains computed directly with 2D finite volume

program. The following conclusions can be drawn from the experimental and inter-model validations:

- The experimental and the inter-model validations have confirmed that the equivalent homogeneous layer wall model can replicate the peak heat gains of walls with thermal bridges with the accuracy primarily limited by the estimate of the R -values.
- When measured R -values are used, the EHL model agreed within $\pm 2.6\%$ of the experimental results. When standard methods recommended by ASHRAE for estimating the R -values were used, the peak heat gains for six of walls were predicted within $\pm 7.7\%$ of the peak heat gain determined using the measured CTFs. For the seventh wall, an insulated steel stud wall mounted on reinforced concrete slab, a peak heat gain error of 19.3% was observed. This is primarily due to an 11.3% deviation of the handbook R -value from the measured R -value.
- The inter-model validation also confirmed that the equivalent wall for the steel stud walls predicts the peak heat gain within $\pm 2.5\%$ of that of the actual wall provided that the R -values were determined using the 2D numerical model. The errors in the R -values computed with standard method were in the range 0.5% to 11.3%. For the cold frame steel stud test wall with the R -value error of 11.3%, the peak heat gain error was 7.3%.
- In its current form, the equivalent homogeneous layer wall model is suitable for sandwich type linear thermal bridge constructions with one composite layer only. For walls with multiple composite layers, the resistance would have to be apportioned. It is expected that this will work well but has not been validated.

- The use of either air-to-air or surface-to-surface R -values for equivalent wall generation depends on the procedure used to determine the overall R -value or U -values. For R -values determined using either isothermal plane or the parallel path correction method the use of either R -value gives the same equivalent homogeneous layer. For R -values determined using the parallel path or zone methods the properties of the EHL wall vary slightly depending on whether the basis is air-to-air or surface-to-surface R -values. If the parallel path extends to air-to-air node in the R -value calculation then the air-to-air R -value should be used in the equivalent layer determination. If the parallel path method combines the facing layers in series with composite layer then the use of either air-to-air or surface-to-surface R -values gives the same equivalent layer.

7.3 Recommendations for Future Work

The recommendations for future work involving improvements to the radiant time series method or dynamic modeling of thermal bridges can be summarized as follows:

- The radiative / convective splits recommended for use with the RTSM fenestration models were based on interior shades with maximum transmittance of 10%. Since some shades, such as light and medium weave drapery fabrics, have higher transmittance, further investigation of radiative / convective splits for higher transmittance interior shades is recommended.
- The improved RTSM peak cooling load over prediction may be reduced further with the use of radiative / convective split that depends on the glazing types,

construction fabrics, and glazing fractions. Investigation of such a correlation is recommended.

- Validation of use of constant radiation coefficient in RTF generation algorithm for large set of zones is recommended for future work.
- A parametric study to cover the three generic steel stud walls with different stud spacings, flange widths and thicknesses and different levels of insulation is recommended as future work.
- The equivalent homogeneous layer wall model as is cannot be used for exposed type thermal bridges. Exposed type thermal bridges may be found in some curtain wall constructions. Extension of the model for exposed type layer thermal bridge construction is recommended for future work.
- Furthermore, while multiple composite layers separated by homogeneous layers may be analyzed by apportioning the resistance between the two layers, this approach has not been validated. This validation should be done.
- The experimental and inter-model validation of the equivalent homogeneous conducted so far have been using design oriented sol-air temperature boundary conditions. It is recommended for future work to validate the model with other types of boundary conditions involving a combination of solar, long wave and convective environments.
- The one-dimensional approximate equivalent homogeneous layers wall model can be implemented as a standalone tool and/or can be integrated with existing building energy analysis and load calculation programs. This would require a two dimensional numerical model with a graphical user interface for geometrical and

material layer specifications, and a sub-program for solving the two-dimensional conduction domain to determine the steady state R -value and generate the one-dimensional equivalent wall. Such a tool, if developed with practicing engineers in mind, would be quite useful and efforts to develop this tool should be undertaken.

REFERENCES

- Alford, J. S., L. Mass, J.E. Ryan, N.Y. Schenectady, F.O. Urban, and Bloomfield, N. J. (1939). "Effect of Heat Storage and Variation in Outdoor Temperature and Solar Intensity on the Heat Transfer Through Walls." *ASHVE Transactions*, 45(1), 369-396.
- Amjad, S., Abdelbaki, A., and Zrikem, Z. (2003). "Transfer functions method and sub-structuration technique for two-dimensional heat conduction problems in high thermal mass systems: Application to ground coupling problems." *Energy and Buildings*, 35(6), 593-604.
- ASHRAE. (1967). *Handbook of Fundamentals*, Atlanta: American Society of Heating, Refrigerating, and Air-Conditioning Engineers, Inc.
- ASHRAE. (1972). *Handbook of Fundamentals*, Atlanta: American Society of Heating, Refrigerating, and Air-Conditioning Engineers, Inc.
- ASHRAE. (2001). *Handbook of Fundamentals*, Atlanta: American Society of Heating, Refrigerating, and Air-Conditioning Engineers, Inc.
- ASHRAE. (2005). *Handbook of Fundamentals*, Atlanta: American Society of Heating, Refrigerating, and Air-Conditioning Engineers, Inc.
- Barbour, C. E., and Goodrow, J. "Thermal performance of steel-framed walls." San Diego, CA, USA, 766-777.

- Billington, N. S. (1987). "Evolution of Environmental Temperature." *Building and Environment*, 22(4), 241-249.
- Brisken, W. R., and Reque, S. G. (1956). " Heat Load Calculations by Thermal Response." *ASHVE Transactions*, 62(1), 391-424.
- Billington, N. S. (1987). "Evolution of Environmental Temperature." *Building and Environment*, 22(4), 241-249.
- Brisken, W. R., and Reque, S. G. (1956). " Heat Load Calculations by Thermal Response." *ASHVE Transactions*, 62(1), 391-424.
- Brown, W. C., and Stephenson, D. G. (1993a). "Guarded hot box measurements of the dynamic heat transmission characteristics of seven wall specimens - Part II." *ASHRAE Transactions*, 99(1), 643-660.
- Brown, W. C., and Stephenson, D. G. (1993b). "Guarded hot box procedure for determining the dynamic response of full-scale wall specimens - Part I." *ASHRAE Transactions*, 99(1), 632-642.
- Brown, W. C., Swinton, M. C., and Haysom, J. C. (1998). "Technique for calculating the effective thermal resistance of steel stud walls for code compliance." *ASHRAE Transactions*, 104(2), 1245-1255.
- Burch, D. M., Seem, J. E., Walton, G. N., and Licitra, B. A. (1992). "Dynamic evaluation of thermal bridges in a typical office building." *ASHRAE Transactions*, 98(1), 291-304.
- Carpenter, S. C., Kosny, J., and Kossecka, E. (2003a). "Modeling Transient Performance of Two-Dimensional and Three-Dimensional Building Assemblies." *ASHRAE Transactions*, 2003, 561-566.

- Carpenter, S. C., Kosny, J., and Kossecka, E. "Modeling transient performance of two-dimensional and three-dimensional building assemblies." Chicago, IL, United States, 566-571.
- Carpenter, S. C., and Schumacher, C. (2003). "Characterization of framing factors for wood-framed low-rise residential buildings." *ASHRAE Transactions*, 109(1), 101-108.
- Carroll, J. A. (1980). "An "MRT Method" of Computing Radiant Energy Exchange in Rooms." San Diego, California, 343-348.
- Carslaw, H. S., and Jaeger, J. C. (1959). *Conduction of heat in solids*, Oxford, Clarendon Press, London.
- Chantrasrisalai, C., and Fisher, D. E. (2007a). "Lighting heat gain parameters: Experimental method (RP-1282)." *HVAC and R Research*, 13(2), 283-303.
- Chantrasrisalai, C., and Fisher, D. E. (2007b). "Lighting heat gain parameters: Experimental results (RP-1282)." *HVAC and R Research*, 13(2), 305-323.
- Chantrasrisalai, C., Iu, I., Eldridge, D. S., and Fisher, D. E. (2003). "Experimental validation of design cooling load procedures: The heat balance method." *ASHRAE Transactions*, 109 (2), 160-173.
- Chen, Y., and Wang, S. (2005). "A new procedure for calculating periodic response factors based on frequency domain regression method." *International Journal of Thermal Sciences*, 44(4), 382-392.
- Clarke, J. A. (2001). *Energy Simulations in Building Design*, Butterworth-Heinemann. .

- Davies, M., Tindale, A., and Littler, J. (1995). "Importance of multi-dimensional conductive heat flows in and around buildings." *Building Services Engineering Research & Technology*, 16(2), 83-90.
- Davies, M. G. (1996). "Time-domain estimation of wall conduction transfer function coefficients." *ASHRAE Transactions*, 102(1), 328-343.
- Fisher, D. E., and Chantrasrisalai, C. (2006). "Lighting Heat Gain Distribution In Buildings." Georgia, Atlanta.
- Gilkey, H. T., D. R. Bahnfleth, and Roose, R. W. (1953). "Cooling a Small Residence House with a Two-Horse Power Mechanical Condensing Unit." *ASHVE Transactions*, 59(1), 283-304.
- Gorgolewski, M. (2007). " Developing a simplified method of calculating *U*-values in light steel framing." *Building and Environment, Volume 42(1)*, 230-236.
- Hittle, D. C. (1992). "Response Factors and Conduction Transfer Functions." 1-42.
- Hottel, H. C., and Sarofim, A. F. (1967). *Radiation Transfer*, McGraw-Hill, New York.
- Houghten, F. C., J. C. Blackshaw, E. M. Pugh, and McDermott, P. (1932). "Heat Transmission as Influenced by Heat Capacity and Solar Radiation." *ASHVE Transactions*, 38(1), 232-284.
- Iu, I., Eldridge, D. S., Chantrasrisalai, C., and Fisher, D. E. (2003). "Experimental validation of design cooling load procedures: The radiant time series method." *ASHRAE Transactions*, 109(2), 139-150.
- James, J. (1937). " Cooling Load Analysis of A Bank." *ASHVE Transactions*, 43(1), 327–344.

- Karambakkam, B. K., B. Nigusse, and Spitler, J. D. "A One-dimensional Approximation for Transient Multi-dimensional Conduction Heat Transfer in Building Envelopes. ." *Nordic Symposium on Building Physics*, Reykjavik, Iceland.
- Kayan, C. F. (1950). "Electric Analogger Studies on Panels with Embedded Tubes." *ASHVE Transactions*, 56(1), 205-222.
- Klems, J. H. (2002). "Solar heat gain through fenestration systems containing shading: Summary of procedures for estimating performance from minimal data." *ASHRAE Transactions*, 108(1), 512-524.
- Kosny, J., and Christian, J. E. "Reducing the uncertainties associated with using the ASHRAE zone method for R-value calculations of metal frame walls." San Diego, CA, USA, 779-788.
- Kosny, J., and Christian, J. E. (1995b). "Reducing the uncertainties associated with using the ASHRAE zone method for R-value calculations of metal frame walls." *ASHRAE Transactions*, 101(2), 779-788.
- Kosny, J., and Christian, J. E. (1995c). "Thermal evaluation of several configurations of insulation and structural materials for some metal stud walls." *Energy and Buildings*, 22(2), 157-163.
- Kosny, J., Christian, J. E., and Desjarlais, A. O. (1997a). "Metal stud wall systems - thermal disaster, or modern wall systems with highly efficient thermal insulation." 1320, 153-179.
- Kosny, J., Christian, J. E., and Desjarlais, A. O. (1997b). "Thermal breaking systems for metal stud walls - can metal stud walls perform as well as wood stud walls?" *ASHRAE Transactions*, 103(1), 518-536.

- Kosny, J., and Kossecka, E. (2002). "Multi-dimensional heat transfer through complex building envelope assemblies in hourly energy simulation programs." *Energy and Buildings*, 34(5), 445-454.
- Kosny, J., Petrie, T. W., and Christian, J. E. (1997c). "Thermal bridges in roofs made of wood and light-gauge steel profiles." *ASHRAE Transactions*, 103(1), 537-549.
- Kossecka, E. (1998). "Relationships between structure factors, response factors, and z-transfer function coefficients for multilayer walls." *ASHRAE Transactions*, 104(1), 68-77.
- Kossecka, E., and Kosny, J. (2002). "Influence of insulation configuration on heating and cooling loads in a continuously used building." *Energy and Buildings*, 34(4), 321-331.
- Kratz, A. P., and Konzo, S. (1933). "Study of Summer Cooling in the Research Residence at the University of Illinois." *ASHVE Transactions*, 39(1), 95 –118.
- Kusuda, T. (1969). "Thermal Response Factors for Multi-layered Structures of Various Heat Conduction systems. ." *ASHRAE Transactions*, 75(Pt 1), 241-271.
- Leopold, C. S. (1948). "Hydraulic Analogue For The Solution of Problems of Thermal Storage, Radiation, Convection, and Conduction." *ASHVE Transactions*, 54(1), 391-424.
- Mackey, C. O., and Wright, L. T. (1944). "Periodic Heat Flow-Homogeneous Walls or Roofs." *Transactions American Society of Heating and Ventilating Engineers*, 50(1), 293-312.
- Mackey, C. O., and Wright, L. T. (1946). "Periodic Heat Flow-Composite Walls or Roofs." *Transactions American Society of Heating and Ventilating Engineers*, 52(1), 283-296.

- McQuiston, F.C., J. D. P., and Spitler, J. D. (2005). *Heating, Ventilating, and Air Conditioning Analysis and Design*, John Wiley and Sons, New York.
- McQuiston, F. C., J.D. Parker and J.D. Spitler. . (2000). *Heating, Ventilation, and Air Conditioning Analysis and Design.*, John Wiley and Sons, Inc., New York.
- Mitalas, G. P. (1968). "Calculations of transient heat flow through walls and roofs." *ASHRAE Transactions*, 74(2), 182-188.
- Mitalas, G. P., and Stephenson, D. (1967). "Room Thermal Response Factors." *ASHRAE Transactions* 73(1), 2.1-2.10.
- Nakhi, A. (1995). " Adaptive Construction Modeling Within Whole Building Dynamic Simulation," University of Strathclyde, Glasgow, UK.
- Paschkis, V. (1942). "Periodic Heat Flow in Buildings Walls Determined by Electrical Analogy Method." *ASHVE Transactions*, 48(1), 75-90.
- Peavy, B. A. (1978). "A note on response factors and conduction transfer functions." *ASHRAE Transactions*, 84(1), 688-690.
- Pedersen, C. (1997). " HBFORT computer program." Pedersen and Associates. .
- Pedersen, C. O., Fisher, D. E., D. J. Spitler, a., and Liesen, R. J. (1998). *Cooling and Heating Load Calculation Principles*, ASHRAE, Atlanta, GA, USA.
- Pedersen, C. O., Fisher, D. E., and Liesen, R. J. (1997). "Development of a heat balance procedure for calculating cooling loads." *ASHRAE Transactions*, 103(2), 459-468.
- Rees, S. J., Spitler, J. D., Davies, M. G., and Haves, P. (2000). "Qualitative comparison of North American and U.K. cooling load calculation methods." *HVAC and R Research*, 6(1), 75-98.

- Rees, S. J., Spitler, J. D., and Haves, P. (1998). "Quantitative comparison of North American and U.K. cooling load calculation procedures - results." *ASHRAE Transactions*, 104(2), 47-61.
- Rees, S. J., Spitler, J. D., and Xiao, X. (2002). "Transient analysis of snow-melting system performance." *ASHRAE Transactions*, 108 (2), 406-423.
- Romine, T. B., Jr. (1992). "Cooling load calculation. Art or science?" *ASHRAE Journal*, 34(1), 14-24.
- Rudoy, W., and Duran, F. (1975). "Development of an improved cooling load calculation method." *ASHRAE Transactions*, 81(2), 19-69.
- Seem, J. E. (1987). "Modeling of Heat Transfer In Buildings," University of Wisconsin-Madison, Wisconsin, Madison.
- Sowell, E. F. (1988a). "Classification of 200,640 Parametric Zones for Cooling Load Calculations." *ASHRAE Transactions*, 94 (2), 754-777.
- Sowell, E. F. (1988b). "Cross-Check and Modification of the DoE-2 Program for Calculation of Zone Weighting Factors." *ASHRAE Transactions*, 94 (2), 737-753.
- Sowell, E. F. (1988c). "Load Calculations for 200,640 Zones." *ASHRAE Transactions*, 94(2), 716-736.
- Spitler, J. D., Daniel E. Fisher, and Pedersen, C. O. (1997). "Radiant time series cooling load calculation procedure." *ASHRAE Transactions*, 103(2), 503-515.
- Spitler, J. D., and Fisher, D. E. (1999a). "Development of periodic response factors for use with the radiant time series method." *ASHRAE Transactions*, 105(1), 491-509.

- Spitler, J. D., and Fisher, D. E. (1999b). "On the relationship between the radiant time series and transfer function methods for design cooling load calculations." *HVAC & R Research*, 5(2), 125-138.
- Spitler, J. D., McQuiston, F. C., and Lindsey, K. L. (1993a). "CLTD/SCL/CLF cooling load calculation method." *ASHRAE Transactions*, 99, 183-192.
- Spitler, J. D., McQuiston, F. C., and Lindsey, K. L. (1993b). "Development of a revised Cooling and Heating Load Calculation Manual." *ASHRAE Transactions*, 99(1), 175-182.
- Spitler, J. D., and Rees, S. J. (1998). "Quantitative comparison of North American and U.K. cooling load calculation procedures - methodology." *ASHRAE Transactions*, 104(2), 36-46.
- Stephenson, D. G., and Mitalas, G. P. (1971). "Calculation of heat conduction transfer functions for multi-layer slabs." *ASHRAE Transactions*, 77(2), 117-126.
- Stewart, J. P. (1948). "Solar Heat Gains Through Walls and Roofs for Cooling Load Calculations." *Transactions American Society of Heating and Ventilating Engineers*, 54(1), 361-388.
- Strand, R. K. (1995). "Heat Source Transfer Functions and Their Application to Low Temperature Radiant Heating Systems," University of Illinois at Urbana-Champaign, Urbana-Champaign.
- Thomas, L. C., and Antar, M. (1998). "Heat transfer in composite walls: a practical two-dimensional thermal circuit method." *ASHRAE Transactions*, 104(2), 198-209.
- Walton, G. N. (1980). "A new algorithm for radiant interchange in room loads calculations." *ASHRAE Transactions* 86:(2), 190-208.

- Wang, S., and Chen, Y. (2003). "Transient heat flow calculation for multilayer constructions using a frequency-domain regression method." *Building and Environment*, 38(1), 45-61.
- Wilkins, C. K. (1998). "Electronic equipment heat gains in buildings." *ASHRAE Transactions*, 104(1), 1784-1789.
- Wilkins, C. K., and Cook, M. R. (1999). "Cooling loads in laboratories." *ASHRAE Transactions*, 105(1), 744-749.
- Willcox, T. N., C.T. Oergel, S.G. Reque, C.M. Toelaer, W.R. Brisken, and BloomField, N. J. (1954). "Analogue Computer Analysis of Residential Cooling Loads." *ASHVE Transactions*, 60(1), 505-524.
- Zhang, C., and Ding, G. (2003). "A stable series expansion method for calculating thermal response factors of multi-layer walls." *Building and Environment*, 38(5), 699-705.

APPENDIX

APPENDIX A: THE NEW RTF ENGINE VALIDATION

A.1 The New RTF Generating algorithm Validation Results

The new RTF generating program, which based on a reduced heat balance method algorithm given in Section 3.1 has been validated against full-blown heat balance program. The RTF plots shown in Figures A.1 to A.8 are for medium and heavyweight construction zone.

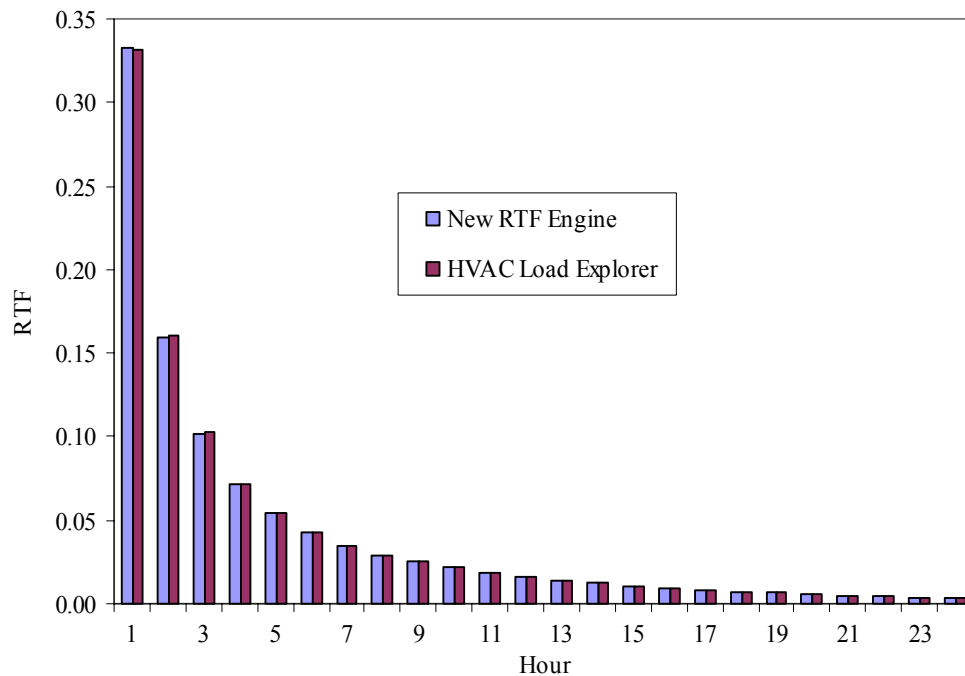


Figure A.1 Non-solar RTF for medium weight construction zone with no carpet for 50% glazing fraction of the exterior facade

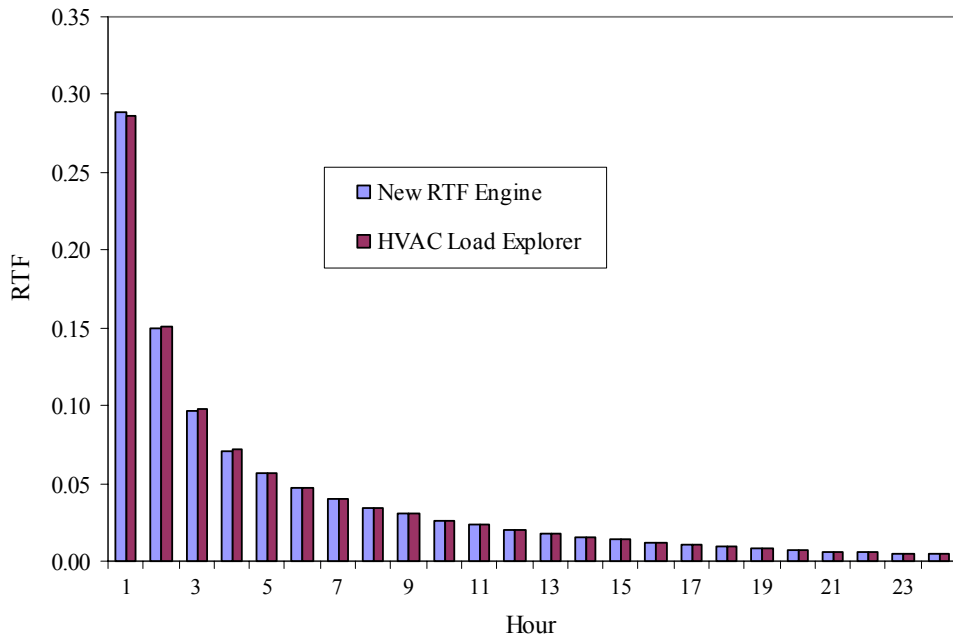


Figure A.2 Solar RTF for medium weight construction zone with no carpet for 50% glazing fraction of the exterior facade

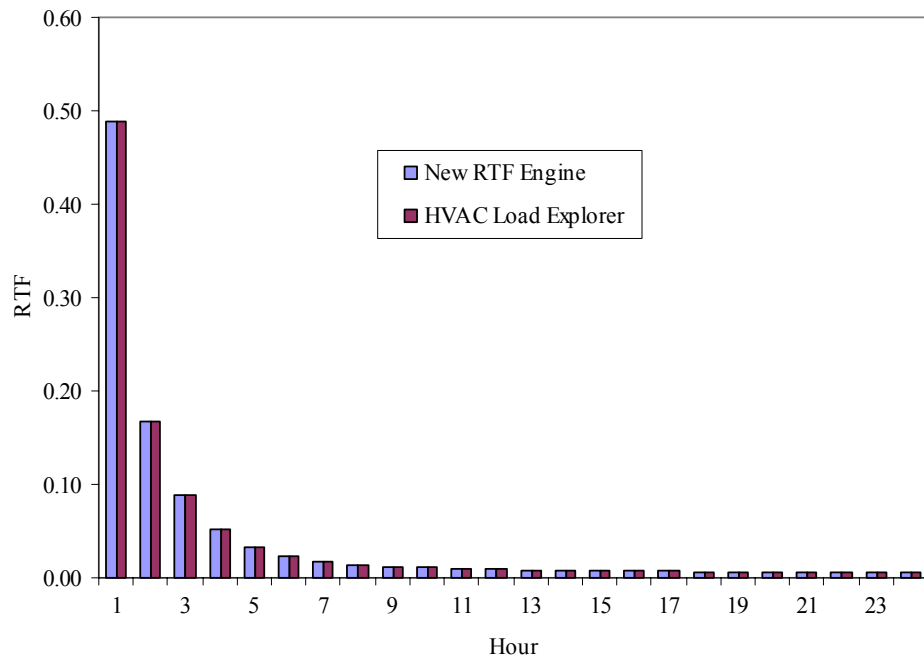


Figure A.3 Non-solar RTF for medium weight construction zone with carpet for 50% glazing fraction of the exterior facade

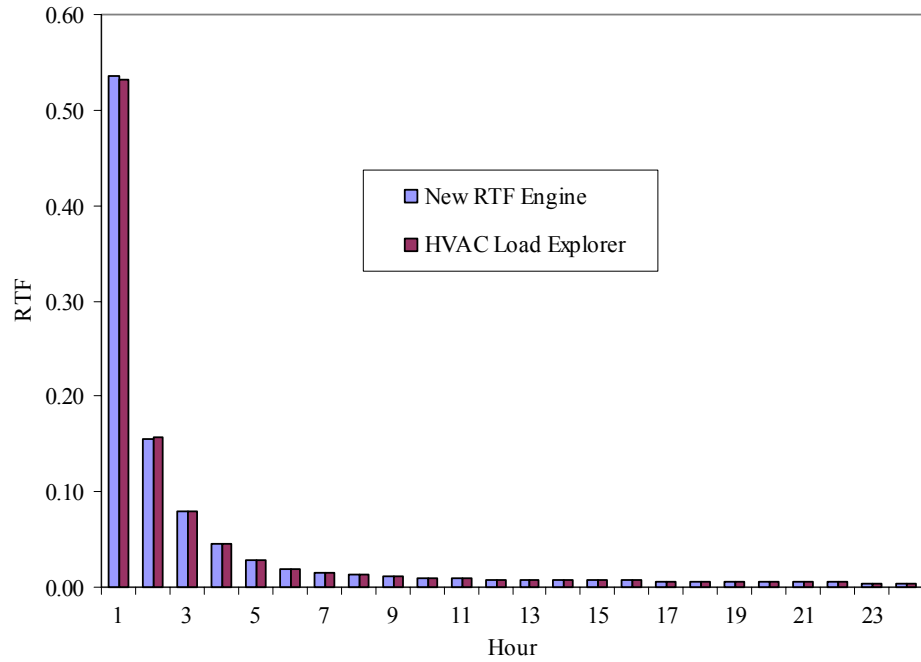


Figure A.4 Solar RTF for medium weight construction zone with carpet for 50% glazing fraction of the exterior facade

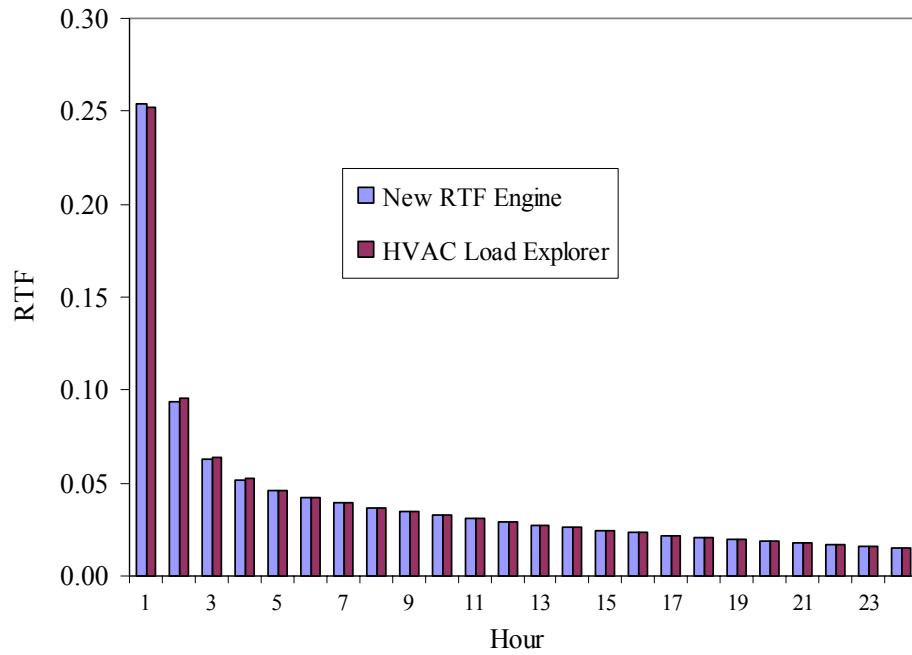


Figure A.5 Non-solar RTF for heavyweight construction zone with no carpet for 50% glazing fraction of the exterior facade

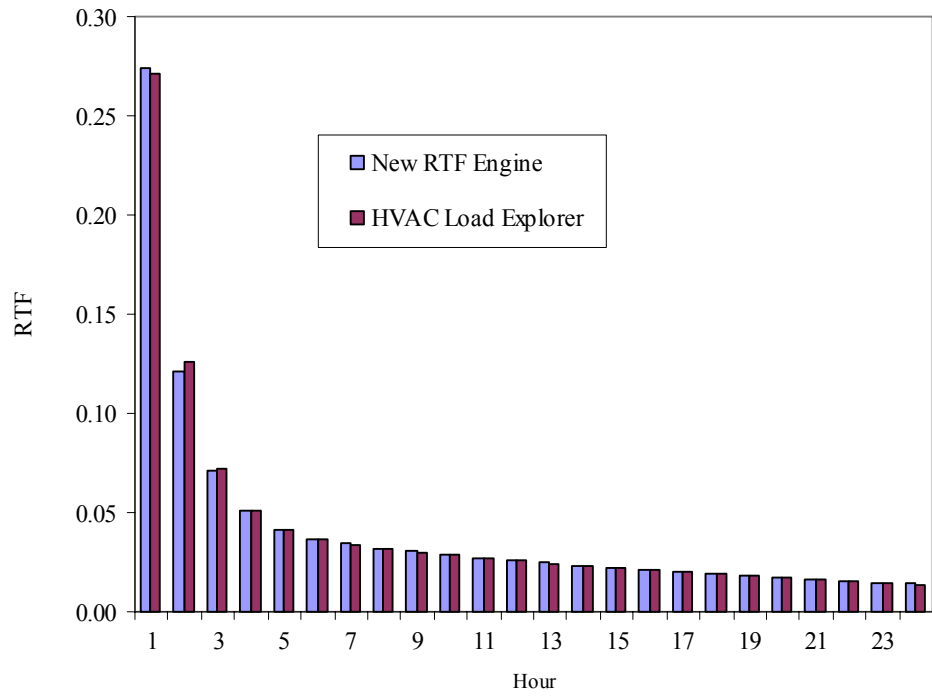


Figure A.6 Solar RTF for heavyweight construction zone with no carpet for 50% glazing fraction of the exterior facade

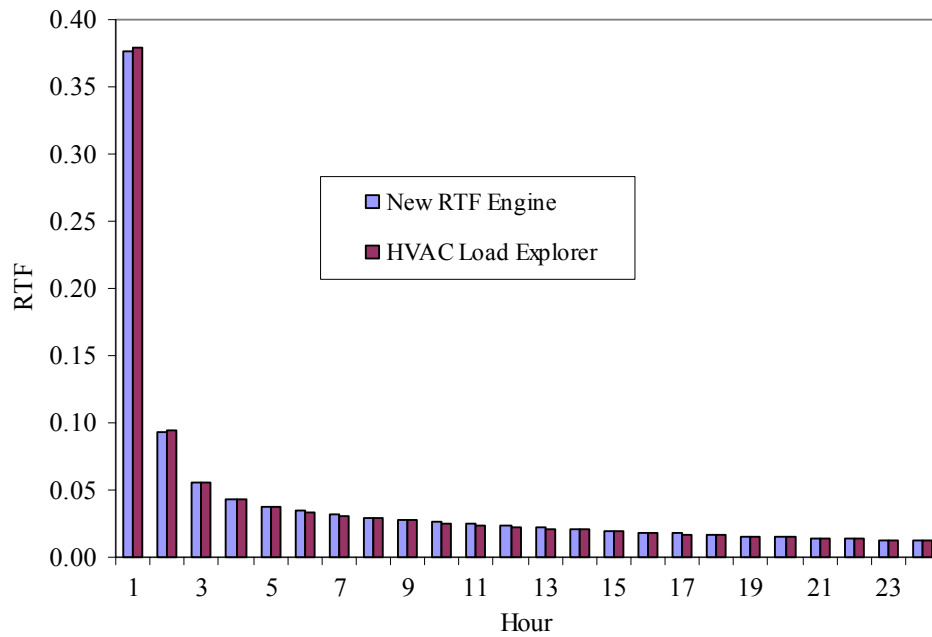


Figure A.7 Non-solar RTF for heavyweight construction zone with carpet for 50% glazing fraction of the exterior facade

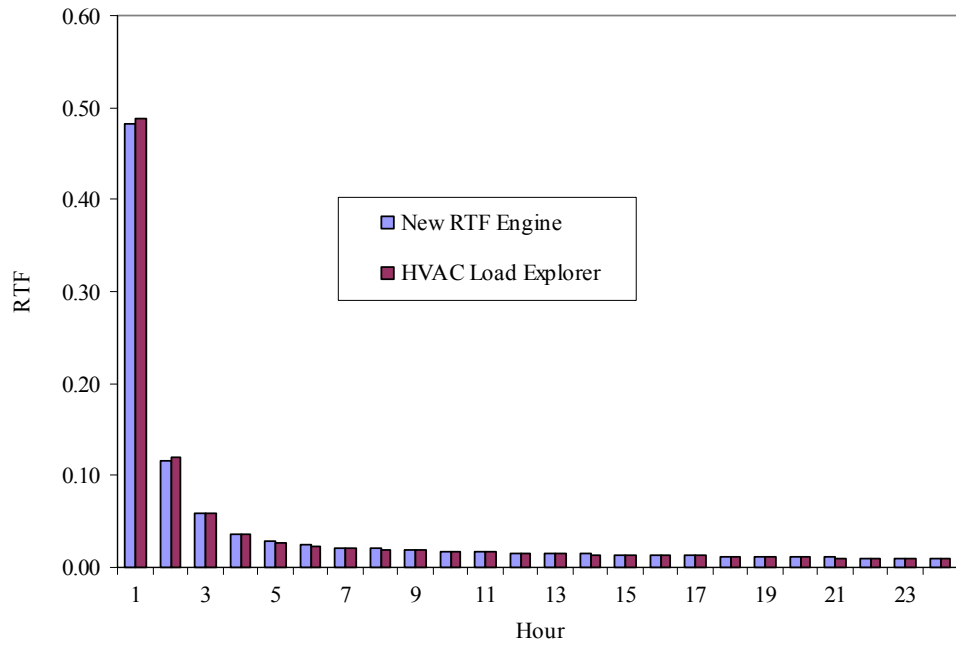


Figure A.8 Solar RTF for heavyweight construction zone with carpet for 50% glazing fraction of the exterior façade

APPENDIX B: 1D FINITE VOLUME METHOD PERIODIC RESPONSE FACTOR GENERATION

B.1 Derivation 1D Finite Volume Numerical Model

Heat conduction in building envelopes is commonly represented by one-dimensional transient heat conduction equation which is expressed as follows:

$$\frac{d(\rho c)\phi}{dt} = \frac{d}{dx} \left(k \frac{d\phi}{dx} \right) \quad (\text{B.1})$$

Where

ρc = is the product of density and specific heat, $\text{J/m}^3 \cdot ^\circ\text{C}$ ($\text{Btu/ft}^3 \cdot ^\circ\text{F}$)

k = is the thermal conductivity of the material, $\text{W/m} \cdot ^\circ\text{C}$ ($\text{Btu-in/ft}^2 \cdot ^\circ\text{F}$)

ϕ = is the temperature, $^\circ\text{C}$ ($^\circ\text{F}$)

t = is the time, s (sec)

x = is the thickness in the direction of the heat flow path, m(in)

Consider a portion of one-dimensional uniform grid shown in Figure B.1. The labels **W**, **P** and **E** denote the grid points, where **P** is the control volume under consideration, and **W** and **E** are the west side and east side neighboring control volumes, respectively. The control volume interfaces are represented by a small letter labels **w** and **e**, and a broken line.

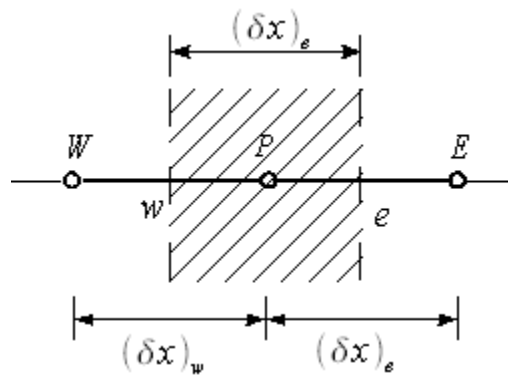


Figure B.1 General one-dimensional grid representation

The one-dimensional transient conduction equations B.1 can be solved using either integral method, by applying conservation of energy / heat to discretized control volumes. These two approaches are discussed as follows:

Integral Method

The first step in formulating a finite volume solution is to integrate the partial differential equation. Hence we step forward in time from some initial condition when solving a transient problem. Hence we integrate from the current time t^n using a fixed time step Δt to a new time t^{n+1} so that:

$$\int_w^e \int_{t^n}^{t^{n+1}} \frac{d(\rho c)\phi}{dt} dt dx = \int_{t^n}^{t^{n+1}} \int_w^e \frac{\partial}{\partial x} \left(k \frac{\partial \phi}{\partial x} \right) dx dt \quad (\text{B.2})$$

If we assume that the grid point value of the dependent variable, in this case temperature, prevails for the whole control volume, then one can approximate the partial with respect to time using backward differencing with time as follows:

$$\int_w^e \int_{t^n}^{t^{n+1}} \frac{d(\rho c)\phi}{dt} dt dx = (\rho c) \frac{\Delta x}{\Delta t} (\phi_P^{n+1} - \phi_P^n) \quad (\text{B.3})$$

The spatial integration of the conduction term in Eq. C.2 results in:

$$(\rho c) \frac{\Delta x}{\Delta t} (\phi_P^{n+1} - \phi_P^n) = \int_{t^n}^{t^{n+1}} \left[\frac{k_e (\phi_E - \phi_P)}{(\delta x)_e} - \frac{k_w (\phi_P - \phi_W)}{(\delta x)_w} \right] dt \quad (\text{B.4})$$

We must now make some assumption about how ϕ_W and ϕ_E vary from one time step to the next. Using fully implicit method, which is unconditionally stable solution scheme results in the following discretized equation:

$$\frac{(\rho c) \Delta x (\phi_P^{n+1} - \phi_P^n)}{\Delta t} = \left[\frac{k_e (\phi_E^{n+1} - \phi_P^{n+1})}{(\delta x)_e} - \frac{k_w (\phi_P^{n+1} - \phi_W^{n+1})}{(\delta x)_w} \right] \quad (\text{B.5})$$

It can be seen that the temporal term is equivalent to first-order backwards differencing in time. The discretized equation can then be said to be first-order accurate in time and second-order accurate in space.

Energy Conservation Method

This method is basically the fundamental concept used in deriving the differential form of the heat equation given in Eq B.1. Applying conservation of energy around the control volume **P** shown in Figure B.1. Ignoring potential energy, kinetic energy and in the absence of internal heat generation, the net inflow of heat into the control volume **P** is equal to the rate of change of the internal of energy of the control volume and is given by:

$$A_w \dot{q}_w'' - A_e \dot{q}_e'' = \Delta \dot{E} \quad (\text{B.6})$$

The heat flux terms crossing the control volume surfaces using the Fourier laws of heat conduction are given by:

$$\begin{aligned} \dot{q}_w'' &= -k_w \frac{\phi_P - \phi_W}{(\delta x)_w} \\ \dot{q}_e'' &= -k_e \frac{\phi_E - \phi_P}{(\delta x)_e} \end{aligned} \quad (\text{B.7})$$

Similarly the rate of change of the internal energy of the control volume is given by:

$$\Delta \dot{E} = \delta V (\rho c) \frac{\phi_P - \phi_P^0}{\Delta t} \quad (\text{B.8})$$

Substituting Eq. B.7 and Eq B.8 into Eq. B.6 yields:

$$-A_w k_w \frac{\phi_P - \phi_W}{(\delta x)_w} + k_e \frac{\phi_E - \phi_P}{(\delta x)_e} = \delta V(\rho c) \frac{\phi_P - \phi_P^0}{\Delta t} \quad (\text{B.9})$$

For equal area in the direction of heat conduction Eq. B.9 reduces to:

$$\delta x(\rho c) \frac{\phi_P - \phi_P^0}{\Delta t} = k_e \frac{\phi_P - \phi_E}{(\delta x)_e} - k_w \frac{\phi_W - \phi_P}{(\delta x)_w} \quad (\text{B.10})$$

Eq. B.10 is identical to Eq. B.5 derived using the integral method. The solution technique adapted here for either these equations require further manipulations to represent the equation in terms of constant coefficient and the nodal temperatures in a form convenient for solving. This is discussed in the following section.

Collecting together terms to form an equation in terms of the nodal values of the dependent variable forms:

$$a_P \phi_P = a_W \phi_W + a_E \phi_E + c \quad (\text{B.11})$$

Where,

$$\begin{aligned}
a_E &= \frac{k_E}{(\delta x)_e}, \\
a_W &= \frac{k_W}{(\delta x)_w}, \\
a_P^0 &= \frac{(\rho c)_P \Delta x}{\Delta t} \\
a_P &= a_W + a_E + a_P^0 \\
c &= a_P^0 \phi_P^n
\end{aligned}
\tag{B.12}$$

Discretization

The discretization scheme used in this formulation is in such way so that it allows to properties uniform over a control volume and allows discontinuities at the control-volume faces (Patankar 1991). The control volumes faces are places at the locations of discontinuities as shown in Figure B.2. The grid points are places at the geometric center of each control volume. Boundary grid points are placed on each boundary. Zero thickness control volumes are used on the boundaries.

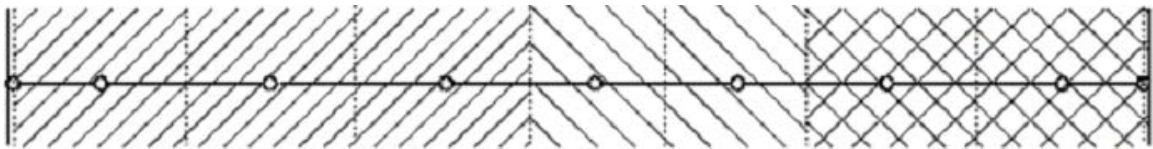


Figure B.2 Discretization for multi-layer construction

Interface Problem

Building envelope involves multi-layer homogenous materials. Therefore, it involves discontinuities in the conductivity of the neighboring cells. This has to be taken care in

the discretization scheme. We have also indicated the need to define the conductivities, k_w and k_e , at each face of the control volume. However, the most important consideration is to arrive at the correct conduction flux formula that can handle discontinuities in conductivities at the control volume faces:

$$\dot{q}_e'' = \frac{k_e(\phi_P - \phi_E)}{(\delta x)_e} \quad (\text{B.13})$$

Where

\dot{q}_e'' = is the conduction heat flux at the interface e , W/m^2 ($\text{Btu/ft}^2 \cdot \text{h}$)

Suppose that we have a one-dimensional grid with different cell sizes as shown below:

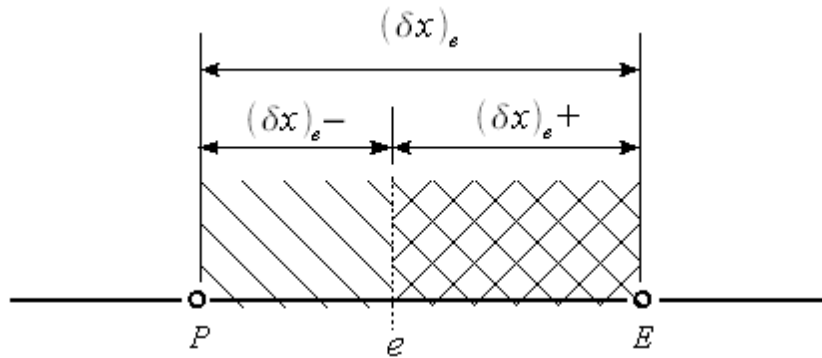


Figure B.3 Control volume interface representation between **P** and **E** grid points

If the conductivities are constant in the respective control volumes, a straightforward one-dimensional analysis leads to:

$$\dot{q}_e'' = \frac{(\phi_P - \phi_E)}{\delta x_{e-}/k_P + \delta x_{e+}/k_E} \quad (\text{B.14})$$

$$a_e = \frac{k_e}{\delta x_e} = \left(\frac{\delta x_{e-}}{k_P} + \frac{\delta x_{e+}}{k_E} \right)^{-1} \quad (\text{B.15})$$

Eq. B.15 allows to model discontinuities in conductivity at control volume faces without need for fine grid use.

Boundary Conditions

In order to generate response factors triangular pulse needs to be specified as initial condition and zero temperature is kept afterwards. This implies that the solution at an interior point is influenced by the conditions at the boundaries. The location of the unit pulse to be applied depends on the type of periodic response to be generated – cross, outside and inside response factors.

The discretization equation B.14 assumes constant flux between neighboring control volume nodes since the temperature is assumed piece wise linear between adjacent the control volumes. The higher order treatment assumes linear variation of the flux between the adjacent nodes.

Linearly varying fluxes assumption between adjacent control volume nodes results in higher order equation for the heat flux (Patankar 1991).

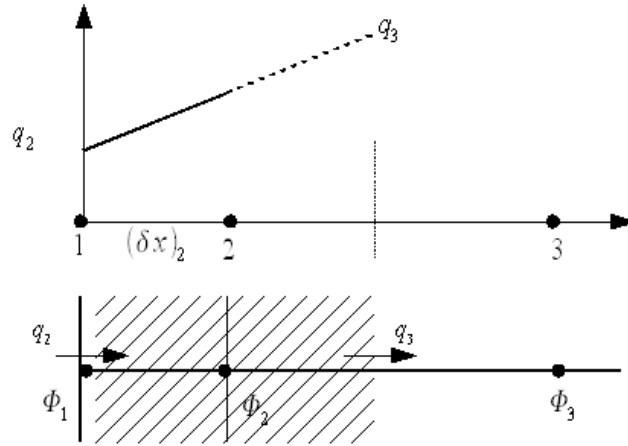


Figure B.4 Control volume at the left boundary and linear varying flux representation

Applying this assumption to the boundary nodes shown in Figure B.4 yields:

$$q_2 = \frac{4}{3} \left[\left(\frac{k_2}{\delta x_{2-}} \right) (\phi_1 - \phi_2) \right] - \frac{1}{3} q_3 \quad (\text{B.16})$$

$$q_3 = \frac{(\phi_2 - \phi_3)}{\delta x_{2+}/k_2 + \delta x_{3-}/k_3} \quad (\text{B.17})$$

The coefficient for the boundary nodes due to the higher order treatment is given by:

$$b_2 = \frac{4}{3} \left(\frac{k_2}{\delta x_2} \right) \quad (\text{B.18})$$

$$a_2 = \frac{4}{3} \left(\frac{\delta x_{2+}}{k_2} + \frac{\delta x_{3-}}{k_3} \right)^{-1}$$

Solution Scheme

Applying the discretization procedures an algebraic equation for each control volume of the form given in Eq. B.11 can be formulated as follows:

$$d^i \phi_i = b^i \phi_{i-1} + a^i \phi_{i+1} + c^i \quad (\text{B.19})$$

where,

d^i = is the coefficient of the i^{th} control volume discretization equation

b^i = is the coefficient of the link to $i-1^{\text{th}}$ control volume in the i^{th} control volume discretization equation

a^i = is the coefficient of the link to $i+1^{\text{th}}$ control volume in the i^{th} control volume discretization equation

c^i = is the constant term in the i^{th} control volume discretization equation

In other words, for the whole discretized domain we have a set of algebraic equations that are coupled via neighboring cells. We can assemble these equations into matrices so that the algebraic problem we have to solve can be expressed as:

$$\mathbf{\Omega} \cdot \mathbf{\phi} = \mathbf{C} \quad (\text{B.20})$$

where

$\mathbf{\Omega}$ = is a square matrix of coefficients for the control volumes

$\mathbf{\phi}$ = is vector containing the temperatures

\mathbf{C} = is vector containing the right hand side constant coefficients

For this linear partial differential equation the solution of the matrix formulation can be determined by using a suitable linear equation solver. The method we apply to solve Eq B.16 depends partly on the properties of the $\mathbf{\Omega}$ matrix coefficients. The matrix equation for a one-dimensional conduction with nine nodes, when fully expanded, looks like:

$$\begin{bmatrix} d^2 & a^2 & 0 & 0 & 0 & 0 & 0 \\ b^3 & d^3 & a^3 & 0 & 0 & 0 & 0 \\ 0 & b^4 & d^4 & a^4 & 0 & 0 & 0 \\ 0 & 0 & b^5 & d^5 & a^5 & 0 & 0 \\ 0 & 0 & 0 & b^6 & d^6 & a^6 & 0 \\ 0 & 0 & 0 & 0 & b^7 & d^7 & a^7 \\ 0 & 0 & 0 & 0 & 0 & b^8 & d^8 \end{bmatrix} \begin{bmatrix} \phi_2 \\ \phi_3 \\ \phi_4 \\ \phi_5 \\ \phi_6 \\ \phi_7 \\ \phi_8 \end{bmatrix} = \begin{bmatrix} c_2 \\ c_3 \\ c_4 \\ c_5 \\ c_6 \\ c_7 \\ c_8 \end{bmatrix} \quad (\text{B.21})$$

A notable property of this matrix is its tri-diagonal structure. This allows the use of a very efficient algorithm known as the Thomas Algorithm or the Tri-Diagonal Matrix Algorithm (TDMA). This is a type of Gauss elimination and can be explained as follows. We can express the equations that make up the matrix as:

$$b^i \phi_{i-1} + d^i \phi_i + a^i \phi_{i+1} = c^i \quad (\text{B.22})$$

Where i is the control volume counter in the range from 2 to 8, and we note that $b^2 = 0$ and $a^8 = 0$. The discretization algebraic equation Eq B.15 for the boundary nodes can be written as follows:

$$d^1 \phi_1 = a^1 \phi_{i+1} + c^1 \quad (\text{B.23})$$

$$d^{nMax} \phi_{nMax} = b^{nMax} \phi_{i-1} + c^{nMax} \quad (\text{B.24})$$

For known boundary temperature condition, which is the case for response factors generation unit triangular pulse, Eqs B.23 and B.24 reduces to:

$$\begin{aligned} d^1 &= 1 \\ a^1 &= 0 \\ c^1 &= \phi_1 \end{aligned} \quad (\text{B.25})$$

And

$$\begin{aligned} d^{nMax} &= 1 \\ b^{nMax} &= 0 \\ c^{nMax} &= \phi_{nMax} \end{aligned} \quad (\text{B.26})$$

Similarly defining two new variables **P** and **Q** for convenience and using the equation for the boundary nodes yields:

$$\phi_1 = P_1 \phi_{i+1} + Q_1 \quad (\text{B.27})$$

Where

$$\begin{aligned} P_1 &= \frac{a^1}{d^1} \\ Q_1 &= \frac{c^1}{d^1} \end{aligned} \quad (\text{B.28})$$

Using the same analogy similar equations can be formulated for the any arbitrary nodes, which will be used to formulate a recursive formula of the form:

$$\phi_i = P_i \phi_{i+1} + Q_i \quad (\text{B.29})$$

and

$$\phi_{i-1} = P_{i-1} \phi_i + Q_{i-1} \quad (\text{B.30})$$

Substituting Eqs. B.25 and B.26 into Eq. B.15 yields:

$$d^i (P_i \phi_{i+1} + Q_i) = b^i (P_{i-1} \phi_i + Q_{i-1}) + a^i \phi_{i+1} + c^i \quad (\text{B.31})$$

Solving for **P** and **Q** gives the recursive formula:

$$P_i = \frac{a^i}{d^i - b^i P_{i-1}} \quad \text{and} \quad Q_i = \frac{c^i + b^i Q_{i-1}}{d^i - b^i P_{i-1}} \quad (\text{B.32})$$

We make a forward sweep, writing for the first equation:

$$P_1 = \frac{a^1}{d^1} \quad \text{and} \quad Q_1 = \frac{c^1}{d^1} \quad (\text{B.33})$$

When the forward sweep is complete we make a backward sweep and write:

$$\phi_{nMax} = Q_{nMax} \quad \text{and} \quad \phi_i = Q_i + P_i \phi_{i+1} \quad (\text{B.34})$$

where M is the total number of cells and the sweep backwards is made with $i=(nMax-1)\dots 2$.

B.2 Finite Volume Method PRF Generation Validation

The 1-D implicit scheme finite volume numerical method PRF generator procedure described in this section has been validated against State Space Method. The validation is done by comparing the PRFs generated using the finite volume method and PRFs determined by converting CTFs generated using the state space method. ASHRAE's Wall10 and Wall37 given in Table B.1 were used for the validation. The PRF plots for these two walls computed using these two procedures are shown in Figures B.5 and B.6. The U -values determined from PRFs sum for Wall10 are $0.890988 \text{ W/m}^2\cdot\text{°C}$ and $0.890976 \text{ W/m}^2\cdot\text{°C}$ for FVM and SSM, respectively. Similarly for Wall37 are $0.225379 \text{ W/m}^2\cdot\text{°C}$ and $0.225373 \text{ W/m}^2\cdot\text{°C}$ for FVM and SSM, respectively

Table B.1 Thermo-physical properties of ASHRAE's Walls (ASHRAE 1997)

Name	Density (kg/m^3)	Specific Heat ($\text{kJ/kg}\cdot\text{K}$)	Conductivity ($\text{W/m}\cdot\text{K}$)	Thickness L (m)	Resistance ($\text{m}^2\cdot\text{K/W}$)
ASHRAE's Wall 10					
A0	0	0	0	0	0.059
A2	2002.0	0.921	1.333	0.100	0.075
B5	91.0	0.841	0.043	0.025	0.578
C2	609.1	0.841	0.381	0.100	0.263
E1	1602.0	0.841	0.727	0.020	0.028
E0	0.0	0	0	0	0.121
ASHRAE's Wall 37					
A0	0.0	0	0	0	0.059
A2	2002.0	0.920	1.333	0.100	0.076
C19	304.3	0.841	0.139	0.305	2.201
B25	91.3	0.841	0.043	0.085	1.937
E1	1602.0	0.841	0.727	0.020	0.026
E0	0.0	0	0	0	0.121

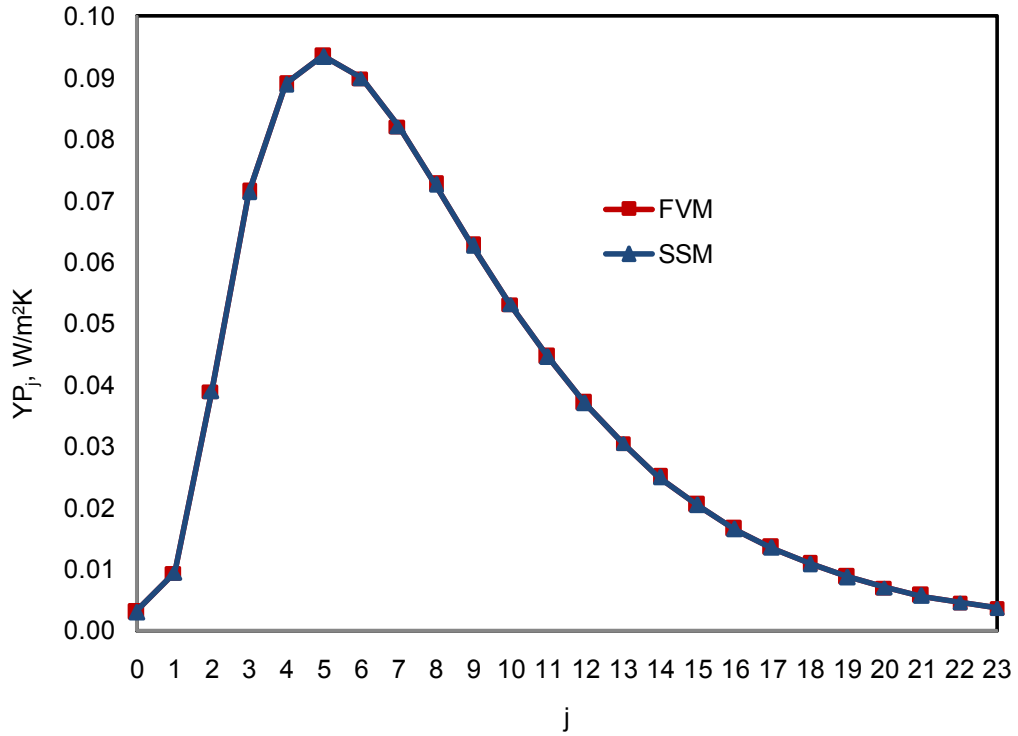


Figure B.5 PRF computed using finite volume method (FVM) and State Space method (SSM) for ASHRAE's Wall10 (ASHRAE 1997)

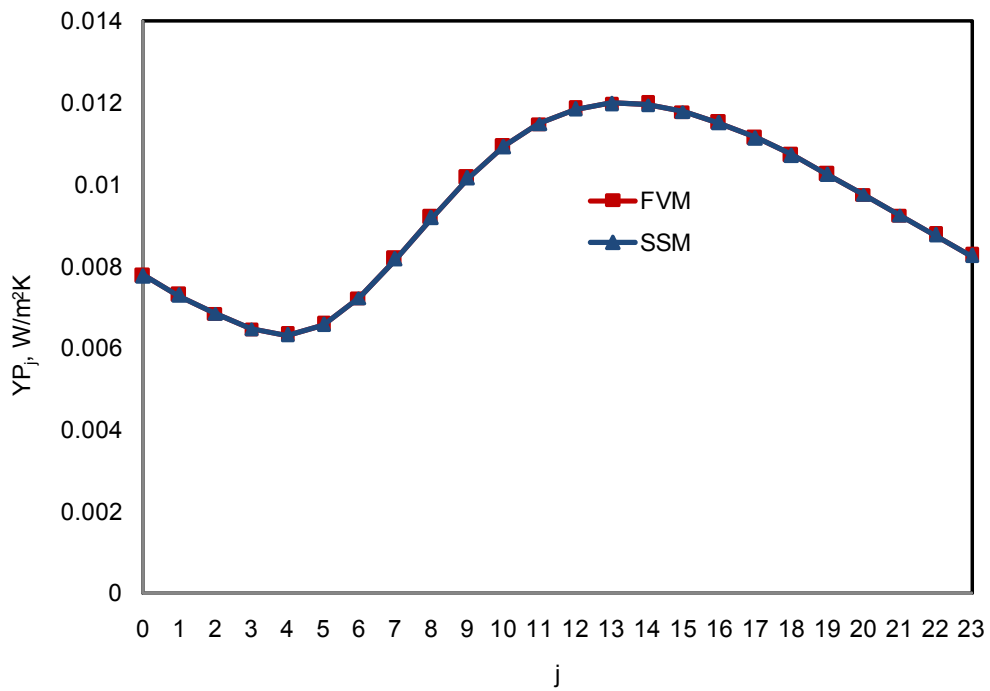


Figure B.6 PRF computed using finite volume method (FVM) and State Space method (SSM) for ASHRAE's Wall37 (ASHRAE 1997)

APPENDIX – C: RTSM IMPLEMENTATION IN OTHER COMPUTING ENVIRONMENTS

C.1 RTF Generator Implementation in SCILAB

```
//RTF Generation: reads periodic response factors and surface area from a text file and sets up
// the zone heat balance matrix and solves for the Radiant Time Factors.
N = 12;
YZP=file('open','C:\SCILAB\PRF.text','old');
SA=file('open','AREA.DAT','last','old'); // opens test file
PRFD=read(YZP,288,2); // reads response factors file
A=read(SA,1,12); // reads surface areas from file
file('close',YZP);
Qgain=1000.;
for j=1:N;
    for i=1:24;
        YP(i,j)=PRFD((j-1)*24+i,1);
        ZP(i,j)=PRFD((j-1)*24+i,2);end;end
PRF=file('open','YZPRF.text','unknown');
write(PRFD,PRFD,'(2(f15.10,2x))');
file('close',PRF);
// creat the system matrix
for j=1:N;
    OMEGA(j,1,1)=ZP(1,j)-YP(1,j);
    for k=2:24;kk=24-k+2;OMEGA(j,1,k)=ZP(kk,j)-YP(kk,j);end;
    for i=2:24;
        for k=1:24;
            kk=k+1; if kk > 24 then, kk=kk-24; else, end;
            OMEGA(j,i,kk)=OMEGA(j,i-1,k);end;end;
end
// define surface areas in the zone
em=[0.9 0.9 0.9 0.9 0.9 0.9 0.9 0.9 0.9 0.9 0.9 0.9];
exec('C:\SCILAB\RTFFUNCTIONS.SCI',-1);
exists('AreaFraction');
exists('InsideRadiationCoef');
exists('MeanRadiantTemperature');
exists('Response');
AF=AreaFraction(A,N,em,N);
for j=1:N;
    MRTVF(j)=1./(1.-A(j)/sum(A));end;
```

```

Iter=0;
while Iter < 10,
    for i=1:N;
        A_MRTVF_Product=0.0d0;
        for j=1:N;
            A_MRTVF_Product=A_MRTVF_Product+A(j)*MRTVF(j);
        end;
        MRTVF(i)=1./(1.-A(i)*MRTVF(i)/A_MRTVF_Product);end;
        Iter=Iter+1; else, end; // Iteration Loop
//
Sigma=5.67E-8;
// Initialize the hourly values of the radiation coefficient
for i=1:24; // number of hours
    for j=1:N; // number of surfaces
        hradbase(j,i) = 4*Sigma*(27+273.15)**3 / (1/MRTVF(j)+(1-em(j)))/em(j);end; // surface
Loop
    end // Hour loop
    for i=1:24;TROOM(i)=24.0;TMRT(i)=24.0;end
    for j=1:N; for i=1:24; TsIn(j,i)=TROOM(i);hrad(j,i)=hradbase(j,i);end;end
    for j=1:N;hcIn(j)=4.68;end
    hcIn(5)=1.25; hcIn(6)=4.37;
// calculate mean radiant temperatures

for Mode=1:2; // Mode 1 for non solar RTF and Mode=2 solar RTF

if Mode==1 then,
    for i=1:24;
        if i==1 then LWRadIntGain = Qgain;
        else LWRadIntGain = 0.0d0; end
        for j=1:N;
            Distribution(j) = AF(j);
            if A(j) == 0 then
                RadPulseDist(j,i) = 0.0;
            else RadPulseDist(j,i) = LWRadIntGain*Distribution(j)/A(j); end,
        end;end
    else,
        for i=1:24;
            if i==1 then LWRadIntGain = Qgain;
            else LWRadIntGain = 0.0d0; end
            for j=1:N; Distribution(j)=0.0;
                if j==6 then Distribution(j)=0.5; elseif j==7 Distribution(j)=0.5; else end
            if A(j) == 0 then
                RadPulseDist(j,i) = 0.0;
            else RadPulseDist(j,i) = LWRadIntGain*Distribution(j)/A(j);end,
        end;end
    end
// iteration starts here
Iter=0;
while Iter < 25 then // iteration for convergence
    for j=1:N;
        for i=1:24;
            C(i)=hcIn(j)*TROOM(i)+hrad(j,i)*TMRT(i)+RadPulseDist(j,i);end
// generate the left hand side system matrix B
    for i=1:24;
        for k=1:24;
            B(i,k) = OMEGA(j,i,k);

```

```

        if i==k then B(i,k) = hcIn(j) + hrad(j,i) + B(i,k);
        else, end
    end; end
BM=file('open','MATRIX.text','unknown');
write(BM,B,(24(f10.6,1x)));
file('close',BM);
// Calculates the surface temperature by matrix inversion and multiplication
BInv = inv(B);
Ts = BInv*C;
for k=1:24;
    TsIn(j,k)=Ts(k);end
end // end of surface loop j
hrad=InsideRadiationCoef(TsIn, TMRT);
TMRT=MeanRadiantTemperature(A, TsIn,hrad);
hrad=InsideRadiationCoef(TsIn, TMRT);
Iter=Iter+1;
else,
    TsIn;
end;
// end if while loop
if(Mode==1) then, [NONSOLARRTF]=Response(A,hcIn,TsIn);
    RTFSUM=sum(NONSOLARRTF)
else,
    [SOLARRTF]=Response(A,hcIn,TsIn);
    RTFSUM=sum(SOLARRTF)
end
end; // end of pulse distribution.
NONSOLARRTF
SOLARRTF

function AF=AreaFraction(A,N,em,N)
    AF=A.*em/(sum(A.*em))
endfunction
function TMRT = MeanRadiantTemperature(A,TsIn,hrad)
    [nS nH]=size(TsIn);
    for i=1:nH;
        A_hrad_Temperature(i)=0.0;
        A_hrad_Product(i)=0.0;
        for j=1:nS;
            A_hrad_Product(i)=A_hrad_Product(i)+A(j)*hrad(j,i);
            A_hrad_Temperature(i)=A_hrad_Temperature(i)+A(j)*hrad(j,i)*TsIn(j,i);end;
        TMRT(i) = A_hrad_Temperature(i)/A_hrad_Product(i);end
    endfunction
function hrad =InsideRadiationCoef(TsIn, TMRT)
    [nS nH]=size(TsIn);
    for i=1:nH;for j=1:nS;
        hrad(j,i)=(0.865+TsIn(j,i)/200)*hradbase(j,i);end;end;
    for i=1:nH;for j=1:nS;
        hrad(j,i)=(0.865 + TMRT(i)/200)*hrad(j,i);end;end
    endfunction
// compute the zone response
function RTF=Response(A,hcIn,TsIn)
    [nS nH]=size(TsIn);
    for i=1:nH;
        RTF(i)=0.0;
        for j=1:nS;

```

```
RTF(i)=RTF(i)+A(j)*hcIn(j)*(TsIn(j,i)-TROOM(j))/Qgain;end;  
end  
endfunction
```

C.2 RTSM Implementation in VBA

The RTSM cooling load calculation procedure has been implemented as a spreadsheets application using VBA programming and worksheet functions. The CTS and RTF were generated using three different approaches:

- Compiled FORTRAN DLL
- VBA sub-program with variable radiation coefficients
- VBA sub-program with constant radiation coefficients

Three thermal zones from ASHRAE head quarter building in Atlanta, Georgia were used as test zones. The hourly cooling loads were calculated for the twelve design days for each zone and the annual peak design day cooling loads were extracted. The hourly design day cooling load for three zones and the three different approaches are shown in Figure C.1 to C.3. The hourly cooling load show very good match. The hourly cooling load error by using constant radiation coefficients was less than $0.02 \text{ Btu/h}\cdot\text{ft}^2$.

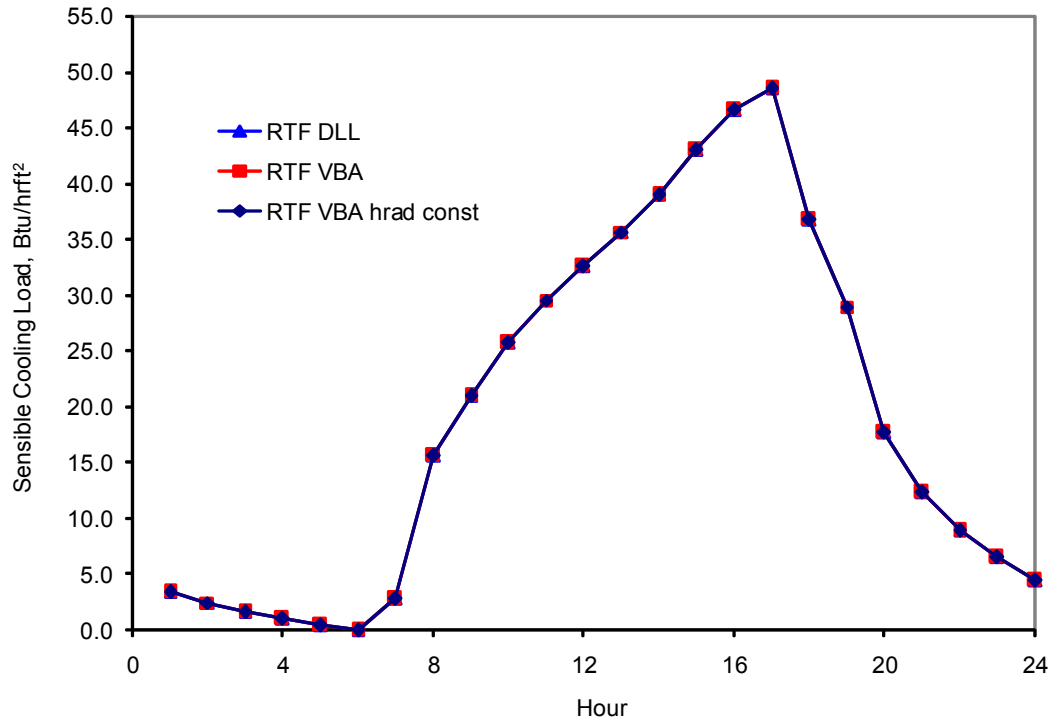


Figure C.1 The RTSM cooling load (per square foot of floor area) for a zone with south and west facing exterior facades

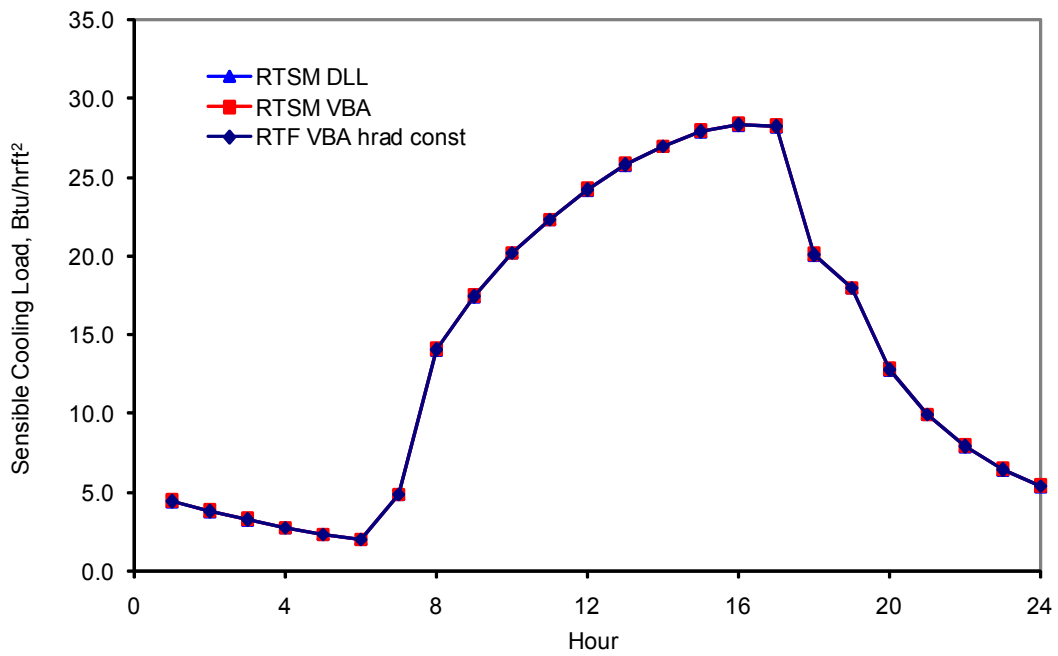


Figure C.2 The RTSM cooling load (per square foot of floor area) for a zone with south facing exterior façade

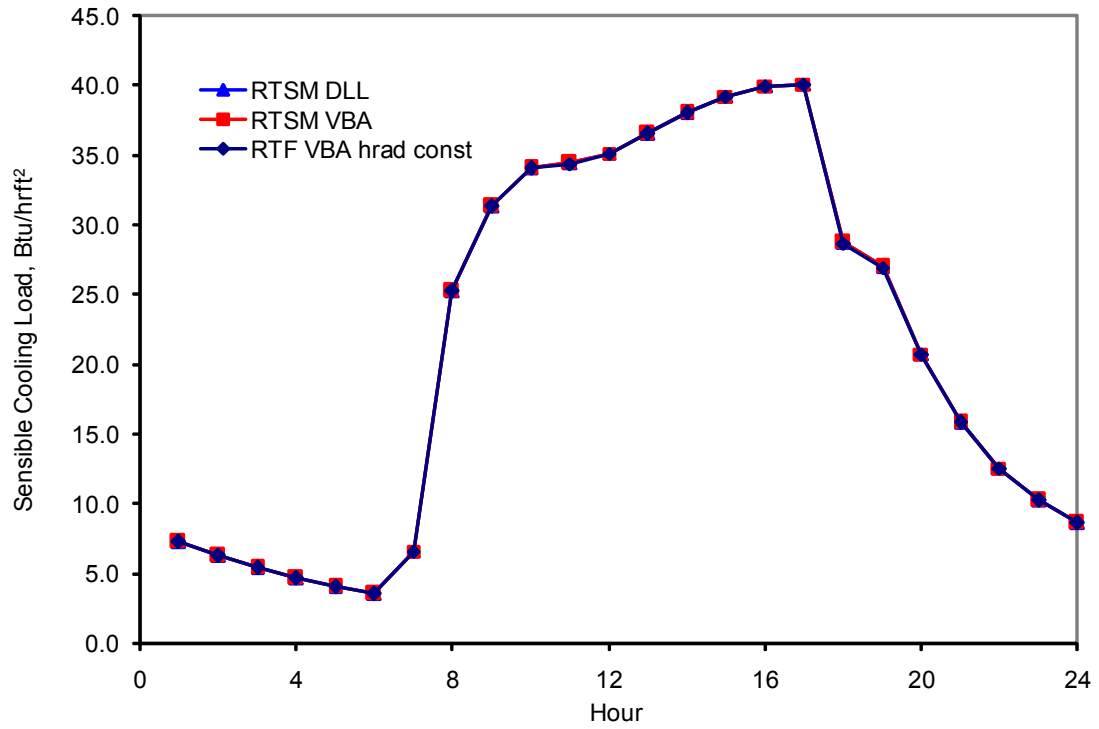


Figure C.3 The RTSM cooling loads (per square foot of floor area) for a zone with north and east facing exterior facades

APPENDIX D: FENESTRATION MODELS FOR HEAT BALANCE AND RTS METHODS

D.1 The Heat Balance Method Fenestration Model

The optical properties (transmittance, reflectance and absorptance) of glazing system are computed from the optical properties of the individual layers using an algorithm developed by Klems (2002). A Multi-layer glazing system representation for system optical properties calculation is shown in Figure D.1 below.

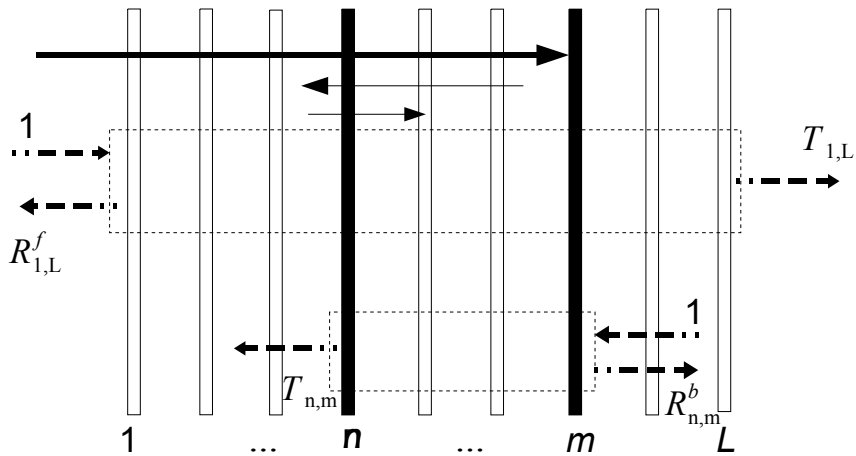


Figure D.1 Multi-layer glazing considered as systems and subsystems
(2005 ASHRAE handbook of Fundamentals)

The glazing system optical properties are computed using recursive relations from the outer pane to the inner pane. The transmittance of the glazing system is computed from the individual layer properties and is given by:

$$T_{n,m+1}(\theta) = \frac{T_{n,m}(\theta)T_{m+1}(\theta)}{1 - R_{n,m}^b(\theta)R_{m+1}^f(\theta)} \quad (\text{D.1})$$

Where,

- $T_n(\theta)$ = isolated-layer transmittance of n^{th} layer (in an L -layer system)
- $T_{n,m}(\theta)$ = transmittance of the subsystem consisting of layers N to M (in an L -layer system)
- R_{m+1}^f = front reflectance of the $m+1$ glazing layer, (-)
- $R_{n,m}^b$ = back reflectance of the subsystem consisting of layers N to M (in an L -layer system, (in))

In the glazing system it is always true that m greater or equal to n , and for a subsystem with single layer $m=n$. With this representation the optical properties a multi-layer glazing system can be computed starting with a single layer and successively adding additional layers. The front and back reflectance of the n glazing layer in the system is calculated from the following recursive expression:

$$R_{n,m+1}^f(\theta) = R_{n,m}^f(\theta) + \frac{[T_{n,m}(\theta)]^2 R_{m+1}^b(\theta)}{1 - R_{n,m}^b(\theta)R_{m+1}^f(\theta)} \quad (\text{C.2})$$

$$R_{n,m+1}^b(\theta) = R_{m+1}^b(\theta) + \frac{[T_{m+1}(\theta)]^2 R_{n,m}^b(\theta)}{1 - R_{n,m}^b(\theta)R_{m+1}^f(\theta)} \quad (D.3)$$

Once the glazing system layer-by-layer transmittance and reflectance are determined, then the n^{th} layer front and back absorptance of the glazing system can be determined. The directional front absorptance of the n^{th} layer in multi-layered glazing system is given by:

$$A_{n:(1,L)}^f(\theta) = \frac{T_{1,n-1}(\theta)a_n^f(\theta)}{1 - R_{1,n-1}^b(\theta)R_{n,L}^f(\theta)} + \frac{T_{1,n}(\theta)R_{n+1,L}^f(\theta)a_n^b(\theta)}{1 - R_{1,n}^b(\theta)R_{n+1,L}^f(\theta)} \quad (D.4)$$

where,

$$A_{n:(1,L)}^f = \text{directional hemispherical front absorptance of the } n^{th} \text{ layer, (-)}$$

The directional back absorptance of the n^{th} layer in multi-layered glazing system is given by:

$$A_{n:(1,L)}^b(\theta) = \frac{T_{n+1}(\theta)a_n^b(\theta)}{1 - R_{1,n}^b(\theta)R_{n+1,L}^f(\theta)} + \frac{T_{n,L}(\theta)R_{1,n-1}^f(\theta)a_n^b(\theta)}{1 - R_{1,n}^f(\theta)R_{n+1,L}^b(\theta)} \quad (D.5)$$

where,

$$A_{n:(1,L)}^b = \text{directional hemispherical back absorptance of the } n^{th} \text{ layer, (-)}$$

Optical properties of the layers are computed at an average wavelength for solar radiation. The absorption in each layer is due to incident solar radiation and multiple reflections within the subsystem (m, n).

D.1.1 Interior Shading Treatment

Klems (2002) glazing system model also is capable of including a single diffuse internal shade layer. The interior shade is assumed as additional layer to the glazing system. The interior shade model for a multi-layer glazing system is based on the following simplifying assumptions:

- the glazing system is completely shaded
- the shading layer is planar
- the shading layer is diffuse reflector.

With this approximation the multi-layer glazing system optical properties are corrected as follows. The beam transmittance of the fenestration system is given by:

$$T_{1,L+1}^{fH}(\theta) = \frac{T_{1,L}^f(\theta)T_s^{fH}}{1 - R_s^{fH} \langle R_{1,L}^b \rangle_D} \quad (D.6)$$

Where,

$T_{1,L}^f(\theta)$ = directional hemispherical transmittance of the glazing system, (-)

$T_{1,L+1}^{fH}$ = directional hemispherical transmittance of glazing system with shade, (-)

$R_{1,L}^b$ = diffuse back reflectance of the glazing system, (-)

T_s^{fH} = transmittance of the shading layer, (-)

R_s^{fH} = reflectance of the shading layer, (-)

The diffuse transmittance of the fenestration system is given by:

$$\langle T_{1,L+1}^{fH} \rangle_D = \frac{\langle T_{1,L}^f \rangle_D T_s^{fH}}{1 - R_s^{fH} \langle R_{1,L}^b \rangle_D} \quad (D.7)$$

Where,

$\langle T_{1,L}^f \rangle_D$ = diffuse transmittance of the glazing system, (-)

$\langle T_{1,L+1}^{fH} \rangle_D$ = average hemispherical transmittance of glazing system with shade, (-)

R_s^{fH} = average hemispherical reflectance of the shading layer, (-)

The beam radiation absorptance of the fenestration system:

$$A_{k:(1,L+1)}^f(\theta) = A_{k:(1,L)}^f(\theta) + \langle A_{k:(1,L)}^b \rangle_D \frac{T_{1,L}(\theta) R_s^{fH}}{1 - R_s^{fH} \langle R_{1,L}^b \rangle_D} \quad (D.8)$$

Where,

$A_{k:(1,L+1)}^f(\theta)$ = directional hemispherical absorptance of the k^{th} layer, (-)

$A_{k:(1,L)}^f(\theta)$ = directional hemispherical front absorptance of the k^{th} layer, (-)

$\langle A_{k:(1,L)}^b \rangle_D$ = average hemispherical back absorptance of the k^{th} layer, (-)

Average hemispherical front absorptance of the fenestration system is given by:

$$\left\langle A_{k:(1,L+1)}^f \right\rangle_D = \left\langle A_{k:(1,L)}^f \right\rangle_D + \left\langle A_{k:(1,L)}^b \right\rangle_D \frac{\left\langle T_{1,L} \right\rangle_D R_s^{fH}}{1 - R_s^{fH} \left\langle R_{1,L}^b \right\rangle_D} \quad (\text{D.9})$$

Where,

$$\left\langle A_{k:(1,L+1)}^f \right\rangle_D = \text{average hemispherical front absorptance of the } k^{\text{th}} \text{ layer with shade, (-)}$$

$$\left\langle A_{k:(1,L)}^f \right\rangle_D = \text{average hemispherical front absorptance of the } k^{\text{th}} \text{ layer, (-)}$$

The directional front absorptance of the shade layer is given by:

$$A_{s:(1,L+1)}^f(\theta) = A_{L+1:(1,L+1)}^f(\theta) = \frac{T_{1,L}(\theta) a_s^f}{1 - R_s^{fH} \left\langle R_{1,L}^b \right\rangle_D} \quad (\text{D.10})$$

Where,

$$a_s^f = \text{Front absorptance of the shading layer, (-)}$$

The average hemispherical absorptance of the shade layer is given by:

$$\left\langle A_{L+1:(1,L+1)}^f \right\rangle_D = \frac{\left\langle T_{1,L} \right\rangle_D a_s^f}{1 - R_s^{fH} \left\langle R_{1,L}^b \right\rangle_D} \quad (\text{D.11})$$

D.1.2 Inward and Outward flow Fraction of Absorbed Component

Computation of inward and outward flow fraction of the absorbed component of the fenestration system with shading requires the inward flow fraction (N_i) of each glazing layers including the shade layer. Thermal resistance network model of the fenestration system has been used to compute the inward and outward flow fraction of the absorbed component of the solar heat gain. The inward-flowing fractions of the absorbed solar heat gain can be estimated using simplified constant thermal resistance model, using the following expressions:

$$AF(\theta) = \sum_{k=1}^{L+1} N_k A_{k:(1,L+1)}^f(\theta) \quad (D.12)$$

$$AF_D = \sum_{k=1}^{L+1} N_k \langle A_{k:(1,L+1)}^f \rangle_D \quad (D.13)$$

$$N_k = \frac{U}{h_{o,k}} \quad (D.14)$$

where,

N_k = inward flow fraction of the absorbed component for the k^{th} layer, (-)

U = U -value of the fenestration system, $\text{W/m}^2 \cdot \text{K}$ ($\text{Btu/h} \cdot \text{ft}^2 \cdot ^\circ\text{F}$)

h_o = effective heat transfer coefficient between the exterior environment and the k^{th} glazing layer, $\text{W/m}^2 \cdot \text{K}$ ($\text{Btu/h} \cdot \text{ft}^2 \cdot ^\circ\text{F}$).

D.1.3 Transmitted and Absorbed Component

The transmitted and absorbed components of the solar radiation for a given fenestration system are computed as follows. The transmitted beam and diffuse solar radiation components are given by:

$$q_T(\theta) = E_{DN} \cos \theta \langle T_{1,L+1}^{fH}(\theta) \rangle \quad (D.15)$$

$$q_{T,d} = (E_d + E_r) \langle T_{1,L+1}^{fH} \rangle_D \quad (D.16)$$

Where,

$$q_T(\theta) = \text{beam transmitted solar heat gain, W/m}^2 \text{ (Btu/h}\cdot\text{ft}^2\text{)}$$

$$q_{T,d} = \text{diffuse transmitted solar heat gain, W/m}^2 \text{ (Btu/h}\cdot\text{ft}^2\text{)}$$

$$E_{ND} = \text{normal direct irradiation, W/m}^2 \text{ (Btu/h}\cdot\text{ft}^2\text{)}$$

$$E_d = \text{diffuse irradiation from the sky, W/m}^2 \text{ (Btu/h}\cdot\text{ft}^2\text{)}$$

$$E_r = \text{diffuse irradiation reflected from the ground or other surfaces, W/m}^2 \text{ (Btu/h}\cdot\text{ft}^2\text{)}$$

$$\theta = \text{angle of incidence between the sun's rays and normal to the surface, radian}$$

The inward and outward flowing fraction of the absorbed solar heat gain components are given by:

$$q_{ai} = E_{DN} \cos \theta \sum_{k=1}^{L+1} A_{k:(1,L+1)}^f(\theta) N_k + (E_d + E_r) \sum_{k=1}^{L+1} \langle A_{k:(1,L+1)}^f \rangle_D N_k \quad (D.17)$$

$$q_{ao} = E_{DN} \cos \theta \sum_{k=1}^{L+1} A_{k(1,L+1)}^f(\theta)(1 - N_k) + (E_d + E_r) \sum_{k=1}^{L+1} \langle A_{k(1,L+1)}^f \rangle_D (1 - N_k) \quad (D.18)$$

Where,

q_{ai} = inward flow fraction of the absorbed component for system, (-)

q_{ao} = outward flow fraction of the absorbed component for system, (-)

D.2 RTSM Fenestration Model

The fenestration model implanted in the RTSM procedure makes use of the Solar Heat Gain Coefficient (*SHGC*), the attenuation coefficient (*IAC*) to account for the shade effect and overall radiative fractions to account for the amount of solar heat gain absorbed by the fenestration system and transmitted into the space. The following section describes the calculation procedure for computing SHGC based on Klems (2002) Model.

D.2.1 Solar Heat Gain Coefficient

For un shaded glazing systems with no strong spectral dependence the solar-weighted spectral band values of the optical properties can be used to estimate the solar heat gain coefficient (Klems 2002) as follows:

$$SHGC(\theta) = T_{1,L}^f(\theta) + \sum_{k=1}^L N_k A_{k(1,L)}^f(\theta) \quad (D.19)$$

$$SHGC_d = \langle T_{i,L}^f \rangle_D + \sum_{k=1}^L N_k \langle A_{k(1,L)}^f \rangle_D \quad (D.20)$$

Where,

$SHGC(\theta)$ = beam solar heat gain coefficient, (-)

$SHGC_d$ = diffuse solar heat gain coefficient, (-)

$T_{(1,L)}^f(\theta)$ = directional hemispherical transmittance of the glazing system, (-)

$A_{k:(1,L)}^f(\theta)$ = directional hemispherical absorptance of the k^{th} layer system, (-)

N_k = inward flow fraction of the absorbed component for the k^{th} layer, (-)

L = number of glazing layers, (-)

The transmitted and absorbed fractions of the glazing systems are calculated from detailed fenestration model described in Section D.1.

VITA

Bereket Asgedom Nigusse

Candidate for the Degree of

Doctor of Philosophy

Thesis: IMPROVEMENTS TO THE RADIANT TIME SERIES METHOD COOLING
LOAD CALCULATION PROCEDURE

Major Field: Mechanical Engineering

Biographical:

Personal Data:

Date of Birth:	Jan 30, 1966
Place of Birth:	Asmara, Eritrea

Education:

Received Bachelor of Science degree in Chemical Engineering from Addis Ababa University, Addis Ababa, Ethiopia, in July 1989.

Received Master of Engineering Science in Mechanical Engineering from the University of New South Wales, Sydney, Australia, in May 1998.

Completed the requirements for the Doctor of Philosophy in Mechanical Engineering at Oklahoma State University, Stillwater, Oklahoma in December 2007.

Experience:

Aug 2005 - Present	Graduate Research Associate Oklahoma State University
--------------------	--

Aug 2003 – July 2005	Fulbright Fellow Oklahoma State University
----------------------	---

Professional Memberships: Phi Kappa Phi Honor Society, American Society of Heating, Refrigerating and Air-conditioning Engineers (ASHRE), and International Building Performance Simulation Association (IBPSA).

Name: Bereket A. Nigusse

Date of Degree: December, 2007

Institution: Oklahoma State University

Location: Stillwater, Oklahoma

Title of Study: IMPROVEMENTS TO THE RADIANT TIME SERIES METHOD
COOLING LOAD CALCULATION PROCEDURE

Pages in Study: 294

Candidate for the Degree of Doctor of Philosophy

Major Field: Mechanical Engineering

Scope and Method of Study:

The objective of the study was improvement of the Radiant Time Series Method (RTSM) cooling load calculation procedure. A series of investigations were carried out, including: improvements to peak cooling load prediction performance, development of a simplified procedure for Radiant Time Factor (RTF) generation, adaptation of the fenestration sub-model to be compatible with currently available manufacturer's data, establishing appropriate radiative fractions for all heat gain types. The simplified RTF generation procedure facilitates implementation in a range of computing environments. Furthermore, an approximate one-dimensional dynamic model for thermal bridges has been investigated and validated against both experimental results and detailed computational results.

Findings and Conclusions:

The Radiant Time Series Method was modified by introducing a dimensionless loss conductance that is readily calculable from the zone geometry and surface characteristic. Along with the revised fenestration sub-model, newly-recommended radiative fractions, and simplified RTF generation procedure, the RTSM performance was validated against the reference method, the heat balance method (HBM) with a large parametric study. The parametric study compared peak cooling loads determined with the improved RTSM procedure to those determined with the HBM for a wide range of building design parameters, for which all combinations formed 2,867,200 different zones. Use of the dimensionless loss conductance caused the maximum overprediction to go from 37% to 18%.

Several additional simplifications were made to facilitate implementation in a range of computing environments. These simplifications included development of a one-dimensional finite volume numerical procedure for generating periodic response factors. This reduced the number of lines of source-code required with the previous state-space method from 2000 to 500 in Fortran 90. In a computing environment with embedded matrix algebra, such as SCILAB, the number of lines of source-code can be further reduced to 150. The new formulation of the RTF generation procedure allows very compact implementation (150 lines of source code, compared to the original procedure, implemented in approximately 4000 lines of Fortran 90 source code) in computing.

The approximate one-dimensional dynamic model of thermal bridges has been validated against published experimental results and also against numerical results generated with a 2D finite volume program. The approximate model can predict peak heat gains within $\pm 2.6\%$ of the experimental measurements, provided accurate steady state thermal resistances are used.

ADVISER'S APPROVAL: Dr Jeffrey D. Spitler
